Università degli Studi di Padova

Dipartimento di Scienze Biomediche

CORSO DI DOTTORATO DI RICERCA IN SCIENZE BIOMEDICHE
31° CICLO

Generation of novel zebrafish models of sarcoglycanopathy

Coordinatore: Ch.mo Prof. Paolo Bernardi
Supervisore: Ch.ma Prof.ssa Dorianna Sandonà
Co-Supervisore: Dott. Marcello Carotti

Dottorando: Dott.ssa Michela Soardi

INDEX

ABSTRACT

Le sarcoglicanopatie sono quattro rare patologie autosomiche recessive appartenenti alla famiglia delle distrofie muscolari di tipo 2 (LGMD2C-F). Esse sono causate da mutazioni nei geni *SGCG, SGCA, SGCB, SGCD* codificanti rispettivamente per γ-, α-, β- e δ- sarcoglicano (SG). I SG formano un complesso tetramerico nel sarcolemma, connesso a quello delle glicoproteine associate alla distrofina (DAPC), essenziale per garantire l'integrità della membrana durante la contrazione muscolare (Bushby, 2009). Mutazioni dei SG causano la perdita/riduzione della proteina mutata e dei partner wild type (WT), alterando le proprietà strutturali del DAPC e aumentando la fragilità del sarcolemma. La maggior parte delle mutazioni sono di tipo missenso e, causando un problema nel folding, portano alla prematura degradazione della proteina mutata effettuata dalla via ERAD (degradazione associata al reticolo endoplasmatico) attraverso il proteasoma (Gastaldello et al., 2008; Bartoli et al., 2008). La conoscenza del meccanismo patologico ha aperto nuove strade a due possibili interventi farmacologici: inibendo la degradazione o assistendo il processo di folding dei mutanti, il complesso dei SG è recuperato riducendo così la fragilità della membrana (Bianchini et al., 2014; Carotti et al., 2018). Questi dati prodotti *in vitro* suggeriscono che molti mutanti sono ancora funzionali, sebbene strutturalmente difettosi. Tuttavia, per la messa a punto di un approccio terapeutico, questi dati necessitano di una validazione *in vivo*, attraverso modelli animali per mimare la malattia umana e recanti quindi mutazioni missenso nei SG. In assenza di modelli murini, un'alternativa promettente per lo studio di molte malattie, fra cui i disturbi muscolari, è rappresentata dallo zebrafish (*D.rerio)*. Tra gli ortologhi dei SG umani, β- e δ-SG sono i più conservati e quindi sono stati scelti per produrre linee knock-out (KO) e knock-in (KI). La bontà dell'uso di questo vertebrato nel mimare la sarcoglicanopatia nasce da uno studio preliminare di Knock-Down con morfolino contro il δ-SG. I morfanti ottenuti hanno mostrato: alterazioni morfologiche, danni alla struttura muscolare e compromissione delle capacità motorie. Grazie a queste premesse, il sistema CRISPR/Cas9 è stato usato per generare modelli KO di β- e δ-SG. In entrambi i casi, l'assenza della proteina provoca la progressiva alterazione della struttura muscolare e delle capacità motorie. Attualmente stiamo usando i KO come background per l'iniezione della sequenza WT o mutata dei SG, sia di origine umana sia di zebrafish. La prima dovrebbe consentire il recupero del fenotipo, mentre quella delle forme mutate permetterà di valutare la capacità dello zebrafish di riconoscerle e degradarle. Questi esperimenti sono della massima importanza per verificare l'idoneità dello zebrafish nel mimare le forme di sarcoglicanopatia causate da mutazioni missenso. La generazione di due modelli KI in zebrafish, β-$SG^{T145R/T145R}$ e δ-$SG^{E264K/E264K}$, prevede l'attivazione della via di riparazione HDR (riparazione omologa diretta). Poiché l'efficienza della ricombinazione omologa è molto bassa, è necessario l'uso di un metodo altamente selettivo per identificare i pesci positivi alla voluta mutazione. Lo screening delle mutazioni somatiche per l'introduzione della mutazione T145R nel gene z-sgcb è stato positivo. Attualmente stiamo aspettando la maturazione sessuale della popolazione F0 per identificare quei pesci in cui ricombinazione sia avvenuta nella linea germinale. Se le linee KI, una volta caratterizzate, mimeranno la patologia umana, rappresenteranno uno strumento fondamentale per testare l'approccio farmacologico proposto *in vitro*, e costituiranno un valido stimolo per la ricerca di base e traslazionale.

ABSTRACT

Sarcoglycanopathy is the collective name of four rare autosomal recessive diseases belonging to the limb-girdle muscular dystrophies type 2 (LGMD2C-F), due to mutations in *SGCG, SGCA*, *SGCB*, *SGCD* genes coding for γ-, α-, β- and δ- sarcoglycan (SG) respectively. SGs form a tetrameric sub-complex on the sarcolemma, closely linked to the dystrophin associated protein complex (DAPC) and play an essential role in assuring membrane integrity during muscle contraction (Bushby, 2009). Mutations in each SG gene cause the loss/reduction of the mutated protein as well as of the wild type (WT) partners with an alteration of the DAPC structural properties and an increased fragility of the sarcolemma. Most of the known disease-causing mutations are missense mutations that results in a folding defective SG, recognized and prematurely degraded by the endoplasmic reticulum associated degradation (ERAD) through the proteasome (Gastaldello et al., 2008). The knowledge of the pathological mechanism opens new avenues to two small molecules-based pharmacological interventions. By inhibiting the mutant degradation or assisting its folding the whole SG complex is recovered on the membrane, suggesting that many mutants are still functional although structurally defective (Bianchini et al., 2014; Carotti et al., 2018). Now for the subsequent preclinical test, these *in vitro* data need to be validated *in vivo.* To accomplish this task, in the absence of suitable rodent models, zebrafish models carrying missense mutations in SGs are needed to mimic the human condition. Among SGs, β- and δ-SG are the most conserved, therefore they were chosen to mimic sarcoglycanopathy in zebrafish. The nearly identical muscle structure with the human one, the ease to set up functional and drug screening test, make this vertebrate an ideal choice for our task. The proof of concept of the suitability of the model came from the knock-down of δ-SG by using the morpholino technique. Morphants showed altered morphology and compromised swimming ability. On these promising data, we decided to generate novel zebrafish lines in which β- or δ-SG genes are modified by using the CRISPR/Cas9 technique. β- and δ-SG Knock-out (KO) animals have been generated and characterized. The absence of the protein led to the progressive alteration of the muscle structure and impairment of the swimming ability. Presently, KO animals are used as the background for the injection of the WT or mutated sequence of the corresponding SG, of human or zebrafish origin. The injection of the WT sequence should allow the rescue of the phenotype, whereas that of the mutated forms will permit to evaluate the ability of the zebrafish ERAD to recognize and degrade a folding defective SG. This data will be of utmost importance to verify the suitability of zebrafish in mimicking those forms of sarcoglycanopathy due to missense mutations. β-SG$^{T145R/T145R}$ and δ-SG$^{E264K/E264K}$ Knock-in (KI) are presently under production. Since the efficacy of the homologoy direct repair is very low, much effort has been devoted to set up a selective procedure to screen the positive fish. Actually, the screening of the somatic recombinants for the introduction of the T145R mutation in z-*sgcb* gene was positive. We are presently waiting for the sexual maturation of the F0 population to perform the outcross with WT in order to identify the founder animals, in which the recombination occurred in the germline. If successfully modelling the sarcoglycanopathy conditions, these KI lines will represent a fundamental tool for testing the proposed pharmacological approach and will be a valuable boost for both basic and translational research.

SUMMARY

Sarcoglycanopathy is the collective name of four rare autosomal recessive diseases belonging to the limb-girdle muscular dystrophies type 2 (LGMD2C-F). Sarcoglycanopathy is characterized, despite the heterogeneous clinical phenotype, by a progressive degeneration of the striated muscle tissue with the consequent loss of deambulation, respiratory complications and, in many cases, cardiac involvement (Kirschner and Lochmüller 2011; Nigro and Savarese 2014).

LGMD2C-F are due to mutations in *SGCG, SGCA*, *SGCB*, *SGCD* genes coding for γ-, α-, β- and δ-sarcoglycan (SG) respectively. SGs form a tetrameric sub-complex of the sarcolemma, closely linked to the major dystrophin associated protein complex (DAPC) and play and essential role in assuring membrane integrity during muscle contraction (Bushby, 2009).

Mutations in each SG gene cause the loss/reduction of the mutated protein as well as of the wild type (WT) partners with an alteration of the DAPC structural properties that leads to an increased fragility of the sarcolemma. The progressive muscle degeneration leads to the onset of the disease.

Finding a cure for this neglected disease still remains a major challenge. Despite the success of both cell and gene therapy in preclinical trials (Tedesco et al., 2012; Pozsgai et al., 2017), preliminary data from them reveal that these approaches are still far from enter clinical therapy (Mendell et al., 2010; Berardi et al., 2014).

In sarcoglycanopathy, most of the known disease-causing mutations are missense mutations. The defect is therefore a single amino acid substitution in a full-length protein that results in a folding defective polypeptide recognized and prematurely degraded by the endoplasmic reticulum associated degradation (ERAD) through the proteasome (Gastaldello et al., 2008; Bartoli et al., 2008). Interestingly, pharmacological interventions aiming to avoid the degradation of these folding defective mutants, allow the recovery of the whole SG complex on the membrane. In particular by blocking the first step, acting on α-mannosidase (Bartoli et al., 2008; Soheili et al., 2012), an intermediate step, inhibiting the E3 ligase HRD1 (Bianchini et al., 2014), or the last one, blocking the proteasome (Gastaldello et al., 2008), additional rounds of folding are forced. Therefore, the protein can acquire a native like conformations, and the SG-complex assembles and localizes at the sarcolemma. The so called “rescue strategy” suggests that many mutants are still functional although structurally defective and prematurely degraded. This evidence opens new avenues of therapeutic interventions for missense mutants. Indeed, by promoting the folding of the defective protein, it could be possible through to the so called “repair strategy”. The idea came from the knowledge related to another loss of functions disease, the cystic fibrosis. Indeed, some missense mutants of the cystic fibrosis transmembrane conductance regulator (CFTR) display folding and trafficking problems and are prematurely degraded likewise many mutated SGs. Therefore, small molecules known as CFTR correctors, acting probably as proteostasis regulator, could be effective also on protein structurally uncorrelated to CFTR (Pacheco et al., 2016).

Indeed, it was evaluated that a small library of CFTR correctors can assist/promote the folding of defective SGs. Importantly, the SG-complex re-localizes to the sarcolemma, restoring the membrane functionality, as evaluated in myotubes of patients (Carotti et al., 2018). These data

represent the proof of concept of the proposed therapeutic approach and need now to be validated *in vivo.* To accomplish this task, we need vertebrate animal models carrying missense mutations in SGs that cause the loss/strong reduction of the tetrameric complex, mimicking the human condition. In the absence of suitable rodent models (Bartoli et al., 2008; Kobuke et al., 2008; Henriques et al., 2018), we decided to adopt zebrafish (*Danio rerio*) to mimic sarcoglycanopathy. Indeed, zebrafish is becoming an ideal model for mimicking genetic diseases thanks to the possibility to easily introduce any desired mutation through the CRISPR/Cas9 genome-editing technologies (Chang et al., 2013). Other advantages are: the nearly identical structure of the fish muscle tissue compared to humans (Guyon et al., 2005); the embryo transparency that permits to easily evaluate any cardiac and/or muscle impairment; the presence of stereotyped movements since the first day of life that allow to measure muscle functionality very early in the development (Kopp et al., 2018; Burgess et al., 2007); the presence of conserved human orthologues of DAPC and of the ERAD elements (Guyon et al., 2005; Chamber et al., 2003 Steffen et al., 2007). Moreover, the possibility to adsorb molecules directly dissolved in fish water, make relatively easy the testing of novel therapeutic molecules (MacRae and Peterson, 2014).

Among SGs, β- and δ-SG are the most conserved, therefore we focused our attention on these zebrafish proteins in order to mimic sarcoglycanopathy in zebrafish.

The proof of concept of the suitability of the model came from the promising results obtained with the transient Knock-Down (KD) of δ-SG (δ-SG_{AUG}MO) by using the morpholino oligonucleotide technique. Treated embryos showed altered phenotype (morphants) with body bending, muscle structure alterations, defective cardiac development and compromised swimming ability.

On these premises, we decided to generate novel zebrafish lines in which β- or δ-SG genes are modified by using the CRISPR/Cas9 technique.

β- and δ-SG Knock-out (KO) animals have been already generated and characterized. The absence of the protein (checked by western blot and immunofluorescence analyses) leads to the progressive alteration of the muscle structure (as evaluated by histochemical analysis) and to the impairment of the swimming ability. Presently, KO animals are used as the background recipient for the injection of the WT or mutated sequence of the corresponding SG, of human or zebrafish origin. The injection of the WT sequence should allow the rescue of the phenotype, whereas that of the mutated forms will permit to evaluate the ability of the zebrafish ERAD to recognize and degrade a folding defective SG. This data being of utmost importance to verify the suitability of zebrafish in mimicking those forms of sarcoglycanopathy due to missense mutations.

β-$SG^{T145R/T145R}$ and δ-$SG^{E264K/E264K}$ Knock-in (KI) are presently under production. It is well known that the efficacy of the homology directed repair to introduce the desired point mutation is very low. Therefore, different approaches, described as successful in literature, are under investigations. Furthermore, the biggest challenge is the screening of the positive embryos that underwent homologous recombination in the germ-line and that can pass the desired mutation to the progeny.

Therefore, many efforts have been devoted to set up a selective and rapid screening procedure to accomplish this task. Actually, the screening of the somatic recombinants for the introduction of the T145R mutation in z-*sgcb* gene was positive. We are presently waiting for the sexual maturation of the F0 population to perform the outcross with WT in order to identify the founder animals, in which the recombination occurred in the germline.

If successfully modelling the sarcoglycanopathy conditions, these KI lines will represent fundamental tools for testing the proposed pharmacological approach and will be a valuable boost for both basic and translational research.

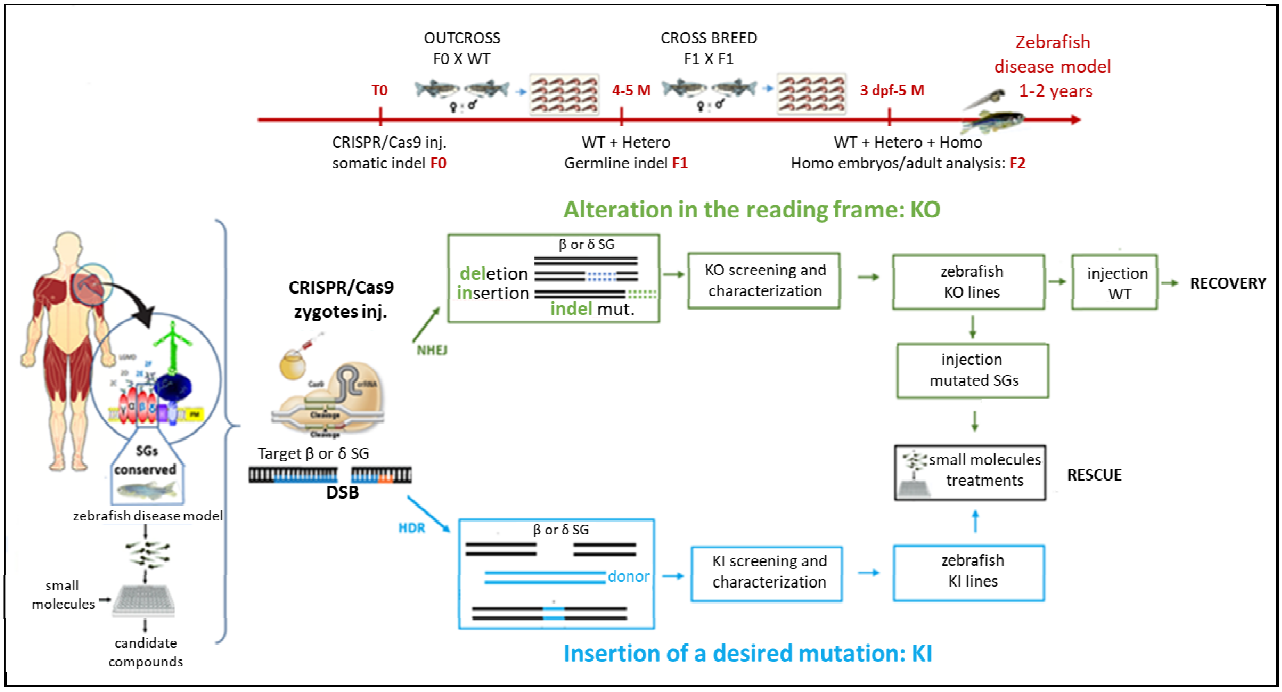

Fig 1. Pipeline of the strategy utilized to produce the KO and KI models of sarcoglycanopathy. CRISPR/Cas9 genome editing technique is used to produce a stable modification in selected locus of zebrafish *sgcb* and *sgcd.* These genes, encoding for β- and δ-SG, are selected because the most conserved between human and zebrafish.

1. INTRODUCTION

1.1 Cytoskeleton of skeletal muscle

Fibres of cardiac and skeletal muscle present a complex structure with a high level of organisation of the constituent proteins to allow a proper contraction. A perfect coordination is required between the contractile unit of muscle fibres, the sarcomere, and the large macromolecular complex, known as costamere, located at the interface between the cell and the extracellular matrix (ECM). The name costamere comes from the Latin word *'costa'* reminiscent of ribs, to identify protein complexes of the cytoskeleton assembled perpendicular to the longitudinal axis of the muscle fibres. Indeed, the complex network of structural and regulatory proteins of costameres tethers the Z-disc and M-band of sarcomere to the sarcolemma, the plasma membrane of striated muscle cells, via the intermediate filaments (IF), filamentous proteins of the cytoskeleton (Henderson et al., 2018; Jakai et al.,2015). The two complexes that compose costameres, the vinculin–talin–integrin system and the dystrophin–glycoprotein complex (DAPC), allow the assembly, the stabilisation and the force transmission between fibres:

- by mechanically connecting the contractile sarcomeres with proteins of the ECM to permit muscle adhesion to ECM;
- by distributing contractile forces from the sarcomere to the basal lamina ('inside-out') and transmitting forces applied externally on the ECM towards the inside of the fibres ('outside-in').

Considering their function, defects in costameres, due to mutations that disorganize their association, usually compromise muscle strength and can often result in cardiac or skeletal myopathies.

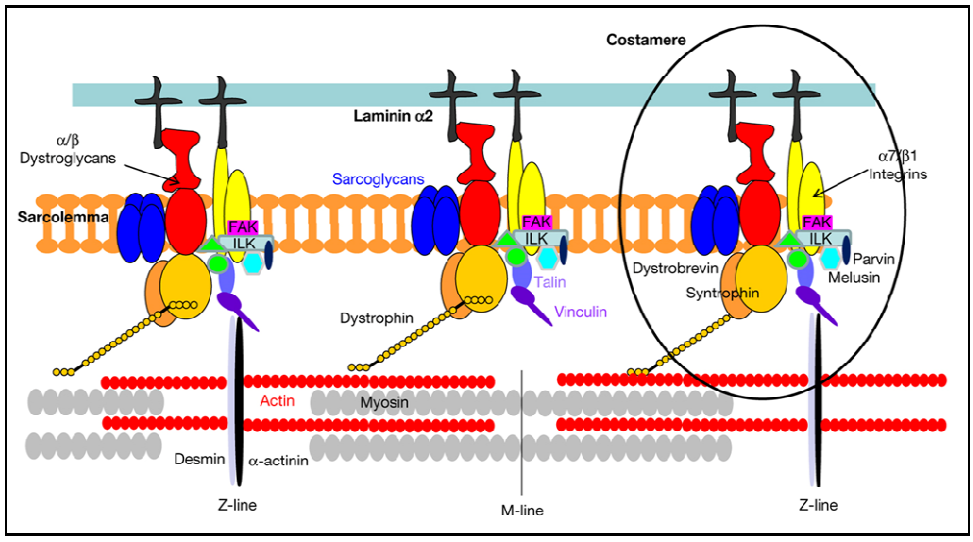

Jakai et al., 2015

Fig 2. Schematic representation of proteins forming costameres in skeletal muscle tissue. Costameres are associated with the sarcolemma that allow muscle adhesion to the ECM. They are composed by the dystrophin–glycoprotein complex and the integrin-talin-vinculin system.

1.1.1. **Dystrophin associated glycoprotein complex (DAPC)**

In 1989, few years after the identification of dystrophin (dys) as the gene responsible for Duchenne muscular dystrophy and its location on sarcolemma, other proteins were co-purified by Campbell and collaborators and the DAPC started to be investigated. In 1991 the DAPC was described as a multimeric protein complex of the sarcolemma, oriented perpendicularly to the longitudinal axis of the muscle fibres, and named in this way because composed of glycoproteins that interact with dys. The location suggests its role as crosslinker between the cytoskeletal F-actin and the ECM, through dys and the laminin-binding protein α-dystroglycan that in turn interacts with the transmembrane polypeptide β-dystroglycan (Hack et al., 2000). Thanks to the structural support of this bridge, the sarcolemma is protected from the long-term mechanical stress of contractile activity, and transmits the force generated by muscle contraction outside the fibres. In agreement with this hypothesis, mutations in genes encoding one of the DAPC components, compromise its backbone structure. Thus, focal ruptures of the sarcolemma, exposing muscle to contraction stresses, promote fibres degeneration and eventually lead to the development of a dystrophic phenotype (Davies and Nowak, 2006).

Furthermore, considering that several signalling molecules bind DAPC core components, a role in cell signalling is also important. For example, neuronal nitric oxide synthase (nNOS) interacts with syntrophins and dystrobrevins, and is implicated in vasodilatation to assure that all the metabolic needed of muscles during contraction are met. Likewise, some DAPC components presenting domains involved in non-structural functions, such as the ATPase activity of α-sarcoglycan, strength the signalling functions. The DAPC can be subdivided into three sub-complexes according to their biochemical characteristics and localisation (Townsend, 2014):

- the sarcoplasmic complex,
- the dystroglycan (DG) subcomplex,
- the sarcoglycan (SG) complex.

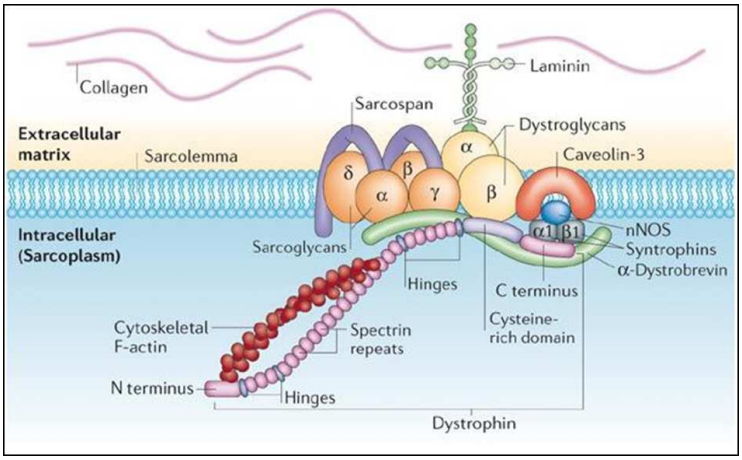

Davies and Nowak, 2006

Fig 3. The DAPC at the sarcolemma. The DAPC comprises sarcoplasmic proteins (dys, α-dystrobrevin, syntrophins and nNOS), transmembrane proteins (β-DG, the SG complex, caveolin-3 and sarcospan) and extracellular proteins (α-DG and laminin). The DAPC provides a strong mechanical link between the intracellular cytoskeleton and the extracellular matrix. Mutations of DAPC couse the, loss/compromission of sarcolemma integrity, and fibres are more susceptible to damage.

1.1.1.1 Sarcoplasmic subcomplex

The sarcoplasmic sub-complex localizes into the cytosol, immediately below the sarcolemma, and consists of dys, syntrophin and dystrobrevin.

Dystrophin

Dys is a large actin-binding protein (437 kDa), enriched at the costameres, lining the inner surface of the sarcolemma, acting as essential fulcrum for the organisation of the DAPC. It is composed of four distinct functional domains: an N-terminal actin-binding domain, a long central rod-domain containing 24 spectrin-like repeats that confers high flexibility to the protein, a cysteine rich domain, and a C-terminal domain. Dys assures the mechanical link between the actin cytoskeleton and the ECM. Indeed, through the N-terminal domain, dys forms a tight link with the actin cytoskeleton, an association reinforced by additional binding sites within some spectrin repeats. At the distal region, dys forms, *via* its cysteine-rich domain, a tight association with the transmembrane protein β-DG that, in turn, provides the interaction with the extracellular component Lamin-2 *via* α-DG (Henderson et al., 2018).

Absence or reduction in dys expression cause the development of Duchenne or Becker muscular dystrophies respectively, characterized also by a dramatic decrease of other DAPC components (Le Rumeur, 2015).

Syntrophin

Syntrophins belong to a family composed by at least three homologous cytoplasmic membrane-associated scaffold proteins directly associated with dys, dystrobrevin and nNOS. Syntrophins strengthen the link between the ECM and cytoskeleton by interacting with F-actin and dys. Furthermore, they play a role in the sarcolemmal localisation of nNOS, and it is thought they associate with kinases, ion channels and several signalling proteins. Therefore, by localizing signalling molecules, syntrophin creates signal-transduction complexes at the DAPC (Adams et al., 2018).

Dystrobrevin

Dystrobrevin is an 80-kDa protein, highly concentrated at the sarcolemma, associated with dys, SGs, IF and nNOS through interactions with syntrophin. Therefore, it cooperates in the stabilization of the sarcolemma (Strakova et al., 2014).

1.1.1.2 α and β-dystroglycans (DG)

DG complex is composed of two heterodimeric, closely associated, α- and β-subunits, which are post-translationally cleaved from a single product of the gene *DAG1.* The α-DG interacts with the β-DG on the extracellular surface. The DG complex assures the physical connection between the cytoplasmic proteins and the ECM. Indeed, the highly glycosylated extracellular protein, α-DG, binds proteins of the ECM (laminin, perlecan, and agrin) while β-DG is a transmembrane protein that binds directly the C-terminal domain of dys, α-dystrobrevin and the SG complex (Johnson et al., 2013).

1.1.1.3 Sarcoglycan complex (SG)

The third complex was discovered in 1994 by Yoshida et al. when, among the four SGs, only three subunits were detected (α-, β-, γ- SGs). In 1996, also δ-SG was discovered, and the structure of the whole complex was described. SGs form a tetrameric complex, by unitary stoichiometry, expressed predominantly on the sarcolemma of striated muscle (Tarakci and Berger, 2016). In addition to these SGs, two other polypeptides, ε-SG, and the ζ-SG, are mainly expressed in smooth muscle and in brain (Townsend, 2014).

SGs are single pass transmembrane glycoproteins, with a small intracellular tail and a large extracellular domain. The SG-complex forms composite molecular relationships with the other DAPC components enforcing the view of its crucial role in stabilising the whole DAPC structure. In particular:

- SGs form a tight side-association with β-DG, sarcospan, syntrophin, nNOS and the extracellular components proteoglycan and biglycan (Rafii et al., 2006; Yoshida et al., 2000);
- the intracellular tail of β- and δ-SG seems to associate directly with the cytoskeletal protein filamin-C and with the C-terminus of dys whereas the N-terminal region of α-dystrobrevin provides an additional secure link between SGs and dys (Chen et al., 2006).

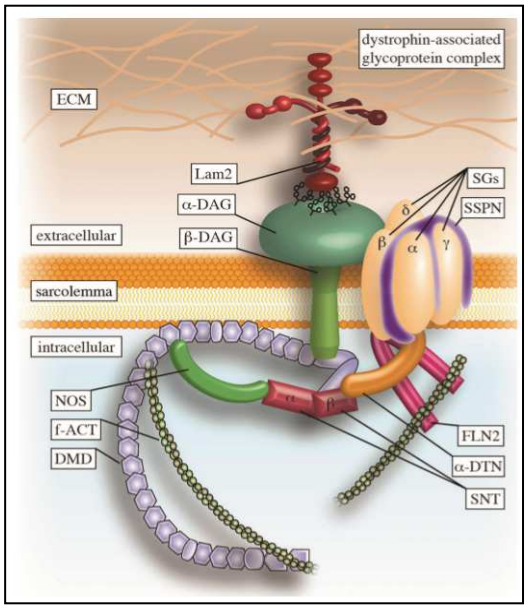

Tarakci and Berger, 2016

Fig 4. SG complex and its interaction with DAPC. The tetrameric complex expressed at the sarcolemma interacts with DAPC elements to strength the mechanical link between the cytoskeleton and the ECM. (Lam2, laminin2; α-, β-DAG, α-, β-DG; SSPN, sarcospan; FLN2, filamin2; α- DTN, α-dystrobrevin; SNT, syntrophin; f-ACT, f-actin; DMD, dys).

1.1.2 SG structure

SGs, with a molecular weight ranging between 35 and 50 kDa, are characterized by a highly conserved primary structure among species, suggesting an important evolutionary role and a secondary structure with β sheets and α-helices.

According the localization of the N-terminal domain, SGs are classified as:

- type I protein (α- SG) since the N-terminal glycosylated domain is extracellular and seems important for cell-cell and cell-ECM interactions;
- type II protein (β, γ, δ- SG) since the C-terminal domain is extracellular. It contains an epidermal growth factor-like domain, which may be a binding site for a yet unidentified ligand and a conserved cluster of five cysteines participating in the formation of intra and intermolecular disulphide bound.

A cysteine cluster is present in the extracellular domain of all SGs and is predicted to be important for the tertiary structure of the protein and the assembly of the whole complex. All four SGs possess putative phosphorylation sites in the intracellular domain, indicating a possible post-translational modulation of the protein or complex (Chen et al., 2006).

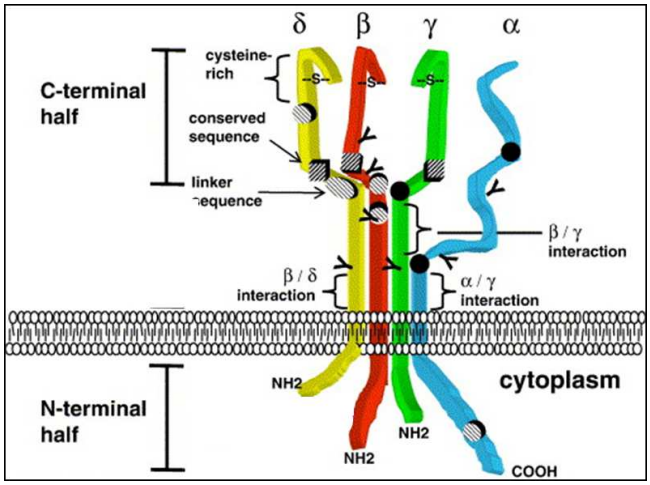

adapted from Chen et al., 2006

Fig 5. Structure of the SG complex. α-SG is a type I transmembrane protein, while the other SGs are type II transmembrane proteins. Intra-molecular disulphide bridge and N-linked glycosylation site are represented by "-S-" and "Y", respectively. Region adjacent to the transmembrane domains are essential for the β/δ-SG and α/γ-SG interaction, whereas the regions distal to the transmembrane domains are important for the β/γ-SG interaction. The C-terminal of β-, δ- and γ-SG form a specific structure consisting of the cysteine-rich motif.

α-Sarcoglycan

α-SG was the first discovered SG and the gene product (*SGCA*) was initially termed adhalin (''*adhal*'', muscle in arabic). After the identification of the other SG subunits and their association as a complex, the subunit was renamed α-SG. α-SG is the most different among SGs from several points of view:

- is not readily cross-linked to other SGs
- is the only SG that, as type I transmembrane protein, displays an amino-terminal extracellular domain with a signal sequence
- an extracellular cysteine cluster is present close to the membrane-spanning domain,

whereas those of the other SGs are located around the C-terminus

- it has a cadherin-like domain (as its homologue ε-SG), supposed to be involved in protein–protein interactions
- it was identified an ATP binding site and an ATPase activity which may serve to modulate the extracellular ATP concentration at the surface of the muscle (Sandonà et al., 2004)

In 1997 the Engvall group discovered another SG protein called ε-SG that showed 47% homology to α-SG at the nucleotide level, and 62% similar at the amino acid one (43% identical). *SGCE* and *SGCA* genes appear to originate from a common ancestor by gene duplication since the gene structure is highly similar. Even if expressed in striated muscle in early development, ε-SG level decreases with the increase in α-SG level, which occurs with the progress in developmental stage. Indeed, in adult tissues ε-SG is primarily localized in non-striated muscle (Liu and Engvall, 1999).

β-, γ-, δ-, sarcoglycans

β-, γ-, δ-SGs are strictly close type II proteins, characterized by:

- nearly identical extracellular C-terminal domains in length (225 amino acids, 224 amino acids, and 224 amino acids, respectively for β-, γ-, δ-SGs). The C-ter includes a cluster of conserved cysteines, in a fixed position, like that of cysteine-containing EGF-like proteins, involved in intramolecular disulphide bonds. Mutations in the cysteine residues are critical and linked to a severe muscular dystrophy (Tarakci and Berger, 2016)
- N-linked glycosylation sites are located in the extracellular domain
- γ-SG and δ-SG, unlike β-SG, share a homology in the whole structure (55% amino acid identity and 70% similarity) and not only in the C-terminal domain. Indeed, initial biochemical characterization did not distinguish the two genes, that probably arisen from a gene duplication event (Yoshida et al., 1994; Nigro et al., 1996B).
- δ- and β-SG are tightly associated since they form the functional core for the assembly of the SG complex (Draviam et al., 2006)

ζ-SG is another type II protein and considering its high homology to γ- and δ-SG (respectively: 72% and 74% similarity; 56% and 57% identities) it was probably originated by gene duplication.

GENE	GENE LOCATION	PROTEIN	TYPE OF TRANSMEMBRANE PROTEIN	EXPRESSION PATTERN	SIZE	N-Gly	Cys	HOMOLOGY	DISEASE
SGCA	17q21	α-SG	type I	striated muscle	50	2	5	ε-SG	LGMD2D
SGCB	4q21	β-SG	type II	striated muscle	43	3	5	γ-, δ-SG (week)	LGMD2E
SGCG	13q21	γ-SG	type II	striated muscle	35	1	4	δ-SG	LGMD2C
SGCD	5q21	δ-SG	type II	striated and smooth muscles	35	3	4	γ-SG	LGMD2F
SGCE	7q21	ε-SG	type I	widely express (high in embryo)	50	1	4	α-SG	myoclonus -dystonia syndrome
SGCZ	8p22	ζ-SG	type II	brain	35	1	4	γ-, δ-SG (strong)	-

Table 1. Features of SGs. The table reports the main feature of SGs. The gene encoding for each SG as well as the gene location are reported. Protein features are also highlight. α and ε- SGs are homologous type I transmembrane proteins, while β-, γ-, δ-SGs are related type II transmembrane proteins with homology in their extracellular carboxyl-termini. Finally, the correlated disease for each SG is reported.

1.1.3 SG complex biogenesis and assembly

The SGs biogenesis occurs in ER where the chain emerges in an unfolded state and undergoes covalent modifications such as N-linked glycosylation and disulphide-bond formation, by the activity of a large array of ER-resident chaperones and enzymes. In detail, the N-glycan, composed by three molecules of glucose, nine of mannose, and two of N-acetilglucosamine is of fundamental importance to binds calnexin (CNX), an integral membrane lectin chaperon, and its luminal paralogue calreticulin (CRT). CNX/CRT recruits several factors to assist the folding of SGs such as: Bip, a chaperon that protects nascent polypeptide from aggregation in the crowded ER environment, and protein disulphide isomerase (PDI) which catalyses disulphide bound formation. Once the SG protein reaches the native conformation, the removal of glucide residues from N-glycan allows the release of the protein from the CNX/CRT cycle.

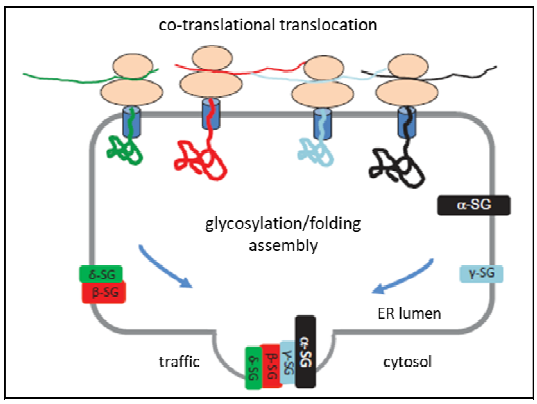

Carotti et al., 2017

Fig 6. SG complex biogeneis. SGs are co-traslationally traslocated into the ER lumen where, after glycosilation, they can be properly folded. The complex can be therefore assembled starting with the β-δ-SG core formation. γ- and α-SGs are then added. When the full tetramer is assembled, it moves toward the sarcolemma to interact with the DAPC.

Correctly folded SGs can now assemble to form the tetrameric complex.

The assembly takes place following a specific pathway and it is a prerequisite for the successful delivery to the plasma membrane (Shi et al., 2004). The first step is represented by the core complex formation, constituted by β- and δ- SG subunits (Draviam et al., 2006). After core formation, γ-SG is added, forming a tightly associated trimer. Cysteine residues of γ-, β-, δ-SGs most likely mediate this linkage through disulphide bound formations. At the final stage, α-SG associates, although in a less tight manner. Therefore, γ-SG acts as a linker to connect α-SG to the β- and δ- SG core.

Once the tetrameric complex is assembled, it moves toward the sarcolemma to interact with the other DAPC components. In detail, it associates with the DG complex and sarcospan *en route* through vesicular transport along microtubule networks from the Golgi apparatus to the cell surface, where the complex is finally anchored (Noguchi et al., 2000).

These data provide support to the assumption that the SG complex behaves as a single unit, in biosynthesis as well as in biochemical analyses and pathogenicity.

Considering this tight assembly, it is possible to understand why a defect in a single subunit results in the loss or marked decrease of the whole complex.

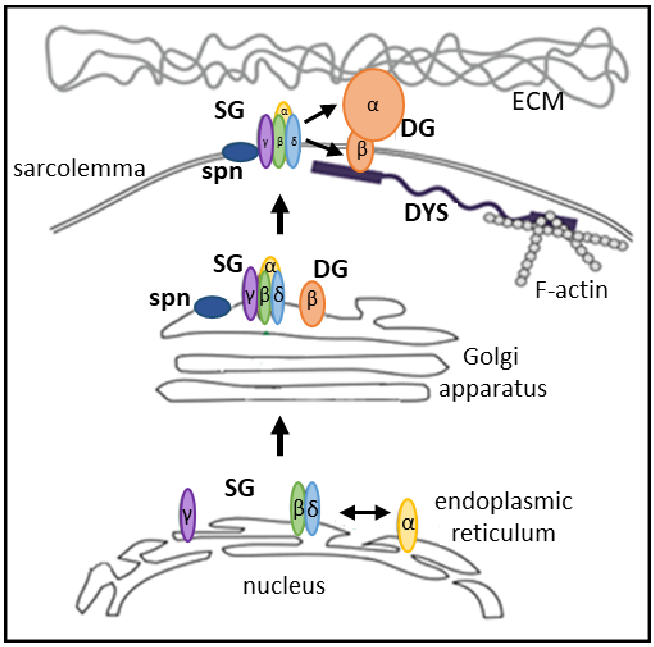

adapted from Hack et al., 2000

Fig 7. SG complex assembly and delivery to the sarcolemma. The SG complex assembly starts with the establishment of a β- and δ-SG core with which γ-SG and α-SG subsequently interact to form the tetramer. Once assembled, the SG complex leaves the ER and, passing through the Golgi apparatus, moves towards the sarcolemma, where interacts with DAPC.

1.1.4. SG role

As located in close proximity and interacting with dys and DG, SGs may couple mechanical and signalling functions in striated muscle (Tarakci and Berger, 2016).

Although the SG complex has not been shown to participate directly in the transmembrane linkage of DAPC, the tightly associated tetrameric complex stabilizes the DAPC on the muscle membrane. This facilitates the interactions between cytoskeleton and the ECM to reinforce sarcolemma from tension produced by contractile activity. This mechanical function is also confirmed by the disorganisation of fibres observable in the absence of SGs expression on the sarcolemma.

Moreover, other functions of SGs are under investigation. For example, the presence of EGF-like repeats, characteristic of some receptors, in β-, γ-, δ-SGs suggests that these particularly strong associated SGs may work as a membrane receptor for a still unidentified ligand, whose position is determined by dys but whose function is carried out also independently from the dys-DG-laminin axis.

Notably, it has been demonstrated that the cytoplasmic tail of SGs becomes phosphorylated after mechanical stimulation, suggesting a role as signalling sensor of contractility (Barton et al., 2006).

Moreover, it was demonstrated that α-SG is a Ca^{2+} Mg^{2+}-dependent ecto-ATPase enzyme. Through the ATP-hydrolysing activity, it could have a role in modulating the extracellular ATP concentration. Therefore, α-SG may represent the catalytic subunit of the of SG complex (Sandonà et al., 2004).

Therefore, although α-β-γ-δ SGs are part of the same complex, the individual SGs may exhibit different functional roles.

1.2 Perturbation of the DAPC causes muscular dystrophy (MD)

After the identification of dys, 30 years ago, as the gene causative of Duchenne and Becker muscular dystrophy (DMD/BMD), a new era began, in which thousands of publications reported the involvement of many proteins in MD.

MD are a group of more than 30 inherited and debilitating disorders characterized by progressive wasting and atrophy of skeletal muscles. The different consequences can span from the loss of ambulance to a dramatic and fatal course due to cardiac and/or respiratory failure (Nigro and Piluso 2015; Shin et al., 2013)

The primary cause for various forms of MD is the mutation in individual genes encoding a number of proteins, including extracellular matrix-, transmembrane- and membrane-associated proteins, cytoplasmic enzymes, and nuclear matrix proteins (Davies and Nowak, 2006). Although these defects can result in different secondary problems/changes, because of the multiple molecular processes that involve the specific proteins, the consequence is generally the generation of an unfavourable environment for muscle regeneration and the promotion of muscle wasting, until the development of the dystrophic phenotype.

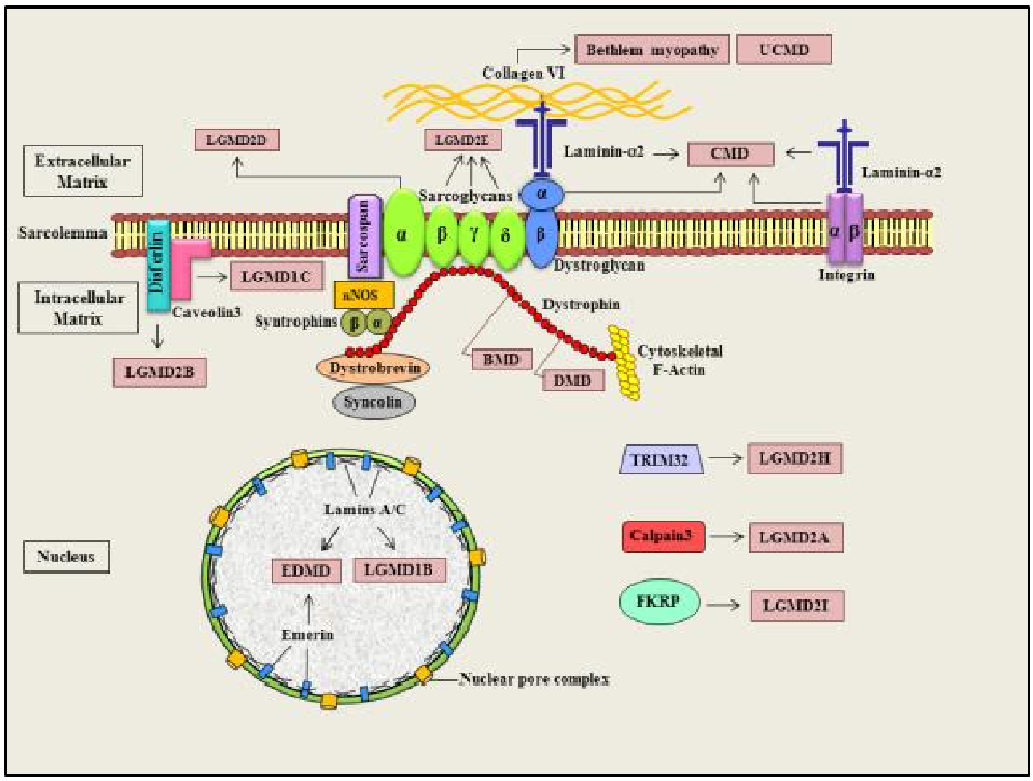

Shin et al., 2013

Fig 8. Schematic representation of various proteins associated with MD. A plethora of MD together with the underlying genetic defects is nowadays known. (BMD, Baker muscular dystrophy; CMD, congenital muscular dystrophy; DMD, Duchenne muscular dystrophy; EDMD, Emery–Dreifuss muscular dystrophy; FKRP, fukutin-related protein; LGMD, limb girdle muscular dystrophy; nNOS, neuronal nitric oxide synthase; TRIM, tripartite motif proteins; UCMD, Ullrich congenital muscular dystrophy).

Despite the heterogeneity of MD, in term of genetic inheritance, clinical onset, and additional non-muscular phenotypes some manifestations remain in common such as:

- infiltration of skeletal muscle by inflammatory cells (macrophages, T cells, neutrophils, mast cell, eosinophils). Inflammation precedes the onset of the disease and persists through later stages (Tidball, 2005).
- alteration in the fluxes of ions and proteins due to focal lesion of the sarcolemma, such as sub-sarcolemmal influx of calcium and loss of creatine kinase (CK). The alteration in the fluxes of ions compromises muscle homeostasis and the activation of various signalling pathways (Culligan and Ohlendieck, 2002).
- Increase of oxidative stress, with ROS production that can damage membrane lipids, structural and regulatory proteins, and DNA (Moylan and Reid, 2007)
- mitochondrial dysfunction since reduction of mitochondrial mass and number, dysregulation of the mitochondrial permeability transition pore opening and defective respiratory chain activities are common features for several MD (Kelly-Worden and Thomas, 2014)
- substitution of contractile tissue with the fibrotic one, and the consequent loss of functional contraction activity (Burks and Cohn, 2011).
- increase of myofibres death, primarily caused by necrosis and secondarily by apoptosis that is exacerbated by physical exercise (Davies and Nowak, 2006).
- impairment of autophagy with concomitant accumulation of damaged organelles (DePalma et al., 2012)
- failure of the regenerative capacity of muscle, as the pool of endogenous satellite cells comes to end, after repeated cycles of regeneration trying to repair the damaged muscle fibres (Shin et al, 2013)
- increase in matrix-metal-proteases (MMP) observed at later stages of the disease progression, that contributes to the sarcolemma (McCaw et al., 2007)

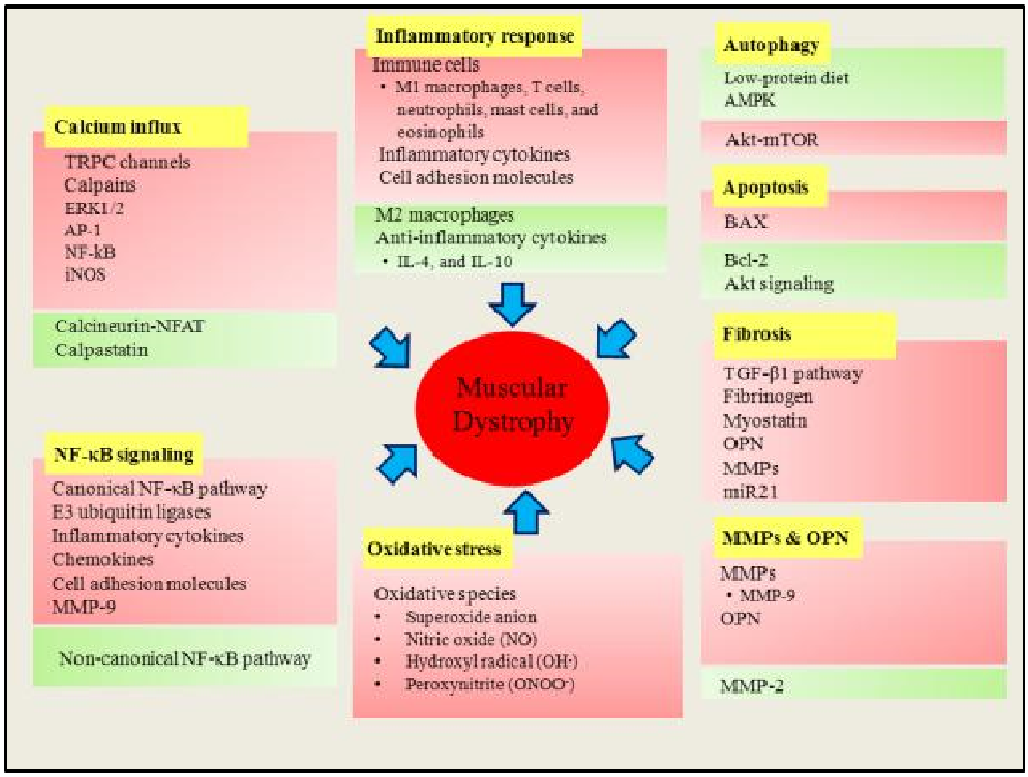

Shin et al., 2013

Fig 9. Mechanisms of muscle wasting in MD. Major molecular processes involved in the pathogenesis of MD are reported (in yellow boxes). Activators or mediators of pathological responses of these processes have been depicted in red boxes. In green boxes are reported some components of each pathway that could improve the dystrophic phenotype

It appears difficult to classify MDs because of the frequent appearance of *de novo* mutations, the intra-familial clinical variability and the problematic correlation of phenotype with genotype (Mathews and Moore, 2003). Nevertheless, according to the pattern of inheritance, MD can be classified as:

- X-linked recessive, as the most worldwide prevalent muscular dystrophy, DMD/BMD
- autosomal dominant as the limb–girdle muscular dystrophy type 1 (AD-LGMD or LGMD1)
- autosomal recessive as the limb–girdle muscular dystrophy type 2 (AR-LGMD or LGMD2)

1.2.1 Limb Girdle muscular dystrophies LGMD

LGMD are a family of heterogeneous disorders, so called because primarily characterized by the involvement of the proximal musculature of the pelvic and shoulder girdle, including sarcoglycanopathy (Guglieri et al., 2008; Nigro and Savarese, 2014).

LGMD are different from the X-linked DMD/BMD as they affect both males and females and show both autosomal dominant (LGMD1) and autosomal recessive (LGMD2) inheritance. Among the LGMD2 sarcoglycanopathy are referred as LGMD2C-F.

The clinical course may be variable, ranging from severe forms with rapid onset and progression, characterized by a Duchenne-like muscular phenotype, to very mild forms allowing affected people to have an almost normal life span and activity (Nigro et al., 2011).

The ongoing classification of LGMDs, reported in the tables below, is based on the involved proteins and the underlying genetic defects.

Gene					Clinical phenotype				
Disease	Locus	Name	Exons	Protein (protein function)	Typical onset	Progression	Cardiomiopathy	sCK	Allelic disorders (OMIM, #)
LGMD1A	5q31.2	TTID	10	myotilin (structural; Z disc)	Adulthood	Slow	Not observed	3-4X	Myopathy, myofibrillar, 3 (609200)
									Myopathy, spheroid body (182920)
LGMD1B	1q22	LMNA	12	lamin A/C (structural; fibrous nuclear lamina)	Variable (4-38y)	Slow	Frequent	1-6X	Cardiomyopathy, dilated, 1A(115200)
									Charcot-Marie-Tooth disease, type 2B1(605588)
									Emery-Dreifuss muscular dystrophy 2, AD(181350)
									Emery-Dreifuss muscular dystrophy 3, AR(181350)
									Heart-hand syndrome, Slovenian type(610140)
									Hutchinson-Gilford progeria(176670)
									Lipodystrophy, familial partial, 2(151660)
									Malouf syndrome(212112)
									Mandibuloacral dysplasia(248370)
									Muscular dystrophy, congenital(613205)
									Restrictive dermopathy, lethal(275210)
LGMD1C	3p25.3	CAV3	2	caveolin 3 (scaffolding protein within caveolar membranes)	Childhood	Slow/ moderate	Frequent	10X	Cardiomyopathy, familial hypertrophic(192600)
									Creatine phosphokinase, elevated serum(123320)
									Long QT syndrome 9(611818)
									Myopathy, distal, Tateyama type(614321)
									Rippling muscle disease(606072)
LGMD1D	7q36	DNAJB6	10	DnaJ/Hsp40 homolog, subfamily B, member 6 (chaperone)	Variable (25-50y)	Slow	Not observed	1-10X	-
LGMD1E	2q35	DES	9	desmin (structural; intermediate filament)	Adulthood	Slow	Frequent	5-10X	Muscular dystrophy, limb-girdle, type 2R(615325)
									Cardiomyopathy, dilated, 1I(604765)
									Myopathy, myofibrillar, 1(601419)
									Scapuloperoneal syndrome, neurogenic, Kaeser type(181400)
LGMD1F	7q32	TNPO3	23	transportin 3 (nuclear importin)	Variable (1-58y)	Slow/ moderate	Not observed	1-3X	-
LGMD1G	4q21	HNRPDL	9	Heterogeneous nuclear ribonucleoprotein D-like protein (ribonucleoprotein, RNA-processing pathways)	Variable (13-53y)	Slow	Not observed	1-9X	-
LGMD1H	3p23-p25	-	-	-	Variable (10-50y)	Slow	Not observed	1-10X	-

Nigro and Savarese, 2014

Table 2. The autosomal dominant forms of LGMD (LGMD1). Usually, LGMD1 have an adult-onset and are mild diseases, indeed affected parents are usually in quite good health at reproductive age. They are relatively rare representing less than 10% of all LGMD.

Gene					Clinical phenotype					
Disease	Locus	Name	Exons	Protein product	LGMD phenotype	Typical onset	Progression	Cardiomiopathy	sCK	Allelic disorders (OMIM, #)
LGMD2A	15q15	CAPN3	24	Calpain 3	ordinary	Adolescence	Moderate/ rapid	Rarely observed	3-20X	
LGMD2B	2p13.2	DYSF	56	Dysferlin	ordinary	Young adulthood	Slow	Possible	5-40X	Miyoshi muscular dystrophy 1 (254130) Myopathy, distal, with anterior tibial onset (606768)
LGMD2C	13q12	SGCG	8	γ-Sarcoglycan	ordinary	Early childhood	Rapid	Often severe	10–70X	
LGMD2D	17q21.33	SGCA	10	α-Sarcoglycan	ordinary	Early childhood	Rapid	Often severe	10–70X	
LGMD2E	4q12	SGCB	6	β-Sarcoglycan	ordinary	Early childhood	Rapid	Often severe	10–70X	
LGMD2F	5q33	SGCD	9	δ-Sarcoglycan	ordinary	Early childhood	Rapid	Rarely observed	10–70X	Cardiomyopathy, dilated, 1L (606685)
LGMD2G	17q12	TCAP	2	Telethonin	ordinary	Adolescence	Slow	Possible	10X	Cardiomyopathy, dilated, 1N (607487)
LGMD2H	9q33.1	TRIM32	2	Tripartite motif containing 32	ordinary	Adulthood	Slow	Not observed	10X	Bardet-Biedl syndrome 11 (209900)
LGMD2I	19q13.3	FKRP	4	Fukutin related protein	ordinary	Late childhood	Moderate	Possible	10-20X	
LGMD2J	2q24.3	TTN	312 or more	Titin	occasional	Young adulthood	Severe	Not observed	10-40X	Cardiomyopathy, dilated, 1G (604145) Cardiomyopathy, familial hypertrophic, 9 (613765) Myopathy, early-onset, with fatal cardiomyopathy (611705) Myopathy, proximal, with early respiratory muscle involvement (603689) Tibial muscular dystrophy, tardive (600334)
LGMD2K	9q34.1	POMT1	20	Protein-O-mannosyl transferase 1	occasional	Childhood	Slow	Not observed	10-40X	Muscular dystrophy-dystroglycanopathy (congenital with brain and eye anomalies), type A, 1 (236670) Muscular dystrophy-dystroglycanopathy (congenital with mental retardation), type B, 1 (613155) Muscular dystrophy-dystroglycanopathy (limb-girdle), type C, 1 (609308)
LGMD2L	11p13-p12	ANO5	22	Anoctamin 5	ordinary	Variable (young to late adulthood)	Slow	Not observed	1-15X	Gnathodiaphyseal dysplasia (166260) Miyoshi muscular dystrophy 3 (613319)
LGMD2M	9q31	FKTN	11	Fukutin	occasional	Early childhood	Moderate	Possible	10-70X	Cardiomyopathy, dilated, 1X (611615) Muscular dystrophy-dystroglycanopathy (congenital with brain and eye anomalies), type A, 4 (253800) Muscular dystrophy-dystroglycanopathy (congenital without mental retardation), type B, 4 (613152)

(*continues*)

Gene					Clinical phenotype					
Disease	Locus	Name	Exons	Protein product	LGMD phenotype	Typical onset	Progression	Cardiomiopathy	sCK	Allelic disorders (OMIM, #)
LGMD2N	14q24	POMT2	21	Protein-O-mannosyl transferase 2	occasional	Early childhood	Slow	Rarely observed	5-15X	Muscular dystrophy-dystroglycanopathy (congenital with brain and eye anomalies), type A, 2 (613150) Muscular dystrophy-dystroglycanopathy (congenital with mental retardation), type B, 2 (613156)
LGMD2O	1p34.1	POMGnT1	22	Protein O-linked mannose beta1,2-N-acetylglucosaminyl transferase	occasional	Late childhood	Moderate	Not observed	2-10X	Muscular dystrophy-dystroglycanopathy (congenital with brain and eye anomalies), type A, 3 (253280) Muscular dystrophy-dystroglycanopathy (congenital with mental retardation), type B, 3 (613151) Muscular dystrophy-dystroglycanopathy (limb-girdle), type C, 3 (613157)
LGMD2P	3p21	DAG1	3	Dystroglycan	singular	Early childhood	Moderate	Not observed	20X	
LGMD2Q	8q24	PLEC1	32	Plectin	singular	Early childhood	Slow	Not observed	10-50X	Epidermolysis bullosa simplex with pyloric atresia (612138) Epidermolysis bullosa simplex, Ogna type (131950) Muscular dystrophy with epidermolysis bullosa simplex (226670)
LGMD2R	2q35	DES	9	Desmin (structural; intermediate filament)	occasional	Young adulthood		A-V conduction block	1X	Muscular dystrophy, limb-girdle, type 2R(615325) Cardiomyopathy, dilated, 1I(604765) Myopathy, myofibrillar, 1(601419) Scapuloperoneal syndrome, neurogenic, Kaeser type(181400)
LGMD2S	4q35	TRAPPC11	30	Transport protein particle complex 11	occasional	Young adulthood	Slow	Not observed	9-16X	
LGMD2T	3p21	GMPPB	8	GDP-mannose pyrophosphorylase B	occasional	Early childhood-Young adulthood		Possible		Muscular dystrophy-dystroglycanopathy (congenital with brain and eye anomalies), type A, 14 (615350) Muscular dystrophy-dystroglycanopathy (congenital with mental retardation), type B, 14 (615351)
LGMD2U	7p21	ISPD	10	Isoprenoid synthase domain containing	occasional	Early / Late	Rapid/ Moderate	Possible	6-50X	Muscular dystrophy-dystroglycanopathy (congenital with brain and eye anomalies), type A, 7 (614643)
LGMD2V	17q25.3	GAA	20	Alpha-1,4-glucosidase	occasional	Variable	Variable (Rapid to slow)	Possible	1-20X	Glycogen storage disease II (232300)
LGMD2W	2q14	LIMS2	7	Lim and senescent cell antigen-like domains 2	?	Childhood	-	Possible	-	

Nigro and Savarese, 2014

Table 3. The autosomal recessive forms LGMD (LGMD2). LGMD2 are much more common than LGMD1. The frequent early onset and progression is correlated with a more severe phenotype.

1.2.2 Sarcoglycanopathies (or LGMD2D-F) and sarcoglycan mutations

Among LGMD2 are four distinct MD subtypes, collectively called sarcoglycanopathy, which are characterized by the loss or strong reduction of SGs at the sarcolemma (Hack et al., 2000; Carotti et al., 2017). Since the second half of the 20th century, sarcoglycanopathies were described as severe disease, clinically similar to DMD, with early-onset and rarely with milder forms showing adolescence- or adulthood-onset. They were originally called autosomal recessive Duchenne-like muscular dystrophy (ARDMD) or severe childhood autosomal recessive muscular dystrophy (SCARDM) (Kloepfer and Talley, 1958). From 1994, when the causative genes were identified the four subtypes were renamed as:

- α-sarcoglycanopathy (LGMD2D) caused by loss-of-function mutations on *SGCA* gene (Roberds et al., 1994)
- β-sarcoglycanopathy (LGMD2E) caused by loss-of-function mutations on *SGCB* gene (Bönnemann et al., 1995; Lim et al., 1995)
- γ-sarcoglycanopathy caused by loss-of-function mutations on *SGCG* gene (LGMD2C) (Noguchi et al., 1995)
- δ-sarcoglycanopathy (LGMD2F) caused by loss-of-function mutations on *SGCD* gene (Nigro et al.,1996A)

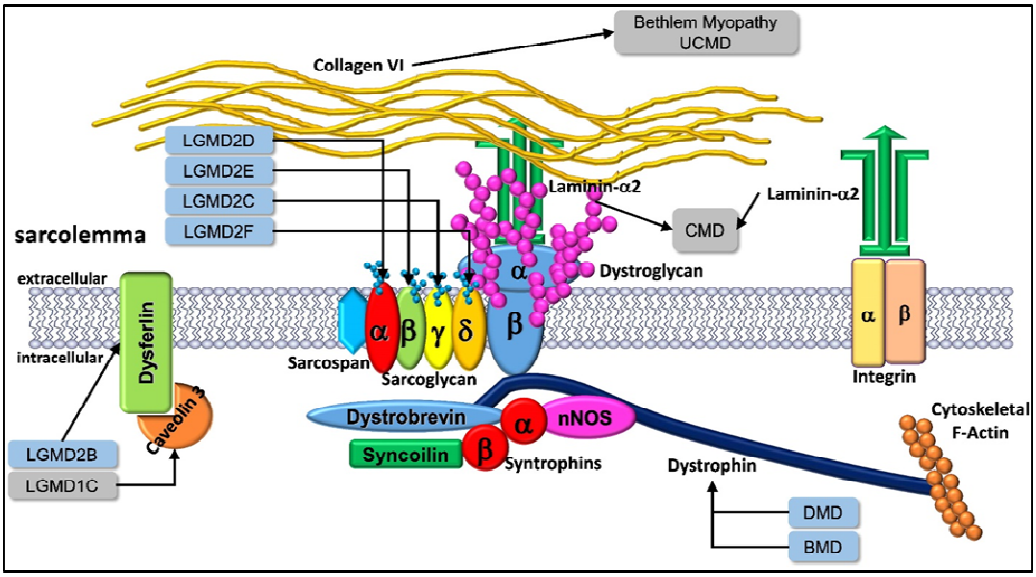

Nigro and Piluso, 2015

Fig 10. Schematic model of SGs in DAPC and LGMD2D-2F. The arrows indicate the involvement of each SG proteins in LGMD. The MD associated to mutations in any component of the DAPC are also reported.

The frequency of sarcoglycanopathy is difficult to evaluate also because related to ethnic clusters and geographic origins of the affected subject. However, it represents 10-20% of all MD cases with normal dys (Fanin et al., 2009; Nigro et al., 2003). In detail, LGMD2D is the most frequently reported, followed by LGMD2C and LGMD2E, with the rarest being LGMD2F.

The clinical profile of sarcoglycanopathy is heterogeneous with both severe and mild forms, even between siblings (Angelini et al., 1998). Mild phenotypes, characterized by late onset and preserved ambulation until adulthood, have been described (Carotti et al., 2017).

However, the clinical picture is usually more severe and rapid than in other LGMD, and more similar to that of DMD patients (Sandonà and Betto, 2009). The disease interferes with the patient's daily functions, rapidly and profoundly reducing the quality of life. Indeed, the progressive proximal muscle weakness compromises the ambulatory capacity, and in the worst cases, patients are wheelchair bound since the adolescence. Moreover, cardiac and respiratory worsening can be fatal if not continuously monitored. Patients can suffer of restrictive ventilatory syndrome therefore needing for respiratory support, and/or dilated cardiomyopathy that requires a concomitant cardiac therapy (Politano et al., 2001; Fanin et al., 2003). Other typical traits are calf hypertrophy, scapular winging, contractures, scoliosis, and increased serum CK (more than 10 times the upper limit).

The most common diagnostic process to identify a LGMD2C-F patient is the immunohistochemical evaluation of the primary defect of the disease. Considering that the diagnosis remains elusive in about 30% of patients, others investigation should be considered, such as: the pattern of muscle involved, the CK level, the family history, and any additional clinical feature (Mercuri et al., 2007 Fisher et al., 2005). However, considering that the protein deficiency could be a secondary effect, the genetic analysis is needed to solve possible confusion in diagnosis (Norwood et al., 2007).

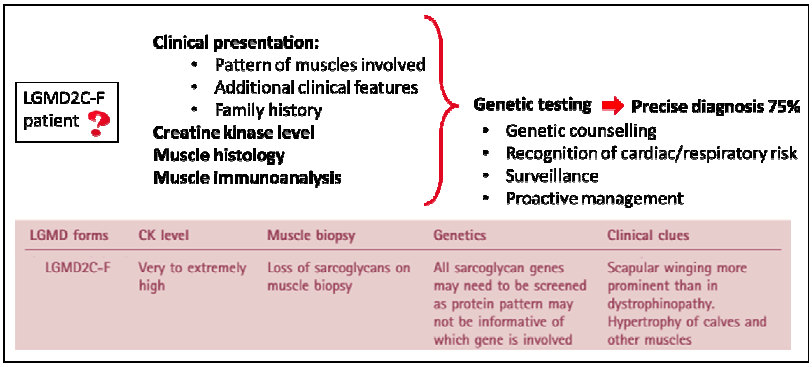

LGMD forms	CK level	Muscle biopsy	Genetics	Clinical clues
LGMD2C-F	Very to extremely high	Loss of sarcoglycans on muscle biopsy	All sarcoglycan genes may need to be screened as protein pattern may not be informative of which gene is involved	Scapular winging more prominent than in dystrophinopathy. Hypertrophy of calves and other muscles

adapted from Bushby, 2009

Fig 11. Steps performed in the LGMD2C-F diagnosis. The different steps needed to diagnose sarcoglycanopathy are represented above. First, the analysis of muscle damage, evaluated with both muscle histology and the increased release of CK, a marker of MD is performed. Then the immunohistochemical analysis highlights the lack of protein that is confirmed by genetic analysis. In the table at the bottom, the typical features of the mentioned investigations for sarcoglycanopathy are reported.

Mutation in any SG gene results in either the loss or strong reduction of the mutated SG and the WT partners as showed in the figure below (12) where the immunofluorescence analysis of patient muscle biopsies is reported. The absence of the mutated SG alters/destroys the association of the other SGs and causes the loss/strong reduction of the whole complex. This alters the structural properties of sarcolemma leading to the progressive muscle degeneration consequent to the loss of function. This finding also suggests that all SGs are required to maintain the integrity of the complex (Carotti et al., 2017).

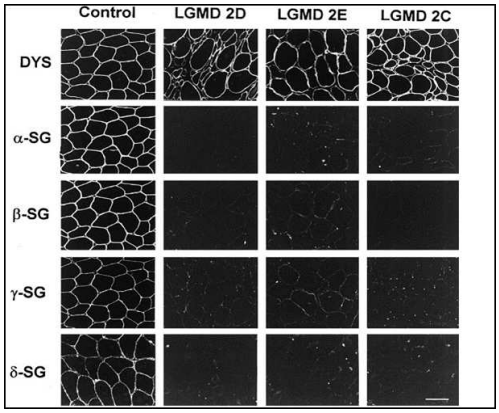

Jung et al., 1996

Fig 12. Immunohistochemical analysis of skeletal muscle biopsies from sarcoglycanopathy patients. Immunostaining of muscle biopsies from LGMD patients suggest that a mutation in any SG produced instability of the remaining WT SG, while dys is less affected.

There is considerable variability in the severity of phenotype associated with SG mutations. This probably depends on:

- the type of mutation. Nonsense and frameshift mutations, as well as those affecting the glycosylation status, seem to have a major impact on the SG complex and, therefore, a more severe clinical outcome (Sandonà and Betto, 2009)
- the quantity of residual protein present. A milder form occurs if traces of SG subunits remain on the cell membrane. Not all SGs are equally destabilized by a mutation. When mutations occur on *SGCA* or *SGCG, r*esidual traces of SGs can be present and limited or no consequence for the DAPC are found (Vainzof et al., 2000; Draviam et al., 2006). On the other hand, *SGCB* and *SGCD* mutations result in the absence of the four SGs from the plasma membrane, as well as in the reduction of dys and DG (Klinge et al., 2008).

However, it must be underlined that exceptions to these generalizations exist. Therefore, a strict correlation between the genotype and the phenotype may be difficult to find. Indeed, some of the SG subunits can be detected on the sarcolemma in some cases of sarcoglycanopathy, meaning that the complete complex formation is not a strict prerequisite for their transport out of the ER.
All known pathogenic variations in SG genes are listed in the Leiden database (http://www.dmd.nl). Mutations can hamper the protein production (no SG synthesis), produce truncated SGs (premature stop codon), or generate a full-length protein with in frame deletions or single amino acid substitutions (missense mutations).

				% of different mutations				
Disease	Gene	Protein	Length (aa)	Null	Frame shift	Missense	In-frame deletion, insertion & duplication	N. different variants
LGMD2D	*SGCA*	α-SG	387	7.1	23.8	65.5	3	84
LGMD2E	*SGCB*	β-SG	318	13.7	25.5	56.9	4	51
LGMD2C	*SGCG*	γ-SG	291	14.5	30.8	40	14.5	55
LGMD2F	*SGCD*	δ-SG	290	21.4	7.1	57.2	14.3	14

Carotti et al., 2017

Table 4. Different protein variants in sarcoglycanopathy. The table reports for each SG gene the percentage of null-, frame shift-, missense-mutation; in-frame deletion, insertion and duplications that are reported for sarcoglycanopathy according to Leiden database (http://www.lovd.org).

The majority of reported cases of sarcoglycanopathy are due to missense mutations.
At least 55, 29, 22, and 8 different missense mutations have been reported in *SGCA*, *SGCB*, *SGCG*, and *SGCD* genes, respectively. The most frequently reported α-SG amino acid substitution is R77C, accounting for more than one-third of cases, followed by R284C and V247M. Of the 29-different known β-SG variants, the S114F amino acid substitution accounts for approximately 45% of all LGMD2E cases. Similarly, the mutation C283Y in γ-SG is responsible for half of all reported LGMD2C cases. Only eight different amino acid substitutions are known for δ-SG, with two variants (A31P and R97N) together accounting for more than half the reported cases of LGMD2F.

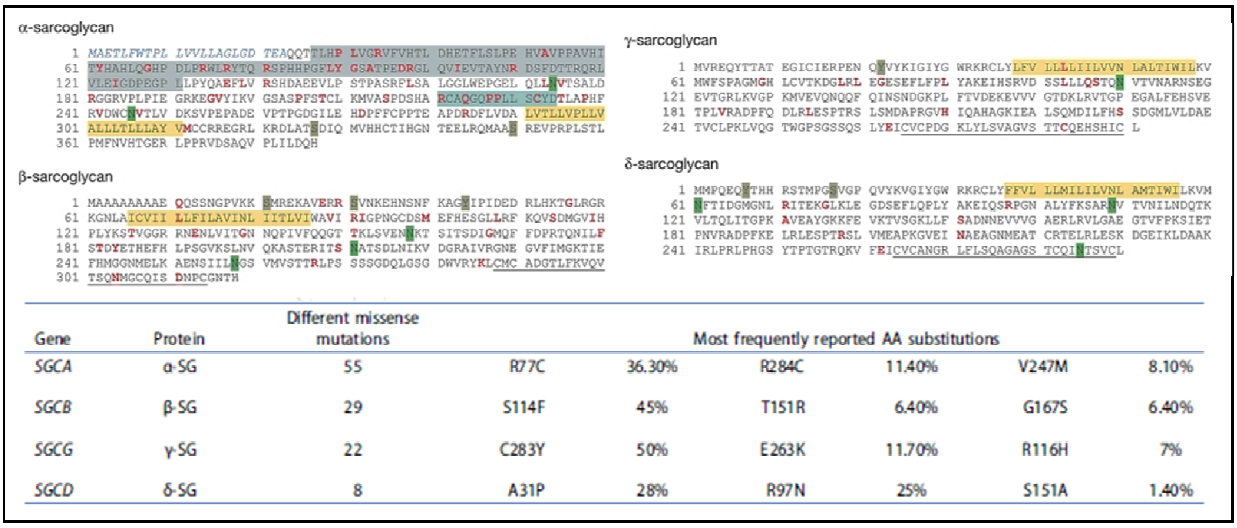

Gene	Protein	Different missense mutations	Most frequently reported AA substitutions					
SGCA	α-SG	55	R77C	36.30%	R284C	11.40%	V247M	8.10%
SGCB	β-SG	29	S114F	45%	T151R	6.40%	G167S	6.40%
SGCG	γ-SG	22	C283Y	50%	E263K	11.70%	R116H	7%
SGCD	δ-SG	8	A31P	28%	R97N	25%	S151A	1.40%

adapted from Sandonà and Betto, 2009 and Carotti et al., 2017

Table 5. Missense mutations in SG. In the top of the panel are reported the amino acid sequence of α-, β-, γ- and δ-SG with all missense mutations responsible for LGMD indicated in red, according to the Leiden database (http://www.lovd.org). In yellow is highlighted the transmembrane domain, in green the putative N-linked glycosylation sites, and in dark green the predicted phosphorylation sites. In α-SG the signal sequence at N-terminus is indicated in italics, the cadherin-like domain is highlighted in grey, whereas the putative ATP-binding site is shown in light blue. In β-, γ- and δ- SG, the putative EGF-like sequence is underlined. The table at the bottom reports also the three most frequent amino acid substitutions for each gene, responsible for LGMD2C-F.

1.2.2.1 Pathogenic mechanism of sarcoglycanopathies

The absence of the protein from muscles of LGMD2C-F patients can be easily explained in the case of a mutation that hampers the protein production or produce truncated SGs. On the contrary, the almost complete loss of the protein in consequence of a single missense mutation is less obvious. Indeed, the fate of such a protein may depend on the QC system supervision, that may recognize the mutated polypeptide as defective and may send it to degradation or may allow its maturation and delivery to the final destination.
Being SGs, membrane glycosylated proteins, this process is carefully monitored in ER. In the ER, WT-SGs undergo folding, glycosylation and maturation, while mutated SGs are recognized as folding defective and become substrates of the ER associated degradation (ERAD).

In detail, if the native form is not achieved after the first round of folding in the CNX/CRT cycle, the folding-sensor UDP-glucose glycosil transeferase 1 (UGGT1) recognizes the unfolded SG and promote additional rounds of folding. However, if the cycles are unproductive, an extensive de-mannosilation of the N-glycan operated by ER-resident mannosidase prevents the action of UGGT1, making the unfolded protein substrate of ERAD (Sandonà and Betto, 2009).

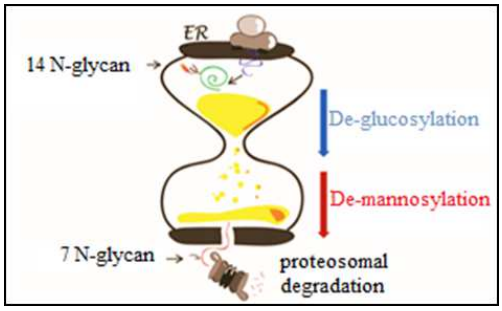

adapted from Pisoni and Molinari, 2016

Fig 13. The hourglass model for timing glycoprotein fate. The removal of glucose residues on the N-glycan, operated by glucosidases promote the entry of SGs into the CNX/CRT cycle. While the extensive de-mannosylation operated by mannosidase stops the folding process and triggers ERAD pathway.

To be degraded, the terminally misfolded SGs must reach the cytosolic multi-protein complex called proteasome. The spatial separation between substrate selection (ER lumen) and degradation (cytosol) requires substrate retro-translocation through the ER lipid bilayer into the cytosol, a process termed dislocation. Chaperons and lectins such as Bip, GRP94 and Os9, target the misfolded protein for dislocation that occurs thanks to a large supramolecular complex integrated in the ER membrane, the dislocons (Sandonà and Betto, 2009). SGs dislocation occurs through the SEL1-HRD1 complex, which also include SEC61, the actual channel. During retro-translocation, a poly-ubiquitin chain (pUb), used as a mark for degradation, is added on lysine residues of misfolded SGs by the coordinated activity of cytosolic and membrane associated E1, E2, E3 ligases (Carotti et al,. 2017). Among the E3 ligases, that differs for substrate specificity, needed to deal with the wide range of protein topologies, HRD1 is one of the main enzyme responsible for the ubiquitination of misfolded SGs. During this process, the SG marked for degradation, can be expelled from ER. Additional elements, belonging to the dislocon, play essential roles in the retrotranslocation process. For example, the p97 ATPase provides the energy and derlin helps the eradication of the pUb-SG from the lipid bilayer allowing the delivery to the proteasome. After retro-translocation, to enter the narrow chambers of the proteasome, the cytosolic enzyme N-glycanase (PNGase) removes the residual N-glycan while the deubiquitinating enzymes (DUBs) remove the pUb chains. Finally, the terminally misfolded SG enters the 20S proteasome catalytic core where it is processed into small fragments.

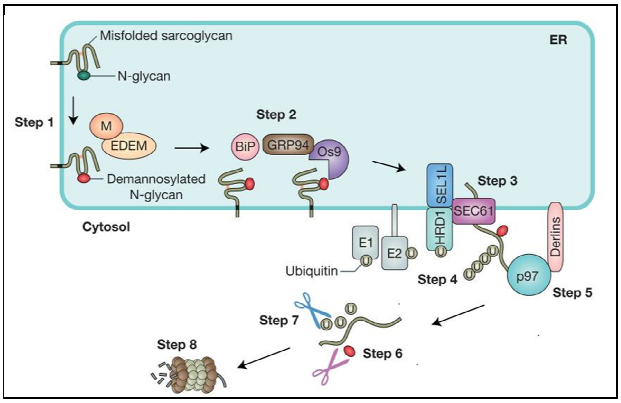

Sandonà and Betto, 2009

Fig 14. ERAD pathway of folding-defective sarcoglycan mutants. This scheme reports the steps of the ERAD pathway responsible for the disposal of a terminally misfolded SG. The de-mannosylation of the N-glycan is the trigger event for the entry of misfolded SG into the ERAD pathway (step1). Chaperons and lectin (Bip, GRP94, Os9) transport SG to the dislocon (step2). The retro-translocation of SG occurs through a complex composed of SEL1, an adaptator protein, HRD1, an E3 ligase, and SEC61, the actual channel (Step 3). During translocations, SGs is poly-ubiquitinated by the coordinated action of E1, E2, E3 ligases (step 4). Notably Hrd1 is one of the E3 ligase. The p97ATPase and the adaptator proteins derlins, are the final players for retro-traslocation (step 5). Before entering the proteasome, the pUb chain is removed by de-ubiquitinase enzymes (DUBs) and the N 7-glycan by PNGase (step 6). Finally, the misfolded SGs is degraded by the proteasome in small polypeptide fragments (step 8).

ERAD is a central system of the secretory pathway of cells, therefore, perturbations in the folding process of proteins can alter the ER homeostasis and perturbation of the folding process can result in disorders called unfolded protein diseases (UPD) (Wang et al., 2012; Vaastyan and Lindquist, 2014).

UPDs can be classified into two groups. The first, results from the failure of ERAD to manage misfolded protein, which in turn can aggregate and accumulate. The precipitation of these aggregates is toxic for the cell and can result in severe pathologic consequences such as in Parkinson or Alzheimer disease.

The second group of disorders is the consequence of the premature degradation of folding defective proteins, as occurring in many cases of cystic fibrosis (CF) and sarcoglycanopathy (Carotti et al., 2017). In these cases, the pathogenic mechanism is represented by a loss of function, even when the folding-defective protein retains, partially or completely, its function. Deciphering ERAD is therefore of fundamental importance not only to shed new light in the pathogenetic mechanisms of UPD but also to identify potential targets for pharmacological therapies.

1.2.2.2 Therapies to treat sarcoglycanopathies

Unfortunately, despite extensive efforts, no effective therapy is currently available to treat sarcoglycanopathy. Until now, the sole pharmacological treatment is the symptomatic administration of corticosteroids, aiming at reducing inflammation, next to supportive interventions designed to preserve the patient's quality of life. Indeed, physiotherapy is necessary to preserve ambulation as long as possible, and respiratory and cardiac assistance may prevent fatal outcome (Narayanaswami et al., 2015).

Causative treatment strategies, such as gene therapy and cell therapy are currently under investigations. Gene therapy seems one of the most convenient strategy since the disease is caused by the loss or strong reduction of the mutated SG and the transfer of the healthy copy of the gene can recover the disease phenotype. Moreover, the delivery of SG genes might be easily accomplished thanks to their small length that allows packaging into different viral vectors. Another innovative therapeutic approach may be the grafting of dystrophic muscles with genetically cured host satellite cells or healthy cells from a donor. However, both approaches present several challenges such as the difficulties of targeting the whole body muscle tissue, and safety problems that can be exacerbated by a long-term therapy needed.

These problems may be overcoming by the use of small molecules that can also ameliorate the compliance of patients. However, for this intent, the clarification of the pathological mechanism is essential for the identification of possible druggable targets. To this intent, the pharmacological inhibition of the proteasome, described in Gastaldello et al., 2008 evidenced for the first time how mutated SGs may be rescued from degradation. Moreover, the rescued SGs were able to correctly assemble with WT partners and localize at the cell membrane. This finding supported the idea that SG mutants may be still functional and opened the route toward a possible therapeutical approached aimed at preventing the degradation of the defective SGs. In the same line of interventions was also the α-mannosidase inhibition with kifunsensine, as reported in Soheili et al., 2012. A few years later, Bianchini et al., identified other ERAD factors involved in the SG degradation, enlarging the list of hypothetical druggable targets and of compounds. Among these, LS-101 and LS-102, inhibitors of HRD1, were tested and reported to efficiently increase the SGs level in a dose dependent manner, allowing also the correct localization of the complex at the sarcolemma of primary myotubes from a LGMD-2D patient (Bianchini et al., 2014).

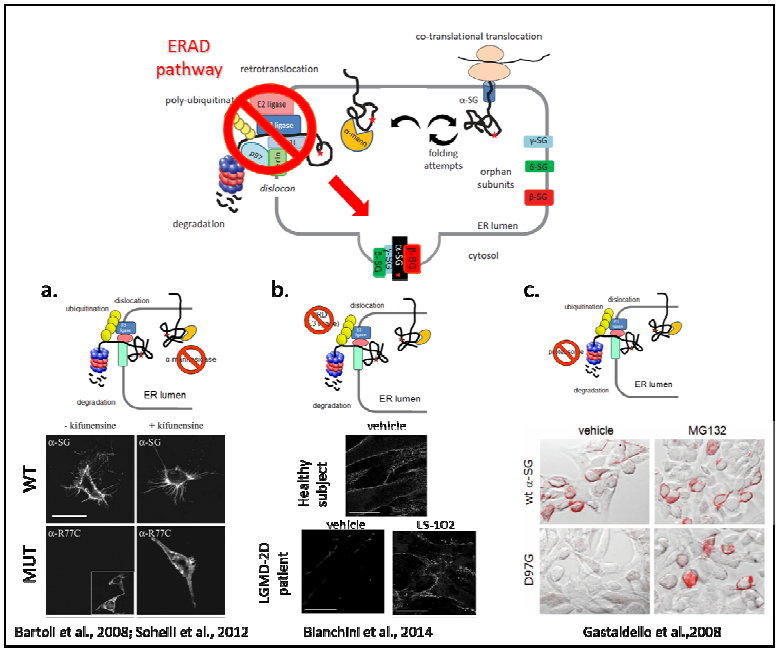

Fig 15. Strategies of SGs rescue as possible therapeutic approach. The upper part of the panel shows that by inhibiting the ERAD pathway involved in sarcoglycanopathy (red sign) the mutated protein, in this case α-SG, can assemble with the WT partners and reach the membrane (red arrow). This representative scheme was better elucidated below, where the block of single degradative step led to the recovery of SGs. (a.), kifunesine blocks the first

step of the pathway, (b.), LS-101, LS-102 block the HRD1 E3 ligase, an intermediate step, and (c.), MG-132, a proteasome inhibitor block the last step of the pathway. In all cases, the SG-complex is recovered at the plasma membrane both in cell models and in myotubes from a LGMD-2D patient.

However, since the inhibition of such important pathways may have important side effects, an alternative small molecule approach has been hypothesized in Carotti et al., 2018 where the attention was focused on the process of folding of the mutated SGs. The idea was to assist the folding process of the defective SG by means of molecules recognised as protein folding correctors. In particular, a number of such compounds has been selected and tested for their activity in recovering those missense mutants of the cystic fibrosis transmembrane regulator channel (CFTR) affecting folding and trafficking of the channel. These compounds named CFTR correctors could help the folding process by acting by two mechanisms. As pharmacological chaperones they can directly bind and stabilize the defective CFTR or, as proteostasis regulators, they can modulate the protein quality control network. In general, a pharmacological chaperone is supposed to be highly specific for a single protein; conversely, a proteostasis regulator should have a wider spectrum of action (Balch et al., 2008).
Since missense mutants of CFTR and SGs share a similar degradative pathway, it seems reasonable to hypothesise that some CFTR correctors, if acting as proteostasis regulators, may be active also on mutated SGs. Indeed, very promising results have been collected by treating cell models and primary myotubes from a LGMD2D patient with several of these compounds. α-SG has no structural similarity with the CFTR chloride channel, therefore the positive effects exerted by CFTR correctors on α-SG is probably due to a general mechanism, that could modulate the activity, composition or concentration of elements of the proteostasis network.
The treatment with some of known correctors induced an increase of the mutated αSG and the re-localization of the SG-complex at the plasma membrane. More interestingly, and for the first time, the functional recovery of the rescued complex was assessed through an *in vitro* functional assay, aimed at measuring the release of the cytosolic enzyme CK from myotubes upon exposure to stressful conditions. Indeed, myotubes form LGMD2D patient released higher amount of CK in comparison to myotubes from a healthy subject. However, after pre-treatment with a corrector, C17, the CK release was significantly reduced, suggesting a stabilization of the sarcolemma because of the SG complex rescue. These data published in Carotti et al., 2018, are attached before the results section because part of this PhD thesis.

1.2.2.3 Animal models of sarcoglycanopathy

The availability of animal models of sarcoglycanopathy greatly facilitated the investigation of the pathogenic mechanisms of the disease. Indeed, thanks to their use it has been confirmed that the loss of SG complex is the cause of membrane instability and muscle degeneration (Dulcos et al., 1999). Moreover, vertebrate models are valuable tools for the screening and/or development of new drugs (Watchko et al., 2002). Below are briefly described the different sarcoglycanopathy animal models currently available.

The natural occurring LGMD-2F model: the Cardiomyopathic Hamster

Homburger et al., in 1962, described a naturally occurring δ-SG KO model, the BIO 14.6 cardiomyopathic hamster (CMH). In 1994, Yamanouchi et al. reported that the primary absence in δ-SG results in a secondary decrease or in the absence of the other SGs. Furthermore, dystrophin appears to be less tightly associated with the sarcolemma and α-DG is destabilized at the extracellular surface, consistent with what observed in LGMD2F (Duclos et al., 1999). However, it was the group of Nigro that identified a deletion in the 5'-untranslated region of exon 1 of the *sgcd* gene that results in the loss of the protein (Nigro et al., 1997).

Phenotypically, the CMH is characterized by fiber atrophy, central nuclei and skeletal muscle necrosis that begins at 1 to 2 months of age. Dilated cardiomyopathy may have fatal consequences (Sakamoto et al., 1997). Defects in sarcolemma permeability of CMH are like those present in the dystrophin-deficient *mdx* mouse and maybe they are the reason of calcium elevation in myofibres, the main cause of the dramatic consequences of the disease (Straub et al.,1998).

SG Gene KO Mice

Sgca, Sgcg, Sgcb, Sgcd null mice have been generated (Hack et al.,1998; Duclos et al., 1999; Vainzof et al.,2008). All four mRNAs including the truncated mRNA of each targeted gene have been detected, thus, the expression level of the SG complex is determined post-translationally.

These animals show dystrophic changes in both skeletal muscle and heart (except for α-SG KO mice, a feature in common with the majority of LGMD2D patients). Skeletal muscle fibres begin to degenerate about 2 weeks after birth with cell infiltration, fibrosis, and changes in plasma membrane integrity. Indeed, SGs null mice show membrane permeability defects evaluated with the increased Evans blue uptake and CK efflux. These animals are also characterized by a destabilization of some DAPC components, in particular DGs and sarcospan meaning that the SG complex is critical for their localization and function. However, heterogeneity in the interactions between members of the SG complex itself as well as in their relationship with DAPC components led to differences among the four KO murine models.

Sgcb and *Sgcd* null mice develop a more severe muscular dystrophy in comparison to *Sgca* and *Sgcg* null mice. The severity of the disease is correlated with the reduction of SG expression. Indeed, in β-and δ-SG KO muscles, remnant SGs are hardly observed on the sarcolemma unlike the other two milder models. Moreover, the loss of complex in *Sgcb* and *Sgcd* null mice, occurs also in vascular smooth muscle, where a trimeric ε-β-δ SG complex exist, causing vasculature constriction and the possible ischemic damage that may exacerbate the skeletal and cardiac pathology (Coral-Vazquez et al., 1999). The absence of α- and γ- SG from the vascular smooth muscle can explain why *Sgca* and *Sgcg* null mice display a less severe phenotype.

SG KI Mice

Considering that sarcoglycanopathy is mainly due to missense mutations, KI animal models mimicking the human condition should be mandatory to better investigate the pathology and to test potential drugs capable of correcting SGs defect.

Two KI mouse models have been generated: α-SG H77C/H77C and β- SG T151R/T151R KI (Kobuke et al., 2008; Bartoli et al., 2008; Henriques et al., 2018).
Unexpectedly, contrarily to the human R77C α-SG and T151R β-SG mutants, which are both prematurely degraded in the human context, the corresponding murine mutants fail to mimic this condition. No sign of muscular dystrophy was detected at various ages (between 4 and 88 weeks), and even upon exposition of mice to stressful conditions. In both α-SG and β-SG, the mutation does not affect the assembly and the targeting of the SG and DAPC complex at the membrane. In the α-SG H77C KI mouse, a possible explanation for the absence of a phenotype could be that the residue at position 77 in mouse (a His) is not the exact counterpart of the human residue (an Arg), even if, according to their basic nature, they should display similar characteristics/behaviour. However, mouse and human α -SG present additional amino acid variations, therefore it is possible that, in the α-SG H77C/H77C, the interactions with other residues compensate for the presence of the mutation. On the other hand, another explanation is that, in mouse, a more permissive quality control system allows the skipping of proteins otherwise recognized as defective in human. This hypothesis seems supported by the finding that also the β -SG-KI mouse fails to develop the expected dystrophic phenotype. Indeed, in this KI animal the mutations is on a conserved residue, located in a region with high homology between mouse and human. Thus, it appears that a missense mutation is insufficient to cause the loss of SGs in mice, because of the less stringent rules of the mouse QC (Henriques et al., 2018). Unfortunately, few comparative studies of proteomes between the two species have been reported until now. Therefore, it appears difficult to give conclusive explanations of the reason why mouse fails in recapitulating the human pathological phenotype when a missense mutation is present in SGs. On the other hand, this behaviour means also that the SGs, even though defective, are functional and strengthens the suitability of therapeutic approaches aimed at protecting mutated SGs from degradation. Considering the need of vertebrate models for testing the efficacy of small molecules identified by *in vitro* studies, a promising alternative to the lack of murine models is represented by zebrafish.

1.3. Zebrafish as model organism

Although reliable data from developmental, biological, biochemical, pharmacological studies are usually obtained through laboratory rodent, experiments with murine models are expensive, time consuming, and limited by ethical consideration.
Other organisms such as *D. melanogaster* and *C. elegans* can serve as powerful model systems for many biological processes and are amenable for large-scale screens. However, being invertebrate, they cannot be utilized to address the development and function of vertebrate-specific features. This forces toward the identification and use of other vertebrates, such as zebrafish (*D. rerio*). Indeed, even if zebrafish is obviously very different from humans, as vertebrate follows an evolutionarily-conserved program of development and presents highly conserved genes and molecular processes (Ota and Kawahara, 2014).

Characteristic of model animals	Model animals		
	Fly	Zebrafish	Mouse
Similarity to human disease	–	++	+++
Similarity to human genome	+	++	+++
Large-scale mutagenesis	+++	+++	+
Gene disruption	+++	+++	+++
Gene replacement	+	+	+++

–, not a strength; +, ++, +++, relative strength of the model in each category.

Ota and Kawahara, 2014

Table 6. Specific features of different invertebrate and vertebrate animal models. The similarity to human disease, to human genome and different type of genetic manipulation are compared in strength for each model. Zebrafish appears an excellent alternative model between the typical invertebrate, the fly, and the typical vertebrate, the mouse.

Zebrafish is a freshwater fish originating from the Ganges river belonging to the family of cyprinids (Dahm, 2006). The name came from the characteristic four horizontal blue metallic stripes alternating with many thinner white lines, which run along the body and the fins.

Fig 16. Specimen of a female (front) and male (behind) zebrafish. Females can be recognized for larger belly sizes while males tend to have a more yellowish colour and red gills.

Since 1970's, when Streisinger began to use zebrafish in research, this little vertebrate became a very popular worldwide animal model both in basic and preclinical research. No other vertebrate model organism has grown in popularity as quickly as zebrafish. Its reputation was firmly established during the nineties of the 20th century when big genetic screening projects in US and Europe led to the discovery of thousands of mutants that gave novel insights into the functions of essential human developmental genes. This is also evident by the increasing number of publications, in which there is the description of the use of this organism. In the early 1990's there were less than 100 zebrafish-related publications annually submitted. This number rose to ~1,000 at the turn of the century and now are on an average of approximately 3,500 per year.

A number of reasons support the use of zebrafish as animal model. First because, as mentioned before, being a vertebrate, it is related to mammals and uniquely positioned to bridge the gap between its vertebrate and invertebrate counterparts. Indeed, 71% of human proteins, and 82% of disease-causing human proteins, have an orthologue in zebrafish (Bradford et al., 2017). This similarity is particularly important also in the field of muscle pathology. Indeed, the striking similarities between fish and mammalian muscle, and the presence of stereotyped movement during development, permits to easily measure any alterations in muscle function (Gibbs et al., 2013). Second, because zebrafish reproduces by external fertilization and because of the transparency during the first phase of development, concluded at 4-5 dpf, all stages of embryogenesis are accessible. Third, the high number of embryos in each progeny, together with the ability of embryos to adsorb drugs dissolved in fish water, allow to carry out high throughput

screening of compounds that would not be possible in mammalian (MacRae and Peterson, 2014). Fourth, the small size reduces housing space and husbandry costs.
Lastly, genome-editing approaches are well established in zebrafish, permitting to introduce any desired mutation rather easily by the microinjection of fertilized eggs (Chang et al.,2013; Li et al., 2016). The rapid development permits quick identification and characterization of mutated fish lines, many of which are available through the Zebrafish International Resource Centre (ZIRC) to facilitate systematic functional studies of the vertebrate genome (Bradford et al., 2017).
Nevertheless, several caveats must be taken into account. First, since they are not mammals they lack lungs, mammary gland, prostate gland and limbs, which make the fish model unusable to study these tissues and organs. Second, fish are poikilothermic and usually maintained below 30 °C, which may not be optimal for those mammalian agents adapted to be active at 37 °C during evolution. Third, since the zebrafish genome is partially tetraploid, it is more difficult to produce loss-of function mutations in certain genes (Postlethwait et al., 2007).

1.3.1 Zebrafish as model organism for human diseases and drug testing

Zebrafish has emerged as an excellent model organism to study human disease, to recognise novel therapeutic strategies, and to develop functional assay for pharmacological experiments.
Numerous human disorders have been recapitulated in zebrafish models (Ota and Kawahara, 2014; Dooley and Zon, 2000). For example, zebrafish has emerged as a powerful vertebrate model system to study hematopoietic disorders and cardiovascular diseases thanks to the rapid heart development, completed at 72 hpf (Bournele et al., 2016). Moreover, it is an ideal model for the cancer research, both because human homologs oncogenes and tumour suppressor have been identified, and because signalling pathways regulating cancer development are conserved (Xie et al., 2015).
Zebrafish can be used also to investigate depressive disorders, evaluated through behavioural or cognitive test, because its neuroanatomical, neuroendocrine, neurochemical characteristics are similar to mammalian ones (Nguyen et al., 2014). Zebrafish kidney is simple and accessible for investigation of kidney diseases (Bogert et al., 2013). Moreover, the phenotypes of several zebrafish models very closely display the severity of the human clinical presentation, even better than the corresponding mouse models, as occurs for the dys deficient zebrafish. It exhibits a severe motor phenotype by 4 days of life and die by 2 weeks of life, while dystrophin-deficient mdx mice have a very mild phenotype that only moderately impacts muscle function and survival (Berger and Curie, 2013). Zebrafish starts therefore to be compared to humans in terms of biological processes and range of phenotypes assayed such as pain, sedation, tumour metastasis, vascular tone, behavioural analysis and muscle damage.

Human gene	Zebrafish gene	Zebrafish model	Reference	Human condition
DMD	*dmd*	morpholino mutant (*sapje*) mutant (*sapje-like*)	Guyon 2003 Bassett 2003; Berger2011 Guyon 2009	Duchenne muscular dystrophy
LAMA2	*lama2*	mutant (*caf*) mutant (cl501)	Hall 2007 Gupta 2012	Congenital muscular dystrophy (MDC1A)
ITGA7	*itga7*	morpholino	Postel 2008	Congenital muscular dystrophy
LMNA	*lmna*	morpholino	Vogel et al 2009; Koshimizu 2011	Multiple forms of dystrophy
COL6A1	*col6a1*	morpholino	Telfer 2010	Ullrich congenital muscular dystrophy; Bethlem myopathy
COL6A3	*col6a3*	morpholino	Telfer 2010	Ullrich congenital muscular dystrophy; Bethlem myopathy
DUX4		overexpression	Wallace 2011; Mitsuhashi 2013	Facioscapulohumeral muscular dystrophy
DNAJB6	*dnajb6b*	morpholino	Sarparanta 2012	Limb-girdle muscular dystrophy
DAG1	*dag1*	morpholino mutant	Parsons 2002 Gupta 2011	Limb-girdle muscular dystropy (MDDGC9)
SGCD	*sgcd*	morpholino	Guyon 2005; Cheng 2006; Vogel 2009	Limb-girdle muscular dystrophy
TCAP	*tcap*	morpholino	Vogel 2009; Zhang 2009	Limb-gidle muscular dystrophy
DUX4		overexpression	Mitsuhashi 2013	Facioscapulohumeral muscular dystrophy
DYSF	*dysf*	morpholino	Kawahara 2011; Roostalu 2012	Myoshi myopathy; limb-girdle muscular dystrophy
POMT1	*pomt1*	morpholino	Avsar-Ban 2010	Multiple forms of dystroglycanopathy
POMT2	*pomt2*	morpholino	Avsar-Ban 2010	Multiple forms of dystroglycanopathy
FKRP	*fkrp*	morpholino	Thornhill 2008; Karahara 2010; Lin 2011; Wood 2011	Multiple forms of dystroglycanopathy
FKTN	*fktn*	morpholino	Lin 2011; Wood 2011	Multiple forms of dystroglycanopathy
ISPD	*ispd*	morpholino	Roscioli 2012	Multiple forms of dystroglycanopathy
B3GNT1	*b3gnt1*	morpholino	Buysse 2013	Walker-Warburg syndrome
GTDC2	*gtdc2*	morpholino	Manzini 2012	Walker-Warburg syndrome
MTM1	*mtm1*	morpholino	Dowling 2009	Myotubular myopathy
DNM2		overexpression	Gibbs 2013	Centronuclear myopathy
CCDC78	*ccdc78*	morpholino	Majczenko 2012	Congenital myopathy with internal nuclei and cores
NEB	*neb*	morpholino	Telfer 2012	Nemaline myopathy
RYR1	*ryr1b*	mutant (*ryr*)	Hirata 2007	Multiple forms of congenital myopathy
SEPN1	*sepn1*	morpholino	Deniziak 2007; Jurynec 2008	Multiple forms of congenital myopathy
DES	*desma* *desmb*	morpholino morpholino	Vogel 2009; Li 2013 Li 2013	Myofibrillar myopathy
CAV3	*cav3*	morpholino	Nixon 2005	Caveolinopathies

Gibbs et al., 2013

Table 7. List of the zebrafish muscular dystrophies models. The table reports the gene mutated in each muscular dystrophy and the corresponding zebrafish models obtained with different genetic technologies.

Considering the expanding number of zebrafish models for muscle diseases, as reported in table 7, a corresponding wide repertoire of techniques has been developed for the analysis of muscle structure and function in zebrafish. Motor behaviours can be measured since two days post fertilization, when zebrafish embryos have developed a robust escape response, such as a rapid swimming away from the stimulus. At approximately 5 days post fertilization, *larvae* begin swimming spontaneously and swim behaviours, such as velocity and turn frequency, can be precisely quantified, using imaging systems like the Noldus DanioVision or the Viewpoint Zebrabox (De Marco et al., 2016). Together, these sequential motor behaviour tracking systems provide a simple and non-invasive evaluation and quantification of muscle function (Kopp et al., 2018).

In developing zebrafish muscles, myofiber integrity can be easily checked using an optical phenomenon called birefringence. Indeed, when viewed under polarized light, myofiber appear as bright under a dark background. However, when muscle damage occurs an increase of areas of shadows can be detect and directly quantified to measure loss/damage of muscle (Zulian et al., 2014). Skeletal muscle can be also visualized using immunohistochemistry or fluorescent probes or by using reporter proteins expressed by tissue-specific promoters (Shahid et al., 2016). Furthermore, the transparency of zebrafish embryos permits elegant optical assays of muscle structure and function that would not be possible in mammalian systems.

Large-scale drugs screening is not feasible in mammals due to cost, ethical concerns and time requirement, but are feasible with invertebrate models or cultured cells. However, such assays, in invertebrates or cells, lack of the functional outcome; moreover *in vivo* experiments allow the evaluation of pharmacokinetic and pharmacodynamics. Zebrafish offers the combination of invertebrate advantages (small size, rapid development, large numbers) and vertebrate biological relevancy, therefore it represents an ideal tool for drug screening experiments.
Compounds to be tested can be directly dissolved in the fish water, because easily adsorbed by embryos, therefore, the evaluation of dose-response relationships and the elucidation of mechanisms of toxicity can be performed in high-throughput screening format.
Questions about relevance to humans remain of central importance in using zebrafish in drug discovery. Indeed, considering the phylogenetic distance between zebrafish and humans a precise correlation between the output from zebrafish screenings and the human biology is required.
Considering that 82% of disease-causing human proteins have an orthologue in zebrafish and that most of the physiologic processes (absorption and excretion, detoxification, etc) are highly conserved, drug effects should be similar and a direct correlation between effects in zebrafish and humans could be done (MacRae and Peterson, 2014).

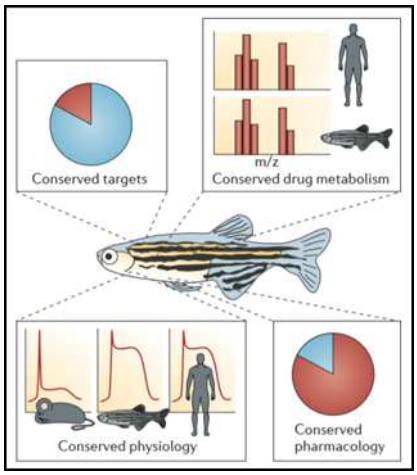

MacRae and Peterson, 2014

Fig 17. Goodness of zebrafish as model for drug testing. Although zebrafish enable *in vivo* studies on a large scale, questions remain about how relevant the findings are for drug discovery. Recent studies have begun to elucidate the degree of conservation between humans and zebrafish physiology, which share 82% of disease-associated targets and a large number of drug metabolism pathways. Zebrafish physiology is often well conserved with humans (sometimes more than rodent physiology is), for example see the cardiac electrophysiology (illustrative electrocardiogram (ECG) tracings from each organism are shown). Several compounds discovered in zebrafish screens have been shown to exhibit similar effects in rodent models and humans.

To screen potential therapeutic compounds, embryos are therefore treated with compounds for several days and the toxicity is evaluated by considering guidelines reported in the Fish Embryo Acute Toxicity (FET) Test (OECD Guidelines for the Testing of Chemicals, 2013). However, one of the most substantial issues is the challenge of controlling and quantifying drug exposures. Although it is easy to control the concentration of a drug in fish water, it is more difficult to predict how much drug will be absorbed.

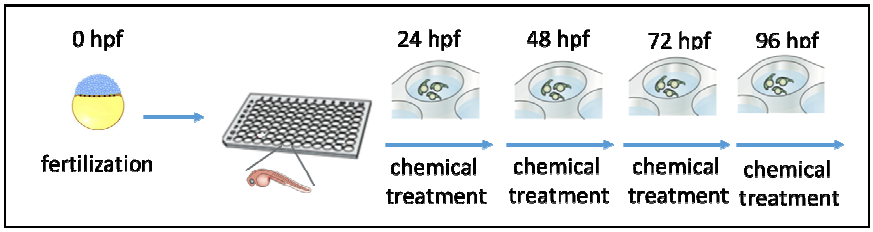

Fig 18. Set up of a screening-toxicity test for chemicals. After 24 hours post fertilization (hpf), embryos are placed in a multi-well plate and treated with different concentrations of the same chemical or with different type of molecules dissolved in fish water. Chemicals are changed periodically, and fish are followed for several days.

1.3.2. Zebrafish muscle development

During the development of the zebrafish musculature, three different structures are recognizable: adaxial cells, muscle precursors, and the horizontal myosepta. In the presomitic mesoderm, the adaxial cells are visible as large cuboidal cells adjacent to the notochord. Muscle precursors, probably a subcategory of adaxial cells, are the first to show striation in myotome (Felsenfeld et al., 1990). They lie adjacent to the notochord, in the region of the myosepta.

The horizontal myosepta is a fibrous layer that divides the myotome into a dorsal and a ventral part and is visible for the first time at approximately 28 hpf.

The development of the axial musculature is therefore rapid and predictable: all the myotomes are present at 30 hpf and the adaxial muscle cells are striated at 36 hpf. The muscle represents approximately the whole mass of the tail and of the trunk and, due to the optical transparency of the zebrafish, can be easily visualized (Gibbs et al., 2013).

Zebrafish skeletal muscle shares many molecular and histological features with mammalian muscle and appears nearly identical to human muscle at the ultrastructural level. This includes preservation of the components of the DAPC, the excitation-contraction coupling machinery, and the contractile apparatus, three features that are of upmost importance to study and understand the pathogenesis of human muscle disease (Berger et al., 2012).

1.3.2.1 DAPC and SG expression in zebrafish

Zebrafish DAPC, as occurring in humans, plays a very important role in muscle architecture and in the organization of myosepta.

Comparative genomics studies have identified orthologues of many members of the DAPC, highlighting the crucial functional significance of these proteins.

The use of antibodies developed for mammalian SGs, able to cross-react with the zebrafish proteins, allowed to analyse the localization of the human protein orthologues of the DAPC in adult zebrafish (Chambers et al., 2003). From these experiments, it emerged that DAPC is express on the sarcolemma and myosepta. The genomic and EST sequences data of the zebrafish genome allowed identifying sequences with a high level of identity of five of the six known SGs in humans with α-SG being the less conserved one (Steffen et al., 2007; Chambers et al.,2003). All these data confirm the goodness of the zebrafish as a model for studying the physiology and pathology of skeletal muscle.

1.3.3. Quality Control System in zebrafish

The endoplasmic reticulum quality control systems (ERQC) is a key element to regulate protein homeostasis and it has been shown to exist in organism from yeast to human. Misfolded proteins that start the maturation process in the ER are processed through the ER associated degradation (ERAD). First, they are recognised in the ER as unfolded/misfolded, then retro-traslocated into the cytosol and poly-ubiquitinated prior to be degraded by the cytosolic 26S proteasome. Recently, evidence is emerging regarding the conservations of this pathway also in zebrafish. First, OS-9, an ER resident lectin that target misfolded protein to ERAD, was identified in the lumen of ER in zebrafish (Wang et al., 2007). Components involved in the ERAD retrotranslocation channel, such as Derlin1 and 2, the E3 ligase gp78, and other adaptor proteins, such as Sel1l, are also described in literature to be involved in the zebrafish ERAD pathway (Saslowsky et al., 2010; Chen et al., 2014; Barbieri et al., 2018). Moreover, a zebrafish mutant for the 26S proteasome was described, resulting in a reduction of the proteasome activity (Imai et al., 2010)

1.4 Genome editing technologies

Targeted genome engineering, which means genome modification in a predetermined locus of different cell types or whole organisms, has become a powerful and broadly applicable tool for biomedical research (Cox et al., 2015).

The potential applications of such genome-editing technologies range from biotechnology, to preclinical studies, until therapeutics. Generation of various animal models is useful to determine the functions of specific genes evaluating the phenotypic consequences of their inactivation (gene knockout), or mutation at the single-nucleotide or structural level (gene knock-in). Furthermore, they may be of upmost importance to set up preclinical drug studies. Finally, the knowledge of the genetic basis of diseases improved the development of targeted genome editing based therapy, involving the correction or inactivation of deleterious mutations, or the introduction of protective mutations (Schwank et al., 2013).

The use of programmable nucleases can artificially produce gene disruptions, DNA insertions, targeted mutations, or chromosomal rearrangements in a predictable and controlled manner (Segal and Meckler, 2013). To date, four major classes of programmable nucleases have been developed to enable site-specific genome editing and are classified into two categories based on their mode of DNA recognition:

- meganucleases (Boissel t al., 2014), zinc finger nucleases (ZFNs) (Miller et al., 2007), and transcription activator–like effector nucleases (TALENs) (Li et al., 2011), that use protein-DNA interactions to bind the selected DNA target
- clustered regularly interspaced short palindromic repeat (CRISPR)-associated nuclease Cas9 (Sander and Joung, 2014), a RNA-guided nucleases (RGNs) that uses simple Watson-Crick base-pairing rules between an engineered short RNA guide molecule and the target DNA site.

These different types of nucleases share the same mechanism of action, *i.e.* the cleavage of the target DNA in a site-specific manner, which in turn triggers endogenous DNA repair systems and the consequent targeted genome modification. However, each of them has unique characteristics.
Meganucleases are endonucleases recognizing long (>14-bp) DNA binding sites and are also responsible for the cleavage of target sequences (Boissel et al., 2014).
ZFNs and TALENs are chimeric enzymes consisting of a DNA binding domain fused to the sequence-diagnostic FokI nuclease domain (Miller et al., 2007; Li et al., 2011).
Re-targeting of meganucleases ZFNs and TALENs requires complex re-engineering cloning since the DNA-binding domain of these nucleases determines their unique site specificity (Kim and Kim, 2014).
By contrast, CRISPR/Cas9 is easier to customize. Indeed, Cas9 protein is invariant and can be easily retargeted to new DNA sequences by changing only the small portion (20-nt) of the RNA guide (gRNA) that base pairs directly with the target DNA (Sander and Joung, 2014). Moreover, Cas9 offers several potential advantages over ZFNs and TALENs, including higher editing efficiency and consistency, with a more specific cleavage, performed usually between the 17th and 18th base in the target sequence. Moreover, the possibility to act on methylated genomic sites and to induce simultaneously multiplex DSBs by the delivery of a combination of distinct gRNAs, enlarges the range of action of the CRISPR/Cas9 system (Cox et al., 2015).

	Zinc finger nuclease	TALEN	Cas9	Meganuclease
Recognition site	Typically 9–18 bp per ZFN monomer, 18–36 bp per ZFN pair	Typically 14–20 bp per TALEN monomer, 28–40 bp per TALEN pair	22 bp (20-bp guide sequence + 2-bp protospacer adjacent motif (PAM) for *Streptococcus pyogenes* Cas9); up to 44 bp for double nicking	Between 14 and 40 bp
Specificity	Small number of positional mismatches tolerated	Small number of positional mismatches tolerated	Positional and multiple consecutive mismatches tolerated	Small number of positional mismatches tolerated
Targeting constraints	Difficult to target non-G-rich sequences	5′ targeted base must be a T for each TALEN monomer	Targeted sequence must precede a PAM	Targeting novel sequences often results in low efficiency
Ease of engineering	Difficult; may require substantial protein engineering	Moderate; requires complex molecular cloning methods	Easily re-targeted using standard cloning procedures and oligo synthesis	Difficult; may require substantial protein engineering
Immunogenicity	Likely low, as zinc fingers are based on human protein scaffold; FokI is derived from bacteria and may be immunogenic	Unknown; protein derived from *Xanthamonas* sp.	Unknown; protein derived from various bacterial species	Unknown; meganucleases may be derived from many organisms, including eukaryotes
Ease of *ex vivo* delivery	Relatively easy through methods such as electroporation and viral transduction	Relatively easy through methods such as electroporation and viral transduction	Relatively easy through methods such as electroporation and viral transduction	Relatively easy through methods such as electroporation and viral transduction
Ease of *in vivo* delivery	Relatively easy as small size of ZFN expression cassettes allows use in a variety of viral vectors	Difficult due to the large size of each TALEN and repetitive nature of DNA encoding TALENs, leading to unwanted recombination events when packaged into lentiviral vectors	Moderate: the commonly used Cas9 from *S. pyogenes* is large and may impose packaging problems for viral vectors such as AAV, but smaller orthologs exist	Relatively easy as small size of meganucleases allows use in a variety of viral vectors
Ease of multiplexing	Low	Low	High	Low

Cox et al., 2015

Table 8. Comparison of different programmable nuclease platforms. Due to its easier customization and high editing activity in comparison to that of other nucleases, Cas9 appears an ideal tool to genome engineering (ZFN, zinc-finger nuclease; TALEN, transcription activator-like effector nuclease; PAM, protospacer adjacent motif).

All the cited engineered nucleases “edit” the genome by introducing targeted double-strand DNA break (DSB) at specific genomic loci. The DNA lesion activates the endogenous repair machinery that acts through two possible mechanisms, depicted in Fig. 19, depending on the cell state and the presence of a repair template (Kim and Kim, 2014):

- the non-homologous end-joining (NHEJ) allows the direct ligation of the break ends. It is the most efficient repair system, but it is error prone, because often causing small insertions and deletions (named indel mutations) to occur in bridging the break site. Indels introduced into the coding sequence of a gene can cause frameshift mutations that lead to mRNA degradation by nonsense-mediated decay or to the production of non-functional truncated proteins.

- homology-directed repair (HDR): mediates the precise repair at the targeted locus in the presence of a donor repair template. If the donor is exogenously introduced and contains point mutations or specific DNA sequences, the repair ends with the stable desired modification of the genomic locus. The donor template can have long homology arms flanking the insertion sequence, if it consists of a double-stranded DNA construct (dsDNA) or of a plasmid DNA; or it can be a short single-stranded DNA oligonucleotides (ssDNA) with homology arms as short as 40bp (Salsman and Dellaire, 2017).
  Even if HDR is less efficient than NHEJ, it is a high-fidelity mechanism. Indeed, the exogenously provided DNA template, which presents sequence similarity to the cleaved site, is effectively used to repair the lesion. Indeed, the end of the ssDNA, generated after its cleavage, provides a substrate for the assembly of Rad51, a recombinase DNA-dependent ATPase that defines the first step of HDR, by forming a nucleoprotein filament on single-stranded. This suppresses the potentially mutagenic pathways of NHEJ, while promoting more precise HDR. Physiologic HDR is active only during the S/G2 phase of the cell cycle, when the duplication of DNA provides the homologous donor template (Escribano-Diaz et al., 2013). However, with an exogenously provided template, HDR takes place also in G1 phase. Moreover, HDR can collaborate or compete with NHEJ that is also active, and generally prominent (Rothkamm et al., 2003). Consequently, cell type and state, target genomic locus and repair template features can affect the repair efficiency.

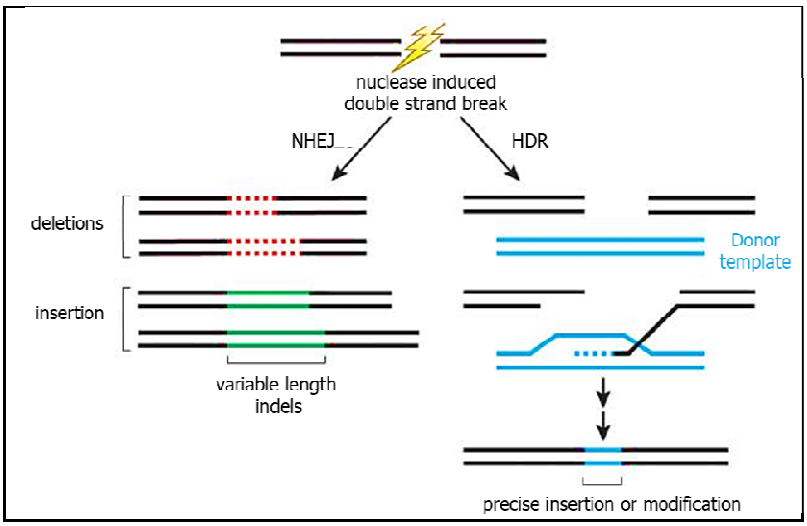

adapted from Sander and Joung, 2014

Fig 19. Nuclease-induced genome editing. Nuclease-induced double strand breaks (DSBs) can be repaired by non-homologous end joining (NHEJ) or homology-directed repair (HDR) pathways. Imprecise NHEJ mediated repair can produce insertion and/or deletion mutations of variable length at the site of the DSB. HDR-mediated repair can introduce precise point mutations or insertions of DNA sequences carried by a single-stranded or double stranded DNA donor template.

1.4.1 CRISPR/Cas9 genome editing technique

The clustered regularly interspaced short palindromic repeat (CRISPR) associated to Cas9 endonucleases are defence mechanisms against invading plasmid-viral genetic elements evolved in prokaryotes and archaea (Jinek et al., 2012). CRISPR repeats were initially discovered in the 1980s in E. coli (Ishino et al., 1987), but their function was not defined until 2008 by Deveau and colleagues, who demonstrated that together with Cas9 protein, they are essential components of the type II adaptive immune system in bacteria and archaea (Deveau et al., 2008).

Functionally, CRISPR/Cas system targets and destroys foreign nucleic acids in a sequence-specific fashion as RNA-guided endonuclease complexes (RGEN), thanks of a RNA-DNA target binding. During preliminary exposure, in the “adaptive-acquisition” phase, exogenous DNA from viruses or plasmids is cut into small fragments called protospacer, which are then incorporated into the bacterial genome at the CRISPR *loci* as spacers sequences of approximately 20bp in length. The insertion occurs between arrays of conserved 20–50 bp, the CRISPR repeats. These *loci* are flanked by a cluster of Cas genes, which encode some of the enzymatic machinery utilized for CRISPR/Cas function.

During any subsequent infection, the second phase namely “crRNA biogenesis” takes place. The CRISPR *loci* are transcribed, and transcripts are processed to generate a single long pre-CRISPR RNAs (pre-crRNA). The pre-crRNA is then processed into an active genetic library of many spacer-derived short 20 nt CRISPR RNAs (crRNAs). crRNAs guide Cas9 to the specific 20-bp DNA target via Watson-Crick base pairing. As the crRNA array is transcribed, a unique auxiliary small RNA, termed trans-activating CRISPR RNA (tracrRNA), that facilitates both the processing of the crRNA array into units and the recruitment of the Cas9 endonuclease, hybridizes to the repeat sequences, creating the double stranded RNA structure crRNAs:tracrRNA (Lau and Davie., 2017).

In the last phase called "interference", the crRNA:tracrRNA binds the CRISPR-associated endonuclease Cas, inducing a conformational rearrangement in the enzyme to form a central channel where the target DNA can be accommodated. The crRNA base pairs with the 20-nt specific region of the target immediately adjacent of a DNA sequence of a few nt, called protospacer adjacent motive (PAM), specific for each prokaryote and recognised by the Cas enzyme. Cas proteins from other species than *S. pyogenes* recognize therefore different PAM sequences. The tracrRNA enhances Cas double-stranded (ds) breaks. This provides the prokaryotic cell with a sequence specific and adaptable mechanism for the cleavage of foreign DNA (Kick et al.,2017).

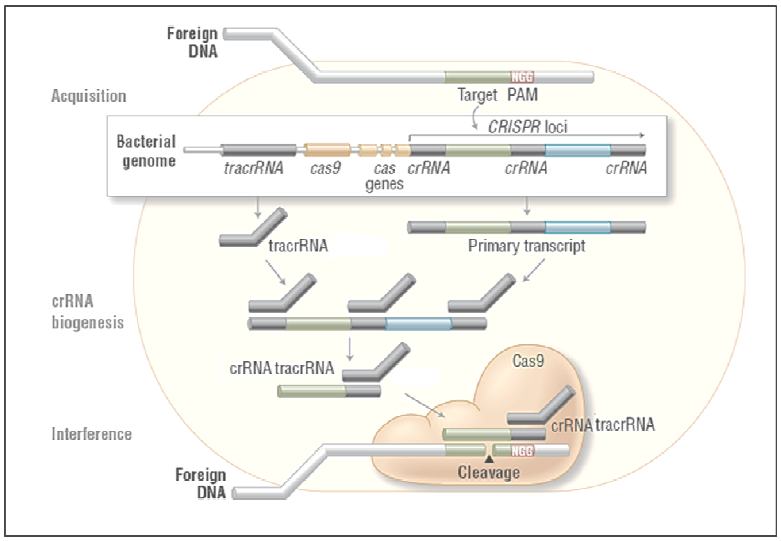

Reis et al., 2014

Fig 20. The CRISPR Cas9 adaptive immune system of bacteria and archaea. The three phases of the prokaryotic adaptive immunity are shown: first, the foreign DNA is acquired into the prokaryotic genome, and then it is processed until the biogenesis of a crRNA that hybridizes with tracrRNA. The RNA complex brings Cas9 to the DNA target, recognised thanks to a perfect base pair of 20 nt between the target DNA and the crRNA. The final event is the DSB operated by the nuclease.

Three types of CRISPR/Cas systems are known in nature, each of which uses distinct mechanisms to carry out the three-step process to produce CRISPR-mediated adaptive immunity (Wiedenheft et al., 2012). Among them, the Type II is the best characterized and the simplest in certain key aspects. One important difference is that its surveillance complex requires only a single Cas9 endonuclease unlike the Type I and Type III (Chylinski et al., 2014).

The first published example of an engineered CRISPR/Cas system for genome editing was in 2012, when Doudna and Charpentier labs demonstrated that S. pyogenes Cas9 (SpCas9) could be guided by a programmable chimeric dual-RNA to target and cleave various DNA sites in vitro (Jinek et al., 2012).

Following the initial proof-of-principle study, a flurry of papers published in 2013 showed that this platform also functions efficiently in a variety of cells and whole multicellular organism such as: *D.rerio* (Chang et al., 2013) *C. elegans* (Friedland et al., 2013), *D. melanogaster* (Yu et al., 2013) and mice (Yang et al., 2013).

1.4.2.1 CRISPR Cas9 as new tool in molecular biology

The type II RNA-directed DNA CRISPR/Cas9 system from *S. pyogenes* has been adapted for inducing sequence-specific DSBs and targeted genome editing of any gene of interest (Sander and Joung, 2014). In the simplest and most widely used form of this system, two components must be introduced into and/or expressed in cells or an organism to perform genome editing: the Cas9 nuclease and a single guide RNA (sgRNA), consisting of the fusion of a crRNA (carrying the sequence of interest) and a fixed tracrRNA joined by a small loop. Thanks to this simplified systems there is no longer the need for the accessory tracrRNA, and for RNase III to mature the crRNA:tracrRNA complex.

Site specificity of DNA cleavage by the Cas9 endonuclease depends on two factors: the base-pair complementarity between the first 20 nts of the sgRNA and the target DNA sequence, and a PAM sequence close to the complementary region at the target site (Jinek et al., 2012).

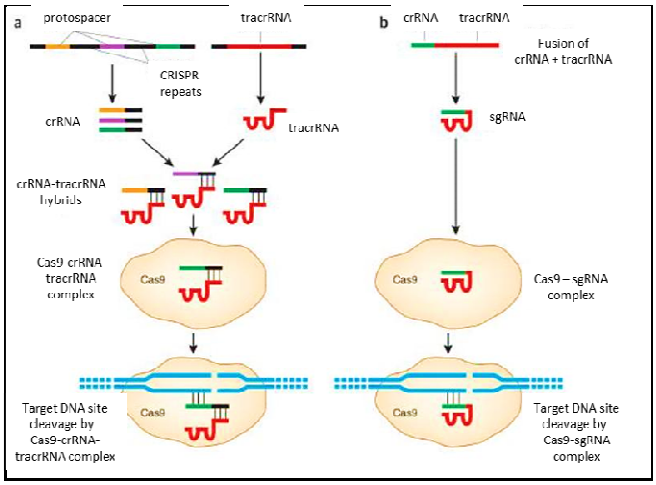

Sander and Joung, 2014

Fig 21. The simplified CRISPR/Cas9 system for genome editing purposes (b) compared with the natural one (a). A chimeric gRNA composed by the fusion of crRNA with a portion of tracrRNA is able to base pair with the target DNA, bringing the Cas9 endonuclease at the target site to mediate the DSB.

1.4.2.2 Key elements of the CRISPR/Cas9 system

To perform the DSB on the target DNA, key elements need to be present, particularly the Cas9 endonuclease, the gRNA in the form of crRNA:tracrRNA or sgRNA, and the PAM sequence at the cutting site.

<u>Cas9 endonuclease</u>

Cas9, the hallmark protein of type II systems, is a DNA endonuclease guided by two RNA molecules (crRNA:tracrRNA) or by the engineered chimeric sgRNA.

Cas9 can site-specifically cleave dsDNA, resulting in the activation of the DSB repair machinery through the NHEJ or HDR, if co-delivered with a donor template. The DSB is produced by two distinct nuclease domains on Cas9. The HNH nuclease domain resides in the mid-region of the protein and cleaves the complementary strand three base pairs upstream the PAM sequence. The RuvC-like domain, located at the amino terminus, cleaves the non-complementary strand within three to eight nts upstream of the PAM sequence.

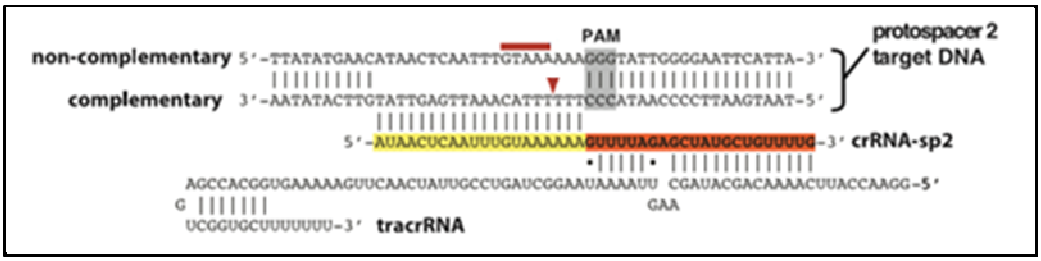

Jinek et al., 2012

Fig 22. CrRNA:tracrRNA target binding and cleavage sites on target DNA. The complementary region of crRNA to tracrRNA is highlighted in orange, with the protospacer target DNA in yellow. The PAM sequence on the protospacer target DNA is highlighted in grey; the cleavage sites are represented by a red arrowhead for the complementary strand and a red line for the non-complementary strand.

To date, engineered variants of the Cas9 nuclease have been adopted in genome-editing protocols in which those point mutations add beneficial features to the enzyme (Sander and Joung, 2014). D10A mutation in the active site RuvC, transforms Cas9 into a nickase, unable to create DSB but only single strand breaks. Thus, introducing a couple of nickases directed by a pair of appropriately oriented gRNAs, should produce staggered ssDNA cuts expected to generate 5' overhang ends. In the presence of a donor template, these nicks are preferentially repaired by HDR, thus improving the rate of homologous recombination.

Another Cas9 variant is a nuclease-deficient enzyme (dCas9) with mutations in both the RuvC and HNH domains, and therefore unable to cleave DNA but conserving just the DNA binding activity to the PAM sequence. This variant, fused with different effector domains, can be used to specifically target any region of the genome to induce for example gene silencing or activation depending on the particular effector present. Thus, Cas9 has the capability not only to edit genomes, but also to act as a transcriptional regulator. Furthermore, it can be used as imagining tool if dCas9 is fused to reporter proteins such as the enhanced Green Fluorescent Protein (eGFP).

When used for genome editing, Cas9 can be introduced in cells or organisms either as a recombinant protein or as its codifying mRNA. The protein would be more effective than Cas9 mRNA because it could act immediately following injection without translational delay (Zhang et al., 2018). Moreover, optimized version of the Cas9 bearing a nuclear localization signal (NLS), such as the SV40 NLS, fused to one or both protein *termini* facilitate endonuclease entrance into the eukaryotic nucleus, improving the editing activity (Hwang et al., 2013).

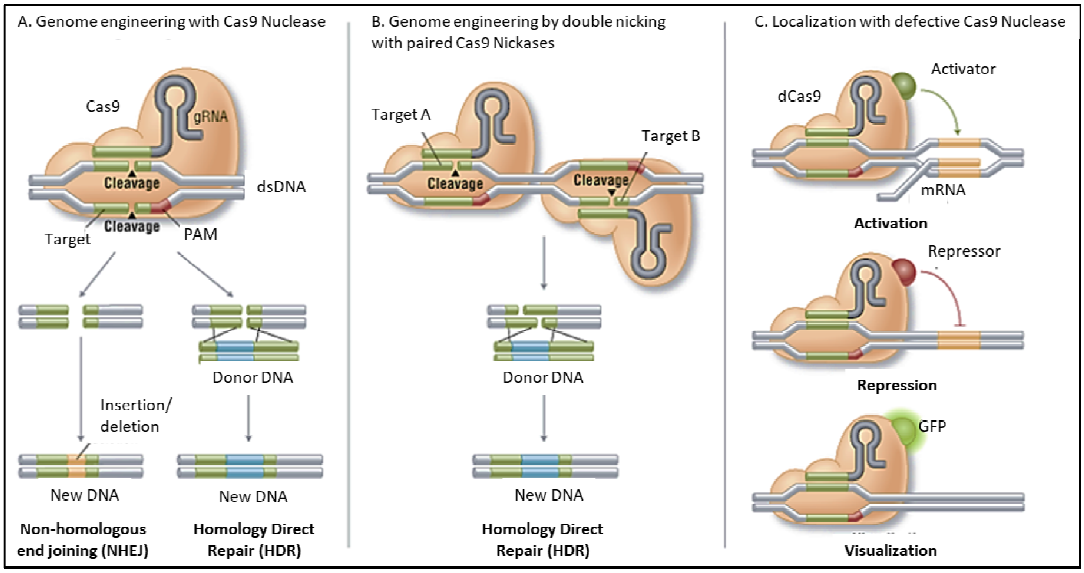

Reis et al., 2014

Fig 23. Overview of various Cas9-based applications. The WT form (A), induces indel mutations through the NHEJ repair pathway or specific sequence replacement or insertion, by the HDR activation in the presence of a donor template. Cas9 nickase, as mutated in one of the two nuclease domains (B), produces a single strand break and can improve the HDR when delivered in pairs into the cells. The dCas9 (C) has lost the cutting activity because both nuclease domains are mutated. dCas9 can be use as gene repressor or activator, if fused to activator/repressor domains or as a reporter when fused to fluorescent proteins (GFP) enabling the imaging of specific genomic loci.

Protospacer Adjacent Motif (PAM)

Targeting and DNA cleavage by Cas9 requires a short (3–9 bp) sequence motif located immediately downstream the target DNA locus, and that it is not recognized by the 20-nt guide sequence. This motif is termed Protospacer Adjacent Motif (PAM) (Wu et al., 2014).

PAM vary, according to Cas9 orthologues, in different prokaryote species. For biotechnological applications, the simplest and most commonly used system is the one derived from *S. pyogenes*, comprising the Cas9 enzyme that recognizes the 5'-NGG PAM sequence (Jinek et al., 2012).

Mismatches within or nearby the first few nucleotides of PAM inhibit heteroduplex formation and resulted in a decreased cleavage efficiency (Sternberg et al., 2014).

Species/Variant of Cas9	PAM Sequence
Streptococcus pyogenes (SP); SpCas9	NGG
SpCas9 VRER variant	NGCG
SpCas9 EQR variant	NGAG
SpCas9 VQR variant	NGAN or NGNG
Staphylococcus aureus (SA); SaCas9	NNGRRT NNGRR(N)
Neisseria meningitidis (NM)	NNNNGATT
Streptococcus thermophilus (ST)	NNAGAAW
Treponema denticola (TD)	NAAAAC

Tab 9. Different types of PAM sequences recognized by Cas9 orthologues. Cas9 proteins with more stringent PAM sequences may result in fewer off-target effects. Indeed, cleavage requires a sequence less frequently distributed in the genome then the most used 5'NGG PAM of the *S. pyrogenes* system.

guide RNA: crRNA-tracrRNA or sgRNA

To achieve site-specific DNA recognition and cleavage, Cas9 must be complexed with both the crRNA and the trans-activating crRNA (tracrRNA), that is partially complementary to the crRNA (Kotani et al., 2015). This interaction creates an RNA secondary structure in which the 5'- 20 nts of the crRNA are available for target DNA binding, thus determining the Cas9 nuclease specificity. The bulk of the tracrRNA downstream of the crRNA base pairing region is free to form additional RNA structures and to interact with Cas9.

Cas9 can be programmed to target a specific locus, by using a single engineered chimeric RNA that retains the base-pair interactions occurring between the tracrRNA and the crRNA. This single transcript effectively fuses the 3' end of crRNA to the 5' end of tracrRNA, thereby mimicking the dual-RNA structure required to guide site-specific DNA cleavage by Cas9. The so-called single guide RNA (sgRNA) displays all the features needed and sufficient for targeted DNA cleavage and induce efficient genome editing (Hwang et al., 2013).

The "seed" region (8–12nt) located at the 3' end of the protospacer sequence of the target DNA is crucial for the interaction with crRNA and subsequent cleavage by Cas9. Therefore, mismatches at the 3' of the protospacer, adjacent to the PAM site, are less tolerated than those in the 5' region of the sequence.

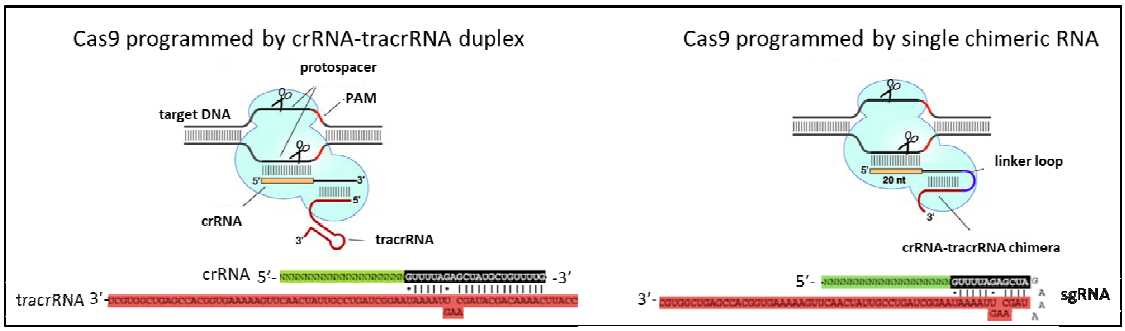

adapted from Hyongbum and Jin-Soo, 2014

Fig 24. gRNA systems. CRISPR RNA (crRNA) and trans-activating crRNA (tracrRNA) form the dual RNA complex naturally occurring in prokaryotes (left) to bring Cas9 on the target. Alternatively, a single-chain guide RNA (sgRNA) derived from the fusion of crRNA with tracrRNA can be used to bring for the complex with Cas9 (right). In green are the 20nt necessary for the DNA target base pairing within the crRNA (green and black). In red is the tracrRNA. In the sgRNA is also visible the small loop allowing the fusion of the two RNA molecules.

The simplicity of CRISPR/Cas9 systems is the reason of its widespread use. Complicated protein engineering is not necessary since Cas9 remains the same and mutagenesis can be directed to diverse genomic locations by simply changing the sgRNA. Nowadays several libraries of gRNAs, consisting of ~64,000 to ~87,000 guides, are available, and several web tools are dedicated to the assisted-design of gRNA (Varshney et al., 2016). gRNAs can be chemically synthetized and purchased in the form of crRNA:tracrRNA, or *in vitro* transcribed in the form of sgRNA.

The ~100 nt long sgRNA, with over 50% G/C content and with a guanine nucleotide adjacent to the PAM motif, ensures high rates of mutagenesis and can be easily prepared by annealing two complementary oligonucleotides followed by *in vitro* transcription (Ran et al., 2013). The choice of the promoter used to express gRNAs can limit the options for potential target DNA sites. The T7

promoter requires that the transcribed RNA initiates with GG, therefore the sgRNA should have the 5'GGN18N- form. Considering that the PAM motif recognized by Cas9 is NGG, gRNAs expressed from T7 promoter are limited to target sites matching the sequence 5'GGN18NGG; such sites are expected to occur every 1 in 128 bp in the genome. On the contrary, SP6 promoter is more flexible than the T7, tolerating a G/A change at the first two positions from the transcription start site. The derived sgRNA can therefore target site matching the form 5'-(G/A)(G/A)-N18-NGG-3', extending the theoretical targeting range to 1 site every 32 bps (Hwang, et al., 2013).

The efficacy of gene editing depends on the easiness with which a modification 'threshold' is achieved. This parameter is influenced by the efficiency of delivery of genome editing molecules, the DSB repair pathway used and the fitness of the edited cells in comparison to the parental one. The rate of editing is greatly influenced by the success of nucleases and/or donor templates delivery. CRISPR/Cas9 system can be delivered *in vitro* into cultured cells, or *in vivo* into embryos or whole organisms. To do that, several approaches can be used, including electroporation, liposome transfection, microinjection, transduction by non-integrating viral vectors and recombinant purified proteins (Liu et al., 2017).

Finally, to increase the successful rate of gene editing it is also essential to avoid deleterious and permanent off-target mutations. Experiments of whole-genome sequencing of Cas9-edited cell lines revealed a low incidence of off-target mutation, suggesting a good specificity of Cas9-mediated genome editing. However, the presence of subsets of off-target sites with high sequence similarity to the target must be carefully evaluated by computational analysis before the choice of the gRNA (Hruscha et al.,2013).

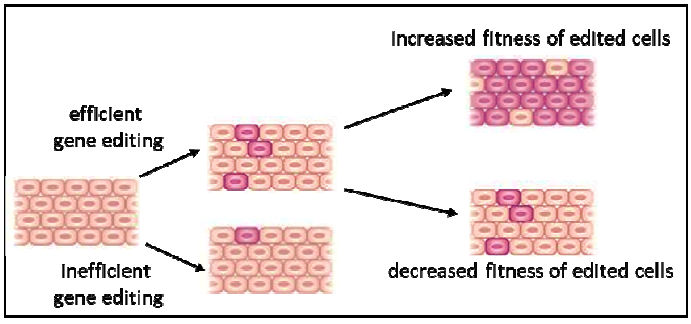

adapted from Cox et al., 2015

Fig 25. Efficiency of genome editing in target cells. Genome editing efficiency in cultured cells depends on the starting number of edited cells (depicted in pink) and by the acquisition or loss of fitness consequent to editing. Unedited cells are depicted in brown

Despite some challenges and possible drawbacks, CRISPR/Cas9 system represents an effective and versatile biotechnological tool, which has and will continue to have significant impact in genome engineering, especially for the generation of new animal models.

1.4.2.3 CRISPR/Cas9 in zebrafish

For decades, the mouse has been the most popular model organism in validating the function of genes, even though large-scale validation of candidate genes in mice is limited by many factors, such as the small number of progeny, the lethality of many KO in utero, and the cost of animal housing.

A promising alternative for functional genomics analysis is represented by zebrafish for several aspects, such those widely described above (paragraph 1.3).

In addition, the zebrafish genome, along with the mouse and human genomes, has been sequenced to a degree that can be considered ‘‘complete” (Howe et al., 2013; http://www.ensembl.org/Danio_ rerio/Info/Index).

Furthermore, zebrafish is particularly amenable to genetic studies. KD, KO and KI models are used to study gene function and evaluate the correlation with the human ones. A recent, large-scale exome-sequencing project aimed at identifying genes putatively causing developmental disorders was performed using morpholino-mediated KD (Deciphering Developmental Disorders Study 2015). However, morpholino caused significantly more off-target induced phenotypes than what previously believed (Kok et al., 2014). Indeed, 80% of the morphant phenotypes were not recapitulated by an actual genetic KO of the matching gene, meaning that most of the KD phenotypes are the result of off-target events.

Many genomic projects are therefore now based on ZFNs, TALENs and CRISPR/Cas9 systems, three genome-engineering platforms that have been successfully exploited in zebrafish, to systematically targeting human disease-related genes. In addition, many of the reagents and protocols for generating these customized DNA nucleases are freely available. Among these three approaches, ZFNs and TALENs, even if well working in zebrafish (Doyon et al., 2008; Bedell et al., 2012), are very challenging to design. Conversely, customized CRISPR/Cas9 displays an easier design and a substantial reduced cost. Importantly, CRISPRs were significantly more efficient in generating genetic mutations in zebrafish when compared to ZFNs or TALENs. Indeed, to identify germline-transmitting founders with ZFNs or TALENs, it is typically necessary to screen 60 embryos/founder while for CRISPR, 10 embryos are enough (Zhang et al., 2018). In addition, since the CRISPR/Cas9 system can target multiple genomic loci, it increases the mutagenesis throughput 10-fold and reduces the animal husbandry needed to identify single mutant carriers. Multiplexing can be also relevant considering that zebrafish frequently have duplicated paralogs or functionally redundant genes (Jao et al., 2013). Another important advantage regards the possibility to mutate with success target sites located in genomic locus previously shown untargetable by TALENs. This was established by the first pioneer study of CRISPR/Cas9 genome-editing in zebrafish, which has displayed the robustness and power of the CRISPR/Cas9 platform (Hwang et al., 2013).

Using zebrafish embryos, CRISPR RNA guided nuclease (RGN) can effectively introduce indel mutations by the NHEJ, so that gene function is lost (targeted gene knock-out) or may introduce specific mutations by the HDR (targeted gene knock-in) (Li et al., 2016).

Mosaic (or chimera) embryos, derived by the micro-injection of CRISPR components, are screened to evaluate mutations rate in various manner such as the T7EI mismatch assay, Surverior assay, high resolution melt (HRM) analysis, PCR subcloning and sequencing (Dahlem et al., 2012; Chang et al., 2013). The indel mutation rate derived from NHEJ repair pathway can be about 75–90%.

Therefore, less than 10 embryos are enough to determine the F0 indel mutation rate and the following germline transmission (Jao et al., 2013). On the contrary, homology directed repair has a much-reduced efficacy. Homologous recombination rate is estimated at 10-15% in chimeras and only 1-3% occurs in the germline. Consequently, a much higher number of zebrafish must be screened to identify those in which the desired mutation is present in the germline and can therefore transmitted to the progeny.

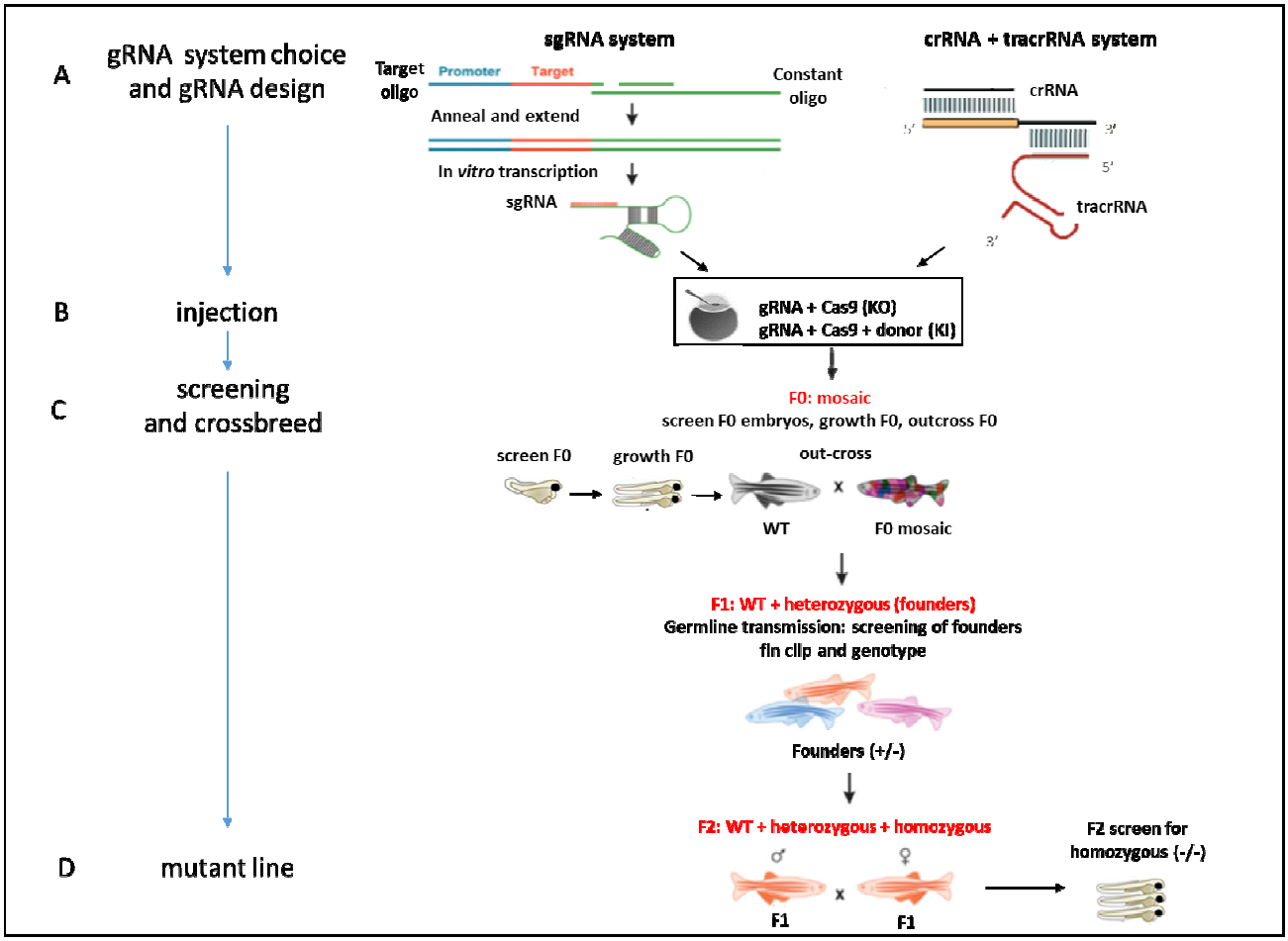

adapted from Varshneyetal, 2015

Fig 26. Strategy for zebrafish genome engineering with CRISPR. Workflow depicting the steps in a zebrafish CRISPR/Cas9 genome editing experiment. The gRNA can be used as both a sgRNA or as crRNA:tracrRNA (A). The gRNA is injected together with Cas9 protein or cas9 mRNA into 1/ 2-cell stage zebrafish to generate a KO. To activate the HDR and generate a KI (B), the system needs to be co-injected with a donor template. Mutagenesis efficiency is evaluated for each gRNA using different methods including T7 endonuclease, heteroduplex mobility shift assay (HMA), and sequencing. Successfully mutagenized F0 animals are raised to adulthood and crossed to WT animals. F1 animals are genotyped, sequenced and crossbred to fix the mutation (C). In the F2 progeny, mutated homozygous can be identified and phenotype-genotype correlations can be carried out (D).

It is important to underline that even if gene KO is a fundamental mechanism for deciphering protein function *in vivo*, most KO genes did not display a readily observable embryonic phenotype (Kettleborough et al., 2013). This effect most likely represents the general limitations of the single gene inactivation in assessing human disease. Indeed, there are a variety of ways in which mutations can influence protein function and reflect on pathology.

To facilitate the generation of human disease models and to enable functional analysis of different protein domains, HDR-mediated precise gene editing is a valuable approach. However, the establishment of pure animal lines with specific point mutations is still a challenging task because of the still low efficiency (Zhang et al., 2018).

Furthermore, because the efficiency of NHEJ in inducing indel is much higher than that of HDR-induced point mutations, it is often difficult to identify the latter in the background of indel mutations. The commonly used genotyping methods mentioned before, are all powerful tools to detect mutations; however, it is difficult to use them to differentiate specific HDR mutations and in particular to separate them from the indel ones.

To evaluate if the HDR mutations are present in F0 and subsequently to check if they occurred also in the germline, it is possible to introduce in the donor template not only the mutated sequences but also silent mutations. This would allow for the design of mutant-specific primers that only detect the mutated sequence of interest, introduced by HDR, without amplifying indels and WT sequence.

Finally, to further improve germline transmission of HDR-induced point mutations, several key factors and manoeuvres may be used to modulate the HDR efficiency such as:

- the use of SCR7, an inhibitor of the DNA ligase IV, that joins the ends of DNA break (thus suppressing NHEJ) and of RS-1, a stimulator of Rad51, that promotes HDR (Chu et al., 2015; Ma et al., 2016).

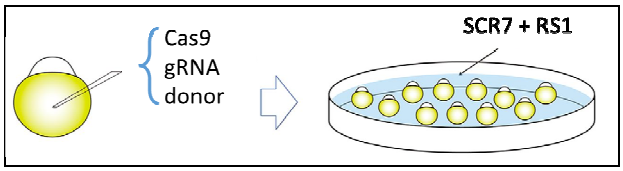

Zhang et al., 2018

Fig 27. SCR7 and RS1 to improve HDR pathway. After the injection of the CRISPR/Cas9 systems and the donor template, a combination of the two molecules is added in a concentration useful to increase the HDR without determine off target effects on zebrafish embryos due to NHEJ activation.

- the choice of the type of DNA donor (ssDNA dsDNA, or plasmid). ssDNAs contain flanking sequences, of at most 20-50 bp on each side, that are homologous to the target region. They can be oriented in either the sense or antisense direction, relative to the target locus, and it is showed that different orientations can influence the efficiency (Armstrong et al., 2016). Nonetheless, there is no consensus on the better strand to use. Other studies suggest that the injection of a plasmid with longer homology arms of at least 800 bp, flanking the desired mutation, can increase the efficacy of the system (Irion et al., 2014) However, the results are so far controversial, probably because of sequence-dependent effects.

- the control of the timing for Cas9 expression, as it has been reported that the germ line cells in zebrafish are concentrated in the primordial germ cells (PGCs) from 32-cell stage. However, since PGC cells undergo asymmetrical mitosis, their proportion decreases with embryonic development. This suggests that earlier HDR starts, higher probability for HDR to occur in the germ cells there is. Moreover, the embryonic development is much faster in the zebrafish than in mammals; hence, a little time gap will lead to great difference in editing efficiency in the germline (Zhang et al., 2018; Kimmel et al., 1995). By using Cas9 protein instead of mRNA, the efficiency of HDR germline transmission increases about six times. This could be due to the immediate availability of Cas9 protein in early phases of embryonic development when the cell number is still low, leading to increased chance for editing events to occur in the germ cells (Ma et al., 2016).

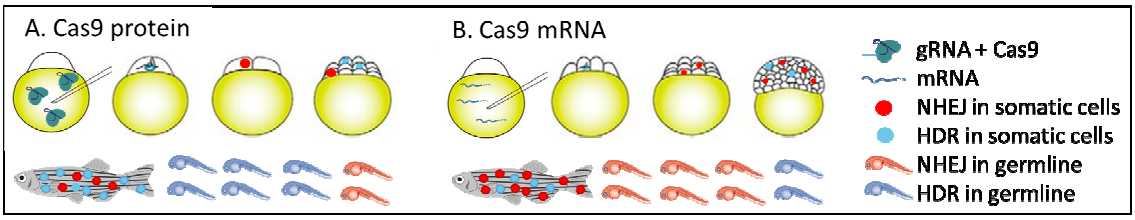

Zhang et al., 2018

Fig 28. comparison of germ line mutation transmission between the use of Cas9protein and Cas9mRNA. Cas9 protein (left pannel) promotes mainly HDR pathway as evidenced by an higher level of light blue dots. This allow an higher germline trasmission of the precise modification produced by HDR (blue embryos) in comparison to the Cas9 mRNA (right pannel).

2. AIM OF THE PROJECT

Sarcoglycanopathies are rare autosomal recessive limb girdle type 2 dystrophies (LGMD2C-F) due to mutations in *SGCA, SGCB, SGCD* and *SGCG* genes coding for α-, β-, δ- and γ-sarcoglycan (SG) respectively. SGs assemble into a single unit within the dystrophin-associated protein complex (DAPC), assuring sarcolemma stability during muscle contraction. The most frequently reported mutation in sarcoglycanopathy are missense mutations. The presence of a single amino acid substitution yields to a folding defective protein recognized by the QC machinery and degraded by the ubiquitin-proteasome system. Although structurally defective, SG mutants are still functional. Indeed, by saving mutants from degradation or by assisting/promoting their folding, the SG-complex can reach and strengthen the sarcolemma. Established the proof of concept *in vitro*, now these pharmacological approaches need the *in vivo* validation. Unfortunately, the currently available animal models are unsuitable for this purpose. Therefore, my work was mainly focused on the generation and characterization of novel models of β- and δ-SG sarcoglycanopathy in zebrafish (*D. rerio*). In the absence of rodent models, zebrafish appears the ideal vertebrate for modelling sarcoglycanopathy. Indeed, in addition to the advantages of this fish over mammals in terms of size, rapid development, large numbers of offspring, zebrafish and mammals have high similarity in gene sequences, conservation of cellular pathways, concordance in developmental phenotype and almost indistinguishable muscle tissue. Moreover, it is becoming easy to manipulate the zebrafish genome by the CRIPSR/Cas9 technology, allowing the generation of both KO and KI models. Finally, thanks to the ability to absorb drugs dissolved in fish-water, and vertebrate biological relevance, zebrafish is an ideal model for testing new drugs (in small, as well as large-scale) not feasible in mammals due to cost, time required and ethical concerns.

β- and δ-SG have been chosen for editing through the CRISPR/Cas9 technique because they are the most conserved SG orthologues. Moreover, knock down experiments resulted in skeletal and cardiac abnormalities, well mimicking the most severe forms of LGMD2E and 2F. Finally, emerging evidence indicates that the ERAD elements and the ubiquitin-proteasome system, responsible for the premature degradation of SG mutants in mammals, are conserved and active in zebrafish.

On these premises, by using the CRISPR/Cas9 system, I have generated and characterized β- and δ-SG KO lines whereas the generation of β-SG and δ-SG KI lines is ongoing. Null-SG zebrafish will mainly serve for the transient expression, by oocyte injection, of mutated sequences of β- and δ-SG and will permit to evaluate the ability of the zebrafish ERAD to recognize and degrade a folding defective SG. Moreover, they will permit to enlarge the number of SG mutations that can be tested for the recovery by pharmacological treatments.

In addition to be a fundamental tool to test *in vivo* our pharmacological approach for sarcoglycanopathy, the novel zebrafish models of sarcoglycanopathy will represent a valuable adjunction to the currently existing vertebrate models for basic and translational research. Moreover, they could become a versatile platform for any future *in vivo* screening of libraries composed of approved drugs as well as novel compounds.

3. MATERIALS AND METHODS

3.1 Animals husbandry and maintenance

Zebrafish were maintained in the facility of the University of Padova according to the standard protocols described by Kimmel et al.,1995. Fish are kept at 28,5°C in conditioned saline aerated aquaria system (Aquarienbau Schwarz, GöttingenC Germany; ZebTech, TECNIPLAST; MüllerCPfleger) with a photoperiod of 12 hours of light and 12 of dark. Fish received the amount of food per day equivalent to the 4% of their body weight, with three daily rations, one with dry food (TetraMin) and twice with living *Artemia salina* nauplia. In about three months fish reach sexual maturity. Male and female were mated in the afternoon, divided by a transparent plastic separator, that is removed the day after when the coupling began. After the eggs deposition and fecundation, they were maintained at 28°C in fish water (0.5 mM NaH2PO4, 0.5 mM NaHPO4, 0.2 mg/l methylene blue, 3 mg/l instant ocean pH7/8). From 6-10 days post fertilization (dpf) zebrafish *larvae* were fed once a day with dry Artemia powder (Novotom, JBL).

3.2 Ethics statement

This study was carried out in accordance with the recommendations in care and use of laboratory animals of the Italian Parliament L.LGS n26/2014. All procedures on animals were approved by the Italian Ministry of Health n.753/2018-PR.

3.3 Antisense Morpholino Oligonucleotide (MO) design and injection

To KD the expression of δ-SG by blocking its translation, zebrafish WT zygotes are injected with a published MO against the δ-SG mRNA starting translation region (δ-SG_{AUG}MO) (Cheng et al., 2006). The δ-SG_{AUG}MO (300 nmol) is ordered from Gene Tools, LLC (Philomath, OR) and 1mM stock solution is prepared and stored at -20°C. On the day of injection, the MO is heated at 65°C for 5 min to denature any secondary structures of the oligo, cooled on ice and spun briefly. The δ-SG_{AUG}MO working solution is injected with concentrations ranging from 0,1 mM to 0,3 mM, with 1X phenol red dye and 1X Danieau injection buffer. Zygotes eggs were arranged along the wedge-shaped troughs in the microinjection chamber plate. The working solution is placed in a hypodermic needle to penetrate the chorion and 8 nL of the solution were released in the zygote. The injection was performed by using a WPI pneumatic PicoPump PV820 injector. As control a standard morpholino (StdMO) was utilised.

3.4 CRISPR CAS9 design and injection for Knock-out production

The sgRNA (table 14 at the end of the chapter) were designed by using the chop-chop software (http://chopchop.cbu.uib.no/). The guides with the lowest level of off target event and the highest score in matching the desired sequence are selected. The sgRNAs are produced according the protocols of Gagnon et al., 2014 by using the MEGAScript kit SP6 (Ambion). Zebrafish WT zygotes are injected with 8 nl of a solution containing 70 ng/µl of sgRNA, 300 ng/µl of Cas9 NLS (Nuclear Localization Signal) protein (Neb), 1X Phenol red dye and 1X Danieau injection buffer by

using a WPI pneumatic PicoPump PV820 injector. Some uninjected embryos are kept as control and both groups were grown at 28.5°C in fish water.

3.5 CRISPR CAS9 design and injection for Knock-in production

The sgRNA were designed by using the chop-chop software (chopchop.cbu.uib.no/) (Labun et al., 2016). The guide with the lowest level of off target event and the highest score in matching the desired sequence is selected. The sgRNAs (β-SG^{T145R}KI guide1, δ-SG^{E264K}KIguide1; δ-SG^{E264K}KIguide2) are produced according the protocol of Gagnon et al., 2014 by using the MEGAScript kit SP6 (Ambion). All the gRNA in the form of crRNA:tracrRNA (β-SG^{T145R}KI guide1, β-SG^{T145R}KI guide2) were purchased from IDT DNA Technologies (Chen et al., 2014) . The gRNAs are reported at table 15 at the end of the chapter.
The donor templates (see tables 16 and 17 for the sequence of the donor employed) harbouring the desired mutations β-SG$^{T145R/T145R}$ and δ-SG$^{E264K/E264K}$ present also silent mutation to avoid the re-cutting of the donor after its insertion by Cas9 enzyme, and a diagnostic restriction site for HindIII and DraI respectively. Silent mutations were designed taking into account the zebrafish codon usage (https://www.kazusa.or.jp). ssDNA donors were synthesized by Sigma Aldrich or IDT DNA Technologies. All the donors were synthesized with phosphorothioate linkages at their ends, to prevent degradation by cellular exonucleases. For β-KI, also a double strand donor was constructed amplifying a 1600 bp region of the beta SG gene, extending from intron 2 to intron 5, with the following primers:

Fwd 5'-AAACGAATTTATGTTCATCAGAGTG-3'
Rev 5'-TCAGGTCAGTATCCTCAGCAGT-3'

The resulting PCR product was cloned into the PCRII vector (Thermo Fisher). A first round of site directed mutagenesis was performed to introduce the mutations ablating the PAM sequence and the seed region with the following primers:

Fwd 5'-GTAAATTACAGGTGGTATTtaGaCAGGGaAACACAAAGCTGA-3'
Rev 5'-TCAGCTTTGTGTTGCCCTGtCtaAATACCACCTGTAATTTAC-3'

A second round of mutagenesis was performed to introduce the mutations changing the Threonine 145 in Arginine and introducing the diagnostic HindIII restriction site with the following primers:

Fwd 5'- ATTtaGaCAGGGaAACAgAAAGCTtAGTGTAGAGGAAGATAA-3'
Rev 5'-TTATCTTCCTCTACACTaAGCTTTcTGTTtCCCTGtCtaAAT-3'
(in lower case are reported the nucleotide changed with respect to the WT sequence).

This construct was used in conjunction with β-SG^{T145R}KI guide1. Starting from this plasmid, another construct was generated for the use with β-SG^{T145R}KI guide2. Mutations altering the PAM sequence and the seed region recognized by β-SG^{T145R}KI guide2 were introduced by mutagenesis

using the following primers:

Fwd 5'- CAgAAAGCTttcaGTcGAaGAAGATAAGACGTCTATT-3'
Rev 5'- AATAGACGTCTTATCTTCtTCgACtgaaAGCTTTcTG-3'

All constructs were verified by sequencing. The plasmids for the injection were purified with a midi prep kit (Qiagen).
Zebrafish WT zygotes are injected by using a WPI pneumatic PicoPump PV820 injector. About 8 nl per embryo were injected and some uninjected embryos are kept as control. Both pools were grown at 28.5°C in fish water. Considering the difficulty in KI generation, several techniques were used:

- injection of working solution with 70ng/µl of sgRNA, 300ng/µl of Cas9 protein, 50ng/µl single strand oligo (ssDNA) donor template, 1X Phenol red dye and 1X Danieau injection buffer. The sgRNAs are produced according the protocol of Gagnon et al., 2014 by using the MEGAScript kit SP6 (Ambion).
- injection of working solution with 70ng/µl of sgRNA, 300ng/µl of Cas9 protein, 50 ng/µl plasmid donor template (800 nt each arm) 1X Phenol red dye and 1X Danieu injection buffer. The sgRNAs are produced according the protocol of Gagnon et al., 2014 by using the MEGAScript kit SP6 (Ambion).
- injection of working solution with crRNA:tracrRNA, Cas9 and donor templates. CrRNA e tracrRNA were preannealed before the injection: 300 pmoles of crRNA were mixed with 300 pmoles of tracrRNA in 100 µl nuclease free duplex buffer (IDT), heated at 95°C for 5 minutes and allowed to cool to room temperature. Afterward, 3 µl of the resulting crRNA-tracrRNA complex were mixed with 3 µl of Cas9 (IDT DNA Technologies) protein 0.5 µg/µl, and incubated at 37°C for 10 min. To this RNP complex, were added 50 ng of DNA donor, 1X Phenol red dye and 1X Danieau injection buffer. To ameliorate the efficacy of KI, these injected embryos are also treated with SCR-7 (Sigma-Aldrich), able to block the NHEJ, and with RS-1 (Sigma-Aldrich), to increase the HDR activity (Zhang et al., 2018). The molecules were dissolved in DMSO at a concentration of 20 mM and added after the injection diluted 1:1000 in fish water. After 6 hours of treatments the water with molecules was replaced with fish water.

3.6 cDNAs expression constructs and injection

Human β- and δ-SG cloning and mutagenesis:
pCDNA3.1 DYK (flag tag) vectors coding for full length human β- and δ-SG were purchased from Genscript. The cds for beta and delta SG were transferred from pcDNA3.1 DYK to the pCS2+ vector by PCR amplification with primers harboring appropriate restriction enzyme sequences.
Mutagenesis to generate human βSG-T151R was performed with the following mutagenic primers:
Fwd 5'-GTTTTTCAGCAAGGGACAAgAAAGCTCAGTGTAGAAAAC-3'
Rev5'- GTTTTCTACACTGAGCTTTcTTGTCCCTTGCTGAAAAAC
Mutagenesis to generate human δSG-E262K was performed with the following mutagenic primers:
Fwd 5'- AGGCAGAAGGTCTTCaAGATCTGCGTCTGCG-3'

Rev 5’- CGCAGACGCAGATCTtGAAGACCTTCTGCCT -3’

Zebrafish β- and δ-SG cloning and mutagenesis:
Total RNA was extracted from 100 mg of muscular tissue of adult zebrafish with TriSure reagent (Bioline). 1 µg of total RNA was reverse transcribed with BioLine Sensifast cDNA synthesis kit. The amplification of the full-length cDNA coding for δ-SG was performed with Accuprime Pfx (Thermo Fisher) with the following primers harboring KpnI sequence at their 5’ ends:
Fwd 5’- TAAGCTGGTACCATGATGACCCAGGAACAGTGC-3’
Rev 5’- AGCTTAGGTACCGAGGCATAAGTTGCTGCTCATC-3’.
The resulting PCR product was cloned in pCDNA3 HisTop (6X His tag) after digestion with KpnI.
Mutagenesis to generate δE264K was performed with the following primer:
Fwd 5’-CGAGACAGACTGTCTTTaAaGTGTGTGTCTGTCCCAA-3’
Rev 5’-TTGGGACAGACACACACtTtAAAGACAGTCTGTCTCG-3’
Amplification of β-SG was performed with the following primer, harboring XhoI sequence (fwd) and PstI sequence (rev):
Fwd 5’-TAAGCTCTCGAGATGGCGTCGGAGCAGGAAATCTCA-3’
Rev 5’- AGCTTACTGCAGGTGCGCTGCCCCACACGG-3’
The resulting PCR product was cloned in pCMV-Flag vector. Mutagenesis to generate βT145R was performed with the following primers:
Fwd 5’-ATTCCGGCAGGGCAACAgAAAGCTGAGTGTAGAGG-3’
Rev 5’-CCTCTACACTCAGCTTTcTGTTGCCCTGCCGGAAT-3’

All WT and mutated zebrafish cDNA were transferred by PCR to the pCS2+ vector for *in vitro* transcription. All mutagenesis reactions were performed with the GeneArt Site Directed Mutagenesis kit (Thermo Fisher) according to the manufacturer’s instruction. All constructs were verified by sequencing. For zebrafish injections, plasmids were purified with midi prep columns (Qiagen). A solution of plasmid ranging from 10 to 50 ng/µl were prepared with Danieau solution and phenol red.

3.7 mRNAs production and injection

WT and mutated mRNA are produced for the injection. The first is utilized to rescue the fish phenotype, while the second will be utilise to study the activity of CFTR correctors. cDNAs coding for full length beta or delta SG, WT or mutated, were cloned into the pCS2+ vector. The vectors were linearized with NotI, and *in vitro* transcribed with the Sp6 mMessagemMachine kit (Thermo Fisher) according to the manufacturer’s instruction. The resulting capped mRNA was purified by LiCl precipitation and re-suspended in nuclease free water. The quality of the mRNA was evaluated running an aliquot on a denaturing polyacrylamide gel with 8M urea. The concentration of the mRNA was evaluated by UV spectroscopy with a Nanodrop spectrophotometer (Thermo Fisher). Different concentrations are tested 150-,100-,50 ng/µl in a working solution composed also of 1X phenol red dye and 1X Danieu injection buffer. The injection was performed by using a WPI pneumatic PicoPump PV820 injector.

3.8 DNA extraction

The genomic DNA was prepared by using the HotSHOT protocol (Meeker et al., Biotechniques 2007). DNA was extracted both from the tail of adult fish and from the whole embryos at 48 hours post fertilization (hpf).

- For the embryos the dechorionation is not necessary. Each embryo was placed in a tube with a 0,16 mg/ml tricaine solution in fish water. After 2 min, tricaine is discarded and the tube is filled with 50 µl DNA lysis buffer (NaOH 50 µM). Tubes are heated at 95 °C for 20 min, cooled at 4°C for 5 min, and 5 µl of Tris HCl 1M pH 7,5 were added to neutralize the DNA sample. To determine the somatic indel frequency the DNA is extracted from 9 embryos and 1 WT as control.
- The adult fish are anesthetized with 0,16 mg/ml tricaine MS-222 solution until gill movement is slowed. A small piece from the end of the tail is cut with a bistoury and transferred into a tube with 50 µl of DNA lysis buffer. Quickly the fish is placed in tank with fresh water for the recovery. The tube is labelled in the same manner of the tank with the corresponding fish. Tubes are heated at 95 °C for 20 min, cooled 5 min at 4°C, ant 5 µl of Tris HCl 1M pH 7,5 were added to neutralize the DNA sample.

3.9 Genotyping of sarcoglycan mutants

3.9.1 PCR for KO

All PCR amplicons are usually 150-200 bp. PCR was performed in a 20 µl total volume reaction with 10-200 ng of genomic DNA template, extracted respectively from embryos or adult tail, 5µM of each primer, 10 µl of a 2x PCR Master Mix (Thermo Fisher, 0.05 U/µl Taq polymerase, buffer, 0.4 mM of each dNTPs, 4 mM magnesium chloride). Primers were designed by primer design software (*Primer blast*). Initial denaturation at 95 °C for 5 minutes was followed by 35 cycles of 30 seconds at 95 °C, 30 seconds at 60 °C, 30 seconds at 72°C, ending with a final extension of 5 minutes. The PCR product was confirmed by analysis of its size running 5 µl on a 2% agarose gel. In the following table are reported the primers used for the β-δ SG KO amplifications.

primers	sequence
β-SG$_{ex2}$KO	
FW	5'-CAAATGTCCACAGGAAATCTCA-3'
RV	5'-AATGAGAGCAAGCAGAAAAAGC-3'
δ-SG$_{ex1}$KO	
FW	5'-CCATCTTTAAGGGGTGTCAGAG-3'
RV	5'-GAATCTGAATGTCCGTCTGTCA-3'
δ-SG$_{ex2}$KO	
FW	5'-ACAGTGCCCTCATAGGAACAAT-3'
RV	5'-CTTCTAAAGGCGGTTCAAAGAA-3'

Table 10. List of primers

To distinguish between WT, homozygotes and heterozygotes, in F1 or F2 two concomitant amplifications are performed. The first is performed with primers able to amplify only a WT sequence, while in the second the amplification occurs only if the INDEL mutations are present. In the presence of a heterozygote sequence both amplification will occur. The 20 µl total volume reaction is performed with 30 ng of genomic DNA template, extracted from embryos, 5 µM of

each primer, 10 µl of 2x PCR Master Mix (Thermo Fisher, containing 0.05 U/µl Taq polymerase, buffer, 0.4 mM of each dNTPs, 4 mM magnesium chloride). Primers are designed by primer design software (*e.g. Primer blast*). Initial denaturation at 95 °C for 5 minutes is followed by 35 cycles of 30 seconds at 95°C, 30 seconds at 58°C, 30 seconds at 72°C, and a final extension at 72°C for 5 minutes. The PCR product is confirmed by analysis of its size using 2% agarose gel electrophoresis: 15µl of sample are loaded and the run is performed at 80V.
In the following table are reported the primers used for the β-SG$_{ex2}$KO amplifications.

primers	sequence
β-SG$_{ex2}$KO	
FW WT	5'-GGAGAGACTCCACAAGACAGGA-3'
RV	5'-CTGCATCTCTAGGAGTTTGACTGT-3'
FW MUT	5'-GAGGAGAGACTCCACAGACTCC-3'
δ-SG$_{ex1}$KO	
FW WT	5'-AGCCATGGTCAGGATGGTAAG-3'
RV	5'-TGGAGGAACCCTTTGTCTGC-3'
FW MUT	5'-ACTTGGTCAGCCATGGTTCA-3'
δ-SG$_{ex2}$KO	
WT	5'-TGTTGTGTTGCATCTTTGCATTTTGG-3'
RV	5'-GCAACGTTTCCGCCAGCC-3'
RV MUT	5'-GGCAACGTTTCCGCCGTAG-3'

Table 11. List of primers

3.9.2 Heteroduplex Mobility Assay (HMA)

Mutagenesis efficiency is tested after DNA extraction and amplification through the HMA. After denaturation at 95°C for 15' and slow renaturation, the PCR products are loaded on a 10% 29:1 polyacrylamide gel to look for additional heteroduplex bands with respect to the WT single band.

3.9.3 PCR for KI

To evaluate the efficacy of the sgRNA in cutting the DNA on exon 4 to produce the β-SG$^{T145R/T145R}$ KI and on exon 8 of δ-SG to change the 264 aa E with K, an amplification with specific primers for β- and δ-SG is performed. The 20 µl total volume reaction is performed with 30 ng of genomic DNA template, extracted from 9 injected embryos and a WT as control, 5 µM of each primer, 10 µl PCR Master Mix (Thermo fisher, 0.05 U/µl Taq polymerase, buffer, 0.4 mM of each dNTPs, 4 mM magnesium chloride). Initial denaturation at 95 °C for 5 minutes is followed by 35 cycles of 30 seconds at 95°C, 30 seconds at 60°C, 30 seconds at 72°C, ending with 95°C for 4 minutes and cooled to 15°C. The PCR product is confirmed by analysis of its size using 2% agarose gel electrophoresis, 5µL of sample are loaded and the run is performed at 80V.

primers	sequence
β-SG$^{T145RKI/T145R}$ KI	
FW	5'-AAAGTGTATTGATCCAGGCGAT-3'
RV	5'-GTAAGGACAATGAGTGTGAGCG-3'
δ-SG$^{E264K/E264K}$ KI	
FW	5'-TCCCAACGGAAAACTCTTCTTA-3'
RV	5'-GAATCTGAATGTCCGTCTGTCA-3'

Table 12. List of primers

F1 embryos are used for the screening of positive fish at homology directed repair. 10 ng of purified DNA are used for the amplification with a primer called genotype (recognizing the WT sequence) and an allele specific oligonucleotide (ASO) primer recognizing only the mutated sequence. ASO primer were designed with their 3' sequence recognizing the mutation introduced to alterate the PAM sequence or the seed region sequence. The selectivity of ASO primer for the mutated sequence was initially checked amplifying a control plasmid containing the mutated (generated by site directed mutagenesis) or the WT sequence. For the screening of fish injected with the plasmid donor, the primer recognizing the WT sequence (see table 13: β-SG$^{T145R/T145R}$ KI genotype RV2) was designed in a region external to the sequence of the homology arms, to avoid the amplification of the injected plasmid. The 20 µl total volume reaction is performed with 10ng of genomic DNA template, extracted from F1 embryos, 5 µM of each primer, 10 µl PCR Master Mix (thermo fisher, 0.05 U/µl Taq polymerase, buffer, 0.4 mM of each dNTPs, 4 mM magnesium chloride). Primers are designed either manually or by primer design software (*e.g. Primer blast*).
Initial denaturation at 95 °C for 5 minutes is followed by 38 cycles of 30 seconds at 95°C, 30 seconds at 63°C, 30 seconds at 72°C, ending with 95°C for 4 minutes The PCR product is confirmed by analysis of its size using 1,5% agarose gel electrophoresis, 15µl of sample ae loaded and the run is performed at 80 mV.

Once identified positive samples, another amplification was performed with an ASO primer oriented in the opposite direction (see table 13: β-SG$^{T145R/T145R}$ KI ASO guide 1 RV) to check the presence or absence of undesired indels also on the upstream region of DNA.
In the following table are reported the primers used for the β-SG$^{T145R/T145R}$ and δ-SG$^{E264K/E264K}$ amplifications.

primers		sequence
β-SG$^{T145RKI/T145R}$ KI genotype		
	FW	5'-TGCAGCTTTGATGAATATAAGAGAC-3'
	RV	5'-GCTTTCTTAACAAAACAAAAGGTGT-3'
	RV2	5'-CGAATGAGTATGCTTTAATCAGG-3'
β-SG$^{T145RKI/T145R}$ KI ASO guide 1		
	FW	5'-TGTGTAAATTACAGGTGGTATTTAGA-3'
	RV	5'-GCTTTCTGTTGCCCTGTCTA-3'
β-SG$^{T145RKI/T145R}$ KI ASO guide 2		
	RV	5'-ACGTCTTATCTTCTTCGACTGAA-3'
δ-SG$^{E264K/E264K}$ KI genotype		
	FW	5'- CATCTTTCTCATATGCTGTGATGAT-3'
	RV	5'- AAGACGTGTCCCAGATGGAG-3'
δ-SG$^{E264K/E264K}$ KI ASO		
	FW	5'-TGCCAGAGGGAAAAGCCAGT-3'

Table 13: List of primers

3.9.4 Allele Cloning

The allele of heterozygous and homozygous fish were cloned in the pGem-T easy vector (Promega) by TA cloning, according to the manufacturer's instructions.

3.9.5 Sanger sequencing

To confirm mutants, positives samples at the HMA or cloned DNA are sequenced. An aliquot of PCR product is purified with ExoSapand sequenced with 3.2 pmoles of the forward or reverse primer. The sequences obtained are analysed for the presence of INDEL mutations for KO or for the presence of the desired point mutation for β-SG, T145R, and δ-SG, E264K.

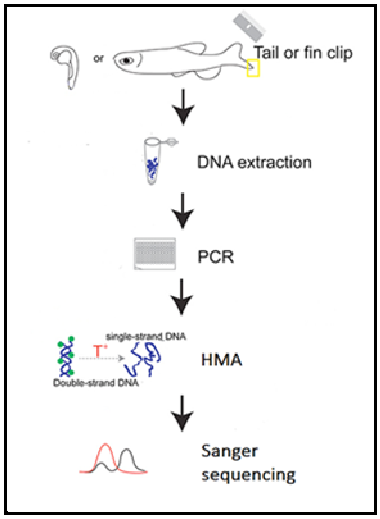

adapted from Xing, L et al., 2014

Fig 29. Protocol for zebrafish genotyping. DNA extraction from whole tissue of embryo or fin clip of adult fish is followed by PCR amplification and HMA analysis, to detect different genotypes.

3.9.6 Determination of somatic indel frequency

At 48hpf, 9 injected embryos and 1 uninjected were sacrificed for DNA extraction, PCR amplification, HMA analysis and Sanger sequencing, to evaluate the efficacy of the gRNA in inducing somatic mutations.

3.9.7 Confirmation of germline transmission

Once injected putative founders are grown to sexual maturity, reach at 3 months, they are crossbreed with WT to obtain the filial generation F1. At 48 hpf, the genomic DNA from the F1 clutches is extracted as described above from 9 embryos to evaluate if the INDEL mutations occurs also in the germline, and from 40 embryos to evaluate if the desired point mutations are acquired to the F1. The genomic DNA is screen using HMA, PCR and enzymatic digestion, and the result is confirmed by Sanger sequencing.

3.9.8 Identification of adult heterozygotes

Putative adult heterozygotes are anaesthetized, and the fin clipped. The fish are identified after PCR amplification and HMA. The results are confirmed by Sanger sequencing and cloning

3.9.9 Establishment of homozygous lines

Once heterozygotes are grown to fertile adults after 3 months can be crossbreed to obtain the filial generation F2 where the homozygotes can be identified with the technique described above.

3.10 Western Blot

The protein analysis is performed on both adult zebrafish and embryos. After anesthetizations, the protein equivalent for 10 embryos at 3- 5 days post fertilizations (dpf) for a mini gel or 15 for a larger gel are dissolved in 2 µL 2X SDS-sample buffer per embryo and incubated for 5 min at 95°C. A mechanical homogenisation is not necessary since cells dissolved rapidly in the buffer. After a

full speed centrifugation, to remove insoluble particles, the samples are loaded on a 10% polyacrylamide gel. Adult zebrafish are anesthetized and killed by cutting the head with a bistoury. The skin is removed, and muscles are dissected and mechanically homogenized with lysis buffer (SDS 3%, EGTA 0.1 mM in Tris Hcl 20 mM, pH7). The homogenates are centrifuged, quantified with BCA assay (Thermo Fisher), and boiled in SDS sample buffer. 30 µg for a mini gel and 100 µg for a larger gel are loaded per lane. Proteins are separated by 10% SDS page and blotted onto a nitrocellulose membrane (10mA, 10 min) stained with Ponceau Red for 3 min, blocked 1h in 10% not fat dry milk in PBST (0,5% Tween-20 in PBS), incubated overnight at 4°C with primary antibody diluted in 5% non-fat dry milk PBST. The day after the membrane is washed for 5 min for 4 times and incubated 1 hour with the secondary antibodies peroxidase conjugated anti-rabbit or anti-mouse IgG diluted 1:2000 in TBST milk 5%. The membrane is washed again 4 times, 5 min each, and incubated 5 minutes in ECL turbo (Euroclone). The signal was detected using an Alliance 9 Mini Chemiluminescence Imaging System (Uvitec).
Band intensities were normalized against total protein loading (evaluated by Ponceau red staining) or against β-actin.
Primary Antibodies used for Western blot

- A 43 KD anti β-sarcoglycan mouse monoclonal antibody is purchased from Novocastra (NCL-L-b-SARC) and diluted 1:200 in 5% non-fat dry milk PBST
- The polyclonal antibody 32 KD anti δ-sarcoglycan rabbit (113813 Abcam) and used at a dilution of 1:200 in 5% non-fat dry milk PBST

3.11 Whole mount immunofluorescence

Embryos at 5 dpf are fixed with 4% paraformaldehyde (PFA) in phosphate buffer saline (PBS) at 4°C overnight. Fixed embryos are transferred in methanol (MeOH) overnight at -20°C. The samples are permeabilized with acetone for 7 min -20°C and rehydrated with increasing concentration of PBS in MeOH (5min MeOH 75%, 5min MeOH 50%, 5min MeOH 25%, PBS 100%). Embryos are washed with PBTX (1X PBS + 1% Triton X 100) 3 times for 10 min, and 3 times for 30 min and blocked with the blocking buffer (10% goat serum, 0,8% Triton X-100,1% BSA in 1× PBTX) for 3 hours at 4°C. After blocking, the samples were incubated with the respective primary antibodies diluted in the incubation buffer (1% goat serum, 0,8%Triron X-100, 1%BSA in 1× PBTX) at 4°C for 2 days. The sample are washed again with PBTX (1X PBS + 1% Triton × 100) 3 times for 10 min and 3 times for 30 min. Embryos are incubated for one day at 4°C in the dark, with the secondary antibody diluted in the incubation buffer. After washing with PBTX (1X PBS + 1% Triton X 100) 3 times for 10 min and 3 times for 30 min, samples are embedded in 1,5% low melting agarose on a glass dish for acquisition of images on a confocal microscopy (Leica TCS SPE). Images are analysed with the software Fijiand transformed into TIFF images by Photoshop (Adobe systems).

Primary Antibodies used for confocal immunofluorescence:

- anti β-sarcoglycan mouse monoclonal antibody (Novocastra NCL-L-b_SARC) diluted 1:200 in I-buffer

- anti δ-sarcoglycan rabbit polyclonal antibody (generous gift from V. Nigro, University of Naples, Italy Nigro et al., 1996*b*) diluted 1:100 in I-buffer.

Secondary antibodies used for confocal immunofluorescence:

- Alexa488 goat anti-mouse (Invitrogen) diluted 1:500 in the incubation buffer for anti β-sarcoglycan.
- Alexa488 goat anti-rabbit (Invitrogen) diluted 1:1000 in the incubation buffer for anti δ-sarcoglycan

3.12 Immunofluorescence of zebrafish cryosections

Embryos of 3dpf are fixed in 4% PFA in PBS overnight at 4°C. Samples are washed in PBS 1X and permeabilized in PBTX 2% (1XPBS + Triton X 100 2%) overnight at 4°C. Embryos are blocked in BSA 1%, DMSO 1%, PBS 1X for 1 hour at room temperature (RT) and then incubated with Phalloidin (SIGMA, 2,5µg/µL in DMSO) diluted 1:1000 in PBTX 1% for 3 hours at RT. Embryos are embedded in 1,5% low melting agarose on a glass dish for acquisition on the confocal microscopy (Leica TCS SPE).

3.13 Hematoxylin & eosin adult zebrafish cryosections

Adult zebrafish are anesthetized and killed according to the standard protocol. Muscle tissue are collected and frozen in liquid nitrogen. Hematoxylin and eosin (H&E) stained sections (7 mm) are stained for 5 min each in hematoxylin and eosin, dehydrated with ethanol and xylenes, mounted with Permount, and examined by light microscopy. All sections were photographed under a Zeiss HBO 50 fluorescence microscope to characterize the skeletal muscles. Difference among the WT and δ-SGs MO pools are calculate with ImageJ software.

3.14 Immunofluorescence analysis of adult zebrafish cryosections

Adult zebrafish are anesthetized and killed according to the standard protocol. Muscle tissue are dissected out and frozen in liquid nitrogen. Seven-millimetre-thick frozen transverse sections are immunolabeled with anti β-SG (Novocastra 1:200) and anti δ-SG (Abcam 1:100) and revealed with Alexa 488 monoclonal anti mouse- and with Alexa 488 polyclonal anti rabbit-conjugated secondary antibodies respectively (Invitrogen).

3.15 Birefringence assay

Muscle birefringence was analysed by taking advantage of muscle fibres anisotropy. Anesthetized WT and δ-SGs MO embryos of 5 dpf are analysed by using two polarizing filters in a Leica M165FC stereomicroscope. The first filter allows the polarized light to illuminate the fish and the second one (analyzer), where the fish are placed, restricts detected light to refracted light coming from muscle fibres. The top polarizing filter is twisted until the light refracting through the muscle was visible.

3.16 Motor activity

3.16.1 Touch evoked escape response assay

The ability to escape after touching embryos with a small tip is evaluated at 5dpf for WT, δ-SG MO, δ-SG KOex1, δ-SG KOex2, β-SG KOex2. Fish are subdivided into four groups according to their ability to escape:

- score 3 means embryos with normal motility to swim;
- score 2 means embryos with minor motility;
- score 1 means embryos with strong motility impairment
- score 0 means embryos with no motility and ability to escape

3.16.2 Embryos locomotion assay

β-SG_{ex2}KO, δ-SG_{ex1}KO, δ-SG_{ex2}KO embryos were collected immediately after spawning and raised in fish water in a light- and temperature-controlled incubator. At 5 dpf *larvae* were placed in a 96-well plate (1 larva per well, 300 µL of FW medium) in the observation chamber of the DanioVision tracking system (Noldus Information Technology, NL). DanioVision is equipped with an IR-sensitive camera, a temperature controller unit and a power supply to control light intensity. From 5 dpf *larvae* locomotor activity was tracked for 3-4 consecutive days and then analyzed by Ethovision 11 software (Noldus Information Technology, NL). The IR-sensitive camera was set to 25 frames per second. Locomotor activity of each larva was calculated as the total distance moved during a 6 min time window. A minimal distance movement of 0.2 mm was used. Fish are kept under 12:12 LD cycles (lights on at 08:00, lights off 20:00). The same procedure was performed for *juvenile* (30 dpf) zebrafish placed in a 9-well plate**.**

3.16.3 Adult fish locomotion assay

From 60 dpf fish locomotor activity was tracked for 3 consecutive days and then analyzed by Ethovision 11 software (Noldus Information Technology, NL). The IR-sensitive camera was set to 5 frames per second. Locomotor activity of each larva was calculated as the total distance moved during a 6 min time window. A minimal distance movement of 2 mm was used. The IR table has a dimension of 120*120 cm and tanks of 8 or 12 cm are used according the size of the fish. Fish are kept 12:12 LD conditions. For light sources, an array of LED strips is used, and irradiances are set at 0.17 W/m^2 for the 12:12 LD cycle.

3.17 Dechorionation

Until 3 dpf, embryos are protected with a chorion that can be manual eliminated to perform analysis before the 3 dpf. A tear is gently made in the chorion with sharp forceps and that the embryo is helped to falls out.

3.18 Statistical analysis

Results from different groups of animals (wild type/mutated) will be analysed using two-way ANOVA with as post hoc-test the Student t-test at two-tailed independent sample. The significant level is fixed at 5%.

name	sequence
β-SG$_{ex2}$KOguide1 **β-SG$_{ex2}$KOguide2**	GAGGAGAGAGACTCCACAAG GCGCCGATGAAGAAGTCCA
δ-SG$_{ex1}$KO	GGACTTGGTCAGCCATGGTC
δ-SG$_{ex2}$KO	GAGTGGGGATCTACGGCTGG

Table 14. List of the sgRNA used for KO generation

name	sequence
β-SG ^{T145R} KIguide1 **β-SG ^{T145R} KIguide2**	GCAGCTTTGTGTTGCCCTGC CAACACAAAGCTGAGTGTAG
δ-SG ^{E264K} KIguide1	GACAGTCTGTCTTCGGTCCA
δ-SG ^{E264K} KIguide2	GATAAGAAGAGTTTTCCGTT

Table 15. List of the sgRNA used for KI generation

ssDNA donor template:

β-KI 1 sense: used in conjunction with β-KI T145R guide 1 (GCAGCTTTGTGTTGCCCTGC):
5'T*GCTTTGAATGATTGTATGAGAAAGTGTATTGATCCAGGCGATGTCTGTGTAAATTACAGGTGGT
ATTTAGACAGGGAAACAGAAAGCTTAGTGTAGAGGAAGATAAGACGTCT*A3'

β-KI 2 antisense: used in conjunction with β-KI T145R guide 1 (GCAGCTTTGTGTTGCCCTGC):
5'A*TGCCCAAATCGCTGACAATAGACGTCTTATCTTCCTCTACACTAAGCTTTCTGTTTCCCTGTCTAAATAC
CACCTGTAATTTACACAGACATCGCCTGGAT*C3'

β-KI 3 sense: used in conjunction with β-KI T145R guide 1 (GCAGCTTTGTGTTGCCCTGC):
5'T*AAATTACAGGTGGTATTTAGACAGGGAAACAGAAAGCTTAGTGTAGAGGAAGATAAGACGTCT*A3'

β-KI 4 sense: used in conjunction with β-KI T145R guide 2 (CAACACAAAGCTGAGTGTAG):
5'T*GTCTGTGTAAATTACAGGTGGTATTCCGGCAGGGCAAC AGA AAG CTT TCA GTC GAA GAA
GATAAGACGTCTATTGTCAG*C3'

β-KI 5 antisense: used in conjunction with β-KI T145R guide 2 (CAACACAAAGCTGAGTGTAG):
5'G*CT GAC AAT AGA CGT CTT ATC TTC TTC GAC TGA AAG CTT TCT GTT GCC CTG CCG
GAA TAC CAC CTG TAA TTT ACA CAG AC*A3'

- Mutations ablating PAM sequence
- Mutations altering seed region
- Mutation substituting T145/R
- Mutation introducing HindIII restriction site
- Mutations recognized by ASO primer

Table 16. List of the ssDNA donor template used for β-SG T145R generation: ssDNA donor were synthesized from Sigma Aldrich or IDT Dna technologies. Different donors were employed, all with phosporothioate modifications at their 5' and 3' ends (*)

ssDNA donor template:

δ-KI 1 sense: used in conjunction with δ-KI E264K guide 1 (GACAGTCTGTCTTCGGTCCA): C*GCCAGCAAAATCAAGCTCCCACGTCTGCCAGAGGGAAAAGCCAGTACATCTGGACCAAGACAGACT GTCTTTAAAGTGTGTGTCTGTCCCAA CGGAAA*A
δ-KI 2 antisense: used in conjunction with δ-KI E264K guide 1 (GACAGTCTGTCTTCGGTCCA): T*TTTCCGTTGGGACAGACACACACTTTAAAGACAGTCTGTCTTGGTCCAGATGTACTGGCTTTTCCCTC TGGCAGACGTGGGAGCTTGATTTTGCTGGC*G
δ-KI 3 sense: used in conjunction with δ-KI E264K guide 2 (GATAAGAAGAGTTTTCCGTT): C*CACCTCTGGACCGAGACAGACTGTCTTTAAAGTGTGTGTCTGTCCCAATGGCAAGCTTTTTTATCAC AAGCAGGAACTGGCTCTACTTGCCAGATGA*G
δ-KI 4 antisense: used in conjunction with δ-KI E264K guide 2 (GATAAGAAGAGTTTTCCGTT): C*TCATCTGGCAAGTAGAGCCAGTTCCTGCTTGTGATAAAAAAAGCTTGCCATTGGGACAGACACACAC TTTAAAGACAGTCTGTCTCGGTCCAGAGGTG*G

Mutations ablating PAM sequence
Mutations altering seed region
Mutation substituting T145/R and introducing DraI restriction site
Mutations recognized by ASO primer

Table 17. List of the ssDNA donor template used for δ-SG E264K generation: ssDNA donor were synthesized from Sigma Aldrich or IDT Dna technologies. Different donors were employed, all with phosporothioate modifications at their 5' and 3' ends (*).

4. PUBLISHED PAPER

Repairing folding-defective α-sarcoglycan mutants by CFTR correctors, a potential therapy for limb-girdle muscular dystrophy 2D

Human Molecular Genetics, 2018, Vol. 27, No. 6 969–984

doi: 10.1093/hmg/ddy013
Advance Access Publication Date: 16 January 2018
Original Article

ORIGINAL ARTICLE

Repairing folding-defective α-sarcoglycan mutants by CFTR correctors, a potential therapy for limb-girdle muscular dystrophy 2D

Marcello Carotti[1,†], Justine Marsolier[2,3,†], Michela Soardi[1], Elisa Bianchini[1,4], Chiara Gomiero[5], Chiara Fecchio[1], Sara F. Henriques[2,3], Romeo Betto[6], Roberta Sacchetto[5], Isabelle Richard[2,3] and Dorianna Sandonà[1,*]

[1]Department of Biomedical Sciences, University of Padova, 35131 Padova, Italy, [2]Genethon, Evry F-91002, France, [3]INSERM, U951, INTEGRARE Research Unit, Evry F-91002, France, [4]Aptuit, 37135 Verona, Italy, [5]Department of Comparative Biomedicine and Food Science, University of Padova, Agripolis, 35020 Legnaro, Padova, Italy and [6]Neuroscience Institute (CNR Padova), 35131 Padova, Italy

*To whom correspondence should be addressed at: Department of Biomedical Sciences, University of Padova, Via Ugo Bassi 58/B 35131, Padova, Italy. Tel: +39 0498276028; Fax: +39 0498276049; Email: dorianna.sandona@unipd.it

Abstract

Limb-girdle muscular dystrophy type 2D (LGMD2D) is a rare autosomal-recessive disease, affecting striated muscle, due to mutation of *SGCA*, the gene coding for α-sarcoglycan. Nowadays, more than 50 different *SGCA* missense mutations have been reported. They are supposed to impact folding and trafficking of α-sarcoglycan because the defective polypeptide, although potentially functional, is recognized and disposed of by the quality control of the cell. The secondary reduction of α-sarcoglycan partners, β-, γ- and δ-sarcoglycan, disrupts a key membrane complex that, associated to dystrophin, contributes to assure sarcolemma stability during muscle contraction. The complex deficiency is responsible for muscle wasting and the development of a severe form of dystrophy. Here, we show that the application of small molecules developed to rescue ΔF508-CFTR trafficking, and known as CFTR correctors, also improved the maturation of several α-sarcoglycan mutants that were consequently rescued at the plasma membrane. Remarkably, in myotubes from a patient with LGMD2D, treatment with CFTR correctors induced the proper re-localization of the whole sarcoglycan complex, with a consequent reduction of sarcolemma fragility. Although the mechanism of action of CFTR correctors on defective α-sarcoglycan needs further investigation, this is the first report showing a quantitative and functional recovery of the sarcoglycan-complex in human pathologic samples, upon small molecule treatment. It represents the proof of principle of a pharmacological strategy that acts on the sarcoglycan maturation process and we believe it has a great potential to develop as a cure for most of the patients with LGMD2D.

[†]These authors contributed equally to this work.

Received: December 5, 2017. **Revised:** December 5, 2017. **Accepted:** December 30, 2017.

Introduction

Limb-girdle muscular dystrophy type 2D (LGMD2D) is an autosomal recessive disease caused by mutations in the *SGCA* gene coding for α-sarcoglycan (α-SG). α-SG is a single-pass transmembrane glycoprotein that together with β-, γ-, and δ-SG forms a tetrameric complex localized into the sarcolemma of striated muscle (1,2). Sarcoglycan complex, as part of the dystrophin-associated protein complex (DAPC), plays a key role in assuring sarcolemma stability during muscle contraction, and seems involved in signaling processes (3). LGMD2D, as well as the other forms of sarcoglycanopathy (LGMD2E, 2C and 2F) can be classified as loss of function (LOF) disease because defects in the specific sarcoglycan are typically responsible for the absence/strong reduction of the mutated protein with the secondary deficiency of the wild type partners (4). In the last few years, by studying the pathogenesis of LGMD2D, it has been established that the LOF condition is the consequence of the activity of the protein quality control (QC) system of the cell. In fact, the majority of LGMD2D genetic defects are missense mutations originating a folding-defective protein that is recognized by the endoplasmic reticulum-QC and delivered to degradation through the ubiquitin-proteasome system (5,6).

Moreover, different missense mutants of α-SG can be properly rescued at the plasma membrane, by targeting the degradative pathway (5–8). This evidence also suggests that, although mutated, these proteins retain their functionality and that the development of novel therapeutic strategies, aiming to reduce the disposal of the mutants, would be fruitful for patients. To this intent, being the presence of a folding-defective α-SG the main cause of pathogenicity in LGMD2D, it is conceivable a 'repair strategy' by means of small molecules facilitating the folding process of the mutants that can therefore pass the quality control and move at the proper site of action.

Protein misfolding is involved in hundreds of genetic diseases, including cystic fibrosis, retinitis pigmentosa, Gaucher's disease, hypogonadotropic hypogonadism (9,10) etc. and the molecules proposed to revert this condition are also numerous. Such compounds can directly act on the improperly folded protein, as pharmacological chaperones, or indirectly by fostering the folding process, as proteostasis regulators (11–14). Among them, several compounds known as correctors of the cystic fibrosis transmembrane regulator (CFTR) protein are also included (15,16). CFTR correctors have been developed for their ability to recover at the cell surface type II mutants of the chloride channel defective in folding and trafficking (17,18).

Here, we show that CFTR correctors are effective in recovering also different mutants of α-SG. This evidence has been provided utilizing cell models expressing folding defective forms of α-SG and, more importantly, primary myogenic cells isolated from a patient with LGMD2D. Indeed, in patient's myotubes, upon CFTR corrector treatments, the mutated sarcoglycan increased in content, assembled with the wild type partners, allowing a correct localization of the whole complex at the sarcolemma and consequently a reduction of membrane fragility. These results strongly suggest the feasibility of a protein 'repair strategy' to treat LGMD2D, starting from already available small molecules that act on the maturation process of the α-SG mutants.

Results

Rescue of different mutants of α-sarcoglycan by means of CFTR correctors

In the attempt to find a therapeutic approach for LGMD2D, we assessed 12 CFTR correctors (see Table 1) for their ability to improve expression and traffic of different mutants of α-SG, which undergo similar processing mechanism of type II mutants of the CFTR chloride channel (18).

We tested CFTR correctors in HEK293 cells transiently expressing either the R98H or the D97G mutant of α-SG, as well as in V247M cells, i.e. a population of HEK293 cells that constitutively expresses the V247M-α-SG. These three mutants are responsible for the development of a severe phenotype in patients with LGMD2D [http://www.dmd.nl] and are potentially recoverable as they traffic toward the plasma membrane of cell models by interfering with different steps of the degradative pathway (6–8).

Figure 1 shows the data concerning the R98H mutant of α-SG whereas results from D97G- and V247M-α-SG are reported in Supplementary Material, Figures S1–S3. Cells expressing the α-SG mutant were incubated for 24 h with CFTR correctors at the concentrations reported in Table 1, known to rescue *in vitro* CFTR processing mutants (15,20–24). As negative controls, cells were incubated with compound vehicle (1‰ DMSO), whereas MG132 was utilized as positive control of rescue (6). Cells transfected with the wild type α-SG were utilized for comparison. α-SG expression in total protein lysates was analysed by western blot with a specific antibody (Fig. 1A). As already shown, α-SG antibody recognizes a band of about 55 kDa both for wild type and mutated α-SG, suggesting that the mutants, although folding-defective, are fully glycosylated (6,8). The brief treatment with MG132 (8 h), as expected, induced a modest increase of the mutant content and led to the appearance of an additional band, at lower molecular weight, representing the de-glycosylated form of the protein accumulated by proteasomal inhibition (6,8). The effect of 24 h of incubation with the diverse CFTR correctors, as visible in the western blots, was quantified by densitometric analysis (see graphs in Fig. 1B related to R98H-α-SG and in Supplementary Material, Fig. S1A and C for D97G and V247M mutants, respectively). Data are presented as fold increase of the negative control, i.e. of the mutant protein content in cells treated with the sole vehicle.

Many of the tested CFTR correctors (C5, C6, C4, C13, C14, C17 and C15) were effective on R98H-α-SG, inducing a fold increase of the mutant content ranging from 2.5 to 3 times the level of control (vehicle). Expression of D97G- and V247M-α-SG also raised by similar extent upon treatment with correctors C5 or C4, and C4 or C17, respectively (see Supplementary Material, S1A and C). VX809, a CFTR corrector approved for the treatment of cystic fibrosis, in accordance with its high specificity for cystic fibrosis chloride channel and related ABC proteins (25), was ineffective on α-SG (Fig. 1A and Supplementary Material, Fig. S1A and C). Finally, coherently with its mechanism of action, VX770 was unproductive when tested in V247M cells (Supplementary Material, Fig. S1C). Indeed, this small molecule is a CFTR potentiator, a pharmacological agent that increases the flow of ions through activated CFTR channels, without affecting folding and maturation of the protein (26).

To be significant in a possible therapeutic approach, mutant rescue must comprise trafficking toward the plasma membrane. Therefore, we evaluated the membrane localization of R98H-α-SG on intact cells, upon treatment with some of the most active CFTR correctors. By using an antibody recognizing an extracellular epitope of α-SG, we showed that only traces of R98H-α-SG (Fig. 1C) were present at the surface of untreated cells (vehicle). Conversely, it is possible to appreciate that C5, C6, C13, C14 and C17 successfully induced the localization at the plasma membrane of R98H-α-SG. Indeed, the cell surface signal increased to

Table 1. List of the CFTR correctors with concentrations utilized in this study

CFF name[a]	Original name	Compound[b]	IUPAC name	Concentration μM
C2	VRT-640[c]	C	2-{1-[4-(4-Chloro-benzensulfonyl)-piperazin-1-yl]-ethyl}-4-piperidin-1-yl-quinazoline	5
C3	VRT-325[d]	B	4-Cyclohexyloxy-2-{1-[4-(4-methoxy-benzensulfonyl)-piperazin-1-yl]-ethyl}-quinazoline	10
C5	corr 5a[e]	H	4, 5, 7-trimethyl-N-phenylquinolin-2-amine	15
C6	corr 5c[e]	I	N-(4-bromophenyl)-4-methylquinolin-2-amine	10
C9	KM11060[f]	F	7-chloro-4-(4-(4-chlorophenyl sulfonyl)piperazin-1-yl)quinoline	10
C4	corr 4a[e]	E	N-[2-(5-Chloro-2-methoxy-phenylamino)-4'-methyl-[4, 5']bithiazolyl-2'-yl]-benzamide	10
C13	corr 4c[e]	Q	N-(2-(3-acetylphenylamino)-4'-methyl-4, 5'-bithiazol-2'-yl)benzamide	5
C14	corr 4d[e]	R	N-(2'-(2-methoxyphenylamino)-4-methyl-5, 5'-bithiazol-2-yl)benzamide	5
C17	15jf[g]	A	N-(2-(5-chloro-2-methoxyphenylamino)-4'-methyl-4, 5'-bithiazol-2'-yl)pivalamide	2
C15	corr 2b[e]	S	N-phenyl-4-(4-vinylphenyl)thiazol-2-amine	15
	VX809[h] Lumacaftor	U	3 -(6-(I -(2, 2- difluorobenzo[d][l, 3]dioxol-5-yl) cyclopropa-necarboxamido)-3-methylpyridin-2-yl)benzoic acid	6
	Glafenine[i]		2, 3-dihydroxypropyl 2-[(7-chloroquinolin-4-yl)amino]benzoate	10

[a]Name according to the list of the Cystic Fibrosis Foundation [https://www.cff.org/CFTR-Chemical-Compound.pdf].
[b]Name according to [WO2014086687].
[c]WO2004111014 A.
[d]US20050059687 A1.
[e]Pedemonte *et al.* (2005) (15).
[f]Robert *et al.* (2008) (20).
[g]Yoo *et al.* (2008) (21).
[h]US2011257223.
[i]Robert *et al.* (2010) (22).

level similar to wild type control (Fig. 1C). In related experiments, D97G-α-SG localized at the plasma membrane upon incubation with corrector C5, whereas V247M-α-SG regained the ability to reach the cell surface upon treatment with both C4 and C17 (Supplementary Material, Fig. S1B and D).

Among the tested molecules, only VX809 and glafenine have been already approved for clinical use in other diseases (27,28). Therefore, the cytotoxicity of the remaining CFTR correctors was evaluated by measuring the release of the cytosolic enzyme LDH in the medium of V247M cells, upon 24 h of incubation. Results reported in Supplementary Material, Figure S4 show that these CFTR correctors, at the concentrations utilized, were safe with the only exception of C4, which produced a statistically significant, although very modest, cell damage at 10 μM.

Dose-response effects of CFTR correctors on α-SG mutant content

The dose-dependent effect, in terms of increase of the α-sarcoglycan mutant content, was then evaluated for the most promising correctors. In Figure 2A, it is evident that the protein level of R98H-α-SG increases by increasing the C6 corrector concentration, to reach a plateau at the higher doses. At the same time, none or negligible signs of toxicity were evident at the most effective concentrations, whereas the highest dose tested (50 μM) was toxic for the cells. Indeed, damaged cells released the cytosolic enzyme LDH (Fig. 2B), and cell viability dropped around 20% that of the control cells, as determined by the MTT assay (Fig. 2C). A comparable trend was observed for corrector C5, as assessed in cell expressing the D97G mutant of α-SG (Fig. 2D–F). Finally, increasing concentrations of corrector C17 were tested in V247M cells. As reported in Figure 2G, this small molecule has a very narrow window of efficacy, as the level of V247M-α-SG increased in the 1 to 8 μM range of concentrations, but dropped to value similar to the untreated cells at higher concentrations (12 and 16 μM). To understand this trend, we evaluated the effect of the small molecule on cell integrity and vitality at the diverse concentrations. No statistically significant release of the cytosolic enzyme LDH was recorded at any concentration tested (Fig. 2H), implying that cells were undamaged by the treatment. However, cell viability was reduced, declining from approximately 80% at 2 μM C17 (the concentration utilized in most of the experiments), to approximately 50% of control at the highest concentrations, as determined by the MTT assay (Fig. 2I). This could be due to either a lower number of cells or a slowdown of cell metabolism. Therefore, to verify a possible effect on cell proliferation, we measured the cell number at the beginning and at the end of the incubation time with C17. We recovered a progressively reduced number of cells from wells with increasing concentrations of the corrector C17 (Supplementary Material, Fig. S5). Therefore, considering the absence of cell death (Fig. 2H) but the reduced number of cells recovered, we hypothesize that corrector C17 exerted a cytostatic effect on proliferating cells.

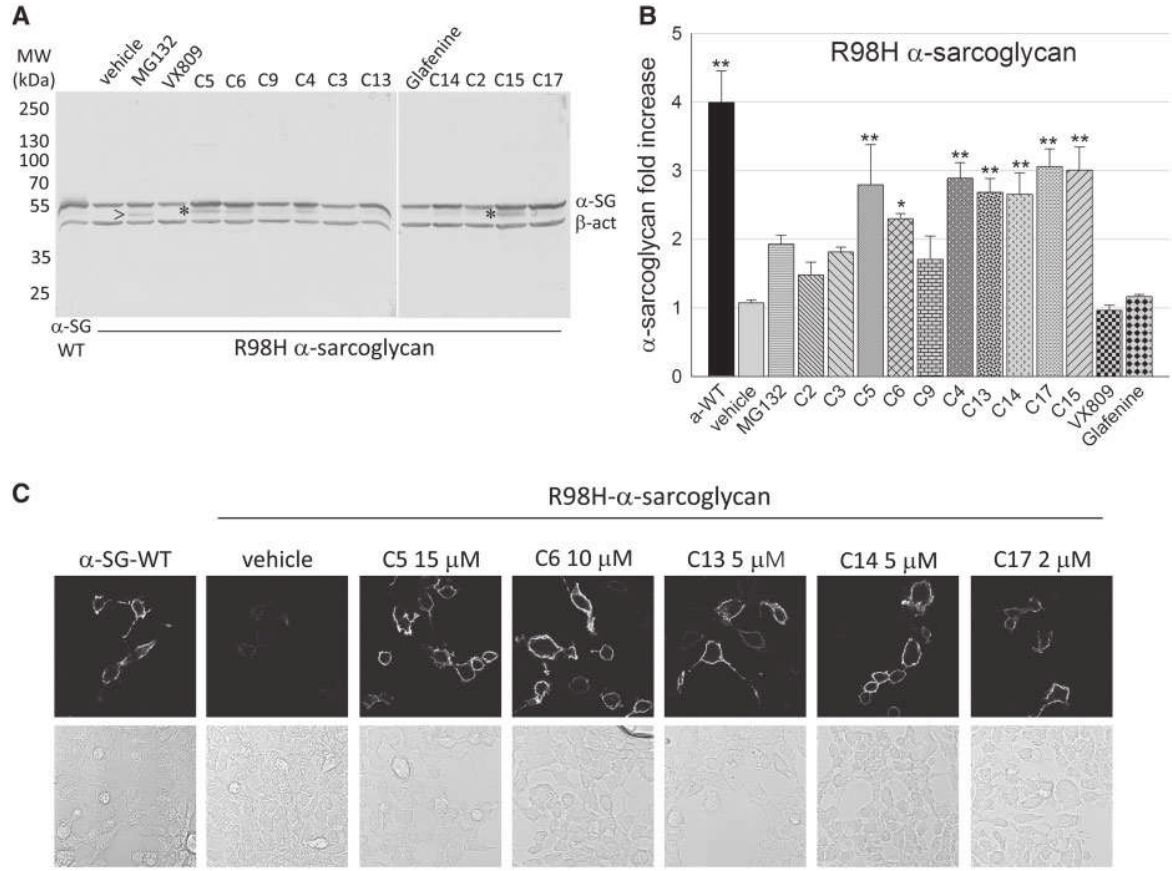

Figure 1. CFTR correctors promoted increase and traffic of R98H-α-sarcoglycan. (**A**) Representative western blot of total protein lysates from HEK-293 cells transiently expressing the R98H form of α-SG and treated with the indicated CFTR correctors, at the concentrations reported in Table 1, MG132 10 μM, as in (6) or vehicle (1‰ DMSO); lysate from cells expressing wild type-α-SG was used for comparison. Membranes were incubated with primary antibodies against α-SG and β-actin, used as loading control; arrowhead indicates the de-glycosylated form of the protein (6), whereas asterisks indicate the immature form of the protein recognized by the α-SG antibody. (**B**) Quantification of α-SG content by densitometric analysis of western blots from at least four independent experiments. The average amount of α-SG (± SEM), is expressed as fold increase of the protein content compared with the negative control (vehicle). Statistical analysis was performed by One-way ANOVA test - multiple comparisons Dunnett test; n.s., $P > 0.05$; *$P \leq 0.05$; **$P \leq 0.01$. (**C**) Membrane localization of α-SG in HEK293 cells expressing R98H-α-SG treated with either vehicle or the indicated CFTR correctors. For comparison, cells expressing wild type-α-SG were also analysed. Localization was evaluated by confocal immunofluorescence analysis of intact cells immuno-decorated with an antibody recognizing an extracellular epitope of α-SG. The primary antibody was revealed with the secondary Alexa Fluor 594-conjugated anti-mouse antibody. Images were recorded with a Leica SP5 laser scanning confocal microscope at the same setting conditions and magnification. Below each image the same field in light transmission was recorded.

Rescue of the folding defective R77C-α-SG by CFTR correctors: single and combined administration

The R77C amino acid substitution is the most frequently reported mutation responsible for LGMD2D [http://www.dmd.nl], consequently it was mandatory to verify the effectiveness of CFTR corrector treatments on this mutant. This mutant tends to aggregate when expressed in HEK293 cells (29), and, probably for this reason, the incubation with MG132 failed to rescue the protein at the cell membrane (6). Therefore, we decided to seek out a different cell model to better mimics the condition observed in human subjects where R77C-α-SG is absent or strongly reduced, and the sole γ-SG is expressed in variable residual amount (30,31). As HER911 cells concomitantly transfected with β-, γ-, δ- and R77C-α-SG were utilized to successfully rescue the mutant at the cell surface upon α-mannosidases inhibition (5), we decided to adopt a similar system. However, to overcome variability associated with a quadritransfection model, we generated a cell line, hereafter named βγδ-cells, in which the cDNAs coding for the wild type β-, γ-, δ-SG were stably integrated in the genome of HER911cells by lentivirus transduction (Supplementary Material, Fig. S6). The subsequent transfection with either wild type or R77C-α-SG led to the production of the final cell model. Here, we show that the level of R77C-α-SG transfected in βγδ-cells (either untreated or treated with the sole vehicle) was very low, about 20% in comparison to wild type (Fig. 3A and B; Supplementary Material, Fig. S6D) and the protein was almost undetectable at the plasma membrane (Fig. 3C, vehicle), well mimicking the condition present in patient's muscle cells (30,31). Therefore, we exploited this model to assess the efficacy of some of the most effective CFTR correctors, administered either as single molecule or in combination. We found that the presence of the other sarcoglycan subunits had a stabilizing effect on the rescued mutant. In fact, treatment with C5, C9, C17 and C4 induced a three to four-fold increase of R77C-α-SG protein content (Fig. 3A and B).

On the other hand, these compounds had no effect on the wild type form of proteins, as observed when treatments were applied in βγδ-cells transfected with either WT-α-SG (Supplementary Material, Fig. S7A) or the unrelated GFP protein (Supplementary Material, Fig. S7B). Moreover, in βγδ-cells, no

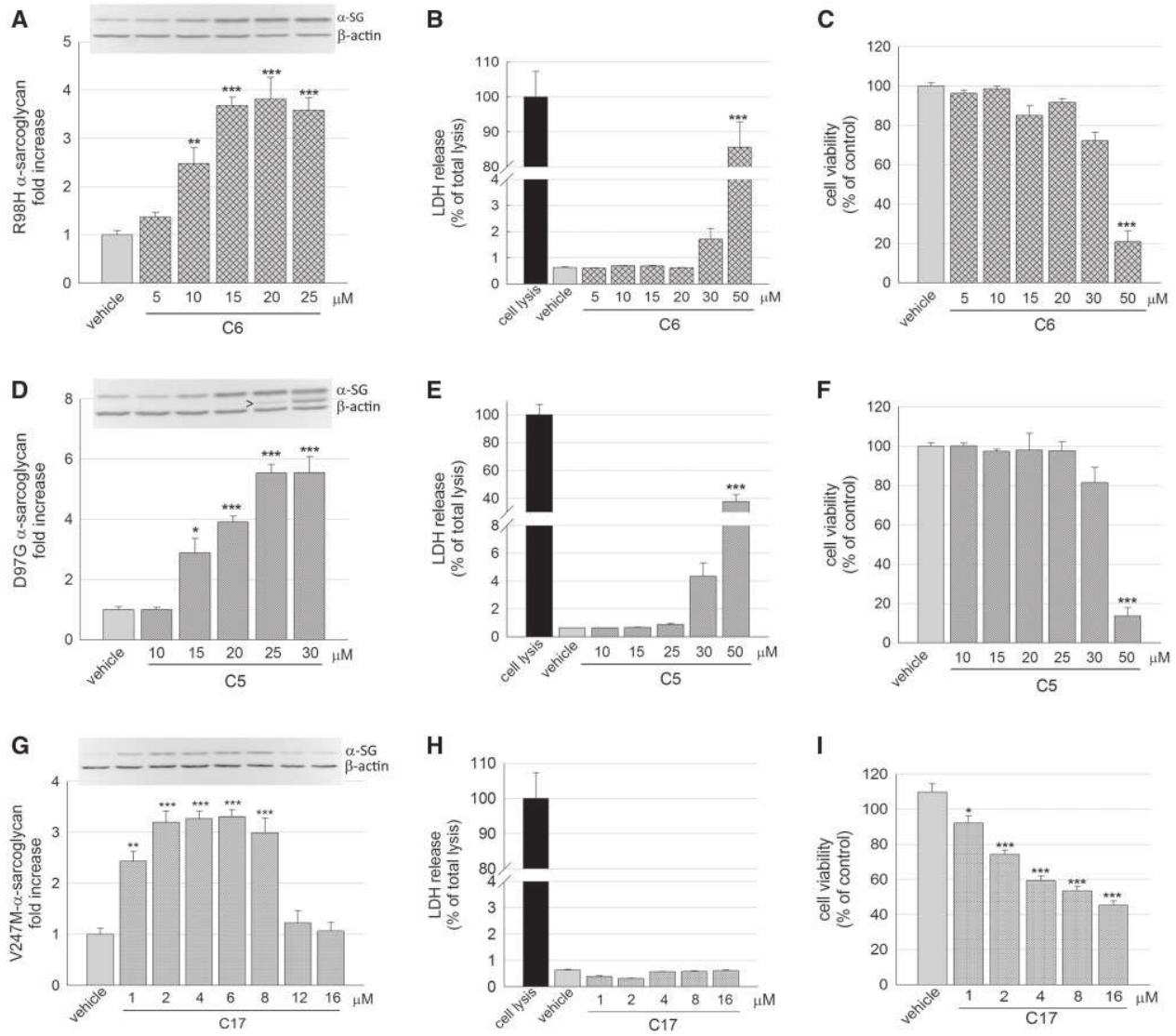

Figure 2. Corrector C6, C5 and C17 induced a dose-dependent increase of different α-SG mutants without major toxic effects. (**A**, **D**, **G**) Quantification of α-SG content in HEK293 cells expressing R98H-α-SG (A), D97G-α-SG (D) or V247M-α-SG (G) treated for 24 h with increasing concentrations of the indicated correctors. α-SG protein content was determined by WB and densitometric analysis on total protein lysates from at least three independent experiments. Above each graph is reported a representative western blot; β-actin was used as loading control. Arrowhead indicates an extra band recognized by the α-SG antibody that probably represents an immature form of the protein. (**B**, **E**, **H**) Cytotoxicity of correctors evaluated as the release of the cytosolic enzyme LDH in the culture medium of cells expressing R98H-α-SG treated with increasing concentration of C6 (B), D97G-α-SG treated with increasing concentration of C5 (E) or V247M-α-SG treated with increasing concentration of C17 (H). LDH release is expressed as percentage of the total amount of enzyme in cell lysate. (**C**, **F**, **I**) cell viability evaluated by measuring the metabolism of cells expressing R98H-α-SG treated with increasing concentration of C6 (C), D97G-α-SG treated with increasing concentration of C5 (F) or V247M-α-SG treated with increasing concentration of C17 (I). Cell viability was expressed as percentage (± SEM) toward cells treated with vehicle. Statistical analysis was performed by One-way ANOVA test - multiple comparisons Dunnett test; n.s., $P > 0.05$; *$P \leq 0.05$; **$P \leq 0.01$; ***$P \leq 0.001$.

effect was exerted by C5, C9, C17 and C4 on the transcription rate of both the wild type and R77C form of α-SG transiently transfected in the cell model (Supplementary Material, Fig. S8A and B, respectively), as well as on WT-β-SG constitutively expressed by the cells (Supplementary Material, Fig. S8C), as determined by quantitative RT-PCR. Altogether, these data suggest that correctors exert their effect specifically on the mutated form of proteins leaving unaltered the mRNA expression controlled by the heterologous promoter.

Remarkably, the rescued protein localized at the plasma membrane, as proven by the intense cell-surface staining of not-permeabilized cells (Fig. 3C). Notably, the combined C17 + C4 administration, each corrector at half dose of the single application, resulted in a more robust effect, as the total mutant content reached that of the wild type (Fig. 3B). In addition, the intensity of the fluorescence signal at the plasma membrane was significantly higher than the one obtained by individually applied correctors (Fig. 3C), as evaluated by using the ImageXpress microscope system (Fig. 3D). Then, we evaluated the effect of the co-administration of C17 + C5, also in this case used at halved dose. In Supplementary Material, Figure S9 is reported the quantification of the cell membrane staining

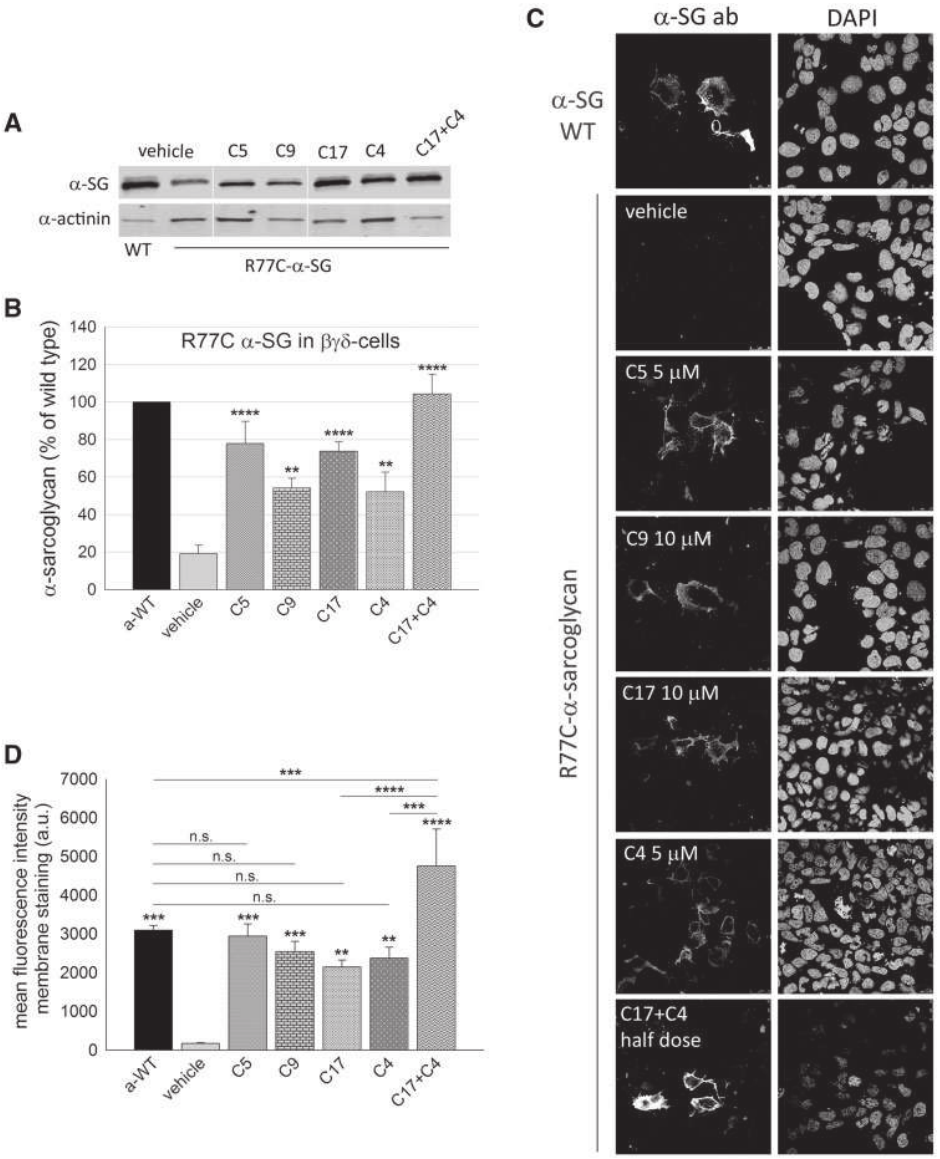

Figure 3. Rescue of the folding-defective R77C-α-SG by means of CFTR correctors. (**A**) Western blot of protein lysates from βγδ-cells transiently expressing R77C-α-SG and treated for 24 h with corrector C5 5 μM, C9 10 μM, C17 10 μM, C4 5 μM. One sample was treated with the combination of corrector C17 and C4 (each one-half dose). Cells expressing wild type-α-SG were utilized as positive control. Membrane were probed with antibodies against α-SG and α-actinin, used as loading control. (**B**) quantification by densitometric analysis of α-SG protein bands on at least three independent Western blot experiments. The average amount of α-SG (± SEM) is shown as percentage of the protein content in cells expressing the wild type form. Statistical analysis was performed by One-way ANOVA test - multiple comparisons Dunnett test; $^{**}P \leq 0.01$; $^{****}P \leq 0.0001$. (**C**) IF confocal analysis of βγδ-cells expressing R77C-α-SG and treated for 24 h with the indicated correctors. Intact cells (not permeabilized) were immune-decorated with an anti α-SG antibody, recognizing an extracellular epitope, revealed by the secondary Alexa Fluor 594-conjugated anti-mouse antibody. Cells expressing wild type-α-SG are shown as positive control. On the right of each image is reported the same field with nuclei stained by DAPI. Images were recorded with a Leica SP5 laser scanning confocal microscope at the same setting conditions and magnification. (**D**) mean fluorescence intensity of membrane staining of βγδ-cells expressing R77C-α-SG treated for 24 h with vehicle (negative control) or the indicated correctors; βγδ-cells expressing WT-α-SG were used as positive control. Fluorescence values from at least three independent experiments, performed in triplicate, were recorded by using the ImageXpress microscope system. Mean values (± SEM) were normalized for the number of cells positive for both α-SG and DAPI under permeabilization condition to consider transfection efficiency. Statistical analysis was performed by One-way ANOVA test - multiple comparisons Bonferroni test; n.s., $P > 0.05$; $^{**}P \leq 0.01$; $^{***}P \leq 0.001$; $^{****}P \leq 0.0001$.

upon CFTR corrector treatment. Also in this case, the co-administration resulted in the additional increase of the cell surface α-SG rescue in comparison to the single-compound administration. All this considered, we conclude that the mutant R77C-α-SG can be successfully rescued *in vitro* by CFTR corrector treatments and those correctors may have an additive and even a synergic effect when administered in combination.

Corrector C17 increases the α-SG mutant level in myotubes from a LGMD2D patient

To validate the data collected with cellular models, we assessed the efficacy of CFTR correctors in rescuing SG-complex directly in human samples. Indeed, we had the opportunity to use myogenic cells derived from a small bioptic fragment of a patient

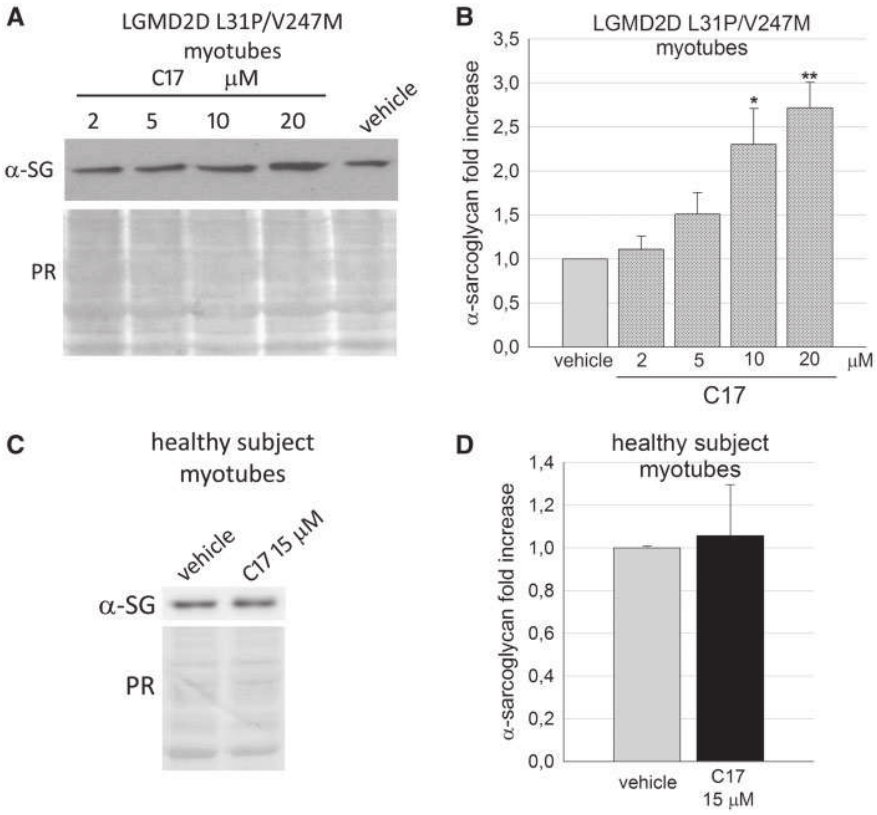

Figure 4. Corrector C17 induced a dose dependent increase of α-SG mutant in LGMD2D myotubes. (**A**) representative western blot of total protein lysates of myogenic cells from a patient carrying the L31P/V247M α-SG mutations grown and differentiated for 7 days and treated for the last 48 h with either 1‰ DMSO (vehicle) or increasing concentrations of corrector C17, as indicated. α-SG protein was revealed with specific primary antibody, the Ponceau red staining (PR) is reported and utilized to normalize the total amount of proteins loaded in each lane. (**B**) quantification by densitometric analysis of α-SG protein bands of three independent western blot experiments, as described in (A). The average amount of α-SG (± SEM) is expressed as fold increase of the protein content present in myotubes treated with vehicle. Statistical analysis was performed by One-way ANOVA test - multiple comparisons Dunnett test; $^{*}P \leq 0.05$; $^{**}P \leq 0.01$. (**C**) myogenic cells from a healthy subject were grown and differentiated for 7 days and treated for the last 48 hours with either 1‰ DMSO (vehicle) or 15 μM C17. Total protein lysates were analyzed by Western blot as described in (A). (**D**) quantification by densitometric analysis of wild type α-SG protein bands of three independent Western blot experiments as described in (C). Statistical analysis was performed by unpaired two-tailed Student's *t*-test.

with LGMD2D carrying the L31P and V247M mutations on the *SGCA* alleles. After 7 days of differentiation, we examined the myotubes derived from these cells by immunofluorescence-confocal analysis. As expected, in comparison to the healthy subject, myotubes from the patient with LGMD2D expressed a low level of SGs, with only traces of the α-SG protein at the myotube surface (Supplementary Material, Fig. S10).

Thereafter, we treated the LGMD2D myotubes with three CFTR correctors or vehicle. Since one of the α-SG mutation is the V247M substitution, we firstly tested C17, the most effective 'V247M-α-SG corrector' as assessed in the cell model. Figure 4A and B shows that the small molecule induced a dose-dependent increase of α-SG mutant, with 10 μM C17 being the concentration needed to elicit a statistical significant increase of the mutant level. On the contrary, 48 h of incubation with 15 μM C17 were ineffective on the level of the endogenous, wild type form of α-SG, expressed by the healthy subject's myotubes, used as control (Fig. 4C and D). These data confirm what already observed with the βγδ-cells (Supplementary Material, Fig. S7) and suggests that corrector C17 is either directly acting on the α-SG mutants or, more probably, on cellular pathways specifically handling the mutant, or on both.

The recovery of the mutant protein elicited by C17 increased with the length of the incubation time, as shown in Figure 5A and B, reporting representative western blots and the densitometric quantification of three independent experiments over a period from 48 to 96 h. Importantly, no evident sign of toxicity was observed neither at 10 nor at 15 μM C17, and at any time point. In fact, the differentiated LGMD2D cells show no major alterations in the morphology of the elongated myotubes nor overt signs of cytotoxicity, such as membrane blebbing or cells detaching from the plate, even after 96 h of incubation (Fig. 5C).

Treatment with corrector C17 stabilized the α-SG mutant in patient's myotubes

The increase of α-SG mutant level, observed in LGMD2D myotubes treated with corrector C17, could be the result of either the transcriptional upregulation of *SGCA* gene or the stabilization of the protein. For the first issue, we studied the effect of the small molecule on *SGCA* transcription by quantitative RT-PCR analysis. For the second issue, we evaluated the rate of α-SG protein disappearance after blocking protein synthesis by cycloheximide. No statistical significant effect was detected on the endogenous *SGCA* transcription, as shown in Figure 6A reporting the average amount of α-SG mRNA in LGMD2D myotubes after 48

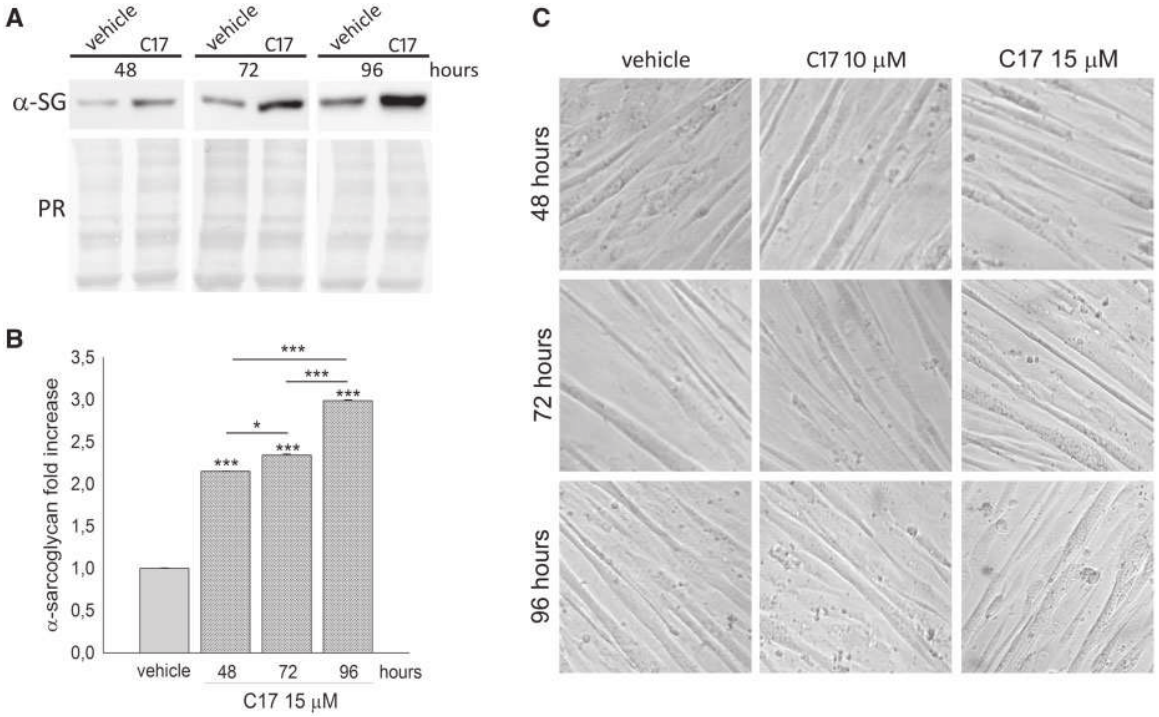

Figure 5. Corrector C17 induced a time dependent increase of mutated α-SG, without toxicity, in LGMD2D myotubes. (**A**) myogenic cells from a patient carrying the L31P/V247M α-SG mutations were grown and differentiated for 7 days and treated with 1‰ DMSO (vehicle) or 15 μM C17 for the indicated time intervals. α-SG protein content was evaluated by western blot of total myotube lysates. The Ponceau red staining (PR) is reported to normalize the total amount of proteins loaded in each lane. (**B**) quantification by densitometric analysis of α-SG protein bands of three independent western blot experiments, as described in (A). The average amount of α-SG (± SEM) is expressed as fold increase of the protein content present in myotubes treated with vehicle for the same incubation interval. Statistical analysis was performed by One-way ANOVA test - multiple comparisons Bonferroni test; $^{*}P \leq 0.05$; $^{***}P \leq 0.001$. (**C**) phase contrast images of myotubes treated with either 1‰ DMSO (vehicle) or C17 at the concentration and time intervals indicated to evaluate possible toxic effects. All images were recorded at the same magnification.

h of treatment with corrector C17 compared with control (vehicle). This data on the transcription of the endogenous *SGCA* gene, confirms what observed when sarcoglycans were exogenously expressed in βγδ-cells (Supplementary Material, Fig. S8).

On the other hand, a clear stabilizing effect was observed on the mutated α-SG expressed by the patient's myotubes upon C17 incubation. In Figure 6B and C are reported a representative western blot and the densitometric quantification of the α-SG level at different time points after the addition of the protein synthesis inhibitor, cycloheximide. In defect of protein neosynthesis, the α-SG mutant in untreated myotubes (vehicle) rapidly diminished during the first 6 h, to reach a value of approximately 50% of the initial level after 24 h. Conversely, the decline of α-SG mutant, accumulated thanks to the C17 treatment, is slower, being only 15% after 6 h and 30% of the initial value at the last time point.

Rescue and traffic of sarcoglycan complex in patient's myotubes upon CFTR corrector treatments

The accumulation of α-SG mutant is therapeutically effective only if followed by SG-complex assembly and localization at the sarcolemma. Therefore, we examined the localization at the myotube surface of both α-SG and δ-SG by antibodies recognizing extracellular epitopes of the two proteins. δ-SG is marker of SG-complex assembly because it is considered the key subunit that forms with β-SG the core complex to which γ- and α-SG associate later to move eventually toward the plasma membrane (32–34). In Figure 7, showing immunofluorescence-confocal images of 7-day-old myotubes, it is undoubtedly evident that the amount of the surface-resident sarcoglycans is extremely low (very faint fluorescence signal) in the absence of any treatment (vehicle). Conversely, the signal for both α- and δ-SG dramatically increased at the sarcolemma after 48 h of incubation with C17, suggesting the treatment successfully recovered the SG-complex at the proper cellular location in human pathological specimens.

Treatment with corrector C5 and C6 resulted in very similar effects. Indeed, when C5 and C6 were applied to myotubes from the patient with LGMD2D, the amount of the mutated α-SG (Supplementary Material, S11A and B) increased in comparison to the control (myotubes treated with vehicle), and the SG-complex was recognized at the surface of treated myotubes (Fig. 7).

C17 treatment restores membrane functionality to patient's myotubes *in vitro*

The SG-complex, interacting with dystrophin and dystroglycans, plays a protective role for the sarcolemma during muscle contraction cycles (35,36). In sarcoglycanopathy the SG-complex is severely reduced or absent from sarcolemma and one of the first clinical sign is the elevated serum content of the cytosolic protein of muscle fibers, creatine kinase (CK, more than 10-fold) (37). This feature is common to many other muscular dystrophies in which there is an alteration of the DAPC (38). There is also evidence that the lack of dystrophin increases the fragility of both cardiomyocytes and skeletal myotubes *in vitro*, which respond to osmotic stress by releasing elevated levels of CK (39–40). Therefore, we applied a protocol to check whether the

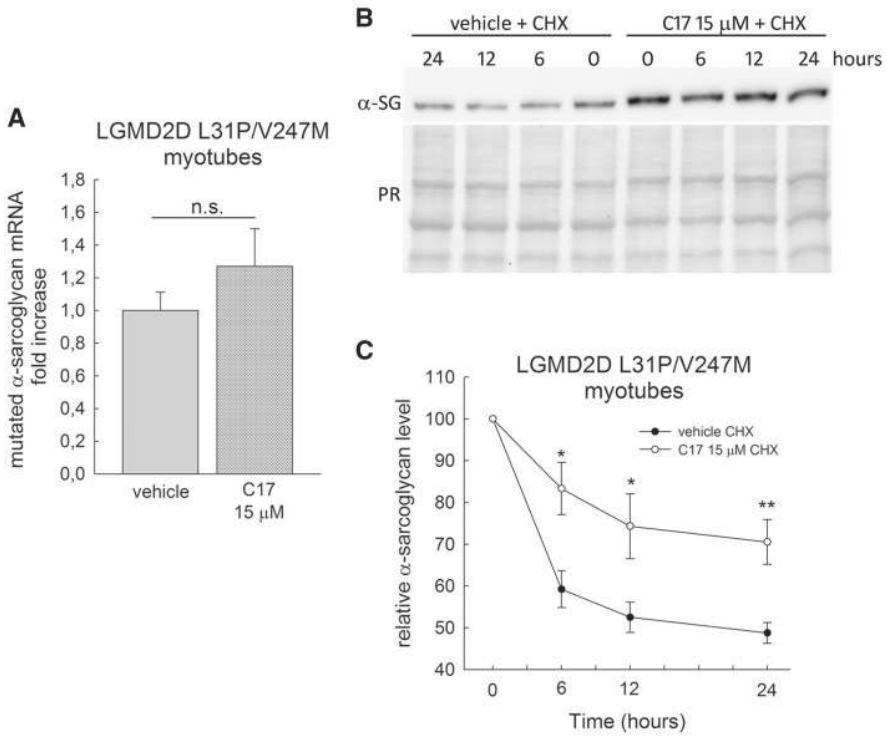

Figure 6. Corrector C17 had no effect on the transcription of SGCA and stabilized α-SG mutant, in LGMD2D myotubes. (**A**) LGMD2D myotubes were treated for 48h with vehicle (1‰ DMSO) or 15 μM C17. The SGCA transcription was evaluated by quantitative real-time PCR (see M&M for details concerning normalization) and reported as mean, ± SEM, relative to DMSO treated control of two independent experiments performed in quadruplicate. Statistical analysis was performed using unpaired two-tailed Student's *t*-test; n.s., $P > 0.05$. (**B**) myogenic cells from a patient carrying the L31P/V247M α-SG mutations were grown and differentiated for 7 days and treated with 1‰ DMSO (vehicle) or 15 μM C17 for 96 h. At the end of incubation, 100 μg/ml cycloheximide was added and myotubes were lysate at the indicated time points. Protein lysate were analyzed by western blot with anti α-SG antibody, the Ponceau red staining (PR) is reported to normalize the total amount of proteins loaded in each lane. (**C**) quantification by densitometric analysis of α-SG protein bands of three independent western blot experiments, as described in (B). The average amount of α-SG (± SEM) is expressed as percentage of the protein present at time 0. Statistical analysis was performed by unpaired two-tailed Student's *t*-test; $^{*}P \leq 0.05$; $^{**}P \leq 0.01$.

presence of the SG-complex, rescued by CFTR corrector treatment, reduced the sarcolemma fragility of the LGMD2D myotubes under stressful conditions. Seven-day-old myotubes were treated for 96 h with vehicle or 15 μM C17. At the end of the treatment, myotubes were maintained 20 min in hypoosmolar conditions (260 and 200 mOsmol) and the release of CK was then measured in the supernatant. Figure 8 shows that myotubes from the healthy subject released very low amount of CK in comparison to the LGMD2D myotubes (treated with vehicle). This occurred at both the hypoosmotic conditions applied and the release from the pathologic myotubes increased by worsening the stress conditions. On the contrary, the release of CK from LGMD2D myotubes pretreated with C17 was significantly reduced in comparison to the vehicle treated control. This suggests the functional improvement of the sarcolemma of the patient's myotubes when the SG-complex is restored upon CFTR corrector treatment.

Discussion

The folding process is a key step for each protein to acquire the functional role. The presence of genetic mutations can lead to a folding-defective polypeptide, usually promptly disposed of by the QC system. The net result is a loss of function even when the folding-defective protein retains, either partially or completely, its function (13,41). This is the pathogenic mechanism of most cases of LGMD2D (7,8), a severe muscular dystrophy, in which more than 50 different missense mutations account for more than 65% of α-SG genetic defects (36). LGMD2D is a rare disease, at present incurable, that could benefit from the use of small molecules acting on either the degradative pathway of the defective mutants, as already shown (5–8), or on the folding/maturation process. In this attempt, we used CFTR correctors, small molecules that promote the recovery of folding-defective mutants of the CFTR protein (17,19). By using these compounds, we show that it is possible to skip the degradation of α-SG mutants, which re-localize at the proper site of action together with the wild type partners. Four different α-SG missense mutations were successfully rescued in cellular models, and importantly, CFTR correctors were effective in primary myogenic cells from a LGMD2D patient. In these cells, the recovered α-SG assembled into a functional SG-complex, which properly localized at, and strengthened the sarcolemma of the patient's myotubes against stressful conditions.

To test the effectiveness of several CFTR correctors, as *in vitro* model we adopted the simple transfection of HEK293 cells with different α-SG mutants, such as R98H-, D97G- and V247M-α-SG. Conversely, for the R77C mutant we needed to better mimic the condition recognizable in pathologic muscle (30,31), and for this reason we generated the novel βγδ-cells,

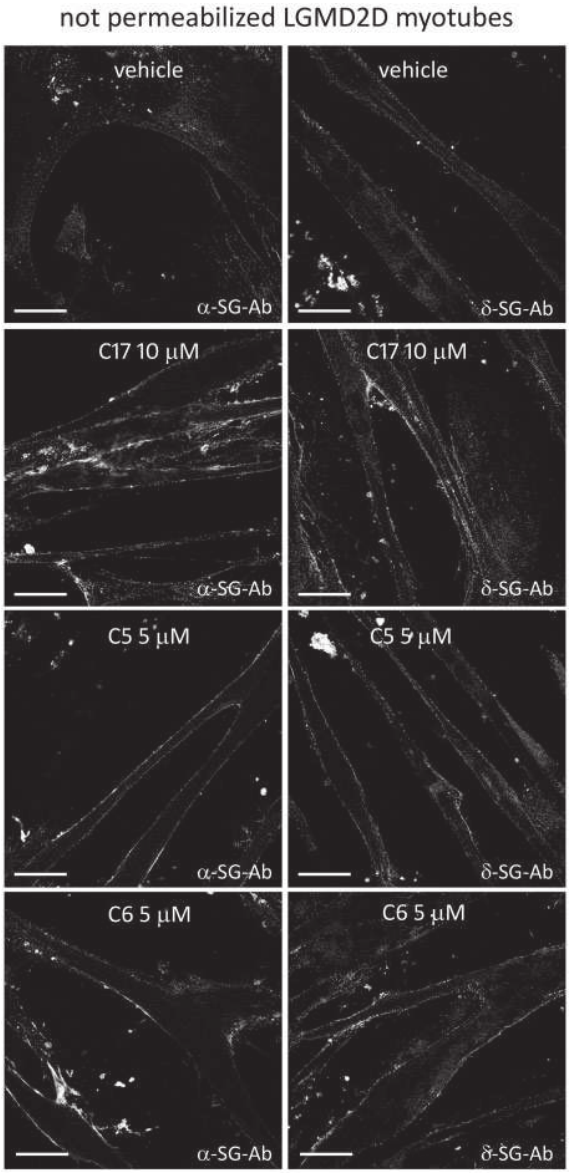

Figure 7. CFTR correctors rescued the sarcoglycan complex in LGMD2D myotubes. Myogenic cells from a patient carrying the L31P/V247M α-SG mutations were grown and differentiated for 7 days and treated for the last 48 h with 1‰ DMSO (vehicle) or the indicated CFTR correctors. At the end of incubation intact myotubes (not permeabilized) were labelled with antibodies recognizing an extracellular epitope of either α-SG (on the left) or δ-SG (on the right), as indicated, to mark the membrane resident sarcoglycans only. Primary antibodies were revealed with the secondary DyLight 488-conjugated anti-rabbit antibodies. Bars indicate 31.75 μm. Images were recorded with a Leica SP5 laser scanning confocal microscope at the same setting conditions.

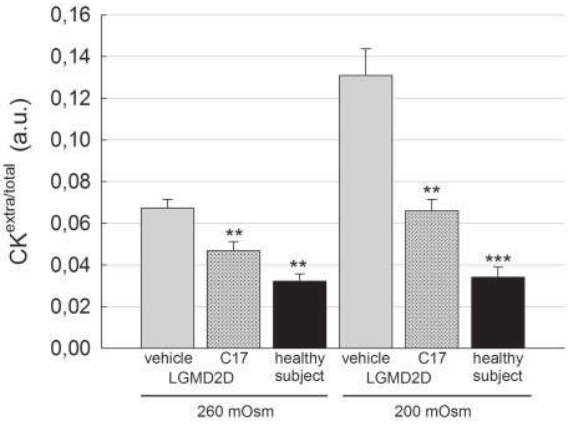

Figure 8. C17 treatment restores membrane functionality to patient's myotubes *in vitro*. Myogenic cells from a patient carrying the L31P/V247M α-SG mutations were grown and differentiated for 7 days and treated for the last 96 h with 1‰ DMSO (vehicle) or 15 μM C17. At the end of the treatment, myotubes were incubated for 20 min in hypo-osmotic solutions as indicated. Then, the cytosolic protein creatine kinase (CK) was measured in the supernatant of myotubes, whereas the intracellular level of the protein was determined after cell lysis. Ratios between extra and total CK values were plotted as average ± SEM of two independent experiments performed in sextuplicate. As reference, the release of CK from myotubes from a healthy subject was assessed at the same hypo-osmotic conditions. Statistical analysis was performed using One-way ANOVA test—multiple comparisons Dunnett test; $^{**}P \leq 0.01$; $^{***}P \leq 0.001$.

constitutively expressing three SGs in which we transfected the mutant. All the mutants checked are rescuable by CFTR corrector treatments as we measured an increase in both quantity (twofold increase was considered significant), and surface localization of the defective proteins (Table 2).

CFTR correctors promote folding and trafficking of type II mutants of the chloride channel, such as ΔF508-CFTR, by two mechanisms. In the first one, correctors are supposed to directly bind and stabilize CFTR, acting as pharmacological chaperones. In the second one, they should modulate the biological capacity of the protein quality control network of the cells, acting as proteostasis regulators (17). In general, a pharmacological chaperone is supposed to be highly specific for a single protein or for conserved motifs of structurally related proteins; conversely, a proteostasis regulator should have a wider spectrum of action (42). α-SG has no structural similarity with CFTR, being a type I protein with a large extracellular N-terminal domain and a short cytosolic C-terminal tail. In our study, we obtained positive results with four mutations, three of them (R77C, D97G and R98H) present in the cadherin-like domain of α-SG, (43) and the last one (V247M) located near the membrane, close to a region probably involved in the interaction with the other SGs (32). Analysing the rescue of the different mutants (Table 2), we can observe that C4 and C17 were effective on all mutants, and C5 on three out of four (those located in the cadherin like domain). This is not surprising for C4 because of its broad activity profile. C4 is active on different processing mutants of CFTR (44,45) as well as on proteins both structurally-correlated and structurally-uncorrelated to CFTR (25,46–49). Moreover, this compound is a weak inhibitor of the E1-E3 ubiquitin ligase cascade (50), therefore could interfere with the degradative pathway of mutants. The effectiveness on α-SG mutants is more surprising for correctors C5 or C17, since they are supposedly specific for ΔF508-CFTR or ABC transporter family, respectively (47,51). On the other hand, both C5 and C17 successfully rescued the I661T mutant of ATP8B1, a protein responsible for the onset of the familial intrahepatic cholestasis, that lacks homology with CFTR (49). Therefore, we can argue that the positive effects exerted by certain CFTR correctors on α-SG is mainly due to a general mechanism, that could modulate the activity, composition or concentration of elements of the proteostasis network. Only VX809 was totally ineffective on α-SG mutants. However, this is in accordance with the high specificity of VX809 for CFTR (47), and ABC proteins sharing common motifs (25), and indeed this small molecule, in combination with Kalydeco (ivacaftor), has been approved by the U.S. FDA as oral treatment for CF since 2015.

Table 2. CFTR corrector efficacy related to specific α-SG mutant expressed in cell models

Corrector	V247M^{HEK293}		R98H^{HEK293}		D97G^{HEK293}		R77C $^{\beta\gamma\delta\text{-cells}}$	
	protein	surface	protein	surface	protein	surface	protein	surface
C2	++	n.d.	−+	n.d.	−	n.d.	n.d.	n.d.
C3	++	n.d.	−+	n.d.	−	n.d.	n.d.	n.d.
C5	−	−	++	√	++	√	+++	√
C6	−	−	++	√	**	n.d.	n.d.	n.d.
C9	++	n.d.	−+	n.d.	−+	n.d.	++	√
C4	++	√	++	n.d.	++	√	++	√
C13	++	n.d.	++	√	**	n.d.	n.d.	n.d.
C14	++	n.d.	++	√	−+	n.d.	n.d.	n.d.
C17	+++	√	+++	√	**	n.d.	+++	√
C15	−	n.d.	+++	n.d.	−+	n.d.	n.d.	n.d.
VX809	−+	−	−	−	−	−	n.d.	n.d.
Glafenine	n.d.	n.d.	−	n.d.	−	n.d.	n.d.	n.d.

√: positive immunofluorescence, −: ineffective, −+: >1X, +: ≥1.5X, ++: ≥2X, +++: ≥3X, **: ≥2X but not statistically significant, n.d.: not determined.

Several CFTR correctors listed in Table 2 would deserve further investigation, in particular by testing different concentrations and, above all, the membrane-localization of rescued mutants. The βγδ-cells transfected with any possible α-SG mutant are a valuable tool to design such experiments, as well as to test additional compounds with improved potency such as, but not limited to, other derivatives of the bithiazole corrector C4 (52). In βγδ-cells transfected with R77C-α-SG we also checked the co-administration of corrector C17 with either C4 or C5. The experience in CF teaches that some promising correctors resulted ineffective in clinical trial when applied individually (53), fostering the research toward the combined use of such compounds. Indeed, the co-administration of C17 + C5 or C17 + C4 resulted in a more effective rescue of the α-SG mutant at the plasma membrane compared with that of either compound applied individually. While the activity of C17 + C5 seems simply additive, that of C17 + C4 suggests a possible synergic mechanism and further work will clarify this point. However, from these data we can suppose that these correctors, even those belonging to the same chemical family (C4 and C17 are two bithiazole derivatives), modulated either different and maybe complementary pathways, or sequential steps of the same pathway during folding and/or trafficking of α-SG toward the plasma membrane. This is remarkable for a future therapy for sarcoglycanopathy, as would permit to treat a wide spectrum of mutations possibly addressing problems distributed along the entire maturation process of sarcoglycans.

We also showed that *in vitro* protein recovery of α-SG mutants was dependent from the dose of the CFTR corrector used (C5, C6 and C17) and that the toxicity on proliferating cells became evident only at very high concentrations. Only corrector C17 showed a very narrow efficacy window (1–8 μM) probably because of a cytostatic effect on proliferating cells exerted at those concentrations. In support of this, there is the observation that no distress sign was evidenced when prolonged treatment and high concentration of C17 were applied on differentiated, non-dividing, LGMD2D myotubes. We are aware that these features are acceptable only for a proof of concept study; however, C17 could represent a lead compound, suitable for efficacy and safety improvement by chemical derivatization.

Even though the data of rescue in cellular models are extremely promising, significantly we validated and reinforced those observations with the results obtained in primary myogenic cells derived from a subject suffering from LGMD2D. Indeed, in patient's myotubes the incubation with C17, C5 or C6 effectively rescued at the sarcolemma the whole SG-complex. The complex, although containing a mutated subunit, was functional as its presence strengthened the sarcolemma, reducing the release of the cytosolic CK protein, under stressful condition.

Experiments with myotubes allowed also to address a few initial issues concerning the mechanism of action of correctors on α-SG. Indeed, our data indicate that corrector C17 had an effect of stabilization on the mutated forms of α-SG only, and this took place without affecting the transcription of the gene. Similar evidence was recorded with βγδ-cells also with correctors C4, C5 and C9. Consequently, we suppose that, acting probably as proteostasis modulators, CFTR correctors help the processes of maturation of α-SG mutants, eventually changing the balance of the biosynthetic/degradative pathways and fostering the assembly with the endogenous partners into a tetramer competent to traffic toward the sarcolemma.

Our strategy is specifically addressing the forms of LGMD2D due to the presence of a missense mutation in the *SGCA* gene. More than 65% of α-SG defects are missense mutations [http://www.dmd.nl] (36) potentially recoverable helping their maturation by corrector treatments. Moreover, many LGMD2D patients are composite heterozygotes, carrying different mutations on the two *SGCA* alleles, and this extends the number of subjects that could benefit from the treatment. Indeed, the recovery of just one allele is predictably sufficient to ameliorate the patient's conditions.

At present it is unknown the amount of sarcoglycan proteins required to reverse the disease phenotype. Surely, 50% of expression guarantees a healthy phenotype, being LGMD2D a recessive disease (1). On the other hand, it is important to remind that disease severity is inversely related to the level of SGs present at the sarcolemma (54–56). Therefore, even a small rescue of SG-complex is expected to ameliorate the patient's conditions. In this framework, the reduced release of CK from pathologic myotubes treated with C17 is significant. Indeed, this is the first observation of a functional rescue of the SG-complex in a human LGMD2D sample upon a pharmacological treatment *in vitro*.

Once at the sarcolemma, a critical issue is the stability of the recovered complex. The presence of a defective α-SG should

lead to a rapid recycling of the tetramer from the sarcolemma, and further work will clarify this point. However, we measured a reduction of the sarcolemma fragility of the LGMD2D myotubes upon corrector treatments, meaning that the SG-complex is sufficiently stable to ameliorate the disease phenotype. We believe that the main issue to overcome in sarcoglycanopathy is to skip mutant degradation, and CFTR correctors, by helping mutant folding, seem to accomplish this task. Then, once assembly and traffic of the tetramer occurred, we expect the interactions among SG-subunits and between SG-complex and elements of the DAPC (33,34) guarantee an adequate structural stability.

Several points need deepening before compounds such as C17, C5, C6, or possibly their derivatives, become actual drugs to treat LGMD2D. Nevertheless, our study represents the proof of principle of a novel pharmacological strategy applicable to a large cohort of patients with LGMD2D. Moreover, we speculate that the same approach is effective with patients suffering from LGMD2C, 2E and 2F, since they share a similar pathogenic mechanism (36). On the other hand, this study, together with other work (48,49), suggests that CFTR correctors could be a significant pharmacological option for many orphan diseases, barely considered by pharmaceutical companies, but with an unmet need to find a cure to ameliorate life condition and life expectancy of patients.

Materials and Methods

Chemicals and treatments

Cycloheximide, glafenine and MG132 were from Sigma-Aldrich, VX809 and VX770 were from Selleck Chemicals, C2, C3, C4, C9 and C17 were a kind gift of the Cystic Fibrosis Foundation, C4, C5, C6, C9, C13, C14 and C15 were from Exclusive Chemistry. All compounds were dissolved in DMSO and the working solution prepared 1000X to have the same content of vehicle (1‰) in each treatment.

Plasmids, cell culture, transfection, and treatments

The full-length cDNA encoding human α-sarcoglycan cloned in the pcDNA3 mammalian expression vector was previously described (57). Plasmids expressing missense mutants of α-sarcoglycan were previously described (6,7).

HEK-293, V247M cells (8), HER-911 and βγδ-HER were grown in Dulbecco's modified Eagle's medium (Sigma) supplemented with 10% fetal bovine serum (FBS) (Gibco) and maintained in a humidified atmosphere containing 5% CO_2 at 37°C.

Immortalized human myoblasts (58) were from the 'Human cell culture platform' of the Myology Institute in Paris. Primary human myogenic cells from an LGMD2D patient were isolated from a bioptic fragment from the Telethon Genetic Bio-Bank facility (8). Myogenic cells were grown in Skeletal Muscle Cell Growth Medium (Promocell) supplemented with 15% FBS (Gibco), named skeletal growth medium (SGM). To start differentiation, myoblasts, grown at confluence, were incubated with DMEM supplemented with 2% Horse Serum (Euroclone), 10 μg/ml human recombinant insulin (Sigma), 100 μg/ml human Apotransferrin (Sigma-Aldrich), named skeletal differentiating medium (SDM). Differentiation was carried out for seven days.

For transient expression, HEK 293 cells were seeded at 50 000 cells/cm^2 and transfected the day after with TransIT-293 (MirusBio) according to manufacturer's instruction. Twenty-four hours after transfection, medium was replaced with DMEM supplemented with 2% FBS containing the indicated concentration of correctors (dissolved in DMSO) or with DMSO alone (final DMSO concentration 1‰).

HER911 or βγδ-cells cells were seeded at 50 000 cells/cm^2 and transfected the day after with 9 μl of Fugene HD Transfection Reagent (E2312 from Promega) and 3 μg of plasmid coding for wild type or mutated α-SG.

MG132 was added 8 h before cell lysis, CFTR correctors were added 24 h before cell lysis or IF assay (transfected HEK293, V247M cells, HER911 and βγδ-cells) and 24–96 h before myotubes lysis, treatment with CHX or IF assay.

After treatments, cells were washed twice with ice cold PBS and lysed with 5% sodium deoxycholate supplemented with complete protease inhibitor (Sigma-Aldrich).

Establishment of a HER911 cell line stably expressing β-, γ -, and δ-sarcoglycan

The stably expressing βγδ-SG clonal cell line was obtained by integration of β-SG, γ-SG, and δ-SG cDNA using lentiviral vectors in HER911 cells. The day following plating cells in 6-well plates, an appropriate volume of lentiviral vector-expressing β-, γ- an δ-SG was added directly into each well containing 1 ml of culture medium, to infect the cells at 100 Multiplicity of Infection (MOI). After 3 h of incubation at 37°C, 1 ml of culture medium was added into each well and cells were incubated at 37°C for an additional 48 h. Each well was subcultured again in 6-well plates and the transduction was repeated two more times as explained above. After three transductions, cells were subcultured in a T-75 culture flask and were maintained at 37°C until 100% of confluence. Then, cells were collected, centrifuged, and resuspended in culture medium at a density of 5×10^5 cells/ml. To obtain clonal cell lines, single cells were sorted by Astrios Beckman Coulter (Brea, CA) from the cell suspension and seeded in 96-well plates in culture medium. After 10 days, a total number of 30 clonal cell lines were selected and subcultured in larger culture plates. All 30 clones were subjected to qPCR analysis to determine the copy-number/genome of each SG and to RT-qPCR analysis to monitor the expression of SGs. One positive SG expressing cell clone was chosen for the next step.

DNA and RNA extraction, qPCR and RT-qPCR from HER911 cells

Genomic DNA (gDNA) and total RNA were extracted using TRIzol reagent (Thermo Fisher Sci.) following the manufacturer's protocol. Total RNA was used as a template for reverse transcription using the MultiScribe RT cDNA kit (Life technologies) according to manufacturer's protocol. gDNA or cDNA from each clone were used as template for qPCR to determine SG-cDNA copy number/genome or sarcoglycan expression, respectively. Amplification was carried out using the ABsoluteQPCR ROXMix (Thermo Fisher Sci.) and the following primers and Taqman probes to β-SG (Forward: 5-CCCGCCTACCCAGTTCCT-3; Reverse: 5-TGTAGCGTACCCAGTCACCACTA-3; Probe: 5-CAGTG GAGACCAGTTGG-3), γ-SG (Forward: 5-AAGTCGGTCCCAAAATG GTAGA-3; Reverse: 5-TGCCGTCGTTGGAGTTGA-3; Probe: 5-CAGAATCAACAGTTTCAG-3), δ-SG (Forward: 5-TGCCTCAGGAG CAGTACACTCA-3; Reverse: 5-CCATAAATCCCCACCTTGTATAC C-3; Probe: 5-ACCGGAGCACCATGCCTGGCT-3). The albumin gene was amplified to normalize the results of copy number/genome of SG-cDNAs, whereas the ubiquitous acidic ribosomal

phosphoprotein (P0) was amplified to normalize the result of SGs expression. All PCR reactions were performed in duplicate and each quantification repeated three times.

RNA extraction from LGMD2D myotubes and RT-qPCR

Total RNA from differentiated myotubes, treated for 48h with 0.1‰ DMSO or C17 15 μM, was extracted with TRIsure reagent (Bioline) according to manufacturer's instructions, and further purified with RNA Clean Up columns (Zymo research). 1 μg of total RNA was reverse transcribed using the SensiFast cDNA synthesis kit (Bioline). Cyclophilin A (*PPIA*), β-2-microglobulin (*B2M*), and ribosomal protein L32 (*RPL32*) were used as reference genes. qPCR was performed in triplicate in a IQ5 Thermal Cycler (Bio-Rad, Hercules, CA, USA) using Biorad iQ Sybr green supermix. The PCR parameters were: initial denaturation at 95°C for 3 min followed by 40 cycles of 10 s at 95°C and 30 s at 55°C for acquisition of fluorescence signal. A melting curve was generated by the iQ5 software following the end of the final cycle for each sample to confirm the specificity of the amplified product. The efficiency of each run was determined by a standard curve and used for calculations. Normalization was performed by geNorm software (https://genorm.cmgg.be/).

Primer sequences were as follows: α-SG forward primer, 5'- C CCCAGACCGTGACTTCTTG-3', reverse primer 5'- TCTCTTCAGC CTTCCCTCCC-3'; *PPIA* forward primer, 5′-TTCATCTGCACTGC CAAGA-3′, reverse primer, 5′-CGAGTTGTCCACAGTCAGC-3′; *B2M* forward primer, 5′-TATCCAGCGTACTCCAAGA-3′, reverse primer, 5′-GACAAGTCTGAATGCTCCAC-3′; *RPL32* forward primer, 5′-CATCTCCTTCTCGGCATC-3′, reverse primer, 5′-CTGGGT TTCCGCCAGTTA-3′.

Data are expressed as means ± SE of three experiments. Comparisons were made using the *t* test, with values of $P < 0.05$ considered statistically significant.

Cycloheximide treatments

LGMD2D myotubes treated for 96h with DMSO or C17 15 μM were incubated with cycloheximide 100 μg/ml for 0, 6, 12 and 24 h. At each time point, cells were lysed with 5% sodium deoxycholate supplemented with complete protease inhibitor and the lysates were stored at -80°C before immunoblot analysis. The intensity of the α-SG signals was normalized to total protein loading, assessed by Ponceau Red staining. Each experiment was performed in triplicate.

Immunoblot analysis

Proteins were quantified by the bicinchoninic-acid protein assay kit (Thermo Scientific), according to manufacturer's instructions. Proteins were resolved by SDS-PAGE, blotted onto a nitrocellulose membrane and probed with selected antibodies (see below). Secondary antibody was horseradish peroxidase-labeled goat anti-mouse IgG (Sigma-Aldrich). Blots were developed with ECL chemiluminescent substrate (Euroclone), and chemiluminescent signals were digitally acquired with a Chemidoc Imaging System (Biorad). In alternative, total proteins lysates were resolved on NuPAGE® Novex® 4–12% Bis-Tris Protein Gels (Thermo Fisher Scientific) and transferred to nitrocellulose membranes (iBlot, Thermo Fisher Scientific) following the manufacturer's instructions. Membranes were blocked in Odyssey Blocking Buffer (Li-Cor) for 1 h at room temperature. Incubations with primary antibodies were carried out at 4°C overnight in Odyssey Blocking Buffer. After 1-h incubation with donkey anti-rabbit IRDye680 and anti-mouse IRDye800 antibodies (EuroBio) at room temperature, proteins were detected by fluorescence in a Odissey imaging system (Li-Cor) following the manufacturer's instructions.

Densitometry was performed with the ImageJ software. The intensities of sarcoglycan bands were normalized for the intensity of β-actin or α-actinin.

Cell viability and cytotoxicity assay

Cells were seeded in a 96-multiwell at a density of 10 000 cells per well. After 24 h, correctors dissolved in 1‰ DMSO were added at the indicated concentrations. After 24 h of treatment, cell viability was determined measuring the bioreduction of MTS (Owen's reagent) by living cells with the Cell Titer 96 Aqueous proliferation assay (Promega) according to the manufacturer's instruction. Cell toxicity was determined measuring the release of LDH in culture supernatant with the Cytotox 96 cytotoxicity assay (Promega) according to the manufacturer's instruction. A maximum LDH release control was performed adding a lysis solution 45 min before adding Cytotox 96 reagent, and LDH release was calculated as (experimental LDH release-blank)/(maximum LDH release-blank)×100.

All spectrophotometric measurements were performed with a Novapath Microplate Reader (Bio-Rad). All experiments were run in sextuplicate.

Hypo-osmotic stress and CK release assay

Myotubes differentiated for 7 days and treated for 96 h with 1‰ DMSO or C17 15 μM were incubated with two hypo-osmotic solutions (260 and 200 mOsm) for 20 min at 37°C. Hypo-osmotic solutions consisted of a salt solution (5 mM HEPES, 5 mM KCl, 1 mM $MgCl_2$, 5 mM NaCl, 1.2 mM $CaCl_2$, 1mM glucose) supplemented with 157 mM sucrose (200 mOsm) or 213 mM sucrose (260 mOsm). Osmolarities were verified with a OM 801 osmometer (Vogel). After the treatment, the supernatant containing the released CK was removed and an equal volume of ice-cold hypo-osmotic solution was added to the cells. The cells were recovered by scraping and lysed by three cycles of freeze-thawing. Released and intra-cellular Creatine Kinase were measured in sextuplicate using the Creatine Kinase Activity Colorimetric Assay Kit (BioVision) according to the manufacturer's instructions.

Confocal immunofluorescence

Immunofluorescence-confocal analyses were performed either in intact cells (not permeabilized) or in permeabilized cells. For the former condition, cells, grown on polylysine-treated glasses, at the end of treatments were incubated for 30 min at 4°C, then gently washed twice with ice-cold PBS and incubated with primary antibodies for 5 h at 4°C. After three gentle washings with ice-cold PBS, cells were incubated with fluorescently labeled secondary antibodies for 2 h at 4°C. Primary and secondary antibodies were diluted in PBS supplemented with 0.5% BSA. After secondary antibody incubation, cells were washed with PBS and then fixed for 15 min with 4% paraformaldehyde in PBS (PFA). After incubation with 50 mmol/L NH_4Cl for 15 min and washing with PBS, nuclei were stained with Hoechst or DAPI. For analysis in permeabilized cells, cells grown and treated as above, were washed with PBS, fixed for 15 min in PBS 3.7% formaldehyde

(Sigma-Aldrich) at room temperature. Slides were rinsed in PBS and permeabilized with PBS 0.5% Triton X-100 (Sigma-Aldrich) for 5 min and then blocked for 30 min with PBS containing 10% SVF to prevent non-specific staining. Incubation with primary and secondary antibody was performed as above described. Cells were examined with a Leica SP5 confocal laser scanning microscope.

Quantification of the mean fluorescence intensity of membrane staining in βγδ-cells transfected with R77C-α-SG was performed by using ImageXpress microscope system (Molecular Devices). Normalization was performed by counting the number of cells positive for both DAPI and α-SG in permeabilization conditions to consider possible differences in transfection efficiency.

Antibodies

Mouse monoclonal antibody specific for α-SG (NCL-a-SARC) was from Leica Biosystem; rabbit monoclonal anti α-SG (AB189254) was from Abcam; mouse monoclonal antibody specific for β-SG, δ-SG, γ-SG and β-actin were from Sigma, rabbit polyclonal antibody specific for α-and δ-SG were produced as previously described (8), rabbit polyclonal antibody specific for α-actinin was from Santa Cruz. Alexa fluor 488, Alexa fluor 594- and DyLight 488-conjugated goat anti-mouse and goat anti-rabbit were from Life Technologies.

Statistical analysis

Data are expressed as means ± SEM. Statistical differences among groups were determined by One-way ANOVA test, followed by either Dunnett test for simultaneous multiple comparisons with control, or Bonferroni test for simultaneous comparisons of all possible contrasts (pairs). When only two groups were considered, statistical analysis was performed by the unpaired two-tailed Student's *t*-test. A level of confidence of $P < 0.05$ was used for statistical significance.

Supplementary Material

Supplementary Material is available at *HMG* online.

Acknowledgements

Giulia Rossetto is kindly thanked for her precious help with primary myogenic cells. Cécile Patissier and Marine Faivre from Genethon INTEGRARE, Evry, are gratefully thanked for their work in generation and characterization of the $\beta\gamma\delta$-cells; Anne-Laure Egesipe and Julie Pernelle, from Istem, AFM Telethon, are gratefully thanked for the valuable help in setup of cell surface fluorescence quantification by ImageXpress. Vincent Mouly and the 'Human cell culture platform' of the Myology Institute Université Pierre et Marie Curie, Paris 6 are gratefully thanked for providing immortalized human myoblasts derived from a healthy subject. Elena Pegoraro and the Telethon Genetic Bio-Bank facility, University of Padova are gratefully thanked for providing the skeletal muscle biopsy of a LGMD2D patient. A special acknowledgement to the Cystic Fibrosis Foundation for providing the first stock of CFTR correctors.

Conflict of Interest statement. None declared.

Funding

Association Françoise contre les Myopathies (18620 to D.S. and I.R.), Italian Telethon Foundation (GEP12058 and GGP15140 to D.S.), University of Padova (CPDA149821/14 to D.S.). Funding to pay the Open Access publication charges for this article was provided by Italian Telethon Foundation.

References

1. Nigro, V. and Savarese, M. (2014) Genetic basis of limb-girdle muscular dystrophies: the 2014 update. *Acta Myol.*, **33**, 1–12.
2. Tarakci, H. and Berger, J. (2016) The sarcoglycan complex in skeletal muscle. *Front. Biosci. (Landmark Ed.)*, **21**, 744–756.
3. Sandonà, D. and Betto, R. (2009) Sarcoglycanopathies: molecular pathogenesis and therapeutic prospects. *Expert Rev. Mol. Med.*, **11**, e28.
4. Kirschner, J. and Lochmüller, H. (2011) Sarcoglycanopathies. *Handb. Clin. Neurol.*, **101**, 141.
5. Bartoli, M., Gicquel, E., Barrault, L., Soheili, T., Malissen, M., Malissen, B., Vincent-Lacaze, N., Perez, N., Udd, B., Danos, O. and Richard, I. (2008) Mannosidase I inhibition rescues the human alpha-sarcoglycan R77C recurrent mutation. *Hum. Mol. Genet.*, **17**, 1214–1221.
6. Gastaldello, S., D'Angelo, S., Franzoso, S., Fanin, M., Angelini, C., Betto, R. and Sandonà, D. (2008) Inhibition of proteasome activity promotes the correct localization of disease-causing alpha-sarcoglycan mutants in HEK-293 cells constitutively expressing beta-, gamma-, and delta-sarcoglycan. *Am. J. Pathol.*, **173**, 170–181.
7. Soheili, T., Gicquel, E., Poupiot, J., N'Guyen, L., Le Roy, F., Bartoli, M. and Richard, I. (2012) Rescue of sarcoglycan mutations by inhibition of endoplasmic reticulum quality control is associated with minimal structural modifications. *Hum. Mutat.*, **33**, 429–439.
8. Bianchini, E., Fanin, M., Mamchaoui, K., Betto, R. and Sandona, D. (2014) Unveiling the degradative route of the V247M α-sarcoglycan mutant responsible for LGMD-2D. *Hum. Mol. Genet.*, **23**, 3746–3758.
9. Denny, R.A., Gavrin, L.K. and Saiah, E. (2013) Recent developments in targeting protein misfolding diseases. *Bioorg. Med. Chem. Lett.*, **23**, 1935–1944.
10. Valastyan, J.S. and Lindquist, S. (2014) Mechanisms of protein-folding diseases at a glance. *Dis. Model.Mech.*, **7**, 9–14.
11. Wang, Y.J., Di, X.J. and Mu, T.W. (2014) Using pharmacological chaperones to restore proteostasis. *Pharmacol. Res.*, **83**, 3–9.
12. Powers, E.T., Morimoto, R.I., Dillin, A., Kelly, J.W. and Balch, W.E. (2009) Biological and chemical approaches to diseases of proteostasis deficiency. *Annu. Rev. Biochem.*, **78**, 959–991.
13. Chaudhuri, T.K. and Paul, S. (2006) Protein-misfolding diseases and chaperone-based therapeutic approaches. *febs J.*, **273**, 1331–1349.
14. Leidenheimer, N.J. and Ryder, K.G. (2014) Pharmacological chaperoning: a primer on mechanism and pharmacology. *Pharmacol. Res.*, **83**, 10–19.
15. Pedemonte, N., Lukacs, G.L., Du, K., Caci, E., Zegarra-Moran, O., Galietta, L.J. and Verkman, A.S. (2005) Small-molecule correctors of defective DeltaF508-CFTR cellular processing identified by high-throughput screening. *J. Clin. Invest.*, **115**, 2564–2571.
16. Cai, Z., Liu, J., Li, H. and Sheppard, D.N. (2011) Targeting F508del-CFTR to develop rational new therapies for cystic fibrosis. *Acta Pharmacol. Sin.*, **32**, 693–701.

17. Birault, V., Solari, R., Hanrahan, J. and Thomas, D.Y. (2013) Correctors of the basic trafficking defect of the mutant F508del-CFTR that causes cystic fibrosis. *Curr. Opin. Chem. Biol.*, **17**, 353–360.
18. Bell, S.C., De Boeck, K. and Amaral, M.D. (2015) New pharmacological approaches for cystic fibrosis: promises, progress, pitfalls. *Pharmacol. Ther.*, **145**, 19–34.
19. Rowe, S.M. and Verkman, A.S. (2013) Cystic fibrosis transmembrane regulator correctors and potentiators. *Cold Spring Harb. Perspect. Med.*, **3**, a009761. pii: a009761
20. Robert, R., Carlile, G.W., Pavel, C., Liu, N., Anjos, S.M., Liao, J., Luo, Y., Zhang, D., Thomas, D.Y. and Hanrahan, J.W. (2008) Structural analog of sildenafil identified as a novel corrector of the F508del-CFTR trafficking defect. *Mol. Pharmacol.*, **7**, 478–489.
21. Yoo, C.L., Yu, G.J., Yang, B., Robins, L.I., Verkman, A.S. and Kurth, M.J. (2008) Methyl-4, 5'-bithiazole-based correctors of defective delta F508-CFTR cellular processing. *Bioorg. Med. Chem. Lett.*, **18**, 2610–2614.
22. Robert, R., Carlile, G.W., Liao, J., Balghi, H., Lesimple, P., Liu, N., Kus, B., Rotin, D., Wilke, M., de Jonge, H.R. *et al.* (2010) Correction of the Delta phe508 cystic fibrosis transmembrane conductance regulator trafficking defect by the bioavailable compound glafenine. *Mol. Pharmacol.*, **77**, 922–930.
23. Loo, T.W., Bartlett, M.C., Wang, Y. and Clarke, D.M. (2006) The chemical chaperone CFcor-325 repairs folding defects in the transmembrane domains of CFTR-processing mutants. *Biochem. J.*, **395**, 537–542.
24. Loo, T.W., Bartlett, M.C. and Clarke, D.M. (2013) Corrector VX-809 stabilizes the first transmembrane domain of CFTR. *Biochem. Pharmacol.*, **86**, 612–619.
25. Sabirzhanova, I., Lopes Pacheco, M., Rapino, D., Grover, R., Handa, J.T., Guggino, W.B. and Cebotaru, L. (2015) Rescuing trafficking mutants of the ATP-binding Cassette Protein, ABCA4, with small molecule correctors as a treatment for Stargardt eye disease. *J. Biol. Chem.*, **290**, 19743–19755.
26. Van Goor, F., Hadida, S., Grootenhuis, P.D., Burton, B., Cao, D., Neuberger, T., Turnbull, A., Singh, A., Joubran, J. and Hazlewood, A. (2009) Rescue of CF airway epithelial cell function in vitro by a CFTR potentiator, VX-770. *Proc. Natl. Acad. Sci. U S A*, **106**, 18825–18830.
27. Wainwright, C.E., Elborn, J.S., Ramsey, B.W., Marigowda, G., Huang, X., Cipolli, M., Colombo, C., Davies, J.C., De Boeck, K., Flume, P.A., TRAFFIC Study Group; TRANSPORT Study Group. *et al.* (2015) Lumacaftor-ivacaftor in patients with cystic fibrosis homozygous for Phe508del CFTR. *N. Engl. J. Med.*, **373**, 220–231.
28. Ginsberg, F., Bourguignon, R.P., Smets, P. and Famaey, J.P. (1983) Tiapride versus glafenine: a double-blind comparative study in the management of acute rheumatic pain. *Curr. Med. Res. Opin.*, **8**, 562–569.
29. Draviam, R.A., Wang, B., Shand, S.H., Xiao, X. and Watkins, S.C. (2006a) Alpha-sarcoglycan is recycled from the plasma membrane in the absence of sarcoglycan complex assembly. *Traffic*, **7**, 793–810.
30. Carrié, A., Piccolo, F., Leturcq, F., de Toma, C., Azibi, K., Beldjord, C., Vallat, J.M., Merlini, L., Voit, T., Sewry, C. *et al.* (1997) Mutational diversity and hot spots in the alpha-sarcoglycan gene in autosomal recessive muscular dystrophy (LGMD2D). *J. Med. Genet.*, **34**, 470–475.
31. Duggan, D.J., Gorospe, J.R., Fanin, M., Hoffman, E.P. and Angelini, C. (1997) Mutations in the sarcoglycan genes in patients with myopathy. *N. Engl. J. Med.*, **336**, 618–624.
32. Shi, W., Chen, Z., Schottenfeld, J., Stahl, R.C., Kunkel, L.M. and Chan, Y.-M. (2004) Specific assembly pathway of sarcoglycans is dependent on beta- and delta-sarcoglycan. *Muscle Nerve*, **29**, 409–419.
33. Draviam, R.A., Shand, S.H. and Watkins, S.C. (2006b) The beta-delta-core of sarcoglycan is essential for deposition at the plasma membrane. *Muscle Nerve*, **34**, 691–701.
34. Allikian, M.J. and McNally, E.M. (2007) Processing and assembly of the dystrophin glycoprotein complex. *Traffic*, **8**, 177–183.
35. Straub, V. and Campbell, K.P. (1997) Muscular dystrophies and the dystrophin-glycoprotein complex. *Curr. Opin. Neurol.*, **10**, 168–175.
36. Carotti, M., Fecchio, C. and Sandonà, D. (2017) Emerging therapeutic strategies for sarcoglycanopathy. *Exp. Opin. Orphan Drugs*, **5**, 381–396.
37. Bushby, K. (2009) Diagnosis and management of the limb girdle muscular dystrophies. *Pract. Neurol.*, **9**, 314–323.
38. Nigro, V. and Piluso, G. (2015) Spectrum of muscular dystrophies associated with sarcolemmal-protein genetic defects. *Biochim. et Biophys. Acta*, **1852**, 585–593.
39. Menke, A. and Jockusch, H. (1995) Extent of shock-induced membrane leakage in human and mouse myotubes depends on dystrophin. *J. Cell Sci.*, **108**, 727–733.
40. Young, C.S., Hicks, Michael R., Ermolova, Natalia V., Nakano, Haruko., Jan, Majib., Younesi, Shahab., Karumbayaram, Saravanan., Kumagai-Cresse, Chino., Wang, Derek., Zack, Jerome A. *et al.* (2016) A single CRISPR-Cas9 deletion strategy that targets the majority of DMD patients restores dystrophin function in hiPSC-derived muscle cells. *Cell Stem Cell*, **18**, 533–540.
41. Noack, J., Brambilla Pisoni, G. and Molinari, M. (2014) Proteostasis: bad news and good news from the endoplasmic reticulum. *Swiss Med. Wkly*, **144**, w14001.
42. Balch, W.E., Morimoto, R.I., Dillin, A. and Kelly, J.W. (2008) Adapting proteostasis for disease intervention. *Science*, **319**, 916–919.
43. Dickens, N.J., Beatson, S. and Ponting, C.P. (2002) Cadherin-like domains in alpha-dystroglycan, alpha/epsilon-sarcoglycan and yeast and bacterial proteins. *Curr. Biol.*, **12**, R197–R199.
44. Grove, D.E., Rosser, M.F., Ren, H.Y., Naren, A.P. and Cyr, D.M. (2009) Mechanisms for rescue of correctable folding defects in CFTR Delta F508. *Mol. Biol. Cell*, **20**, 4059–4069.
45. Caldwell, R.A., Grove, D.E., Houck, S.A. and Cyr, D.M. (2011) Increased folding and channel activity of a rare cystic fibrosis mutant with CFTR modulators. *Am. J. Physiol. Lung Cell Mol. Physiol.*, **301**, L346–L352.
46. Wang, Y., Bartlett, M.C., Loo, T.W. and Clarke, D.M. (2006) Specific rescue of cystic fibrosis transmembrane conductance regulator processing mutants using pharmacological chaperones. *Mol. Pharmacol.*, **70**, 297–302.
47. Van Goor, F., Hadida, S., Grootenhuis, P.D., Burton, B., Stack, J.H., Straley, K.S., Decker, C.J., Miller, M., McCartney, J., Olson, E.R. *et al.* (2011) Correction of the F508del-CFTR protein processing defect in vitro by the investigational drug VX-809. *Proc. Natl. Acad. Sci. U S A*, **108**, 18843–18848.
48. Sampson, H.M., Lam, H., Chen, P.C., Zhang, D., Mottillo, C., Mirza, M., Qasim, K., Shrier, A., Shyng, S.L., Hanrahan, J.W. and Thomas, D.Y. (2013) Compounds that correct F508del-CFTR trafficking can also correct other protein trafficking diseases: an in vitro study using cell lines. *Orphanet. J. Rare Dis.*, **8**, 11.
49. van der Woerd, W.L., Wichers, C.G., Vestergaard, A.L., Andersen, J.P., Paulusma, C.C., Houwen, R.H. and van de Graaf, S.F. (2016) Rescue of defective ATP8B1 trafficking by

CFTR correctors as a therapeutic strategy for familial intrahepatic cholestasis. *J. Hepatol.*, **64**, 1339–1347.
50. Jurkuvenaite, A., Chen, L., Bartoszewski, R., Goldstein, R., Bebok, Z., Matalon, S. and Collawn, J.F. (2010) Functional stability of rescued delta F508 cystic fibrosis transmembrane conductance regulator in airway epithelial cells. *Am. J. Respir. Cell. Mol. Biol.*, **42**, 363–372.
51. Loo, T.W., Bartlett, M.C., Shi, L. and Clarke, D.M. (2012) Corrector-mediated rescue of misprocessed CFTR mutants can be reduced by the P-glycoprotein drug pump. *Biochem. Pharmacol.*, **83**, 345–354.
52. Ye, L., Hu, B., El-Badri, F., Hudson, B.M., Phuan, P.W., Verkman, A.S., Tantillo, D.J. and Kurth, M.J. (2014) ΔF508-CFTR correctors: synthesis and evaluation of thiazole-tethered imidazolones, oxazoles, oxadiazoles, and thiadiazoles. *Bioorg. Med. Chem. Lett.*, **24**, 5840–5844.
53. Clancy, J.P., Rowe, S.M., Accurso, F.J., Aitken, M.L., Amin, R.S., Ashlock, M.A., Ballmann, M., Boyle, M.P., Bronsveld, I.nez., Campbell, P.W. *et al.* (2012) Results of a phase IIa study of VX-809, an investigational CFTR corrector compound, in subjects with cystic fibrosis homozygous for the F508del-CFTR mutation. *Thorax*, **67**, 12–18.
54. Barresi, R., Confalonieri, V., Lanfossi, M., Di Blasi, C., Torchiana, E., Mantegazza, R., Jarre, L., Nardocci, N., Boffi, P., Tezzon, F. *et al.* (1997) Concomitant deficiency of beta- and gamma-sarcoglycans in 20 alpha-sarcoglycan (adhalin)-deficient patients: immunohistochemical analysis and clinical aspects. *Acta Neuropathol.*, **94**, 28–35.
55. Vainzof, M., Passos-Bueno, M.R., Pavanello, R.C., Marie, S.K., Oliveira, A.S. and Zatz, M. (1999) Sarcoglycanopathies are responsible for 68% of severe autosomal recessive limb-girdle muscular dystrophy in the Brazilian population. *Neurol. Sci.*, **164**, 44–49.
56. Boito, C., Fanin, M., Siciliano, G., Angelini, C. and Pegoraro, E. (2003) Novel sarcoglycan gene mutations in a large cohort of Italian patients. *J. Med. Genet.*, **40**, e67.
57. Sandona, D., Gastaldello, S., Martinello, T. and Betto, R. (2004) Characterization of the ATP-hydrolysing activity of alpha-sarcoglycan. *Biochem. J.*, **381**, 105–112.
58. Zhu, C.H., Mouly, V., Cooper, R.N., Mamchaoui, K., Bigot, A., Shay, J.W., Di Santo, J.P., Butler-Browne, G.S. and Wright, W.E. (2007) Cellular senescence in human myoblasts is overcome by human telomerase reverse transcriptase and cyclin-dependent kinase 4: consequences in aging muscle and therapeutic strategies for muscular dystrophies. *Aging Cell*, **6**, 515–523.

5. RESULTS

5.1 Generation of β-SG- and δ-SG-KO zebrafish lines to mimic sarcoglycanopathy

Orthologues of all human muscle specific SGs are expressed in zebrafish (Chambers et al.,2003; Steffen et al., 2007). Protein sequence alignments show that among the four SG proteins, β- and δ-SG are the most conserved, being β-SG (coded by z-*scgb* gene) 75% identical and 87% similar to human orthologue and δ-SG (coded by z-*sgcd* gene) 72% identical and 87% similar to human orthologue. Furthermore, the rational of mimicking sarcoglycanopathy in zebrafish is consequent to both literature (Guyon et al., 2005; Cheng et al., 2006) and our data of δ-SG-knocking down (KD) by morpholino oligo (MO) targeting the translational starting point of the mRNA. As reported in Fig. 30, δ-SG-KD leads to severe abnormality at macro and microscopic level in both skeletal and cardiac muscle, in this well modelling the human condition.

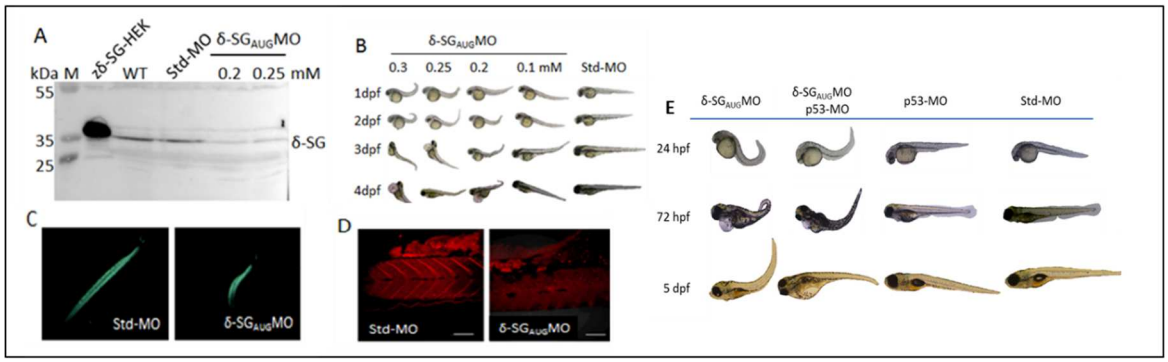

Fig 30. Mimicking sarcoglycanopathy in zebrafish

A) δ-SG MO, targeting the AUG codon of mRNA, reduced the expression of δ-SG in injected zebrafish. Western blot analysis of total protein extracts from 3-dpf *larvae* of WT fish and std-MO or δ-SG_{AUG}MO-2 injected zebrafish. As positive control, proteins from HEK293 cells transiently transfected with a vector expressing the zebrafish δ-SG sequence (zδ-SG-HEK293) were loaded in the gel.

B) Zebrafish injected with δ-SG MO show a curved or bent phenotype, denoting muscle impairment. Zebrafish oocytes, at 1 cell stage, were injected with either the standard control morpholino (std-MO) or the reported concentration of the δ-SG MO. Embryo and *larvae* were analysed at different time points after injection. dpf, days post fertilization

C) δ-SG knock down resulted in altered birefringence, denoting muscle impairment.

D) Decreased expression of the β-SG partner is observed at the myosepta of δ-SG MO injected zebrafish, in this resembling sarcoglycanopathy. 3-dpf zebrafish, injected with either the std-MO or δ-SG MO, were analysed by whole-mount immunofluorescence using an anti-β-SG antibody. Primary antibody was revealed with the secondary DyLight 594-conjugated anti-mouse antibody. Images were recorded with a Leica SP2 laser scanning confocal microscope.

E) The KD of p53 did not determine the rescue of the phenotype. The phenotype derived from KD of δ-SG was not due to the activation of p53.

Confident of the promising results obtained with the δ-SG-KD, we decided to take advantage of the CRISPR/Cas9 system to perform the specific knock out (KO) of β- and δ-SG and select stable mutant lines.

Recent works reported that bacterial type II CRISPR systems can be adapted to create a single guide RNAs (sgRNAs) capable of directing site specific DNA cleavage by the Cas9 nuclease *in vivo* to induce targeted genetic modifications in zebrafish embryos with high efficiency (Hwang et al., 2013). Therefore, we decided to adopt this procedure to target exons 1 or exon 2 of the z-*sgcb* and z-*sgcd*. The initial region of the genes, to limit the possibility of the production of a truncated protein that may retain a partial function, is chosen as target.

Once characterized at the molecular, histological and functional level, these animals will be utilized to transiently express mutated forms of SG in order to check the ability of the zebrafish quality control system to recognize and degrade such defective proteins. Such experiments should give the first hints on the feasibility of mimicking in zebrafish the forms of sarcoglycanopathy caused by missense mutations.

5.1.1 Workflow for KO production

Figure 31 reports the workflow for KO zebrafish production with the indication of the main steps of the entire procedure.

The first delicate step is the design of the suitable sgRNA to target the genomic region of interest. Several software, such as Chop-Chop (chopchop.cbu.uib.no) (Labun et al., 2016) design tools, can help in this operation (see Fig. 32 for details). The sgRNA and the Cas9 protein are then injected into 1-2 cell-zygotes. Part of the embryos, developing after the injection (F0 population), is genotyped to evaluate the somatic frequency of indel mutations generated via NHEJ. The remaining embryos are grown until sexual maturity (about three months) to be outcrossed with WT. The genotyping of the F1 population permits the identification of the founders, those animals in which the mutations occurred also in the germline. Heterozygote founders, when sexually mature are crossbred to obtain the F2 population in which approximately one quarter of fish is WT, two quarter heterozygotes and one quarter mutated homozygotes. From this point the crossbreed of the mutated homozygotes establishes the stable line. Considering any possible drawback of the procedure and the time needed to reach the sexual maturity of fish, the characterization of the novel lines can start approximately 1 years form the first rounds of sgRNA/Cas9 injection.

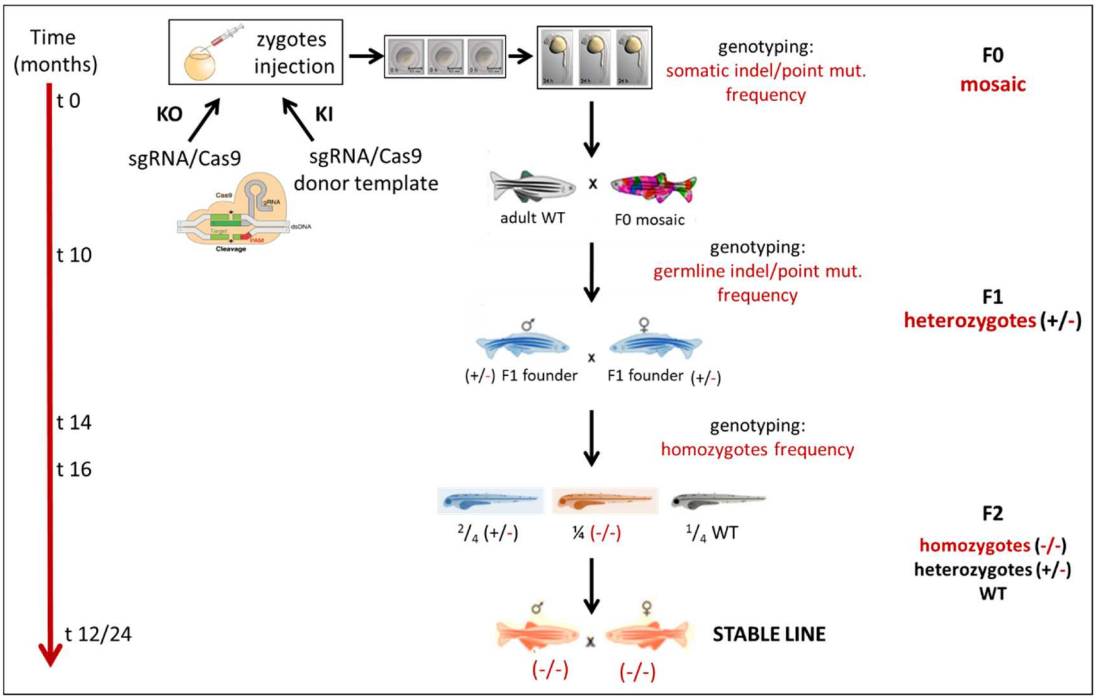

Fig 31. Timeline of KO and KI generation.

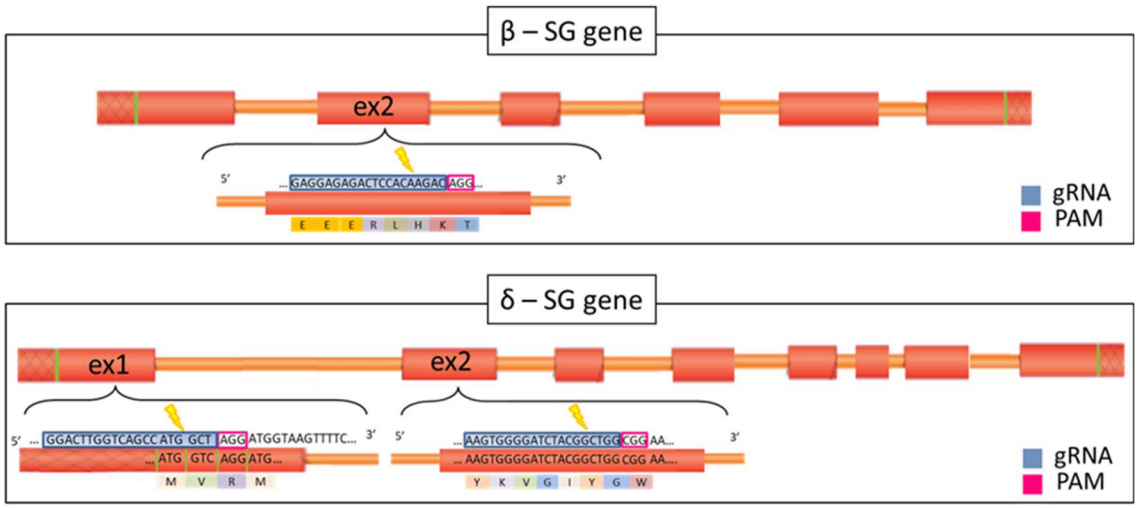

Fig 32. β-SG$_{ex2}$-, δ-SG$_{ex1}$-, δ-SG$_{ex2}$ sgRNAs. Scheme of z-*sgcb* (upper panel) and z-*sgcd* (lower panel) organization. Exons are depicted as red boxes, introns as orange lines, the dimensions are not in scale. The targeted regions are enlarged with the nucleotide sequence recognized by the sg-RNA indicated in blue. For each guide, the PAM sequence, essential for Cas9 activity, is boxed in pink. Lightning bolts represent the putative sites of break from Cas9. The amino acid sequences corresponding to the regions of interest are also reported.

SgRNAs were synthesized from a template generated by the annealing and subsequent extension of oligo A and B (see the Fig. 33). Oligo B corresponds to the constant part of the CRSPR RNA and is common to all reactions. On the contrary, Oligo A contains the sequence of the SP6 promoter, 20 nt of the specific target sequence, and 20 nt overlapping the chimeric gRNA core sequence. 8 nL of a mix containing 70 ng/µL of purified sgRNA of β-SGex2-, δ-SGex1- or δ-SGex2 and 300 ng/µL recombinant Cas9-NLS (nuclear localization signal) were injected into one-two-cell stage zygotes to induces mutagenesis.

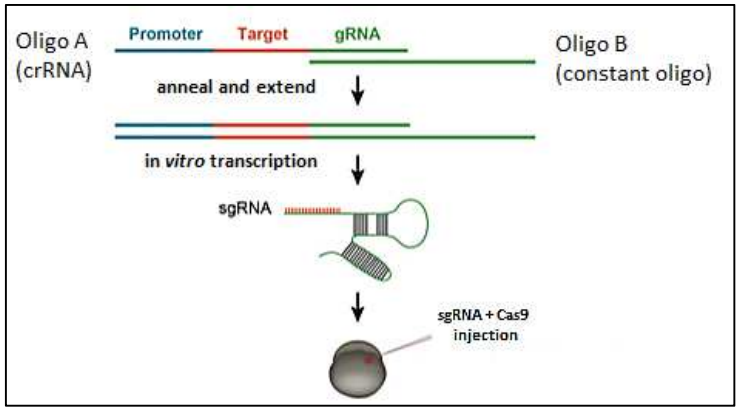

adapted from Varshney et al., 2015

Fig 33. β-SG$_{ex2}$-, δ-SG$_{ex1}$-, δ-SG$_{ex2}$ sgRNA production and injection. General scheme representing the generation by annealing and extension of the template suitable for the *in vitro* transcription of the sgRNAs. After purification, the sgRNA mixed with the Cas9 recombinant protein is micro-injected in fertilized oocytes at one or two cell stages.

5.1.2 Screening of mutants in filial generations

The F0 population, developing from the injected embryos, was screened to evaluate the presence of INDEL mutations generated by the NHEJ activated by the Cas9 DSB. The screening was performed with the heteroduplex mobility assay (HMA) assay, as described in the Materials and Methods section. Embryos in which the NHEJ introduced small deletions or insertions, displayed peculiar heteroduplex migration patterns in comparison to WT. These results were confirmed by Sanger sequencing. The rate of somatic indel mutations in the F0 populations was 75% for β-SG$_{ex2}$, 85% for δ-SG$_{ex1}$ and 80% for δ-SG$_{ex2}$, indicating the goodness of the chosen sgRNAs.

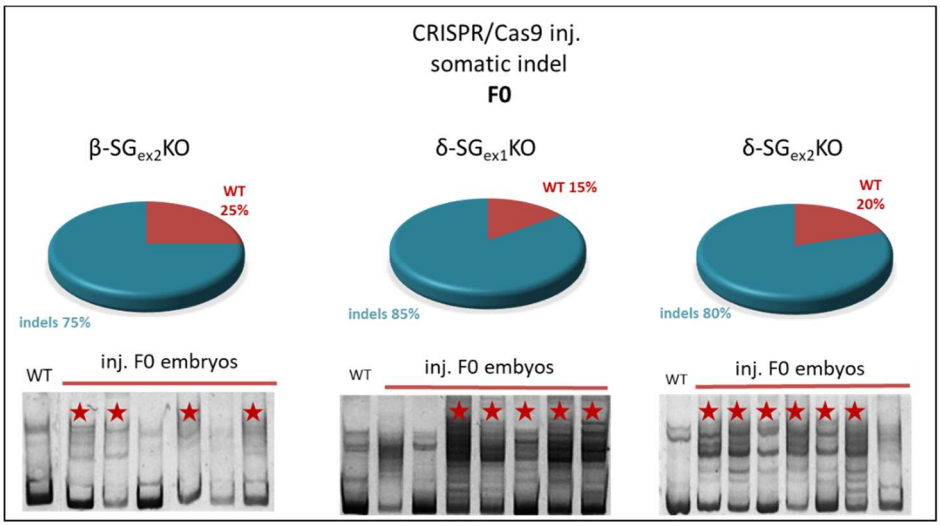

Fig 34. INDEL mutations in F0 populations. WT display a different pattern of migration in comparison to embryos with somatic INDEL mutations. DNA from positive fish was sequenced and the somatic INDEL frequency was evaluated. Stars indicate the positive embryos.

Members of the F0 population were outcrossed with WT zebrafish and the same analysis was performed to evaluate the germline transmission in F1 generation (identification of founders).
The frequency of germline INDEL mutations was evaluated in 45% for β-SG$_{ex2}$in, 41% for δ-SG$_{ex1}$-, and 45% for δ-SG$_{ex2}$. When checked by Sanger sequencing, the electropherograms from heterozygote DNA embryos showed the presence of two different nucleotide sequences starting from the point of the DSB generated by the Cas9 enzyme.

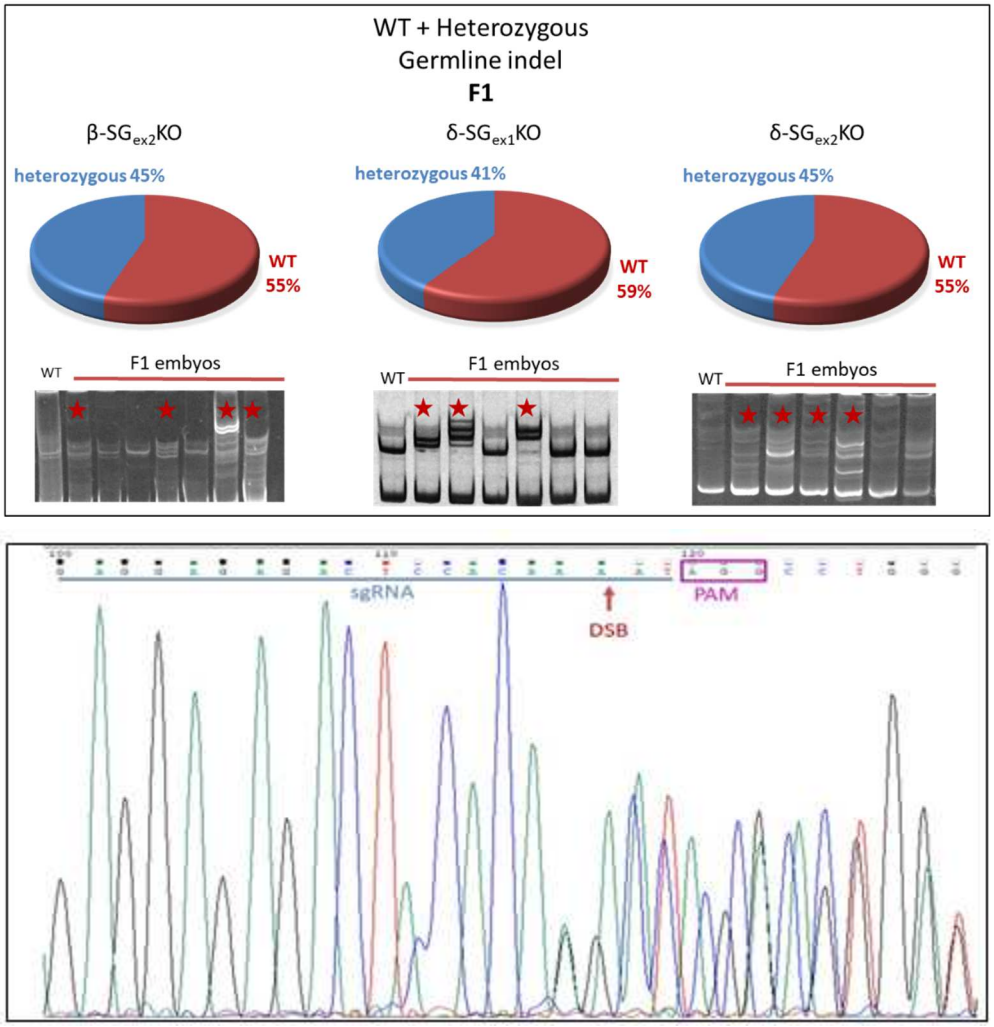

Fig 35. INDEL mutations in F1 populations. HMA assay on F1 embryos injected with β-SG$_{ex2}$-, δ-SG$_{ex1}$-, δ-SG$_{ex2}$ sgRNA/Cas9 and rate of germline transmission of the INDEL mutations as confirmed by Sanger sequencing (top panel). A representative electropherogram of the DNA of a heterozygote embryo is shown in a (bottom panel). The overlapping peaks in the region targeted by β-SG$_{ex2}$ sgRNA (in blue), start close to the PAM site (in purple).

When growth to adulthood, heterozygote mutants, were controlled by DNA sequencing of the targeted locus to establish the mutation/s introduced and to identify the founders of the future generation. To perform this analysis, amplicons obtained by PCR were cloned into the pGEM®-T Easy Vector (Promega).

The following sequence analysis allowed the identification of the specific mutation in each founder that were then accordingly crossed (F1XF1) to generate the F2 population.

The founders selected for the subsequent breeding carried a deletion of 6 bp and of an insertion of 2 bp in z-*sgcb* exon2 (see Fig. 36), a deletion of 4 bp in z-*sgcd* exon2 (see Fig. 37), and of 15 bp at the exon 1/ intron 1 boundary in z-*sgcd* (see Fig. 38). In the first two cases, the mutations are expected to produce an out of frame protein sequence with the appearance of premature stop codons.

In the third case the deletion is expected to result in the loss of the splicing site with the formation of aberrant transcripts. Indeed, for what concern δ-SG$_{ex1}$sgRNA, the retention of the very long intron 1 and the translation of this aberrant transcript should produce an unrelated polypeptide sequence, with the premature emergence of stop codons.

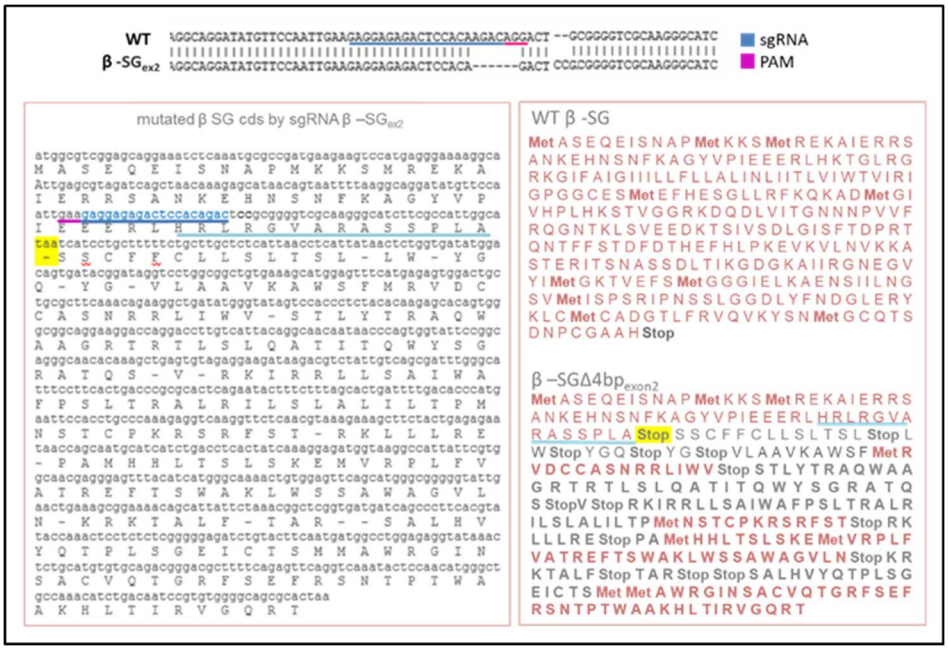

Fig 36. Representation of the mutation on z-*sgcb* and the possible consequence on the β-SG protein. The sequence of the z-*sgcb* region involved by the mutation is reported on top. The mutation corresponds to a deletion of 6 bp and of an insertion of 2 bp in the neighbourhood of the PAM sequence (underlined in pink). The resulting deletion of 4bp is expected to alter the reading frame of the protein with the occurrence of a premature stop codon. The site of β-SG$_{ex2}$sgRNA annealing is underlined in blue. On the left panel is reported the DNA sequence and the corresponding translated sequence of the mutated allele, the site of sgRNA alignment is in blue, the sequence emerging downstream the mutation is underlined in light blue and the premature stop codon (at position 60), in yellow. On the right panel, the WT and the mutated-βSG protein sequences are reported for comparison. The out of frame sequence is underlined in light blue and the premature stop codon is highlighted in yellow.

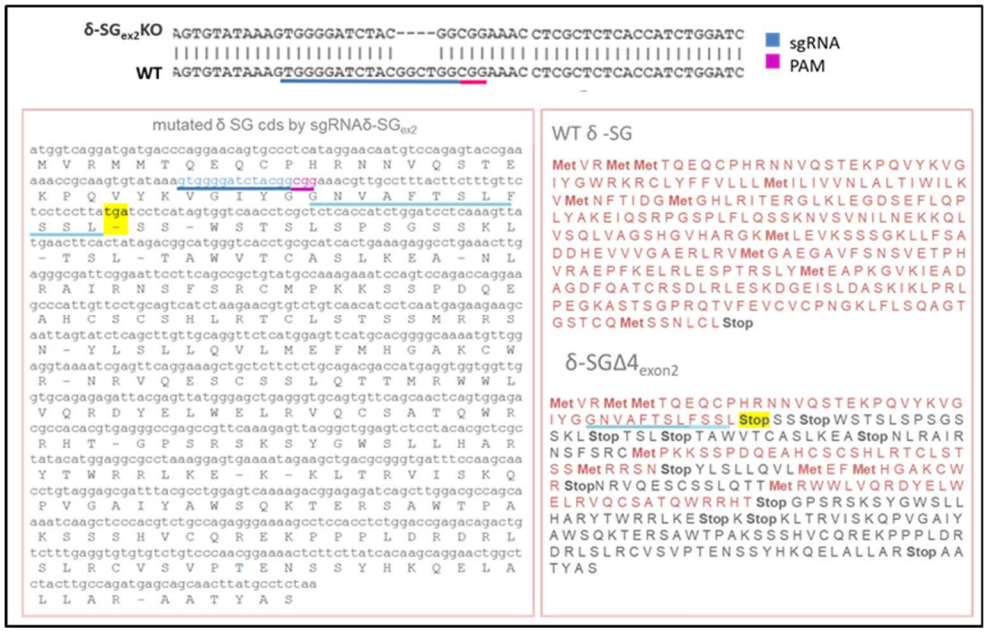

Fig 37. Representation of the mutation on z- ***sgcd*** **and possible consequence on the δ -SG protein.** The sequence of the z-*sgcd* region involved by the mutation is reported on top. The mutation corresponds to a deletion of 4 bp in the neighbourhood of the PAM sequence (underlined in pink). The deletion is expected to alter the reading frame of the protein with the occurrence of a premature stop codon. The site of δ-SG$_{ex2}$sgRNA annealing is underlined in blue. On the left panel is reported the DNA sequence and the corresponding translated sequence of the mutated allele, the site of sgRNA alignment is in blue, the sequence emerging downstream the mutation is underlined in light blue and the premature stop codon (at position 13) in yellow. On the right panel, the WT and the mutated-βSG protein sequences are reported for comparison. The out of frame sequence is underlined in light blue and the premature stop codon is highlighted in yellow.

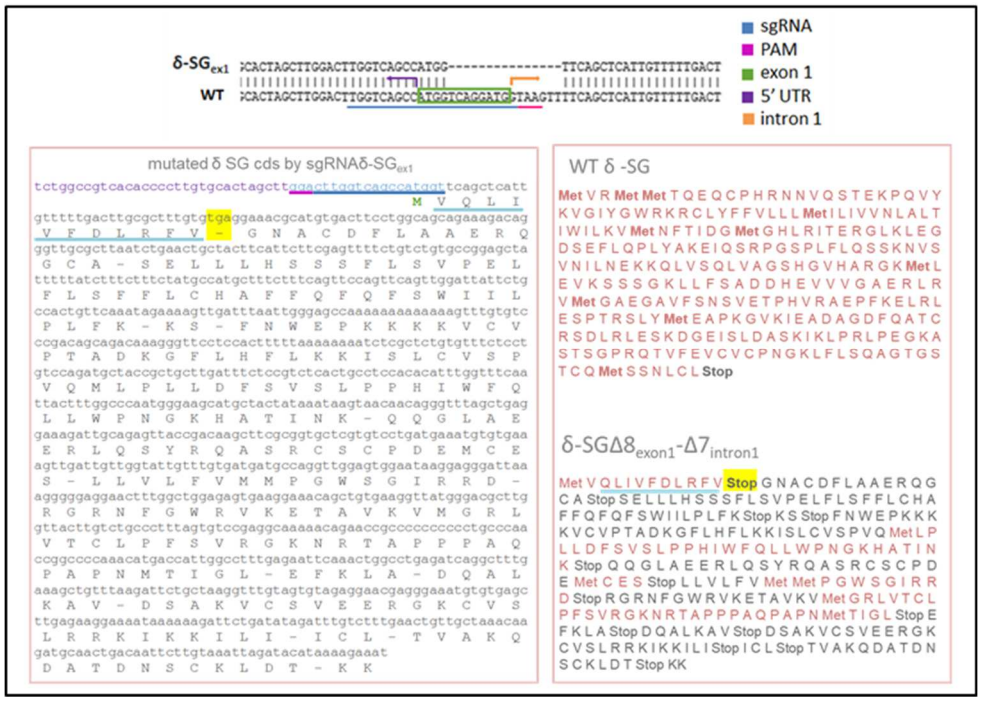

Fig 38. Representation of the mutations on z-*sgcd* and possible consequence on the δ-SG protein. The sequence of the z-*sgcd* region involved by the mutation is reported on top. The mutation corresponds to a deletion of 15bp at the boundary between exon 1 (Δ8bp) and intron 1 (Δ7bp) that is expected to remove the splicing site (top panel). The site of δ-SG$_{ex1}$sgRNA annealing is underlined in blue, the PAM sequence in pink, the sequence corresponding to the coding region of exon 1 is boxed in green, and the starting point of intron 1 is indicated by the orange arrow, the 5' UTR with a purple arrow. On the left panel is reported the DNA sequence and the corresponding translation of the mutated allele, the site of sgRNA alignment is in blue, the final part of 5'-UTR sequence is in purple, the sequence emerging downstream the mutation is underlined in light blue and the premature stop codon (emerging after 12 aa) is in yellow. On the right panel, the WT and the mutated-δ-SG protein sequence are reported for comparison, the novel polypeptide sequence is underlined in light blue and the premature stop codon is highlighted in yellow.

The F2 embryos, generated by the crossbreed of founders, were genotyped by HMA assay and Sanger sequencing. A Mendelian inheritance was observed with an average of ¼ of mutated homozygotes, ½ of heterozygotes and ¼ of wild type homozygotes.

Mutated homozygotes were grown and subsequently crossbred to obtain the stable mutant lines.

The characterization of the β-SG$_{ex2}$KO and δ-SG$_{ex2}$KO lines has been concluded and is described in this thesis, whereas that of δ-SGex1-KO line is still ongoing and therefore is not here reported.

5.1.3 Characterization of β-SG$_{ex2}$KO line

Considering that sarcoglycanopathy is a progressive muscular disease, an important parameter in the characterization of the mutants is the age of the fish. Therefore, to evaluate the impact of the mutation on skeletal muscle, molecular, histological and behavioural analyses were carried out both at the embryo-larval and at the *juvenile*-adult phases.

5.1.3.1 Embryo-larval phase

5.1.3.1.1 Molecular analysis

As expected by the DNA sequence analysis, the mutation on the exon 2 of the *z-sgcb* gene, led to the lack of β-SG protein as investigated by both western blot and whole-mount confocal immunostaining on 5 dpf embryos. Indeed, by the western blot analysis reported in Fig. 39, it is possible to see that the monoclonal antibody specific for β-SG recognized a doublet of bands, around 43KDa in the protein lysate from WT embryos that is absent in the lysate from β-SG-KO animals. The same membrane, probed with a polyclonal antibody specific for δ-SG, showed a strong reduction (almost absence) of the δ-SG partner in the mutated fish, whereas a band of approximately 35 KDa is visible in WT.

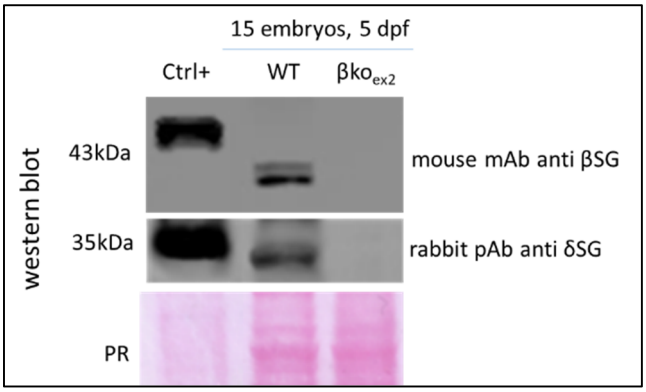

Fig 39. Western blot analysis of protein lysates from 5 dpf embryos of WT and β-SG$_{ex2}$KO zebrafish. Fifteen embryos of both WT and β-KO were lysate according the protocol described in Materials and Methods and loaded on a SDS-PAGE. After blotting, the membrane was probed with a mouse monoclonal antibody (mAb) specific for β-SG and with a rabbit polyclonal antibody (pAb) specific for δ-SG. The first antibody recognized a doublet of bands of approximately 43 KDa only in the WT lane. The δ-SG pAb recognized a band of about 35 KDa in the WT that does not appear in the mutant. As positive control HEK293 cells transfected with z-*sgcd* and human (h)-*SGCB* are used. Below the western blot is reported the Ponceau Red staining of the membrane to control protein loading.

On the other hand, overlapping results were obtained by the whole-mount confocal analysis of 5 dpf embryos. Indeed, as reported in Fig. 40, both the β-SG and δ-SG antibodies strongly marked fish myosepta as well as muscle fibres in WT animals. On the contrary the signal from β-SG Ab is lacking and that from δ-SG Ab is virtually absent from the β-SG ex2 KO.

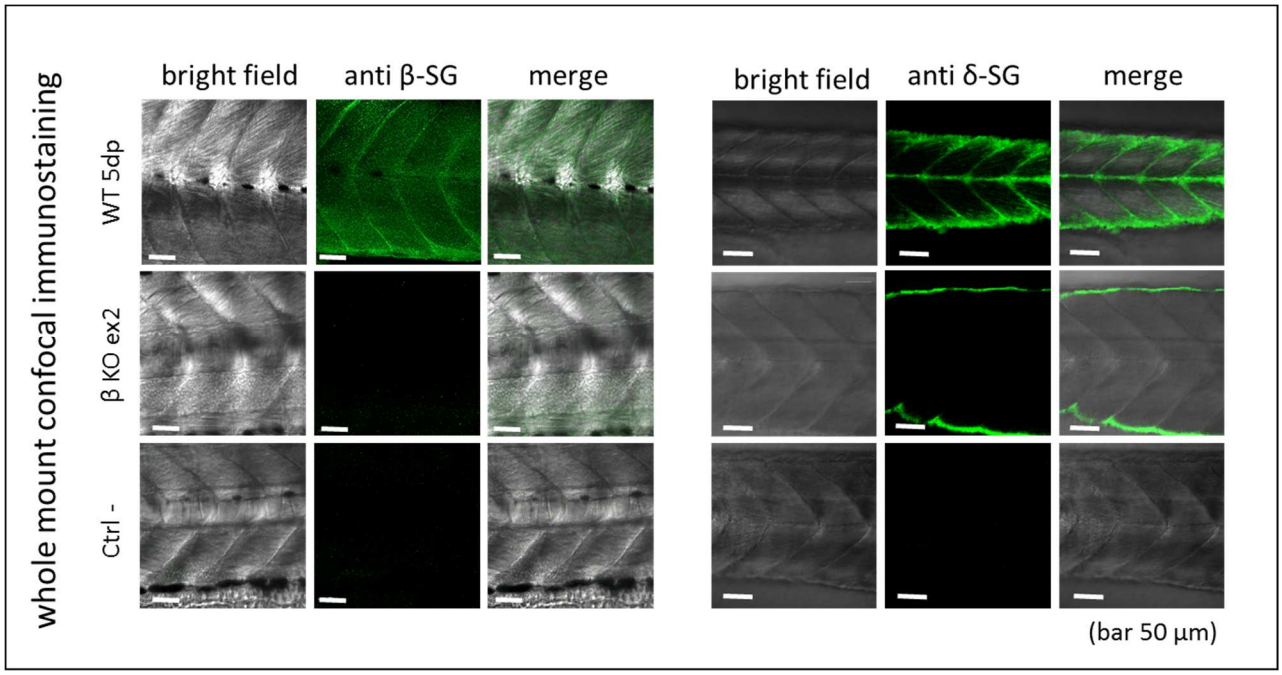

Fig 40. Whole mount confocal analysis of WT and β-SG$_{ex2}$KO embryos. Whole mount immunostaining of 5 dpf embryos of both genotypes was carried out according to what described in Materials and Methods. The primary antibodies specific for β-SG or δ-SG immuno-labelled myosepta and muscle fibres in WT fish. Primary antibodies were revealed by Alexa 488-conjugated secondary antibodies. Images were recorded with a Leica M80 confocal microscope. The bright fields of the immunofluorescent images, as well as the merge of such images, were also reported. No signal for β-SG and traces of δ-SG are visible in mutated embryos as well as in negative control (Ctrl-) fish, treated with the sole secondary antibodies.

These findings resemble what is possible to observe in other KO animal models (Coral-Vazquez et al., 1999) but, importantly, in muscle of LGMD-2E patients (Jung et al., 1996), where the loss of one mutated SG is followed by the absence/strong reduction of the WT partners. As β- and δ-SG play a pivotal role in the assembly and subsequent localization of the complex, it is possible to hypothesize that in the β-SG-KO zebrafish, also the α-SG and γ-SG are missing. Unfortunately, the lack of specific antibodies against the zebrafish proteins, prevented this analysis.

5.1.3.1.2 Morphological and structural analysis

Despite the absence of β-SG, no evident alteration in the fish morphology during the embryo/larval phases was observed.

The development of embryos follows the general morphology score cited in Hermsen et al., 2011 without any evident difference between WT and β-SG$_{ex2}$KO embryos.

At 24 hpf the rudiments of the primary organs become visible, the tail bud becomes more prominent, the embryo elongates, and the trunk myotomes produce weak muscular contractions. The contractions often occur in bursts, at a rate of about eight episodes per minutes. Body axis straightens from its early curvature about the yolk sac; circulation, pigmentation, and fins begin to develop.

At 48 hpf the hatching occurs asynchronously, the morphogenesis of primary organ systems is completed, the contractions begin to involve series of myotomes and become stronger, more coordinated, and more frequent and the pectoral fins appear.
From 72 hpf the swim bladder inflates; food-seeking and active avoidance behaviours appear.
At 4 dpf the yolk begins to be adsorbed and embryos begin to feed independently from the fifth day. All these features were present in the WT as well as in the mutant zebrafish and are summarized in Fig 41.

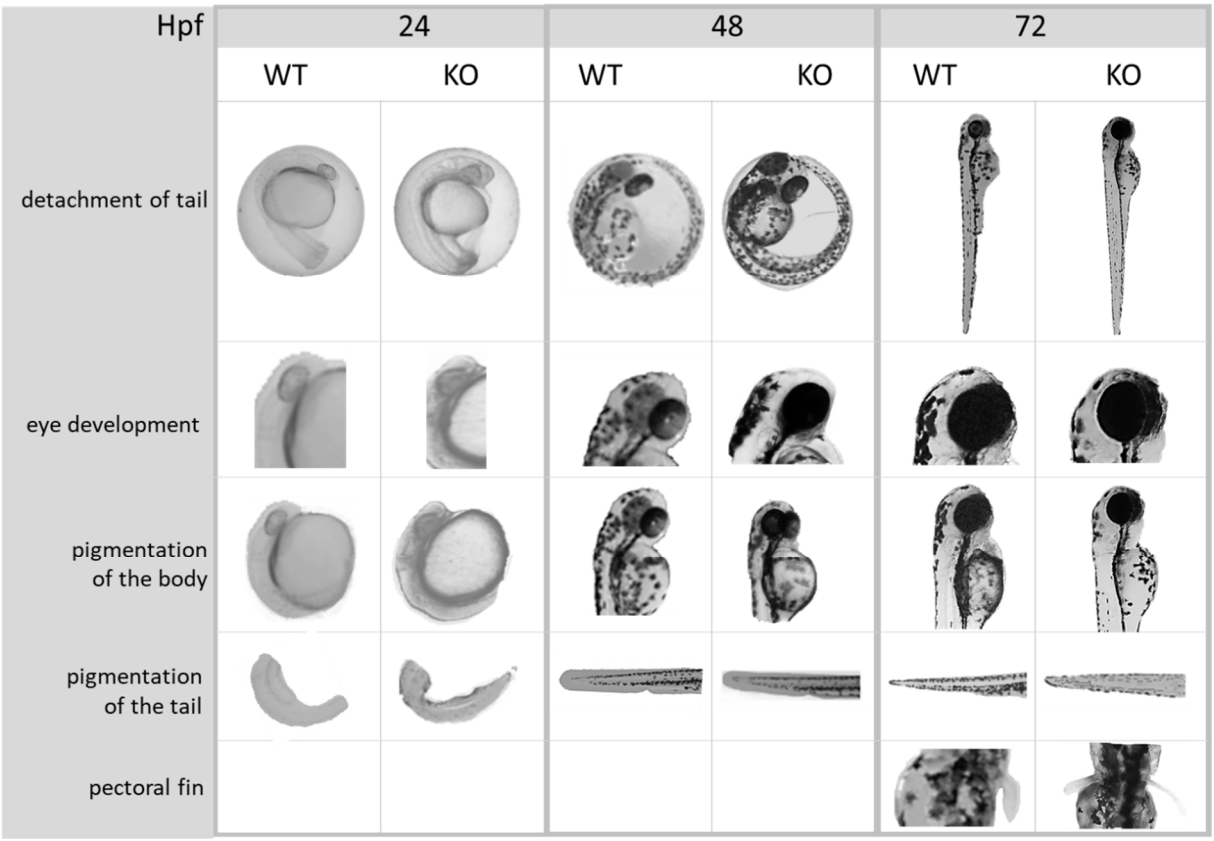

Fig 41. General morphology scoring system showing normal development of β-SG-KO zebrafish embryo and no differences in comparison to WT embryos up to 72 hours post fertilization (hpf).

As expected from the absence of a clear morphological phenotype, and despite the lack of the SG-complex, the organization of myofibres appeared only marginally altered at the embryo-larval stage. Indeed, the staining with the fluorescent probe phalloidin resulted in no major difference between WT and β-SG_{ex2}KO embryos. Phalloidin specifically binds the native quaternary structure of F-actin thus allowing to follow the structure of the myofibrils in adjacent myocytes, which appear less compact in the mutated than in the WT embryos (slightly larger dark zones among myofibrils).

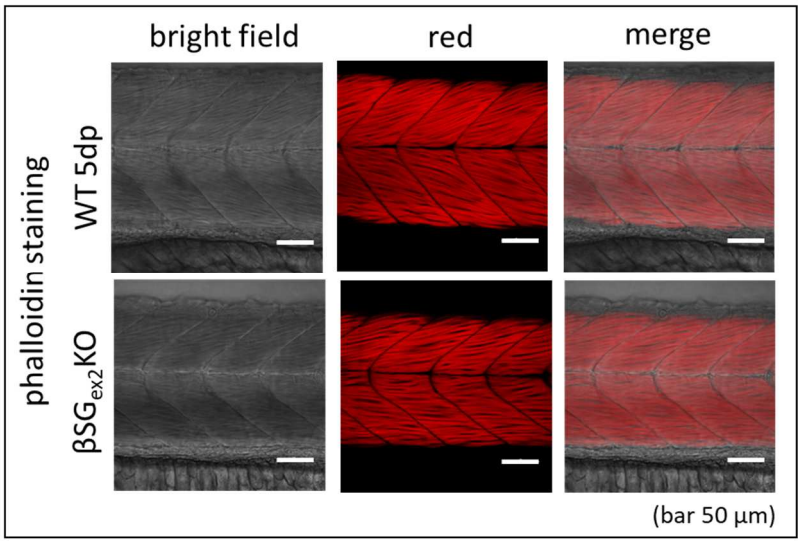

Fig 42. Myofibrils-phalloidin staining of 5 dpf wild type and β-SG-KO embryos. Embryos were stained with phalloidin conjugated to TRITC according to the protocol described in Materials and Methods. Phalloidin is a probe for F-actin, thus allowing the analysis of the skeletal muscle myofibrils that in mutant embryos appear slightly less compact then in WT. Images were recorded with a Leica M80 confocal microscope. The bright fields of the immunofluorescence images, as well as the merge of such images, are also reported.

5.1.3.1.3 Motor behaviour analysis

Locomotion assays during early zebrafish larval development are used to assess muscle performance. Here, we have utilised both the fast touch evoked response assay and the analysis of movement tracking for several days. The touch evoked response assay is used to evaluate the swimming action, which is proportional to muscle force of fast-twitch muscle fibres and measures the capacity of fish to escape in response to an external stimulus, i.e. a gentle touch with a capillary. By 24 hpf, WT zebrafish spontaneously contract their tail muscles and by 48 hpf, exhibit controlled swimming behaviours, with burst swim, accompanied by sharp turns. At 5 dpf, the movement is perfectly controlled and autonomous. Reduction in the frequency of these movements, or other alterations, may indicate a skeletal muscle dysfunction.

The comparative analysis between WT and mutated fish was performed at 5 dpf. A score from 0, inability to escape, to 3, perfect swimming activity, was attributed to describe the swimming escape ability of embryos. No statistical difference among WT and mutants was observed, and to approximately 95% of fish received a score of 3, whereas the remaining 5% received a score of 2. This suggests that no impairment of muscles involved in rapid movements is present at this developmental stage. On the other hand, this finding is in accordance with the negligible disorganization of myofibrils as evaluated with the phalloidin TRITC staining.

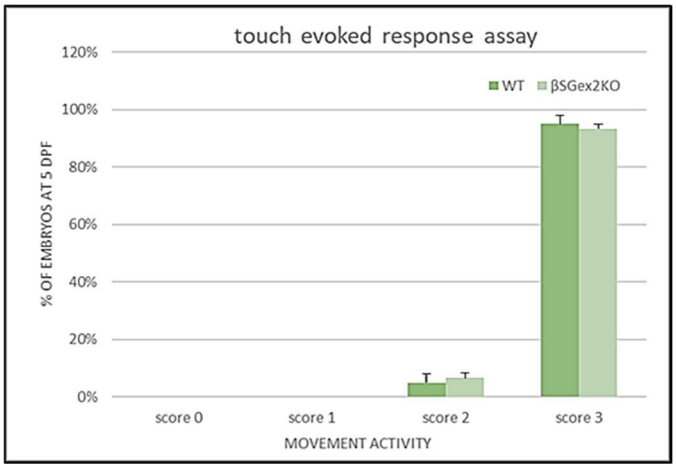

Fig 43. Touch evoked response assay performed with 5 dpf wild type and β-SG-KO embryos. The ability to escape after an external stimulus (tap on the head with a capillary) was evaluated by assigning a score from 0 (no movement), 1 (slow escape velocity), 2 (intermediate escape velocity) to 3 (fast escape velocity) denoting normal swimming activity. No significant difference was recorded between WT and β-SG$_{ex2}$KO during the embryo phase.

To better analyse the swimming performance of β-SGex2KO fish, we decided to record the movements of *larvae* for an extended period by using the DanioVision (Noldus) movement tracking system (DeMarco et al., 2016). This allows the kinematic quantification of motor events. Due to the larvae's small size, these experiments can be performed in multi-well plates.

In zebrafish *larvae*, as in higher vertebrates, locomotor activity is subjected to circadian control since the onset of spontaneous movement at day 4. The circadian clock, regulated by light (circadian rhythms), is needed to synchronize biochemical, physiological and behavioural processes. The pineal gland of zebrafish contains an intrinsic circadian clock that drives rhythmic synthesis of the hormone melatonin. Melatonin, which release is inhibited during the light period, reduces zebrafish locomotor activity significantly. Thus, a distinct day/night activity pattern can be observed (Burgess and Granato, 2007). The circadian rhythms were maintained during the analysed period through cycles of light and dark into the DanioVision.

Zebrafish *larvae* display a defined locomotor repertoire as they can swim, turn and capture prays. These activities, easily monitored by automated video tracking systems, are different between light and dark phases. In detail, following the onset of darkness, *larvae* showed a transient elevation in scoots prior to a gradual drop-off in motor activity. Indeed during dark, large turns with slow performance are recorded. On the contrary, during periods of bright illumination they displayed elevated locomotor activity, probably resembling the natural behaviour of searching for food and escaping from predation. It is therefore beneficial for zebrafish *larvae* to synchronize activity levels to the diurnal cycle (Kopp et al., 2018).

WT and β-SG$_{ex2}$KO embryos (5 dpf) were placed on a 96 multi-well plate (one fish for well) and followed for the next 4 days. After few hours of acclimation to the new environment, zebrafish experimented a constant temperature of 26 °C and 12 hours light/12 hours dark phases and feeding was made during the 2nd light phase. Zebrafish *larvae* of both genotypes swam during the

light phase, and strongly reduced their activity during the dark period. The distance covered in 6 minutes by each embryo for the entire period was recorded and each dot of the graph represents the mean distance (+/- standard error) travelled by WT or β-SG$_{ex2}$KO homozygote *larvae*. Thanks to this analysis, it is possible to appreciate that, during the light phases, the mean distance covered in 6 min by β-SG$_{ex2}$KO fish was slightly lower in comparison to WT, even if not statistically significant when analysed point by point.

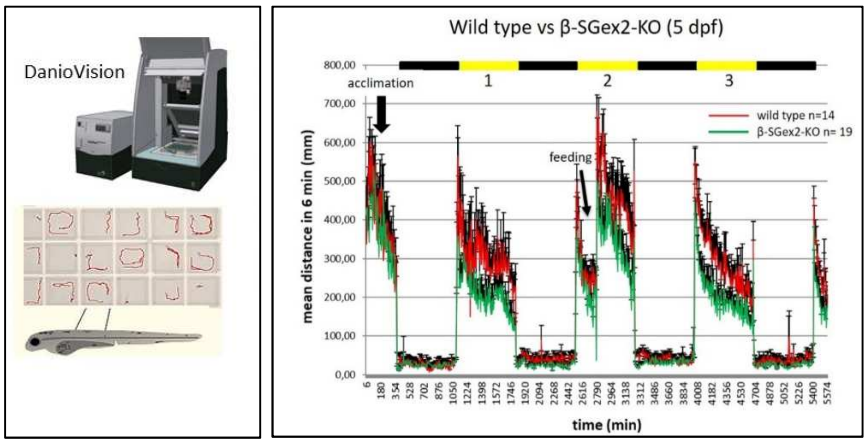

Fig 44. DanioVision (Noldus) movement tracking system and traces from WT and β-SG$_{ex2}$KO *larvae*. The DanioVision apparatus and an example of the plate where embryos are placed (arena) with movement recording are reported on the left panel. The mean distances travelled in 6 min by WT and mutated embryos were plotted in function of time, and standard errors are also indicated. The daily/night phases are pointed out as yellow and black bars, respectively, on top of the graph. During acclimation, fish of both genotypes exhibited an overlapping behaviour, as well as during the dark phases, when the swimming activity is strongly reduced. On the other hand, a difference in the swimming behaviour became visibile during the light phase. Fish of both genotype increased the swimming activity in a comparable way, upon food intake.

When the total distance travelled during the active periods is calculated, it is possible to observe that the mutant embryos are approximately 30% less active then the WT.

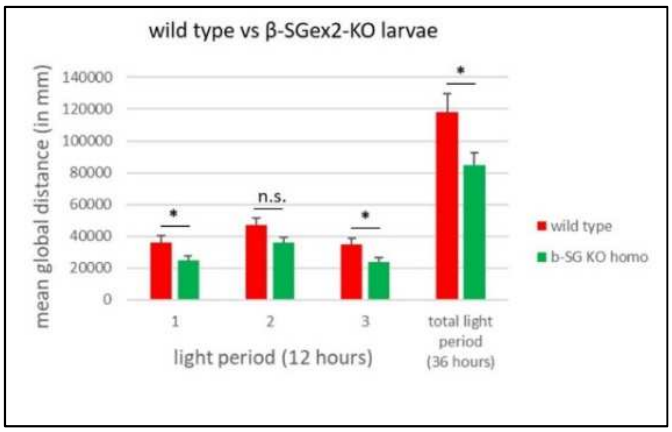

Fig 45. Global distance covered by wild type and β-SG$_{ex2}$KO larvae. The distance covered during the single light phases and in total were measured for both wild type and mutated *larvae* and compared. Mutants moved approximately 30% less than WT. *, P≤ 0.05.

Data collected during the embryo-larval phase showed that the absence of the mutated β-SG corresponds to a strong reduction of the WT partner δ-SG, suggesting of the entire SG-complex loss. Despite the lack of the key SG-complex, the overall phenotype of the fish and particularly the structure of the muscle were nearly normal. Indeed, the ability of the mutated embryos to escape in response to an external stimulus is identical to that of the WT. On the other hand, a more accurate and long-lasting analysis that recorded the fish movements for several days, brought out a statistically significant reduction of approximately 30% of the swimming activity of mutants in comparison to WT. This could be a first indication that the effects of the absence of the SG-complex start to manifest at the functional level, even though the overall structure of muscle was substantially unchanged. Therefore, to evaluate any worsening of the fish condition, we proceeded with the characterization of the β-SG$_{ex2}$KO zebrafish at the *juvenile* and adult stages.

5.1.3.2 *Juvenile*-adult phase

5.1.3.2.1. Morphological analysis

The morphological observation of mutants during the entire development never reveal major differences with age-matched WT fish as depicted in Fig. 41 and in Fig. 46 reporting the pictures of the body and tail of 5-month-old zebrafish of both WT and β-SG$_{ex2}$KO genotype.

Fig 46. Morphological analysis of adult wild type and β-SG$_{ex2}$KO fish.

This suggests that signs of a pathologic condition, if any, are not immediately visible at the external observation, as with the MO-KD model, and that an in-depth analysis is needed. Therefore, we first evaluated the motor behaviour at the *juvenile* stage and later we sacrificed few adult fish (5-month-old) to assess the skeletal muscle condition at the molecular and histological level.

5.1.3.2.2. Motor behaviour analysis

WT and β-SG$_{ex2}$KO fish were placed in suitable wells according to their size. After acclimation, the recording of the movements, with the DanioVision tracking system, was limited to one light phase between two dark phases. This was due to the need of feeding fish daily and to avoid any potential stress related to the small environment in which fish can move. Because of the limited number of animals that can be analysed simultaneously, we focused the attention on the mutated fish, and only one WT was utilized for reference. Nevertheless, it is possible to appreciate that the daily activity of the β-SG$_{ex2}$KO was reduced of approximately 40% if compared to that of WT, suggesting a worsening of the muscle conditions. Other experiments are ongoing to increase the sample size, once fish will grow.

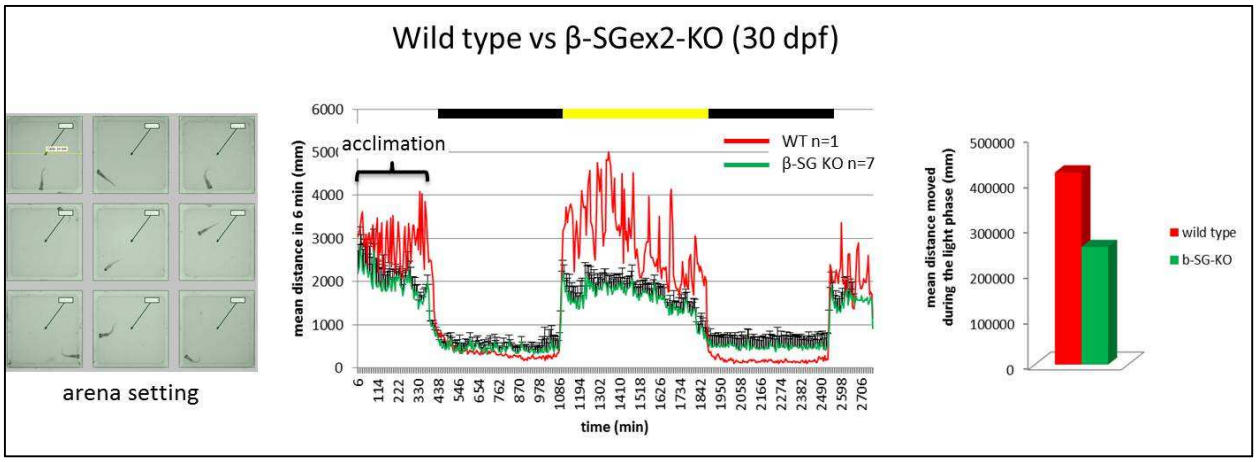

Fig 47. Locomotion assay of wild type and β-SG$_{ex2}$KO zebrafish at the juvenile stage (30 dpf). An example of the arena where 30 dpf zebrafish were placed is reported on the left. The distances travelled in 6 min by WT (1 fish) and mutated zebrafish (the mean of 7 fish) are plotted as a function of time, standard errors are also indicated. The daily/night phases are pointed out as yellow and black bars, respectively, on top of the graph. The quantification of the total distance moved during the light phase is reported in the graph on the right, where results from WT and mutated zebrafish are compared. One of the two WT fish died during the acclimation phase and therefore it was eliminated from the analysis. It is possible to observe a clear reduction of the swimming activity of the β-SG$_{ex2}$KO, however, because of the presence of a single WT animal (control) the statistical analysis cannot be executed.

5.1.3.2.3. Molecular and histological analyses

To evaluate the status of the skeletal muscle of β-SG$_{ex2}$KO at late developmental stage, after the sacrifice of a few animals, we extracted skeletal muscle proteins for western blot analysis and prepared cryosections to perform both immunofluorescence and histological analyses.

The absence of β-SG protein was confirmed by western blot as well as by the immunofluorescence staining of cryosections of skeletal muscles of 5-month-old fish (adult). The strong reduction of the δ-SG partner is also confirmed.

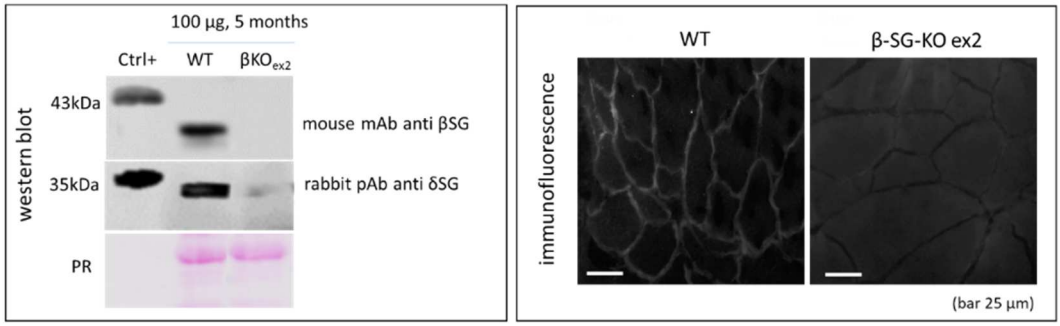

Fig 48. Western blot and immunofluorescence analyses of skeletal muscle from adult zebrafish. Left panel: 100 µg of protein lysates from both WT and β-SG$_{ex2}$KO were loaded on SDS-PAGE. After blotting, the membrane was probed with a mouse monoclonal antibody (mAb) specific for β-SG and with a rabbit polyclonal antibody (pAb) specific for δ-SG. As positive control HEK293 cells transfected with z-sgcd and human h-*SGCB* are used. Ponceau red staining is reported as control of protein loading. Right panel: immunofluorescence staining with β-SG specific antibody of cryosection from trunk muscles of WT and β-SG$_{ex2}$KO adult zebrafish. Primary antibody was revealed by Alexa 488 conjugated secondary antibody. Images were collected with a fluorescent microscope (Zeiss HBO 50), at the same setting conditions. The β-SG specific antibody labelled the sarcolemma of WT fibres, whereas no signal is present in muscle fibres from mutated zebrafish.

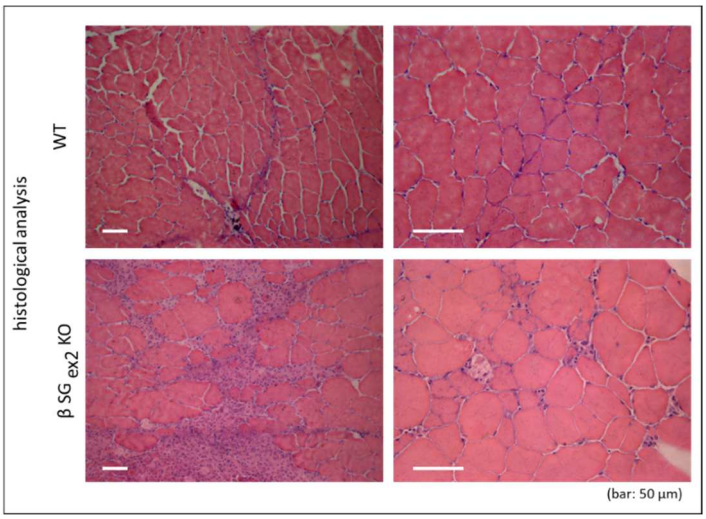

Fig 49. Hematoxylin-eosin staining of skeletal muscle cryosections from wild type and β-SG$_{ex2}$KO adult fish. Histological analysis of muscles from WT and β-SG$_{ex2}$KO zebrafish shows the presence of clear muscle dystrophic features in the mutant fish such as very large or smaller area of fibrosis and heterogeneity in fibres size.

When skeletal muscle cryosections of 5-month-old mutant fish were stained with H&E, a clear myopathic picture became evident. Indeed, features of muscular dystrophy such fibrosis, as well as heterogeneity in fibres size were present. On the contrary the WT muscle presented a well organised structure, with fibres of the same size and nuclei located peripherally. Data collected during the last phases of zebrafish development and in adulthood, confirmed the absence of an evident morphological phenotype, as already observed during the embryo-larval phases. However, the progression of the pathological status is evident both at the structural (histology) and behavioural (movement tracking) levels.

5.1.4 Characterization of δ-SG$_{ex2}$KO line

The characterization of this novel zebrafish lines was performed following the same workflow adopted for the β-SG$_{ex2}$KO line. Results are largely overlapping, therefore data collected during the embryo/larval and *juvenile*/adult phases of zebrafish development have been summarized.

5.1.4.1 Embryo-larval phase

As expected from the data collected for β-SG$_{ex2}$KO line, during the early stage of development δ-SG$_{ex2}$KO line does not display a dystrophic muscular phenotype. Indeed, despite the lack of δ-SG, the development is normal, no major defects are visible in myofibrils and the ability to escape after an external stimulus is conserved (Fig. 50).

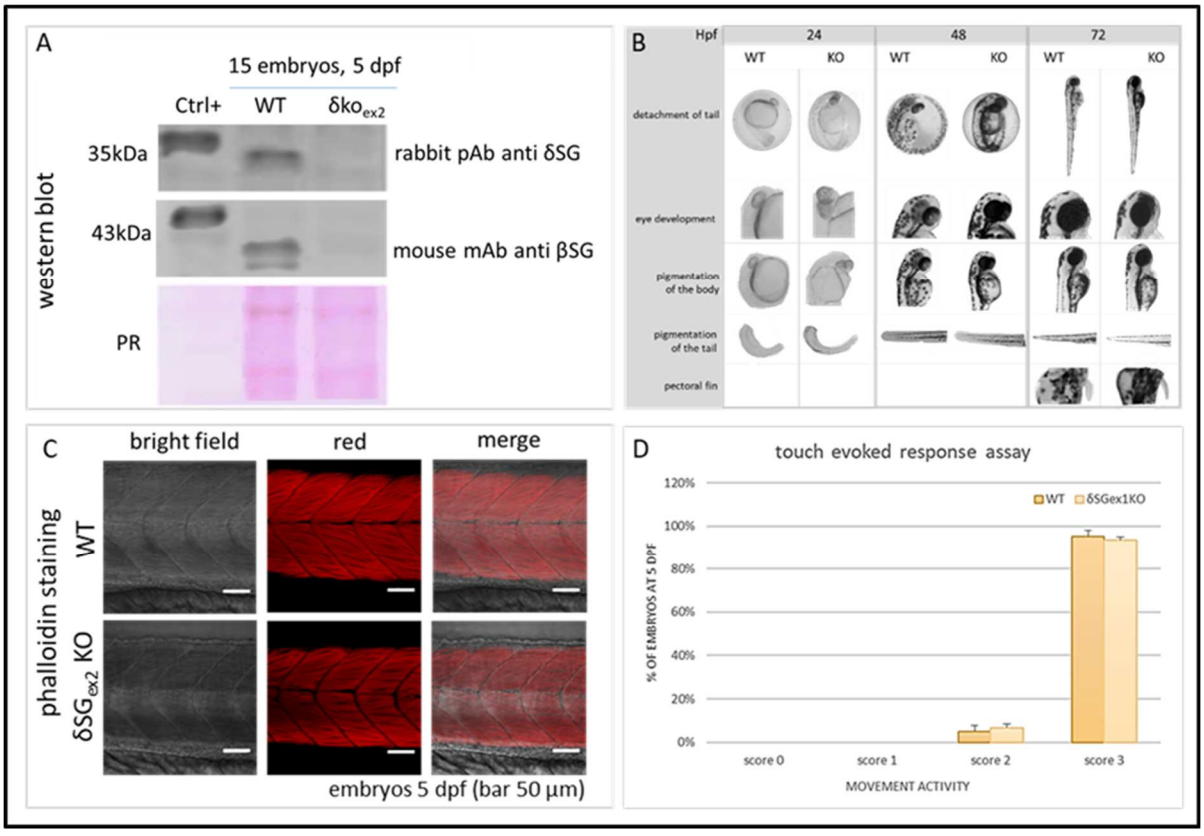

Fig 50. Characterization of embryos-*larvae* phase of δ-SG$_{ex2}$KO line.

A) δ-SG$_{ex2}$sgRNA, targeting exon 2 of z-*sgcd*, prevent the expression of δ-SG in injected zebrafish. Western blot analysis of total protein extracts from 15 embryos at 5-dpf of WT and δ-SG$_{ex2}$KO injected zebrafish. As positive control (ctrl+), proteins from HEK293 cells transiently transfected with a vector expressing the zebrafish δ-SG sequence and the human β-SG one were loaded on the acrylamide gel. After blotting the membrane were probed with a rabbit polyclonal antibody (pAb) to evaluate the expression of δ-SG, and with a mouse monoclonal antibody (mAb) specific for β-SG. As expected, pAb recognize a band at 35 kDa, specific of δ-SG, while mAb recognise the band of β-SG at 43 KDa. dpf, days post fertilization

B) Despite the absence of δ-SG expression evaluated by western blot (A), mutants embryos do not display any morphological alteration, as occurred for β-SG$_{ex2}$KO line. The development follows the general morphology scored cited in Hermsen et al., 2011 explained in detail for the β-SG$_{ex2}$KO characterization. hpf, hours post fertilization.

C) As consequence of the lack of a clear dystrophic phenotype, myofibrils appear only slightly less compact in mutants in comparison to WT embryos at 5 dpf once stained with phalloidin, a probe for F-actin, conjugated to TRITC.

D) The touch evoked escape response is a locomotion assay that allow to rapidly evaluate any possible muscle impairment in the swimming ability of 5dpf embryos after a gentle touch of the body with a capillary. Reduction in the escaping behaviour may indicate a muscle dysfunction. However, as occurred for β-SG$_{ex2}$KO line shown above, no significant differences are detected between WT and mutants, since they can properly escape after the external stimulus.

5.1.4.2 *Juvenile*-adult phase

To investigate if also in this case the muscle damage is progressive, as occurred in β-SG$_{ex2}$KO, the *juvenile*/adult phase were analysed also for δ-SG$_{ex2}$KO. As expected, δ-SG protein is absent, and the strong reduction of the WT partner β-SG is confirmed. Despite a normal external aspect, a clear dystrophic picture is present at the skeletal muscle level (Fig 51).

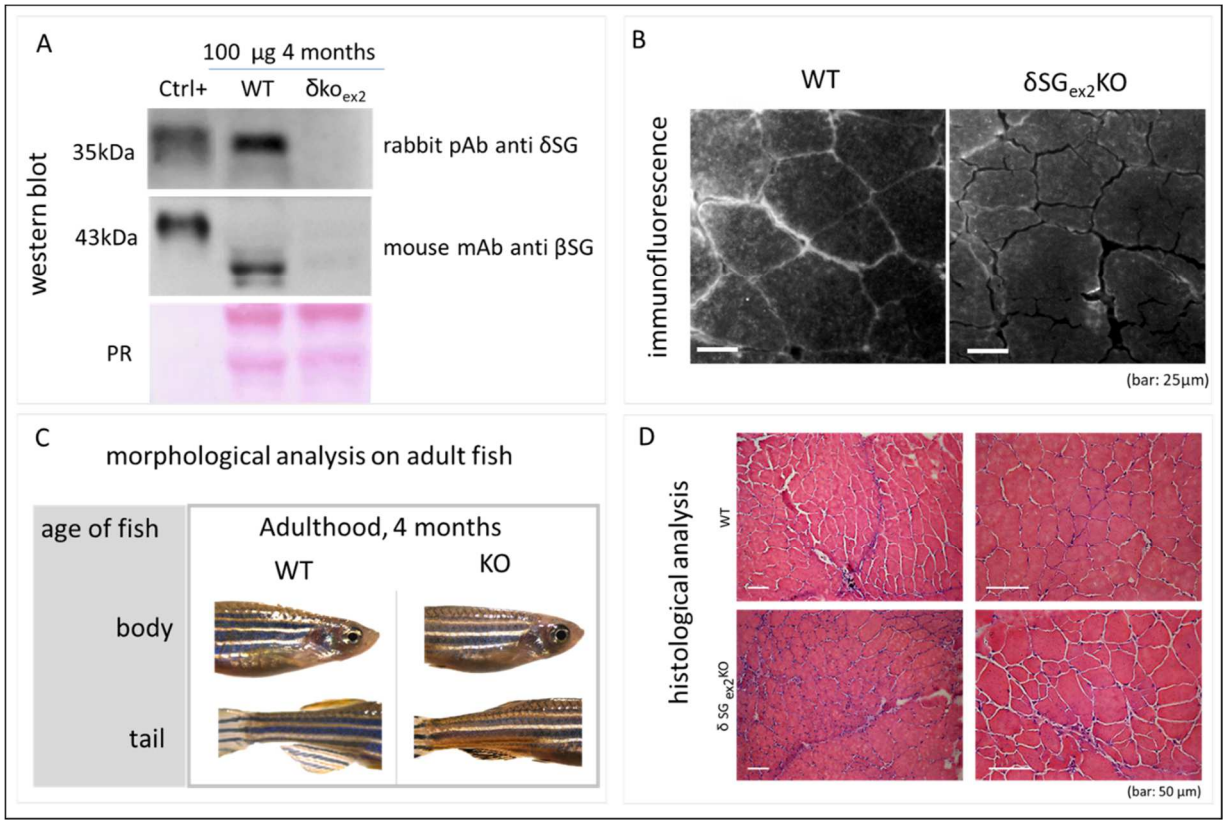

Fig 51. Characterization of *juvenile*-adult phase of δ-SG$_{ex2}$KO line.

(A) 100 µg of protein lysate from both WT and δ-SG$_{ex2}$KO were loaded on a SDS-PAGE and the membrane was probed with both a rabbit polyclonal antibodies (pAb) that recognise a band at 35kDa of δ-SG and a mouse polyclonal antibodies (mAb) that recognise a band at 43 kDa of β-SG. 5 µg of protein lysate from HEK 293 cells transfected with the zebrafish δ-SG and the human β-SG were used as positive control. Ponceau red (PR) staining was reported as positive control. The western blot analysis confirmed the absence of δ-SG protein followed by a strong decrease/absence of β-SG one.

(B) Immunofluorescence staining with a rabbit polyclonal antibodies (pAb) of cryosection from trunk muscle of WT and δ-SG$_{ex2}$KO adult zebrafish, revealed by Alexa 488 conjugated secondary antibodies, confirmed the absence of δ-SG from the membrane.

(C) Despite the absence of δ-SG, no morphological alterations were detected on adult δ-SG$_{ex2}$KO zebrafish in comparison to the WT.

(D) A deeper phenotypical analysis performed on histochemical sections of 4-month-old WT and mutants, stained with hematoxilin-eosin, displayed the beginning of a dystrophic phenotype. Inflammatory infiltrates and fibres of different size, indicating that cycle of regeneration and degeneration occur, were detected.

5.2 WT mRNA injection and protein expression

δ-SG$_{ex2}$KO embryos were injected with 8 nL each of a solution containing 150 ng/µL of an *in vitro* transcribed capped mRNA coding for human WT δSG.

At 24, 48, 72 hpf 15 embryos were lysed in protein extraction buffer, loaded for SDS-PAGE gel and probed with an antibody specifically recognizing only the human protein.

The western blot analysis (Fig 52) showed a strong signal at 24 hpf that progressively decreased because of the dilution occurring in the growing embryos reaching a level like that present in WT embryos. The evaluation of its localization, by whole mount confocal immunostaining, is ongoing.

If the molecular rescue will be confirmed, we will proceed with the injection of the mRNA coding for mutated δ-SG proteins. The comparison of the level of protein of the mutated and WT SG and their localization will help in understanding the ability of zebrafish ERAD in recognizing these mutants as folding defective as occurring in human.

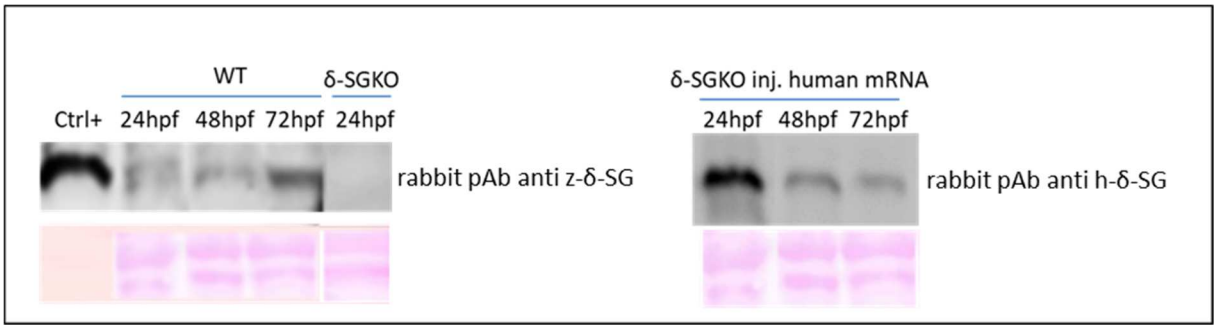

Fig 52. Human protein expression in zebrafish embryos after human WT mRNA injection. The panel on the left shows the absence of the mutated protein in KO embryos since the first 24 hpf in comparison to the time course of the WT endogenous protein expression. The panel on the right shows the time-course of the expression of human δ SG WT.

5.3 Generation of β-SG$_{ex4}$T145R and δ-SG$_{ex8}$E246 KI lines

By sequence alignments of zebrafish and human SG sequences, we identified the conserved amino acids that are mutated in sarcoglycanopathy (highlighted in yellow in Figure 53).

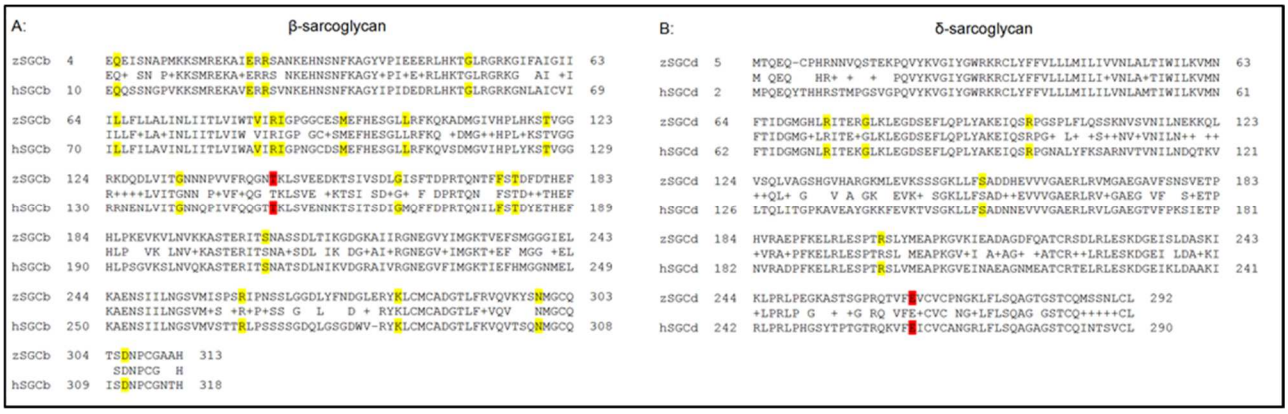

Fig 53. Sequence alignment of zebrafish *versus* human SG proteins. The conserved residues, mutated in sarcoglycanopathy, are highlighted in yellow. The residues of β-SG and δ-SG chosen for KI in zebrafish are indicated in red.

We have chosen the residue at position 145 of z-*sgcb* (in exon 4), corresponding to position 151 in human, and the residue at position 264 of z-*sgcd* (exon 8), corresponding to position 262 in human, to introduce the desired mutations (highlighted in red in Fig 53). The choice fell on these residues, because mapping in well-conserved regions and belonging to the list of mutations proven to be recoverable by targeting the QC system (human T151R-β-SG and E262K-δ-SG) (Soheili et al. 2012). To introduce the mutations in β- and δ-SG, we exploited the ability of the CRISPR/Cas9 system to generate a DSB in a specific preselected site. The DNA damage can be repaired by the activation of the homology direct repair (HDR) if a donor template, carrying the desired mutation, is concomitantly introduced to allow recombination. The last step, although enhanced by the activity of the CRISPR/Cas9 in comparison to the conventional systems, presents anyway a low rate of success. Therefore, with the aim to increase the events in which the HDR occurred successfully, we applied several approaches described as promising in literature (Jasin and Rothstein, 2013; Auer et al., 2014).

In particular, the conventional system, exploiting a sgRNA, was tested in combination with two different donor templates: a short single strand DNA oligos (ssDNA), ranging in length from 65 to 115 nt or a double strand donor (dsDNA) with long homology arms of 800 bp each, cloned into a plasmid. Moreover, to enhance the activity of the Cas9 enzyme, we tried a protocol in which the guide RNA is divided into two molecules, as naturally occurring in bacteria with crRNA and tracrRNA (Kotani et al.,2015). Also in this case, the RNAs were used in combinations with the Cas9 protein and the donor templates above described. Furthermore, the ssDNA oligos were designed

both in antisense and sense orientation. The ssDNA donors were synthesized with phosphorothioate linkages at their 5' and 3' ends, a modification that should improve the efficiency of recombination by increasing the resistance of the donor molecules toward cellular exonucleases (Renauld et al., 2016). Finally, in all these approaches, the SCR7 small molecule, known as inhibitor of NHEJ was tested in combination with RS1, an activator of HDR, to avoid undesired INDEL formation and to improve recombination (Zhang et al., 2018). Several guides and different donors were tested, and the approach based on two RNA molecules + ss-sense-DNA donor, 65 nt long, worked on z-*sgcb* with success. The results until now acquired with the β-SG_{ex4}T145R are reported below.

5.3.1. Workflow for KI production

The steps for KI production are almost identical to that for the KO production, therefore we can refer to Figure 31 for an overall description of the experimental workflow. As in the case of KO, the Chop-Chop (Labun et al., 2016) and IDT CR RNA (integrated DNA technologies for crRNA design) (Chen et al., 2014) tools were used to design and choose the RNA guides with the highest score for predicted cutting activity, and the lowest chance of off-target events (Hruscha et al., 2013). In this case, the choice fell on those guides annealing closest to the point where the desired mutations are planned to be introduced, because of the inverse relationship between KI efficiency and distance of the desired modification from the cut site (Liang et al., 2017; Paquet et al., 2016).

Then, the first step was the evaluation of the gRNAs goodness by measuring the rate of indel mutations introduced by the Cas9 activity. The best guides, resulting in the highest rate of mutagenesis in the neighbouring of the target site, were chosen and micro-injected with Cas9 and the donor templates in 1-2 cell zygotes. At 48 hpf, some F0 injected embryos were genotyped to evaluate the efficacy of HDR at the somatic level. This step is particularly challenging because of the low rate of success of the HDR that results in a low amount of positive DNA in chimeras. Therefore, it was essential to setup a highly sensitive and selective screening method. Once established the rate of somatic recombination, zebrafish of the F0 positive populations, were grown to adulthood to outcross with WT to identify founders, i.e. those fish in which HDR occurred also in the germline where the rate of recombination is, on average, 1-3% (Aurer et al., 2014). Once identified, founders were sequenced in order to verify the presence of the desired β-SG_{ex4}T145R or δ-SG_{ex8}E264K missense mutation and the absence of any indel mutations introduced by NHEJ. Selected founders are then crossbred (F1XF1) to select the mutated homozygotes in the F2 population.

To generate a KI mutant, considering the time-required to perform all the mentioned activity, to setup of the powerful screening method, and the challenges of working with living animal, the time necessary is generally longer than for the KO production.

5.3.2. β-SG$_{ex4}$T145R and δ-SG$_{ex8}$E246K sgRNA production and injection

The gRNAs were designed to target exons 4 and 8, respectively in *sgcb* and *sgcd*, near the point of mutations to increase the efficacy of HDR (see Fig 54). The procedure to produce the sgRNA was the same as described for the generation of the KO lines (see Fig.33). In the approach exploiting two separate molecules of RNA, the crRNA and tracrRNA molecules were chemically synthetized. SgRNA or crRNA:tracrRNA were then co-injected with the donor template into the 1-2 cell zygotes. Donor templates were composed by two homology arms, centred in the point of mutation, with the sequence identical to that of the targeted gene, except for the mutation to be inserted. The length of the ssDNA donors ranged from 115 to 65 nucleotides, whereas the dsDNA donor has homology arms of 800bp each. The sequence of the donor template was designed to introduce silent mutations in the PAM region, recognized by Cas9, and in the seed region of annealing with the gRNA. These silent mutations were introduced to avoid the re-cutting of DNA once the HDR has occurred. Furthermore, another silent mutation was introduced on exon 4 of z-*sgcb*, to generate a diagnostic restriction site for HindIII to simplify the screening of the positive embryos with a simple DNA digestion. On z-*sgcd,* the integration of the desired missense mutation itself (E246K) produces a diagnostic restriction site for DraI that can be exploited for the screening process. In Fig 54 are reported all the features here described.

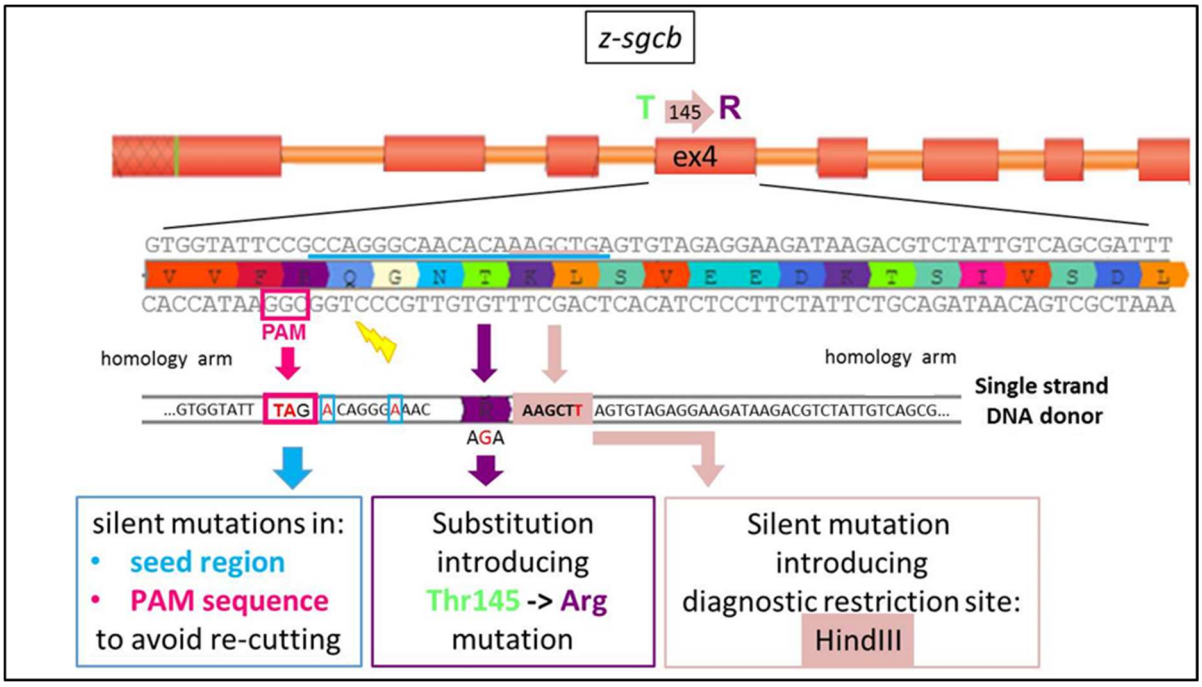

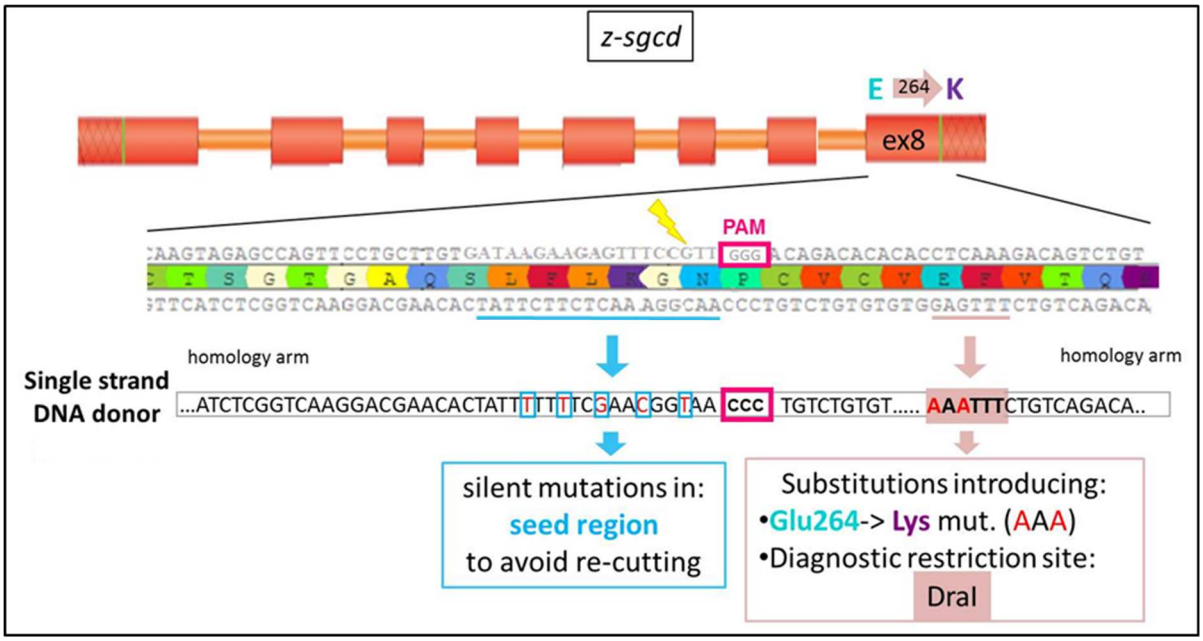

Fig 54. β-SG$_{ex4}$T145R and δ-SG$_{ex8}$E246K gRNA and donor template design. Scheme of z-*sgcb* (upper panel) and z-*sgcd* (lower panel) gene organization. Exons are depicted as red boxes, introns as orange thick lines; the dimensions are not in scale. The targeted regions of exon 4 in z-*sgcb*, and exon 8 in z-*sgcd* are enlarged and both the nucleotide sequence and the corresponding protein sequence are displayed. The region recognized by the gRNAs (guide n°1 for β-SG, n°2 for δ-GS, see Materials and Methods) is underlined in pale blue. For each guide, the PAM sequence, essential for Cas9 activity, is boxed in pink. Lightning bolts represent the putative sites of break from Cas9. The donor templates, with the specific missense mutations and the two-homology arms, are also reported. In the oligo sequence, the silent mutations are boxed in pale blue. The position of the diagnostic restriction sites introduced by the HDR are highlighted in pale pink.

5.3.3 Screening of mutants in filial generations

To evaluate the cutting efficacy of several guides, a preliminary injection with only gRNAs and the Cas9 enzyme was performed. The unique pattern observable by the heteroduplex migration assay, and the Sanger sequencing of injected F0 embryos were used to measure the cutting activity. The best guides for each gene were chosen and utilized in the subsequent experiments of microinjection in combination with the donor templates.

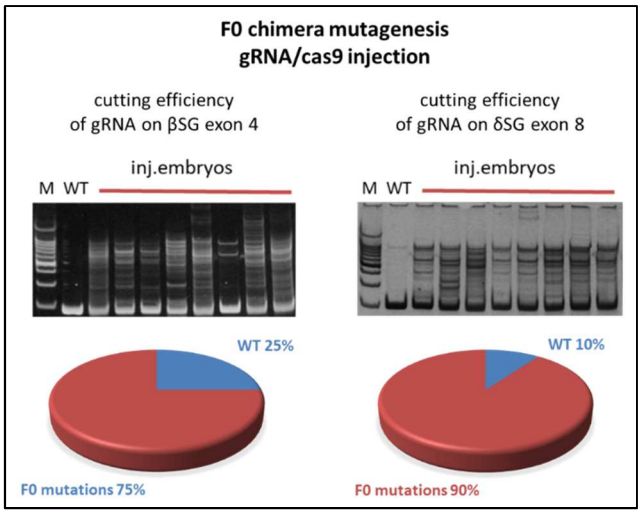

Fig 55. Cutting efficiency of the best gRNAs selected for *sgcb* and *sgcd* respectively. HMA assay on DNA amplified from F0 injected embryos. In this figure are reported the results obtained with the best guides tested for each gene that induced a rate of indel mutations of 75% and 90% in *sgcb* and *sgcd* genes, respectively.

In total were tested two different guides for β-SG in combination with 5 ssDNA donors (differing for length, position and orientations) and 1 plasmid donor, and 2 different guides in combinations with 4 ssDNA donors for δ-SG.

Despite a high cutting activity induced by the gRNA, the rate of HDR falls commonly around 10-15%, at the somatic level (F0 population), and only 1-3% is occurring in germline. Therefore, it was mandatory to setup a powerful tool to discriminate unambiguously the few molecules of positive DNA in the total DNA of the injected chimeras.

To accomplish this task, we setup a PCR amplification based on the use of a reverse primer, external to the region involved in homology recombination, and a forward primer aligning exactly in the region where the silent mutations are located. In this way, amplification should occur only if HDR introduced the sequence of interest. Indeed, the forward primer, called allele specific oligonucleotide (ASO), can discriminate between WT and mutated DNA because extension occurs only if perfectly matching the sequence. In the presence of the parental allele, the mismatches at the 3' end are refractory to primer extension. In Fig. 56 was reported as an example the experimental approach for β-SG. A similar approach was used for δ-SG (data not shown).

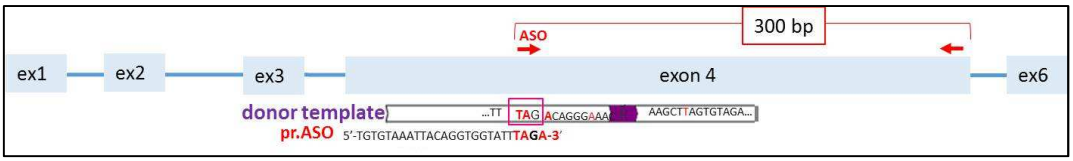

Fig 56. Scheme of the region in exon 4 of *z-sgcb* involved in HDR. Position and features of the oligonucleotides used for the screening of the somatic recombinants are indicated. The dimensions are not in scale. The forward primer (ASO) is able to discriminate between the WT and mutated allele because of the 3' mismatches, refractory to primer extension, formed when alignment occurs with the parental sequence.

The ability to discriminate between WT and mutant was first tested by the amplification of two plasmids harbouring the mutated or the WT sequences. As reported in fig.57 for β-SG, the WT sequence was never amplified, at any annealing conditions, while the mutated sequence was amplified, even under increasingly stringent conditions of annealing.

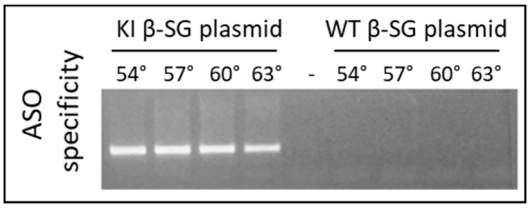

Fig 57. ASO specificity for mutant sequence. Primer ASO are able to distinguish between the mutant sequence, amplified at all the conditions tested, and the WT sequence, never amplified. The different annealing temperatures tested are reported. The most stringent PCR conditions (63°C annealing temperature) was used for the subsequent analysis on the genomic DNA of the injected fish (F0 population).

After the injection of gRNAs and the donor templates, DNA was extracted and amplified with the appropriate ASO primer for β-SG or δ-SG. Until now, we have obtained positive resulted for β-SG using guide n°1 and ssDNA donor n°3 (see Materials and Methods for detail).
After the injection of crRNA, tracrRNA, Cas9 and the ssDNA donor template, 40 embryos of the F0 population were analysed at 48 hpf. After genomic DNA purification, ASO amplification was carried out at the most stringent conditions. Twenty-three out of forty (23/40) fish were positive at ASO amplification, as it possible to observe in figure 58 reporting the picture of the agarose gel electrophoresis in which a pool of 9 samples are examined. A fragment of the correct length (approximately 300 bp) was amplified in about 58% of the analysed samples.

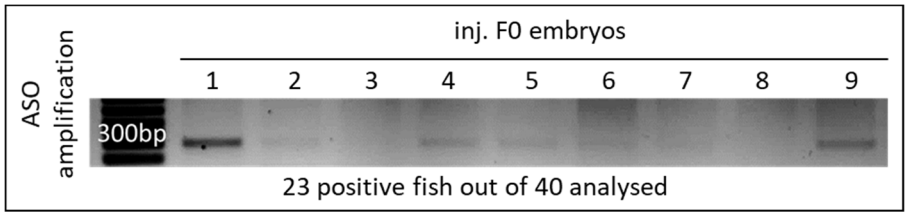

Fig 58. ASO amplification of a representative pool (9/40) of F0 embryos. The 57,5% of injected fish are positive at ASO amplification.

To confirm the result, 12 of the 23 positive samples were sequenced. All of them presented the desired missense mutations T145A on exon 4 of βSG, as well as the silent mutations added to avoid re-cutting of DNA and to introduce the diagnostic restriction site for Hind III. Only 2 of the 12 analysed sequences displayed additional undesired indel mutations in region upstream and downstream the place of recombination. In Fig.59 it is reported the sequence alignment of a representative fragment, between one positive fish at ASO amplification compared to WT. It is

possible to identify the point mutation of interest (boxed in purple) and the silent mutations introduced to avoid DNA re-cutting (boxed in pink) and to generate the diagnostic restriction site Hind III (boxed in pale pink). The region corresponding to the donor sequence is highlighted in yellow.

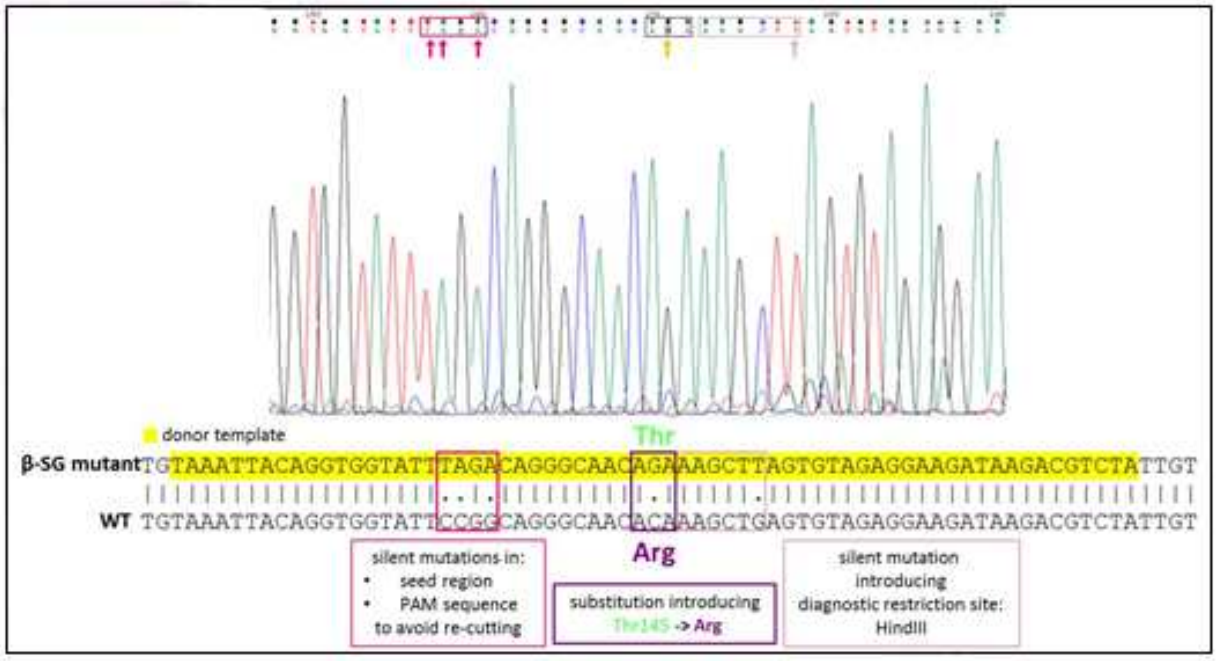

Fig 59. Sequence alignment of a representative β-SG-mutated fragment with wild type. The desired missense mutation, as well as the other silent mutations harboured by the ssDNA donor template were identified in the fragments amplified by primer ASO. Mismatches are boxed in different colours. The desired missense mutation is boxed in purple, the silent mutations in pink and those introducing a diagnostic restriction site for HindIII in pale pink. The region corresponding to the sequence of the template donor is highlighted in yellow. Above the scheme is reported the electropherogram of a representative mutant.

The remaining fish of the F0 population are now growing and will be outcrossed with WT to evaluate the germline rate transmission and to identify founders. Even if it is well known the low frequency of germline transmission, the high frequency of HDR observed in the F0 population, allows for optimistic expectations.

6. CONCLUSION

Sarcoglycanopathies, also known as limb-girdle muscular dystrophy (LGMD) 2C-F, are a group of autosomal recessive muscle wasting diseases that mainly affect the proximal musculature of the scapular and pelvic girdles, due to mutations in the genes coding for α-, β-, γ-, δ- sarcoglycans (SGs) (Nigro and Savarese, 2014).

Sarcoglycanopathies are heterogeneous disorders for both age of onset and phenotype severity. However, they are invariably characterized by a progressive degeneration of the skeletal muscle tissue, with increase of serum CK due to sarcolemma fragility, often ending in loss of ambulation. Additional features are calf hypertrophy, scapular winging, contractures, and scoliosis. Patients can suffer of restrictive ventilatory syndrome with the need for respiratory support, and/or dilated cardiomyopathy that requires a concomitant cardiac therapy. Respiratory and/or cardiac complications can be fatal if not continuously monitored. (Politano et al., 2001; Barresi et al., 1996). Although supportive interventions aim at ameliorate the quality of life of patients, the sole pharmacological treatment, nowadays available, is the symptomatic one with corticosteroids to decrease inflammation (Carotti et al., 2017). Unfortunately, no causative therapeutic approach for sarcoglycanopathy has still reached clinical application.

SGs are four transmembrane glycoproteins of striated muscle that form a tetrameric complex of the sarcolemma. SG-complex is closely linked to the major dystrophin associated protein complex (DAPC) and plays a fundamental role in assuring the membrane integrity during the contraction cycles (Ozawa et al., 2005).

Mutations in any SG genes (*SGCA, SGCB, SGCG, SGCD*) result in the strong reduction or total loss of the affected protein as well as of the WT partners. The disruption of a key membrane complex is responsible for the alteration of the DAPC structural properties that results in an increased membrane fragility. This leads to progressive muscle wasting and the onset of a severe form of dystrophy (Sandonà and Betto, 2009). SGs point mutations reported in the Leiden database (http://www.dmd.nl) are either nonsense, in-frame small deletions/insertion or missense mutations. The latter, producing a full-length protein with a single amino acid substitution, are the most frequently reported (on the whole, more than 65%).

In the last few years, it has been observed that a single amino acid substitution in a full-length SG results in a folding defective protein that is recognized by the quality control (QC) machinery of the cell. The defective SG becomes substrate of the endoplasmic reticulum associated degradation (ERAD) and is discarded through the ubiquitin proteasome system (UPS) (Bartoli et al., 2008; Gastaldello et al., 2008).

Thanks to this knowledge, two possible therapeutic approaches have been hypothesized, for those forms of sarcoglycanopathy due to the presence of missense mutations. Both strategies aim to

recover a functional SG-complex at the proper cellular site, by using small molecules able either to avoid the degradation or to "repair" the folding defective SG (Gastaldello et al., 2008; Soheili et al., 2012; Bianchini et al., 2014; Carotti et al., 2018). Concerning the first approach, it was reported that, by targeting different steps of the degradative pathway, most of the SG missense mutants are recovered on the sarcolemma, thus indicating that these mutants are still functional even if folding defective (Gastaldello et al.2008; Bianchini et al., 2014). The second strategy that would be fruitful for patients, aims to help the folding process of SG missense mutants and it is based on small molecules known as correctors of the cystic fibrosis transmembrane regulator channel (CFTR). These molecules were screened for their ability to assist the folding of the conformational mutants of the chloride channel involved in cystic fibrosis (Gelman and Kopito, 2003). Indeed, many mutations occurring in cystic fibrosis are missense mutations leading to defects in the folding of an otherwise functional CFTR protein, a mechanism that is in common with sarcoglycanopathies. On these premises, CFTR correctors were successfully tested *in vitro* in sarcoglycanopathy models and the proof of concept of this therapeutic approach was described in Carotti et al., 2018. Data from both cell models and notably, primary myotubes from a patient suffering of α-sarcoglycanopathy, strongly suggest the feasibility of a "protein repair strategy" to treat LGMD2D. Indeed, upon CFTR corrector treatments, the amount of the mutated α-SG increases thanks to protein stabilization without any effect on the gene transcription. CFTR correctors act probably as proteostasis regulators by modulating the activity, composition or concentration of proteostasis network elements. The accumulation of α-SG mutants could be therapeutically effective since followed by SG-complex assembly and localization at the sarcolemma. The SG complex, although containing a mutated subunit, is functional as its presence strengthened the sarcolemma, reducing the release of the cytosolic CK protein under stressful condition. The same approach could be effective with LGMD2C, 2E and 2F patients, since all the forms of sarcoglycanopathy share a similar pathogenic mechanism (Carotti et al., 2017).

To move on toward a therapy, the subsequent preclinical step needs to test *in vivo* efficacy and tolerability of these compounds. To this aim, there is the need of vertebrate animals carrying missense mutations in SGs that cause the loss or strong reduction of the tetrameric complex, mimicking the human condition.

Unfortunately, the existing mouse models cannot be used since both the α-$SG^{H77C/H77C}$ and β-$SG^{T153R/T153R}$ mice do not recapitulate the disease. Indeed, the mutated SG and the entire complex properly localize at the sarcolemma and mice develop no dystrophic phenotype (Bartoli et al., 2008; Kobuke et al., 2008; Henriques et al., 2018). On the other hand, the existing KO models not expressing the protein, are therefore unusable to test this pharmacological approach.

In these years, zebrafish (*Danio rerio*) is becoming an ideal animal model for mimicking genetic diseases and in particular muscular disorders for many reasons (Dooley and Zon, 2000). First, it is relatively easy to introduce any desired mutation by applying the CRISPR/Cas9 genome-editing

technology (Chang et al., 2013). Second, in addition to the advantages of this small fish over mammals in terms of size, rapid development, large numbers of offspring, zebrafish also shares with mammals high similarity in gene sequences (Chambers et al., 2003; Steffen et al., 2007), conservation of cellular pathways and almost indistinguishable muscle tissue structures (Guyon et al., 2003). Third, the embryo transparency is useful to evaluate any cardiac or muscle impairment during the initial stages of development (Gibbs et al., 2013). Fourth, the presence of stereotyped movements since the first day of life allows easily observing and measuring any alteration in muscle function (Kopp et al., 2018; Burgess et al., 2007). Moreover, emerging evidence indicates that the ERAD elements and the ubiquitin-proteasome system, responsible for the premature degradation of sarcoglycan mutants in mammals, are conserved and active in zebrafish (Barbieri et al., 2018, Wang et al., 2007; Saslowsky et al., 2010; Chen et al., 2014; Imai et al., 2010). Finally, the ability to adsorb molecules directly dissolved in fish-water makes zebrafish an ideal model for testing new drugs (in small as well as in large-scale) not feasible in mammals due to cost, time requirement and ethical concerns (MacRae and Peterson, 2014).

In this context, my PhD project regards mainly the generation of novel models of LGMD2E and 2C in zebrafish. β-and δ-SG have been chosen since they are the most conserved SGs between human and zebrafish. In particular, protein sequence alignments show that β-SG is 75% identical and 87% similar to human orthologue and δ-SG is 72% identical and 87% similar to human orthologue.

Furthermore, the proof of concept of mimicking sarcoglycanopathy in zebrafish was obtained with the rapid and transient Knock-Down (KD) of δ-SG through the injection of δ-SG morpholino-based antisense oligonucleotides (δ-SG_{AUG}MO) directed against the mRNA translation-starting region. Treated embryos showed a decrease in the δ-SG protein content as evaluated by western blot and confocal immunofluorescence. Interestingly, the decrease in δ-SG expression was accompanied by a strong decrease in β-SG, as occurring in KO mice and in hamster Bio14.6 8 (Durbeej and Campbell, 2002) as well as in LGMD2F patients (Jung et al., 1996). Not only the SG complex, but also the muscle structure resulted affected, since the birefringence assay showed dark zones in muscle fibres, a sign of muscle damage. The effect was dose dependent because by increasing the concentration of δ-SG_{AUG}MO from 0.1mM to 0.3mM a stronger muscle impairment became evident. Moreover, embryos showed altered phenotype (called morphants) with bent body along the major axis, cardiac alteration, as occurring in LGMD2C and 2E, delayed development, and compromised swimming ability evaluated through the touch evoked escape response assay. Indeed, the morphants, when gently touched with a needle, cannot escape since not swimming properly. Both WT and standard MO (Std-MO) injected embryos were used as negative control. This technology, however, can elicit off target effects with a death peak at 1-day post fertilization (dpf) by p53-induced apoptosis (Robu et al., 2007). Therefore, p53 was knocked down to reduce

this unspecific effect of δ-SG_{AUG}MO injection. Finally, to confirm the specificity of the δ-SG_{AUG}MO we performed a rescue experiment by the injection of the human δ-SG mRNA.

However, our aim is the generation of stable mutants. Therefore, the successful results obtained with the MO technique, encouraged us to produce and characterize novel lines of zebrafish mutated in *sgcb* and *sgcd* genes, coding respectively for β- and δ-SG. To this purpose, we applied the CRISPR/Cas9 genome editing technology to obtain both KO and KI zebrafish lines of β- and δ-SG genes.

This system was first discovered as one of the many defence mechanisms active in prokaryotes and archaea against invading DNA and recently was modified for genome editing. The system can easily target virtually any genomic location of interest by a customizable short RNA guide in various organisms, including zebrafish (Mali et al., 2013).

Two novel lines of zebrafish, in which β- or δ-SG have been Knocked-out (KO), have been already generated and characterized at the molecular, morphological, histological, and behavioural levels.

In both β-SG_{ex2}KO and δ-SG_{ex2}KO lines, the absence of the protein interested by KO was verified by western blot and whole-mount immunofluorescence confocal analysis.

Is important to note that, as occurring in patients (Jung et al., 1996), other KO models (Coral-Vazques et al., 1999), and δ-SG KD with MO, the absence of the mutated SG protein is followed by the strong reduction (almost absence) of the WT partners. This is the consequence of the inability to form a regular SG-complex that requires the presence of all the SG members (Carotti et al., 2017). Moreover, β- and δ-SG are considered the two subunits playing a pivotal role in the assembly process, being the core components to which the other SGs subsequently interact with (Townsend et al., 2014). The absence of both β - and δ -SG suggests that also α- and γ-SG are missing or decreased but, unfortunately, the lack of specific antibodies against the zebrafish proteins prevented this analysis.

The absence/alteration of the SG-complex is expected to have a deep impact on the DAPC function and thus on the sarcolemma properties, leading to muscle degeneration. However, according to our data, these are not early effects, as at the embryos-larval stage, the muscle structure is only marginally affected, as probed by staining with fluorescent-phalloidin that evidenced only a slightly less compact organization of the myofibrils in comparison to WT. Consistently, when β- and δ-SG-KO embryos were challenged with a test evaluating the ability to escape from a mechanical stimulus, both mutants showed a behaviour overlapping that of the WT embryos. On the other hand, a deeper analysis of the swimming ability of the mutants, consisting in the recording of their movements in continuously for several days, highlighted a reduction, of about 20-30%, in the total distance moved in comparison to WT embryos.

Sarcoglycanopathy is a progressive disease and, indeed β- and δ-SG-KO zebrafish experienced progressive muscle damage and impairment in muscle function. When the tracking of the distance moved by mutants was recorded at the *juvenile* stage (30 dpf) it was evident that the swimming

capacity of β-SG_{ex2}KO worsened in comparison to the embryonic performance. However, the most remarkable data came from the histological analysis of muscle cryosections from 5 months old mutant, in which a clear and severe myopathic picture was present in comparison to age-matched WT animals.

All this considered, it is possible to conclude that both β-SG_{ex2}KO and δ-SG_{ex2}KO lines develop a progressive muscle dystrophy resembling the condition present in LGMD2E and 2F patients. Presently, the effect of the SG absence at the cardiac and circulatory system levels is under investigation, to evaluate also in these aspects any overlapping with the human conditions (Politano et al., 2001).

Although not definitely concluded, the characterization of these novel zebrafish lines strongly suggests they well resemble the conditions present in LGMD2E and 2F. Moreover, the KO zebrafish lines can be used as background for the injection of the mRNA of β- and δ-SG for the transient expression of many different mutated forms of these SGs.

Indeed, we have already performed a pilot experiment with the injection of the human WT sequence, showing that the protein is expressed at high level during the first 24 hours and then progressively decreases reaching at 48 hours a level similar to that present in the control WT zebrafish. The analysis of the localization, presently ongoing, will tell us if the protein assembles with the other SGs and moves towards the sarcolemma. If the molecular rescue with the WT sequence will be confirmed, we will proceed with the injection of the mRNAs coding for mutated SG proteins. By comparing the protein level and the localization of these mutants with that of the WT, we are confident to understand if the zebrafish ERAD is able to recognize such mutants as folding defective as occurring in human. This would be of upmost importance, because our primary aim is to develop zebrafish models mimicking the forms of sarcoglycanopathy caused by the presence of a missense mutation in the sarcoglycan genes. Moreover, if this system will be fruitful, injected KO zebrafish will be utilized to test compounds allowing to verify safety, efficacy and, importantly, broadness of their activity (how many different mutations can be recovered).

In addition to the KO models, this project aims to generate knock-in (KI) zebrafish, β-$SG^{T145R/T145R}$ and δ-$SG^{E246K/E246K}$ KI, in which directly perform the pharmacological tests. The amino acid substitutions, T145R on exon 4 of z-*sgcb* and E246K, on exon 8 of z-*sgcd*, have been chosen because present in a well conserved region between human and zebrafish SG sequence and because they are among the mutations recoverable *in vitro* by targeting ERAD (Soheili et al., 2012). The introduction of a precise point mutation (KI) is much more complicated than the achievement of a KO mutation.

Therefore, we tested several approaches, described as successful in literature (Jasin and Rothstein, 2013; Auer et al., 2014) that include:

i. The use of either a sense or antisense single strand DNA oligos (ranging in length from 62 to 115 nucleotides) or a double stranded DNA cloned into a plasmid (800 nt long homology arms) to verify the efficacy of short vs long donor templates;

ii. The injection of the Cas9 enzyme with a sgRNA (the simplified system) or with the complex crRNA:tracRNA (the physiological system);

iii. The addition of small molecules acting on the repair pathway of the cell by either blocking the non-homologous end joining (NHEJ), or by increasing the activity of the homologous direct repair (HDR).

To increase the efficacy of HDR, Cas9 must cut close to the point of the mutation needs to be introduced, therefore gRNAs were selected as closest as possible to the mutation site.
The most challenging part in the KI development is the screening of the injected populations since a low percentage of embryos undergoes homology direct repair and even a smaller percentage (about 1-3%) presents the recombination in the germ line. Moreover, the introduced mutation is restricted to one single base and to detect this small change there is the need for a highly sensitive and selective technique, since hundreds or thousands of embryos cannot be all sequenced. Therefore, for the screening step we setup a PCR amplification experiment based on the ability of an allele-specific oligonucleotide (ASO) to amplify only the mutated DNA, which is present in a much lower amount than the WT in the chimera-injected embryos.
Among the different approaches used to induce the homologous recombination, the successful was that based on the use of the crRNA+tracrRNA+Cas9 injection together with the ssDNA sense donor template n°3, 65nt long. Indeed, 58% of F0 injected embryos were positive for somatic homology direct repair, as determined with the ASO-specific PCR amplification. Sequencing analysis established that more than 70% of the positive embryos were free from unwanted indel mutations.
These chimeras, when sexually mature, will be outcrossed with WT animals to verify the presence of the mutation in the germ line and the transmission to the offspring. Once identified the founders, as an additional way to follow the segregation of the missense mutations, we have the possibility to use a diagnostic restriction site, introduced through a silent mutation present in the donor template. In this way, we expect that the occurrence of the pathologic mutations may be anticipated by the recognition of the diagnostic restriction sites for DraI or HindIII, in δ-SG and β-SG, respectively. SG-KI lines are not yet in our hands, however, the high rate of positive embryos

observed in the F0 population allows to be confident for the identification of founders and for the establishment of the stable lines expected by the end of the current/beginning of the next year.

Sarcoglycanopathies are progressively muscle-wasting diseases, with a great impact on the patient's quality of life. Presently, no cure is available; therefore, delivering effective treatments for patients suffering of such diseases is a health challenge, unfortunately still unmet. In the few last years, we have dedicated many efforts to the identification of novel therapeutic strategies for sarcoglycanopathies, also thanks to the disclosure of the pathogenic mechanism of the disease (Gastaldello et al., 2008; Bianchini et al., 2014; Carotti et al., 2018). For the pharmacological approach based on the use of protein folding correctors, we have established, *in vitro*, the proof of concept that is waiting for the *in vivo* validation (Carotti et al., 2018). Unfortunately, the rodent models at present available are unsuitable or unusable to this purpose (Bartoli et al., 2008; Kobuke et al., 2009; Henriques et al., 2018). Therefore, the novel vertebrate models of sarcoglycanopathy produced in zebrafish, and described in this PhD thesis, represent a fundamental tool to test *in vivo* our pharmacological approach for sarcoglycanopathy. Moreover, they could become a versatile platform for any future *in vivo* screening of libraries composed of approved drugs as well as novel compounds. Finally, they are a valuable adjunction to the currently existing vertebrate models for basic and translational research, particularly suited for studying the first stages of the disease development.

7. REFERENCES

Adams M.E., Odom G.L., Kim M.J., Chamberlain J.S., Froehner S.C. Syntrophin binds directly to multiple spectrin-like repeats in dystrophin and mediates binding of nNOS to repeats 16-17. Hum Mol Genet (2018). 27(17):2979-2985.

Angelini C., Fanin M., Menegazzo E., Freda M. P., Duggan D. J., Hoffman E. P. Homozygous α-sarcoglycan mutation in two siblings: one asymptomatic and one steroid-responsive mild limb-girdle muscular dystrophy patient. Muscle Nerve (1998). 21:769-775.

Armstrong G. A. B. et al. Homology Directed Knockin of Point Mutations in the Zebrafish tardbp and fus Genes in ALS Using the CRISPR/Cas9 System. PLOS ONE (2016). 11:e0150188.

Auer T.O., Duroure K., De Cian A., Concordet J.P., Del Bene F. Highly efficient CRISPR/Cas9-mediated knock-in in zebrafish by homology-independent DNA repair. Genome Research (2014). 24:142–153.

Balch W. E., Morimoto R. I., Dillin A. and Kelly J. W. Adapting proteostasis for disease intervention. Science (2008). 916–919.

Barbieri A., Carra S., De Blasio P., Cotelli F., Biunno I. Sel1l knockdown negatively influences zebrafish embryos endothelium. J Cell Physiol (2018). 233(7):5396-5404.

Barresi R., Confalonieri V., Lanfossi M., Di Blasi C., Torchiana E., Mantegazza R., Jarre L., Nardocci N., Boffi P., Tezzon F., Pini A., Cornelio F., Mora M., Morandi L. Concomitant deficiency of α- and γ-sarcoglycans in 20 α-sarcoglycan (adhalin)-deficient patients: immunohistochemical analysis and clinical aspects. Acta Neurophatology (1996).

Bartoli M., Gicquel E., Barrault L., Soheili T., Malissen M., Malissen B., Vincent-Lacaze N., Perez N., Udd B., Danos O. et al. Mannosidase I inhibition rescues the human alpha-sarcoglycan R77C recurrent mutation. Hum. Mol. Genet. (2008). 17(9):1214-21.

Barton E. R. Impact of sarcoglycan complex on mechanical signal transduction in murine skeletal muscle. American Journal of Physiology (2006). 411-419.

Bedell V. M., Wang Y., Campbell J. M., Poshusta T. L., Starker C. G., Krug R. G. II., Tan W., Penheiter S. G., Ma A. C., Leung A. Y. et al. In vivo genome editing using a high- -efficiency TALEN system. Nature (2012). 491(7422):114-8.

Berardi A., Trezza V., Palmery M., Trabace L., Cuomo V. and Campolongo P. An updated animal model capturing both the cognitive and emotional features of post-traumatic stress disorder (PTSD). Front Behav Neurosci. (2014). 8: 142.

Berger J. and Curie p.d.. Zebrafish models flex their muscles to shed light on muscular dystrophies. Disease models and mechanisms (2012). 5(6):726-732.

Bianchini E., Fanin M., Mamchaoui K., Betto R. and Sandona D. Unveiling the degradative route of the V247M a-sarcoglycan mutant responsible for LGMD-2D. Human Molecular Genetics (2014). 23, 3746–3758.

Bogert P.S.T, Huang B.Q., Gradilone S.A., Masyuk T.V, Moulder G.L., Ekker S.C. and LaRusso N.F. The zebrafish as a model to study polycystic liver disease. Zebrafish (2013). 10(2):211-217.

Boissel S., Jordan J., Astrakhan A., Adey A., Gouble A., Duchateau P., Shendure J., Stoddard B.L., Certo M.T., Baker D., Scharenberg A.M.MegaTALs: a rare-cleaving nuclease architecture for therapeutic genome engineering. Nucleic Acids Research (2014). 42:2591–2601.

Bönnemann C. G., Modi R., Noguchi S., Mizuno Y., Yoshida M., Gussoni E., McNally E. M., Duggan D. J., Angelini C., Hoffman E. P., Ozawa E., Kunkel L. M. β-Sarcoglycan (A3b) mutations cause autosomal recessive muscular dystrophy with loss of the sarcoglycan complex. Nature Genetics (1995). 11:266–273

Bournele D, Beis D. Zebrafish models of cardiovascular disease. Heart Fail Rev (2016) 21(6):803-813.

Bradford Y. M., Toro S., Ramachandran S., Ruzicka L., Howe D. G., Eagle A., Kalita P., Martin R., Moxon S. A. T., Schaper K. and Westerfield M. Zebrafish Models of Human Disease: Gaining Insight into Human Disease at ZFIN. ILAR Journal (2017). Vol. 58, No. 1, 4–16.

Burgess H.A., Granato M. Modulation of locomotor activity in larval zebrafish during light adaptation. J Exp Biol. (2007) 210(Pt 14):2526-39.

Burks T. N., Cohn R. D. Role of TGF-β signaling in inherited and acquired myopathies. Skeletal Muscle (2011). 1(1):19.

Bushby K. Diagnosis and management of the limb girdle muscular dystrophies. Pract Neurol. (2009). 314-23.

Carotti M., Fecchio C. and Sandonà D. Emerging therapeutic strategies for sarcoglycanopathy. Expert Opinion on Orphan Drugs (2017). 5:5, 381-396.

Carotti M., Marsolier J., Soardi M., Bianchini E., Gomiero C., Fecchio C., Henriques S. F., Betto R., Sacchetto R., Richard I., Sandonà D. Repairing folding-defective α-sarcoglycan mutants by CFTR correctors, a potential therapy for limb-girdle muscular dystrophy 2D. Hum Mol Genet. (2018). 27(6):969-984

Chambers S. P., Anderson L. V., Maguire G. M., Dodd A. and Love D. R. Sarcoglycans of the zebrafish: orthology and localization to the sarcolemma and myosepta of muscle. Biochemical and Biophysical Research Communications (2003). 303(2): 488-495.

Chang N., Sun C., Gao L., Zhu D., Xu X., Zhu X., Xiong J. and Xi J. J.. Genome editing with RNA-guided Cas9 nuclease in Zebrafish embryos. Cell Research (2013). Vol. 23, 465–472.

Chang N., Sun C., Gao L., Zhu D., Xu X., Zhu X., Xiong J.W. and Xi J.J. Genome editing with RNA-guided Cas9 nuclease in Zebrafish embryos. Cell Research (2013). 23: 465–472.

Chen J. et al. Identification of functional domains in sarcoglycans essential for their interaction and plasma membrane targeting. Experimental Cell Research (2006). 15; 312(9):1610-25

Chen Z., Ballar P., Fu Y., Luo J., Du S., Fang S. The E3 ubiquitin ligase gp78 protects against ER stress in zebrafish liver. J Genet Genomics (2014). 41(7):357-68.

Cheng L., Guo X. F., Yang X. Y., Chong M., Cheng J., Li G., Gui Y. H., Lu D. R. Delta-sarcoglycan is necessary for early heart and muscle development in zebrafish. Biochemical and Biophysical Research Communications (2006). 1290–1299.

Chu V. T., Weber T., Wefers B., Wurst W., Sander S., Rajewsky K. and Kühn R. Increasing the efficiency of homology-directed repair for CRISPR Cas9 induced precise gene editing in mammalian cells. Nature Biotechnology (2015). 33,543–548.

Chylinski K., Makarova K.S., Charpentier E., Koonin E.V. Classification and evolution of type II CRISPR-Cas systems. Nucleic Acids Res (2014) 42(10):6091-105.

Coral-Vazquez R., Cohn R.D., Moore S.A., Hill J.A., Weiss R.M., Davisson R.L., Straub V., Barresi R., Bansal D., Hrstka R.F., Williamson R., Campbel K.P. Disruption of the Sarcoglycan–Sarcospan Complex in Vascular Smooth Muscle: A Novel Mechanism for Cardiomyopathy and Muscular Dystrophy (1999). Cell. 98: 465–474.

Cox D. B. T., Platt R. J. and Zhang F. Therapeutic genome editing: prospects and challenges. Nature (2015). Vol. 21, No. 2, 121-131.

Culligan K. G., Ohlendieck K. Abnormal calcium handling in muscular dystrophy. Basic and Applied Myology (2002). 12:147–57.

Dahlem T. J., Hoshijima K., Jurynec M. J., Gunther D., Starker C. G., Locke A. S. et al. Simple methods for generating and detecting locus-specific mutations induced with TALENs in the zebrafish genome. PLoS Genetics (2012).

Dahm R. The Zebrafish Exposed: "See-through" mutants may hold the key to unraveling the mysteries of embryonic development. American Scientist (2006). Vol. 94, No. 5, 446-453.

Davies K. E. and Nowak K. J. Molecular mechanisms of muscular dystrophies: old and new players. Molecular Cell Biology (2006). 762-773.

De Marco R.J., Thiemann T., Groneberg A.H., Herget U., Ryu, S. Optogenetically enhanced pituitary corticotroph cell activity post-stress onset causes rapid organizing effects on behavior. Nature Communications (2016). 7:12620.

De Palma C., Morisi F., Cheli S., Pambianco S., Cappello V., Vezzoli M. et al. Autophagy as a new therapeutic target in Duchenne muscular dystrophy. Cell Death and Disease (2012). 3:418.

Deveau H., Barrangou R., Garneau J. E., Labonté J., Fremaux C., Boyaval P. et al. Phage response to CRISPR-encoded resistance in Streptococcus thermophilus. Journal of Bacteriology (2008). 190(4): 1390–1400.

Dooley, K. and Zon, I.L. Zebrafish: a model system for the study of human disease Current Opinion in Genetics & Development (2000). 10:252–256.

Doyon Y., McCammon J. M., Miller J. C., Faraji F., Ngo C., Katibah G. E., Amora R., Hocking T. D., Zhang L., Rebar E. J. et al. Heritable targeted gene disruption in zebrafish using designed zinc-finger nucleases. Nature Biotechnology (2008). 26: 702–708.

Draviam R.A., Shand S.H., Watkins S.C. The β-δ-core of sarcoglycan is essential for deposition at the plasma membrane. Muscle Nerve (2006). 34(6):691-701.

Duclos F., Straub V., Moore S. A., Venzke D. P., Hrstka R. F., Crosbie R. H., Durbeej M. et al. Progressive muscular dystrophy in n-sarcoglycan deficient mice. Journal Cell of Biology (1999).

Durbeej M. and Campbell K.P. Muscular dystrophies involving the dystrophin–glycoprotein complex: an overview of current mouse models. Current Opinion in Genetics & Development (2002). 12:349–36.

Escribano-Díaz C., Orthwein A., Fradet-Turcotte A., Xing M., Young J. T., Tkáčˇ J. et al. A cell cycle-dependent regulatory circuit composed of 53BP1-RIF1 and BRCA1-CtIP controls DNA repair pathway choice. Molecular Cell (2013). 49(5): 872–883.

Fanin M., Melacini P., Boito C., Pegoraro E., Angelini C. LGMD2E patients risk developing dilated cardiomyopathy. Neuromuscular Disorders (2003). 303–309.

Fanin M., Nascimbeni A. C., Aurino S., Tasca E., Pegoraro E., Nigro V., Angelini C. Frequency of LGMD gene mutations in Italian patients with distinct clinical phenotypes. Neurology (2009). 1432–1435.

Felsenfeld A. L., Walker C., Westerfield M., Kimmel C., Streisinger G . Mutations affecting skeletal muscle myofibril structure in the zebrafish. Development. (1990). 108(3):443-59.

Fischer D., Walter M. C., Kesper K. et al. Diagnostic value of muscle MRI in differentiating LGMD2I from other LGMDs. Journal of Neurology (2005). 252:538–547.

Friedland A. E., Tzur Y. B., Esvelt K. M., Colaiacovo M. P., Church G. M. and Calarco J. A. Heritable genome editing in C. elegans via a CRISPR-Cas9 system. Nature Methods (2013). 10(8), 741–743.

Gagnon J. A. et al. Efficient mutagenesis by Cas9 protein-mediated oligonucleotide insertion and large-scale assessment of single-guide RNAs. PLOS ONE (2014). 9:e98186.

Gastaldello S. et al. Inhibition of proteasome activity promotes the correct localization of disease causing α-sarcoglycan mutants in HEK293 cells constitutively expressing b-, g-, and d-sarcoglycan. American Journal of Pathology (2008). 170-181.

Gelman, M.S. and Kopito, R.R. Cystic fibrosis: premature degradation of mutant proteins as a molecular disease mechanism. Methods in Mol. Biol (2003). 232:27-37.

Gibbs E.M., Horstick E.J., and Dowling J.J. Swimming into prominence: the zebrafish as a valuable tool for studying human myopathies and muscular dystrophies. FEBS J. (2013) 280(17): 4187–4197.

Guglieri M., Magri F. and Comi G. P. Molecular etiopathogenesis of limb-girdle muscular and congenital muscular dystrophies: boundaries and contiguities. Clinica and Chimica Acta (2005). 361:54–79.

Guglieri M., Straub V., Bushby K. and Lochmuller H. Limb–girdle muscular dystrophies. Current Opinion in Neurology (2008). 21(5):576-84.

Guyon J.R., Mosley A.N., Jun S.J., Montanaro F., Steffen S.L., Yi Zhou, Nogro V., Len I. Zon, Kunkel L.M. Delta-sarcoglycan is required for early zabrafish muscle organization. Experimental cell research (2005). 304(1):105-115

Hack A. A., Lam M. J., Cordier L., Shoturma D. I., Ly C. T., Hadhazy M. A., Hadhazy M. R., Sweeney H. L. and McNally E. M. Differential requirement for individual sarcoglycans and dystrophin in the assembly and function of the dystrophin-glycoprotein complex. Journal of Cell Science (2000). 2535-2544.

Hack A.A., Ly C.T., Jiang F., Clendenin C.J., Sigrist K.S., Wollamn R.L., and McNally E.M. γ-Sarcolgycan deficiency leads to muscle membrane defects and apoptosis independent of dystrophin. J Cell Biol (1998) 142: 1279–1287.

Henderson C.A., Gomez C,G., Novak S,M., Mi-Mi L, Gregorio C,C. Overview of the Muscle Cytoskeleton Compr Physiol. (2018) ; 7(3): 891–944.

Henriques S.F., Patissier C., Bourg N., Fecchio C., Sandona D., Marsolier J., et al. Different outcome of sarcoglycan missense mutation between human and mouse. PLoS ONE (2018). 13(1): e0191274.

Hermsen S.A., Evert-Jan van den Brandhof, Leo T.M. van der Ven, Piersma A.H. Relative embryotoxicity of two classes of chemicals in a modified zebrafish embryotoxicity test and comparison with their in vivo potencies. Toxicology in Vitro (2011). 25(3):745-753.

Homburger F., Baker J.R., Nixon C.W., and Whitney R. Primary, generalized polymyopathy and cardiac necrosis in an inbred line of Syrian hamsters. Med Exp (1962). 6: 339–345.

Howe K., Clark M. D., Torroja C. F., Torrance J., Berthelot C., Muffato M., Collins J. E., Humphray S., McLaren K., Matthews L., McLaren S., Sealy I., Caccamo M., Churcher C., Scott C. et al. Thezebrafish reference genome sequence and its relationship to the human genome. Nature (2013). 496,498–503.

Hruscha, A., Krawitz, P., Rechenberg, A., Heinrich, V., Hecht, J., Haass, C., Schmid B. Efficient CRISPR/Cas9 genome editing with low off-target effects in zebrafish. Development (2013). 140:4982-4987.

Hwang W. Y., Fu Y., Reyon D., Maeder M. L., Kaini P., Sander J. D., Joung J. K., Peterson R. T., Yeh J. R. Efficient genome editing in zebrafish using a CRISPR-Cas system. Nature Biotechnology (2013). 31:227–229.

Hyongbum K. and Jin-Soo K. A guide to genome engineering with programmable nucleases. Nature reviews and Genetics (2014). Vol. 15, 321-334.

Imai F., Yoshizawa A., Fujimori-Tonou N., Kawakami K., Masai I. The ubiquitin proteasome system is required for cell proliferation of the lens epithelium and for differentiation of lens fiber cells in zebrafish. Development (2010). 137(19):3257-68.

Irion U. Krauss J., Nüsslein-Volhard C. Precise and efficient genome editing in zebrafish using the CRISPR/Cas9 system. Development (2014). 141:4827–4830.

Ishino Y., Shinagawa H., Makino K., Amemura M. and Nakata A. Nucleotide sequence of the iap gene, responsible for alkaline phosphatase isozyme conversion in Escherichia coli, and identification of the gene product. Journal of Bacteriology (1987). 169(12): 5429–5433.

Jakai O., Casas-Fraile L., de Munain A. D., Saenz A. Costamere proteins and their involvement in myopathic processes. Expert Reviews in Molecular Medicine, Cambridge University Press (2015). Vol. 17; e12; 1 of 11.

Jao L. E., Wente S. R., Chen W. Efficient multiplex biallelic zebrafish genome editing using a CRISPR nuclease system. Proceeding National Academy Science 110 (2013). 13904–13909.

Jasin M. and Rothstein R. Repair of Strand Breaks by Homologous Recombination. Cold Sprong Harb Perspect Biol (2013). 5(11):a012740.

Jinek M., Chylinski K., Fonfara I., Hauer M., Doudna J. A. and Charpentier E. A programmable dual-RNA-guided DNA endonuclease in adaptive bacterial immunity. Science (2012). 816–821.

Johnson E.K., Li B., Yoon J.H., Flanigan K.M., Martin P.T.,Ervasti J., Montanaro F. Identification of New Dystroglycan Complexes in Skeletal Muscle. PLoS ONE (2013). 8(8): e73224.

Jung D., Duclos F., Aposto B., Straub V., Lee J. C., Allamand V., Venzke D. P., Sunada Y., Moomawi C. R., Leveille C. J., Slaughteri C. A., Crawford T. O., McPherson J. D. and Campbell K. P. Characterization of d - Sarcoglycan, a novel component of the oligomeric Sarcoglycan complex involved in Limb-Girdle muscular dystrophy. The journal of biological chemistry (1996). Vol. 271, No. 50, 32321–32329.

Kelly-Worden M. and Thomas E., Mitochondrial Dysfunction in Duchenne Muscular Dystrophy. Open Journal of Endocrine and Metabolic Diseases (2014). 4:211-218.

Kettleborough R. N., Busch-Nentwich E. M., Harvey S. A., Dooley C. M., de Bruijn E., van Eeden F., Sealy I., White R. J., Herd C., Nijman I. J. et al. A systematic genome-wide analysis of zebrafish protein-coding gene function. Nature (2013). 494–497.

Kick L., Kirchner M., Schneider S. CRISPR-Cas9: From a bacterial immune system to genome-edited human cells in clinical trials. Bioengineered (2017). 8(3):280-286.

Kim H., Kim J. S. A guide to genome engineering with programmable nucleases. Nature Review Genetics (2014). 15(5):321-34.

Kimmel C. B., Ballard W. W., Kimmel S. R., Ullmann B. and Schilling T. F. Stages of embryonic development of the zebrafish. Developmental Dynamics (1995). 203,253–31.

Kirschner J., Lochmüller H. Sarcoglycanopathies. Handb Clin Neurol. (2011). 101:41-6.

Klinge, L. et al. Sarcoglycanopathies: Can muscle immunoanalysis predict the genotype? Neuromuscular Disorders (2008). 934-941.

Kloepfer H. W., Talley C. A. Autosomal recessive inheritance of Duchenne type muscular dystrophy. Annual of Human Genetics (1958). 22(2):138-43.

Kobuke K., Piccolo F., Garringer K.W., Moore S.A., Sweezer E., Yang B., et al. A common disease-associated missense mutation in alpha-sarcoglycan fails to cause muscular dystrophy in mice. Human molecular genetics (2008). 17(9): 1201–1213.

Kok F. O., Shin M., Ni C., Gupta A., Grosse A. S., van Impel A., Kirchmaier B. C., Peterson-Maduro J., Kourkoulis G., Male I. et al. Reverse genetic screening reveals poor correlation between morpholino-induced and mutant phenotypes in zebrafish. Developmental Cell (2014). 32: 97–108.

Kopp R., Legler J., Legradi J. Alteration in locomotor activity of feeeding zebrafish larvae as a consequence of exposure to different enviromental factors. Environ Sci pollut Res (2018). 25:4085-4093.

Kotani H., Taimatsu K., Ohga R., Ota S., Kawahara A. Efficient Multiple Genome Modifications Induced by the crRNAs, tracrRNA and Cas9 Protein Complex in Zebrafish. Plos one (2015). 10 (5).

Labun K., Montague T.G., Gagnon J.A., Summer B.T., Valen E. CHOPCHOP v2: a web tool for the next generation of CRISPR genome engineering. Nucleic Acids Research (2016). 44(W1):W272-W276.

Lau V. and Davie J.R. The discovery and development of the CRISPR system in applications in genome manipulation. Biochem Cell Biol (2017). 95(2):203-210.

Le Rumeur E. Dystrophin and the two related genetic diseases, Duchenne and Becker muscular dystrophies. Bosnian journal of basic medical sciences (2015). 15(3):14-20.

Li M., Zhao L., Page-McCaw P., and Chen W. Zebrafish genome engineering using the CRISPR-Cas9 system. Trends in Genetics (2016). 32(12): 815–827.

Li T. et al. TAL nucleases (TALNs): hybrid proteins composed of TAL effectors and FokI DNA-cleavage domain. Nucleic Acids Research (2011). 39, 359–372.

Liang X., Potter J., Kumar S., Ravinder N., Chesnut J.D. Enhanced CRISPR/Cas9-mediated precise genome editing by improved design and delivery of gRNA, Cas9 nuclease, and donor DNA. J Biotechnol (2017). 241:136-146.

Lim L. E., Duclos F., Broux O., Bourg N., Sunada Y., Allamand V., Meyer J., Richard I., Moomaw C., Slaughter C. et al. Beta-sarcoglycan: characterization and role in limb girdle muscular dystrophy linked to 4q12. Nature Genetics (1995). 257–265.

Liu C., Zhang L., Liu H., Cheng K. Delivery strategies of the CRISPR-Cas9 gene-editing system for therapeutic applications. J Control Release (2017). 266:17-26.

Liu L. A., Engvall E. Sarcoglycan isoforms in skeletal muscle. Journal of Biological Chemistry (1999). 274:38171–38176.

Ma Y., Chen W., Zhang X., Yu L., Dong W., Pan S., Gao S., Huang X. and Zhang L. Increasing the efficiency of CRISPR/Cas9-mediated precise genome editing in rats by inhibiting NHEJ and using Cas9 protein. RNABiology (2016). 13: 605–612.

MacRae C.A., and Peterson R.T. Zebrafish as tools for drug discovery. Nature (2014) 14: 721-731.

Mali P., Luhan Y., Esvelt K.M., Aach J., Guell M., DiCarlo E.J., Norville J.E., Church G.M. RNA-guided human genome engineering via Cas9.Sience (2013). 339(6121):823-826.

Mathews K. D., Moore S. A. Limb-girdle muscular dystrophy. Current Neurology and Neuroscience (2003). 3:78–85.

McCaw P.A., Ewald A.J., Werb Z. Matrix metallo proteinases and the regulation of tissue remodelling. Nature Reviews Molecular Cell Biology (2007). 8:221–33.

McNally E. M., Passos-Bueno M. R., Bönnemann C. G., Vainzof M., de Sá Moreira E., Lidov H. G., Othmane K. B., Denton P. H., Vance J. M., Zatz M. and Kunkel L. M. Mild and severe muscular dystrophy caused by a single gamma-sarcoglycan mutation. Am J Hum Genet. (1996). 59(5): 1040–1047.

Meeker N.D., Hutchinson S.A., Ho L., Trede N.S. Method for isolation of PCR ready genomic DNA from zebrafish tissue. Biotechniques (2007).43(5):601-614.

Mendell J. R., Campbell K., Rodino-Klapac L., Sahenk Z., Shilling C., Lewis S., Bowles D., Gray S., Li C., Galloway G., Malik V., Coley B., Clark K. R., Li J., Xiao X., Samulski J., McPhee S. W., Samulski R. J., Walker C. M. Dystrophin immunity in Duchenne's muscular dystrophy. N Engl J Med. (2010) 363(15):1429-37.

Mercuri E., Pichiecchio A., Allsop J. et al. Muscle MRI in inherited neuromuscular disorders: past, present, and future. Journal of Magnetic Resonance Imaging (2007). 25:433–440.

Miller J.C. et al. An improved zinc-finger nuclease architecture for highly specific genome editing. Nature Biotechnology (2007). 25, 778–785.

Moylan J. S., Reid M. B. Oxidative stress, chronic disease, and muscle wasting. Muscle and Nerve (2007). 35:411–29.

Narayanaswami P., Carter G., David W. et al. Evidence-based guideline summary: diagnosis and treatment of limb-girdle and distal dystrophies: report of the guideline development subcommittee of the American Academy of Neurology and the practice issues review panel of the American Association of Neuromuscular & Electrodiagnostic Medicine. Neurology (2015). 84:1720–1721.

Nguyen M., Stewart A.M., Kalueff A.V. Aquatic blues: modeling depression and antidepressant action in zebrafish. Prog Neuropsychopharmacol Biol Psychiatry (2014). 55:26-39.

Nigro V. Molecular bases of autosomal recessive limb-girdle muscular dystrophies. Acta Myologica (2003). 35–42.

Nigro V., Aurino S., Piluso G. Limb girdle muscular dystrophies: update on genetic diagnosis and therapeutic approaches. Current Opinion in Neurology (2011). 24:429-36.

Nigro V., De Sa' Moreira E., Piluso G., Vainzof M., Belsito A., Politano L. et al. Autosomal recessive limb-girdle muscular dystrophy, LGMD 2F, is caused by a mutation in the sarcoglycan gene. Nature Genetics (1996 A). 195–198.

Nigro V., Okazaki Y., Belsito A., Piluso G., Matsuda Y., Politano L. et al. Identification of the Syrian hamster cardiomyopathy gene. Human Molecular Genetics (1997). 6:601-607.

Nigro V., Piluso G., Belsito A., Politano L., Puca A. A., Papparella S., Rossi E., Viglietto G., Esposito M. G., Abbondanza C., Medici N., Molinari A. M., Nigro G., Puca G. A. Identification of a novel sarcoglycan gene at 5q33 encoding a sarcolemma l35kDa glycoprotein. Human Molecular (1996 B). (8):1179-86.

Nigro V., Savarese M. Genetic basis of limb-girdle muscular dystrophies: the 2014 update. Acta Myol. (2014). 33(1):1-12.

Nigro V., Piluso G. Spectrum of muscular dystrophies associated with sarcolemma protein genetic defects. Biochimica and Biophysica Acta. (2015). 1852(4):585-93.

Noguchi S. E., Wakabayashi E., Imamura M., Yoshida M., Ozawa E. Formation of sarcoglycan complex with differentiation in cultured myocytes. European Journal of Biochemistry (2000). 267:640–648.

Noguchi S., MacNally E. M., Ben Othmane K., Hagiwara Y., Mizuno Y., Yoshida M., Yamamoto H., Bönneman C. G., Gussoni E., Denton P., Kyriakides T., Middleton L., Hentati F., Ben Hamida M., Nonaka I., Vance J., Kunkel L. M., Ozawa E. Mutations in the dystrophin-associated protein γ-sarcoglycan in chromosome 13 muscular dystrophy. Science (1995). 270: 819–822

Norwood F., de Visser M., Eymard B. et al. EFNS guideline on diagnosis and management of limb girdle muscular dystrophies. European Journal of Neurology (2007). 14:1305–12.

Ota S., Kawahara A. Zebrafish: a model vertebrate suitable for the analysis of human genetic disorders. Congenit Anom (2014) 54(1):8-11.

Ozawa, E., Mizuno, Y., Hagiwara, Y., Sasaoka, T., and Yoshida, M. Molecular and cell biology of the sarcoglycan complex. Muscle nerve (2005). 32:563-576.

Pacheco M.L., CFTR Modulators:shedding light on precision medicinefor cystic fibrosis. Front Pharmacol (2016). 7:275.

Paquet D., Kwart D., Chen A., Sproul A., Jacob S., Teo S., Olsen K.M., Gregg A., Noggle S., Tessier-Lavigne M. Efficient introduction of specific homozygous and heterozygous mutations using CRISPR/Cas9. Nature (2016). 533(7601):125-9.

Pisoni G.B and Molinari M. Five Questions (with their Answers) on ER-Associated Degradation. Traffic (2016) 17: 341–350.

Politano L., Nigro V., Passamano L., Petretta V., Comi L. I., Papparella S., Nigro Ge., Rambaldi P. F., Raia P., Pini A., Mora M., Giugliano M. A. M., Esposito M. G., Nigro G. Evaluation of cardiac and respiratory involvement in sarcoglycanopathies. Neuromuscular Disorders (2001). 178-185.

Postlethwait J.H. The zebrafish genome in context: ohnologs gone missing.J Exp Zool B Mol Dev Evol. (2007)15; 308 (5):563-77.

Pozsgai E. R., Griffin D. A., Heller K. N., Mendell J. R., Rodino-Klapac L. R. Systemic AAV-Mediated β-Sarcoglycan Delivery Targeting Cardiac and Skeletal Muscle Ameliorates Histological and Functional Deficits in LGMD2E Mice. Mol Ther. (2017). 25(4):855-869.

Rafii M. S. et al. Biglycan binds to a- and g-sarcoglycan and regulates their expression during development. Journal of Cellular Physiology (2006). 439-447.

Ran F. A., Hsu P. D., Wright J., Agarwala V., Scott D. A. and Zhang F. Genome engineering using the CRISPR-Cas9 system. Nature protocols (2013). Vol.8 No. 11: 2281-2308.

Reis A., Hornblower B., Robb B., Tzertzinis G. CRISPR/Cas9 and Targeted Genome Editing: A New Era in Molecular Biology. NEB expressions Issue I (2014).

Renaud J.B., Boix C., Charpentier M., De Cian A., Cochennec J., Duvernois-Berthet E., Perrouault L., Tesson L., Edouard J., Thinard R., Cherifi Y., Menoret S., Fontanière S., de Crozé N., Fraichard A., Sohm F., Anegon I., Concordet J.P., Giovannangeli C. Improved Genome Editing Efficiency and Flexibility Using Modified Oligonucleotides with TALEN and CRISPR-Cas9 Nucleases. Cell Rep (2016). 14(9):2263-2272.

Roberds S. L., Leturcq F., Allamand V., Piccolo F., Jeanpierre M., Anderson R. D., Lim L. E., Lee J. C., Tomé F. M., Romero N. B. et al. Missense mutations in the adhalin gene linked to autosomal recessive muscular dystrophy. Cell (1994). 625-33.

Robu M.E., Larson J.D., Nasevicius A., Beiraghi S., Brenner C., Farber S.A., Ekker S.C. p53 activation by knockdown technologies. PLoS Genet (2007). 3(5):e78.

Rothkamm K., Kruger I., Thompson L. H. and Lobrich M. Pathways of DNA double strand break repair during the mammalian cell cycle. Molecular Cellular Biology (2003). 23, 5706–5715.

Sakamoto A. et al. Both hypertrophic and dilated cardiomyopathies are caused by mutation of the same gene, d-sarcoglycan, in hamster: an animal model of disrupted dystrophin-associated glycoprotein complex. Proceedings of the National Academy of Sciences of the United States of America (1997). 13873-13878.

Salsman J., Dellaire G. Precision genome editing in the CRISPR era. Biochemistry and Cell Biology (2017). 95(2):187-201.

Sander J. D. and Joung J. K. CRISPR-Cas systems for editing, regulating and targeting genomes. Nature Biotechnology (2014). Vol. 32, 347–355.

Sandonà D., Gastaldello S., Martinello T., Betto R..Characterization of the ATP-hydrolysing activity of α-sarcoglycan. Biochemical Journal (2004). Pt 1:105-12

Sandonà D., Betto R. Sarcoglycanopathies: molecular pathogenesis and therapeutic prospects. Expert Reviews in Molecular Medicine (2009). 11:e28.

Saslowsky D.E., Cho J.A., Chinnapen H., Massol R.H., Chinnapen D.J., Wagner J.S., De Luca H.E., Kam W., Paw B.H., Lencer W.I. Intoxication of zebrafish and mammalian cells by cholera toxin depends on the flotillin/reggie proteins but not Derlin-1 or -2. J Clin Invest (2010). 120(12):4399-4409.

Schwank G., Koo B. K., Sasselli V., Dekkers J. F., Heo I., Demircan T. et al. Functional repair of CFTR by CRISPR/Cas9 in intestinal stem cell organoids of cystic fibrosis patients. Cell Stem Cell (2013). 13(6), 653–658.

Segal D. J., Meckler J. F. Genome engineering at the dawn of the golden age. Annual Review of Genomics and Human Genetics (2013). 14:135-58.

Shahid M., Takamiya M., Stegmaier J., Middel V., Gradl M., Klüver N., Mikut R., Dickmeis T., Scholz S., Rastegar S., Yang L., Strähle U. Zebrafish biosensor for toxicant induced muscle hyperactivity. Sci Rep (2016). 6:23768.

Shi W., Chen Z., Schottenfeld J., Stahl R. C., Kunkel L. M., Chan Y. M. Specific assembly pathway of sarcoglycans is dependent on beta and delta-sarcoglycan. Muscle Nerve (2004). 29:409–419.

Shin J., Tajrishi M. M., Ogura Y., Kumar A. Wasting mechanisms in muscular dystrophy. International Journal of Biochemistry and Cell Biology (2013). 45(10):2266-79.

Soheili T., Gicquel E., Poupiot J., N'Guyen L., Le Roy F., Bartoli M. and Richard I. Rescue of sarcoglycan mutations by inhibition of endoplasmic reticulum quality control is associated with minimal structural modifications. Human Mutation (2012). 33,429–439.

Steffen L.S., Guyon J.R., Vogel E.D., Beltre R., Pusack T.J., Zhou Y., Zon L.I., Kunkel L.M. Zebrafish orthologs of human muscular dystrophy genes. BMC Genomics (2007). 8:79.

Sternberg S. H., Redding S., Jinek M., Greene E. C., Doudna J. A. DNA interrogation by the CRISPR RNA-guided endonuclease Cas9. Nature (2014). 507(7490):62-7.

Strakova J., Dean J. D., Sharpe K. M., Meyers T. A., Odom G. L., Townsend D. Dystrobrevin increases dystrophin's binding to the dystrophin-glycoprotein complex and provides protection during cardiac stress. J Mol Cell Cardiol. (2014).76:106-15.

Straub V., Duclos F., Venzke D. P., Lee J. C., Cutshall S., Leveille C. J., Campbell K. P. Molecular pathogenesis of muscle degeneration in the d-sarcoglycan deficient hamster. American Journal of Physiology (1998). 153(5): 1623–1630.

Tarakci H. and Berger J. The sarcoglycan complex in skeletal muscle. Frontiers in Bioscience, Landmark (2016). 744-756.

Tedesco F. S., Gerli M. F., Perani L. et al. Transplantation of genetically corrected human iPSC-derived progenitors in mice with limb-girdle muscular dystrophy. Science Translational Medicine (2012). 4:140.

Tidball J. G. Inflammatory processes in muscle injury and repair. American Journal of Physiology Regulatory, Integrative and Comparative Physiology (2005). 288:R345–53.

Townsed D. Finding the sweet spot: Assembly and glycosylation of the dystrophin-associated glycoprotein complex. The anatomical record (2014). 297(9):1694–1705.

Vainzof M., Ayub-Guerrieri D., Onofre P.C., Martins P.C., Lopes V.F., Zilberztajn D., Maia L.S., Sell K., Yamamoto L.U. Animal models for genetic neuromuscular diseases. J Mol Neurosci (2008). 34(3):241-8.

Vainzof M., Moreira E. S., Canovas M., Anderson L. V., Pavanello R. C., Passos-Bueno M. R., Zatz M. Partial alpha-sarcoglycan deficiency with retention of the dystrophin-glycoprotein complex in a LGMD2D family. Muscle Nerve (2000). 23:984–988.

Valastyan J.S. and Lindquist S. Mechanisms of protein-folding diseases at a glance. The Company of Biologists Ltd, Disease Models & Mechanisms (2014). 7: 9-14.

Varshney G. K. et al. CRISPRz: a database of zebrafish validated sgRNAs. Nucleic Acids Research (2016). 44:D822–6.

Varshney G. K. et al. High-throughput gene targeting and phenotyping in zebrafish using CRISPR/ Cas9. Genome Research (2015). 25:1030–1042.

Wang S., Kaufman R. J. The impact of the unfolded protein response on human disease. Journal of Cell Biology (2012). 197(7):857–67.

Wang Y., Fu X., Gaiser S., Köttgen M., Kramer-Zucker A., Walz G., Wegierski T. OS-9 regulates the transit and polyubiquitination of TRPV4 in the endoplasmic reticulum. J Biol Chem (2007). 282(50):36561-70.

Watchko J., O'Day T., Wang B., Zhou L., Tang Y., Li J., Xiao X.. Adeno-associated virus vector-mediated minidystrophin gene therapy improves dystrophic muscle contractile function in mdx mice. Human Genetics Therapy (2002). 13(12):1451-60.

Wiedenheft B., Sternberg S. H., Doudna J. A., RNA-guided genetic silencing systems in bacteria and archaea. Nature (2012). Vol. 482, 331–338.

Wu X., Kriz A.J., Sharp P.A. Target specificity of the CRISPR-Cas9 system. Quant Biol (2014) 2(2):59-70.

Xie X., Ross J.L., Cowell J.K., Teng Y. The promise of zebrafish as a chemical screening tool in cancer therapy. Future Med Chem (2015). 7(11):1395-405.

Xing L., Quist T.S., Stevenson T.J., Dahlem T.J., Bonkowsky J.L. Rapid and Efficient Zebrafish Genotyping Using PCR with Highresolution Melt Analysis. J. Vis. Exp. (2014) (84), e51138.

Yamanouchi Y., Mizuno Y., Yamamoto H., Takemitsu M., Yoshida M., Nonaka Y., Ozawa E. Selective defect in dystrophin-associated glycoproteins 50DAG (A2) and 35DAG (A4) in the dystrophic hamster: An animal model for severe childhood autosomal recessive muscular dystrophy (SCARMD). Neuromuscolar disorders (1994). Volume 4, 49–54.

Yoshida M. et al. Biochemical evidence for association of dystrobrevin with the sarcoglycansarcospan complex as a basis for understanding sarcoglycanopathy. Human Molecular Genetics (2000). 1033-1040.

Yoshida M., Suzuki A., Yamamoto H., Mizuno Y., Ozawa E. Dissociation of the complex of dystrophin and its associated proteins into several unique groups by n-octyl P-D-glucoside. European Journal of Biochemistry (1994). 222:1055-1061.

Yu Z., Ren M., Wang Z., Zhang B., Rong Y. S., Jiao R. et al.. Highly efficient genome modifications mediated by CRISPR/Cas9 in drosophila. Genetics (2013). 195(1), 289–291.

Zhang Y., Zhang Z., Ge W. An efficient platform for generating somatic point mutations with germline transmission in the zebrafish by CRISPR/Cas9-mediated gene editing. Journal of Biological Chemistry (2018). 6611-6622.

Zulian A., Rizzo E., Schiavone M., Palma E., Tagliavini F., Blaauw B., Merlini L., Maraldi N.M., Sabatelli P., Braghetta P., Bonaldo P., Argenton F., Bernardi P. NIM811, a cyclophilin inhibitor without immunosuppressive activity, is beneficial in collagen VI congenital muscular dystrophy models. Hum Mol Genet (2014). 23(20):5353-63.

AKNOWLEGMENT

Firstly, I would like to thank my professor Dorianna Sandonà, for conveying to me the passion for research, for her kind availability and because she always promoted opportunities for improving my professional skills. I would like also to thanks my supervisor, Marcello Carotti, who has guided me during these years of Ph.D with his constant attention and help. Indeed, whiteout their constant support this work would not have been possible

Secondly, thank to Chiara Fecchio, for her friendship, valuable advice and for the support that has given me over the years, encouraging me to improve even more.

Moreover, thanks to Giovanni Risato, Martina Scano, Francesca Marostica, Andrea Vettori, and to all the other colleagues, for the contribution and for the wonderful moments spent together.

Finally, thank to my family and to Romano, for their support, help and patience that have helped me to complete this wonderful study and improve my personal development.